



**THE ROLE OF GLUTATHIONE-S-TRANSFERASE IN  
EPITHELIAL MESENCHYMAL TRANSITION (EMT) MODEL  
IN COLORECTAL CANCER AND THE ENHANCEMENT OF  
ADJUVANT THERAPY BY TARGETING  
GLUTATHIONE-S-TRANSFERASE INHIBITOR**

**KOLOREKTAL KANSERDE EPİTELYAL MEZENKİMAL  
GEÇİŞ (EMT) MODELLEMESİNDE  
GLUTATYON-S-TRANSFERAZ'IN ROLÜ VE GLUTATYON-  
S-TRANSFERAZ İNHİBİTÖRÜ HEDEFLERENEREK ADJUVAN  
TERAPİ ETKİNLİĞİNİN ARTTIRILMASI**

**BURÇİN ÖZÇELİK**

**PROF. DR. ALPER B. İSKİT**

**Supervisor**

Submitted to

Graduate School of Science and Engineering of Hacettepe University

as a Partial Fulfillment to the Requirements

for the Award of the Degree of Doctor of Philosophy

in Nanotechnology and Nanomedicine

2018

This work named "The role of Glutathione-S-Transferase in Epithelial Mesenchymal Transition (EMT) Model in Colorectal Cancer and the Enhancement of Adjuvant Therapy by Targeting Glutathione-S-Transferase Inhibitor" by BURÇİN ÖZÇELİK has been approved as a thesis for the Degree of Doctor of Philosophy in Nanotechnology and Nanomedicine by the Examining Committee Members mentioned below.

Prof. Dr. Gülberk UÇAR  
Head

Prof. Dr. Alper B. İSKİT  
Supervisor

Prof. Dr. Aymelek GÖNENÇ  
Member

Assoc. Prof. Dr. İpek EROĞLU  
Member

Assoc. Prof. Dr. Ergin DİLEKÖZ  
Member

This thesis has been approved as a thesis for the Degree of Doctor of Philosophy in Nanotechnology and Nanomedicine by Board of Directors of the Institute of Graduate School of Science and Engineering on ..... / ..... / .....

Prof. Dr. Menemşe GÜMÜŞDERELİOĞLU  
Director of the Institute of  
Graduate School of Science and Engineering

***This thesis is dedicated to my parents and my sister..  
For their endless love, support and encouragement..***

## ETHICS

In this thesis study, prepared in accordance with the spelling rules of Institute of Graduate School of Science and Engineering of Hacettepe University,

I declare that

- all the information and documents have been obtained in the base of the academic rules
- all audio-visual and written information and results have been presented according to the rules of scientific ethics
- in case of using others works, related studies have been cited in accordance with the scientific standards
- all cited studies have been fully referenced
- I did not do any distortion in the data set
- and any part of this thesis has not been presented as another thesis study at this or any other university.

23/10/2018



BURÇİN ÖZÇELİK

## YAYIMLAMA VE FİKRİ MÜLKİYET HAKLARI BEYANI

Enstitü tarafından onaylanan lisansüstü tezimin/raporumun tamamını veya herhangi bir kısmını, basılı (kağıt) ve elektronik formatta arşivleme ve aşağıda verilen koşullarla kullanıma açma iznini Hacettepe Üniversitesine verdiğimi bildiririm. Bu izinle Üniversiteye verilen kullanım hakları dışındaki tüm fikri mülkiyet haklarım bende kalacak, tezimin tamamının ya da bir bölümünün gelecekteki çalışmalarda (makale, kitap, lisans ve patent vb.) kullanım hakları bana ait olacaktır.

Tezin kendi orjinal çalışmam olduğunu, başkalarının haklarını ihlal etmediğimi ve tezimin tek yetkili sahibi olduğumu beyan ve taahhüt ederim. Tezimde yer alan telif hakkı bulunan ve sahiplerinden yazılı izin alınarak kullanması zorunlu metinlerin yazılı izin alarak kullandığımı ve istenildiğinde suretlerini Üniversiteye teslim etmeyi taahhüt ederim.

Yükseköğretim Kurulu tarafından yayınlanan '*Lisansüstü Tezlerin Elektronik Ortamda Toplanması, Düzenlenmesi ve Erişime Açılmasına İlişkin Yönerge*' kapsamında tezim aşağıda belirtilen koşullar haricinde YÖK Ulusal Tez Merkezi / H.Ü. Kütüphaneleri Açık Erişim Sisteminde erişime açılır.

- Enstitü / Fakülte yönetim kurulu kararı ile tezimin erişime açılması mezuniyet tarihimden itibaren 2 yıl ertelenmiştir.
- Enstitü / Fakülte yönetim kurulu gerekçeli kararı ile tezimin erişime açılması mezuniyet tarihimden itibaren ..... ay ertelenmiştir.
- Tezim ile ilgili gizlilik kararı verilmiştir.



23/10/2018

BURÇİN ÖZÇELİK

## ÖZET

# KOLOREKTAL KANSERDE EPİTELYAL MEZENKİMAL GEÇİŞ (EMT) MODELLEMESİNDE GLUTATYON S-TRANSFERAZ'IN ROLÜ VE GLUTATYON S-TRANSFERAZ İNHİBİTÖRÜ HEDEFLERENEREK ADJUVAN TERAPİ ETKİNLİĞİNİN ARTTIRILMASI

**Burçin ÖZÇELİK**

**Doktora , Nanoteknoloji ve Nanotıp Anabilim Dalı**

**Tez Danışmanı: Prof. Dr. Alper B. İSKİT**

**Ekim, 2018, 141 sayfa**

Kolorektal kanser, dünya çapında kanserle ilişkili ölümlerin üçüncü önde gelen nedenidir. Uzak bölgelere yayılmayan kolorektal kanserler için, cerrahi genellikle birincil veya ilk tedavi seçeneğidir. Bununla birlikte, kemoterapi (neoadjuvan, adjuvan ve ileri evre kemoterapi) halen yaygın olarak kullanılmaktadır. Kolorektal kanseri tedavi etmek için birkaç antikanser ajanı mevcuttur, ancak nihayetinde kanser nüksleri meydana gelir. Mevcut tedavilerin başarısında önemli bir engel, kanser hücrelerinin, genellikle geri dönüşü olmayan bir nokta olarak kabul edilen ve en kötü sonuçla ilişkili olan metastazlara neden olan tekrarlayan adaptasyonudur. Bu nedenle, kanser hücrelerinin direncini arttıran mekanizmaları anlamak, özel bir önem taşımaktadır.

Son yıllarda, epitelyal mezenkimal geçişin (EMT), doğal olarak meydana gelen transdiferansasyon programı, kemoterapiye karşı dirençte önemli bir rol oynadığına inanılmaktadır. EMT'nin kemoterapi direncinde ve metastazda kritik bir rol oynadığı yaygın olarak gösterilse de, EMT ile ilaç direnci arasındaki potansiyel sinyalizasyon ağı hala belirsizdir. Glutatyonun (GSH) hem endojen hem de ksenobiyotik kökenli elektrofillerle reaksiyonunu katalize eden bir izozimler ailesi olan Glutatyon S-Transferazlar (GST'ler), doğrudan detoksifikasyon yoluyla ilaç direncinin gelişmesine neden olurlar. GST'lerin pi ( $\pi$ ) ve mu ( $\mu$ ) sınıfları, hücrel sağkalımda ve ayrıca kanser gelişiminde düzenleyici bir rol oynamaktadır.

Bu nedenle, bu çalışmada, HT-29 KRK hücre hattında *in vitro* EMT modeli oluşturulmuş ve EMT, immünohistokimyasal ve biyokimyasal yöntemler kullanılarak gösterilmiştir. HT-29 KRK hücrelerinin epitelyal ve mezenkimal fenotiplerinde GST- $\pi$  ve GST- $\mu$  ekspresyon ve protein düzeyleri belirlenmiştir. Her iki formda oksidatif stres oluşturulmuş ve oksidatif hasar tespit edilmiştir. HT-29 KRK hücrelerinin epitelyal ve mezenkimal fenotiplerinde oksidatif hasar ile GST izoenzimlerinin gen ve protein düzeyleri arasındaki korelasyon belirlenmiştir. HT-29 KRK hücrelerinin her iki fenotipi, FDA onaylı bir GST inhibitörü olan etakrinik asit (ETA) ile muamele edilmiştir. ETA muamelesini takiben GST izoenzimlerinin ekspresyon ve protein düzeyleri belirlenmiştir. Testler GST inhibitörünün KRK'da EMT üzerindeki etkisini araştırmak için HT-29 KRK hücrelerinin oksidatif olarak hasar oluşturulmuş epitelyal ve mezenkimal fenotipleri için tekrarlanmıştır. Epitelyal ve mezenkimal fenotipler, ayrıca yeni terapötik protokolün etkinliğini araştırmak için adjuvan tedavi kombinasyonu ile ve adjuvan tedavi kombinasyonu ve ETA ile tedavi edilmiştir. Boş ve ETA yüklü PLGA-*b*-PEG nanopartiküller ve mPLGA-PEG-SS-ETA nanokonjugatları nanopresipitasyon tekniği ile hazırlanmıştır. Bu nanoformülasyonlar ortalama partikül büyüklüğü, PDI, zeta potansiyeli açısından ve morfolojik olarak karakterize edilmiştir. Nanoformülasyonların ETA yükleme kapasitesi ve yükleme verimliliği, valide HPLC yöntemi ile belirlenmiştir. Optimize edilmiş nanoformülasyonlar, hedefleme çalışmaları için için HT-29 hücrelerinin mezenkimal fenotipine özgü Vimentin (Vim) monoklonal antikoru ile konjuge edilmiştir. Nanoformülasyonların *in vitro* sitotoksitesi L929 hücrelerinde belirlenmiştir. Epitelyal ve mezenkimal fenotipler, hedefe yönelik yeni terapötik protokolün etkinliğini araştırmak için, adjuvan tedavi



kombinasyonu ve ETA yüklü ve mezenkimal fenotip hedefli nanoformülasyonlarla tedavi edilmiştir. İmmün sistemi baskılanmış Wistar sıçanlarda *in vivo* EMT modeli oluşturulmuştur. Yeni hedefe yönelik terapötik protokolün *in vivo* etkinliğini araştırmak için hayvanlar, adjuvan tedavi kombinasyonu ve adjuvan tedavi kombinasyonu ile ETA yüklü ve mezenkimal fenotip hedefli nanoformülasyonlarla tedavi edilmiştir.

HT-29 KRK hücrelerinde *in vitro* EMT modeli başarıyla oluşturulmuştur. HT-29 hücrelerinin mezenkimal fenotipinde, GST- $\pi$ 'nin yüksek ekspresyonu ve protein seviyeleri gözlenmiş, ancak GST- $\mu$  ekspresyon paternlerinde dikkate değer bir fark gözlenmemiştir. ETA, PLGA-*b*-PEG nanopartiküllere başarıyla yüklenmiştir. ETA ayrıca disülfid bağı yoluyla mPEG-PLGA kopolimerine konjuge edilmiş ve sonuçta oluşan polimer nano boyutlu taşıyıcı sistemlere kendiliğinden dönüşmüştür. ETA yüklü nanoformülasyonlar, dar bir boyut dağılımı ile 115-130 nm aralığında elde edilmiştir. Vim mAb konjugasyonu ile her iki nanoformülasyon da mezenkimal fenotipe başarı ile hedeflenmiştir. Hedefe yönelik formülasyonların hücre içine alımları daha yüksek olup, GST- $\pi$  izoenzimi üzerinde daha düşük konsantrasyonlar ile inhibisyon etkisi göstermiştir.

HT-29 KRK hücrelerinin enjeksiyonu ile immün sistemi baskılanmış Wistar ratlarda başarılı bir şekilde *in vivo* EMT modeli oluşturulmuştur. EMT oluşumu gözlenen hayvanlarda GST- $\pi$  izoenzimi ekspresyon seviyelerinde artış gözlenmiştir. ETA yüklü ve mezenkimal fenotipe hedeflendirilmiş nanoformülasyonlar adjuvan tedavi etkinliğini arttırarak oluşan granülom boyutlarında küçülmeyi sağlamıştır.

**Anahtar Kelimeler:** Kolorektal kanser, epitelyal mezenkimal geçiş, GST izoenzimleri, etakrinik asit, immunonanopartiküller, immünonanokonjugatlar, adjuvan tedavi

## **ABSTRACT**

# **THE ROLE OF GLUTATHIONE-S-TRANSFERASE IN EPITHELIAL MESENCHYMAL TRANSITION (EMT) MODEL IN COLORECTAL CANCER AND THE ENHANCEMENT OF ADJUVANT THERAPY BY TARGETING GLUTATHIONE-S-TRANSFERASE INHIBITOR**

**Burçin ÖZÇELİK**

**Doctor of Philosophy, Department of Nanotechnology and Nanomedicine**

**Supervisor: Prof. Dr. Alper B. İSKİT**

**October 2018, 141 pages**

Colorectal cancer is the third leading cause of cancer-related deaths worldwide. For colorectal cancers that have not spread to distant sites, surgery is usually the primary or first treatment option. However, chemotherapy (neoadjuvan, adjuvan and advanced-stage chemotherapy) is still widely used. Several chemotherapeutic agents are available for the treatment of CRC, but eventually cancer relapse occurs. A major impediment in the success of available therapies is the recurrent adaptation of cancer cells, leading to metastases, which are often considered as the point of no return, and are associated with the worst outcome. Therefore, understanding the mechanisms that drive resistance of cancer cells bears special importance.

In the recent years, epithelial-mesenchymal transition (EMT), naturally occurring transdifferentiation program, is believed to play an important role in resistance toward chemotherapeutics. Although EMT is widely demonstrated to play a critical

role in chemoresistance and metastasis, the potential signaling network between EMT and drug resistance is still unclear. Glutathione S-Transferases (GSTs), a family of isozymes that catalyze the reaction of glutathione (GSH) with electrophiles of both endogenous and xenobiotic origins, assist in the development of drug resistance through direct detoxification. The pi ( $\pi$ ) and mu ( $\mu$ ) classes of GSTs play a regulatory role in cellular survival and also in development of cancer.

Thus, in the present study, *in vitro* EMT model was created in HT-29 CRC cell line and EMT was demonstrated using immunohistochemical and biochemical methods. Expression and protein levels of GST- $\pi$  and GST- $\mu$  in the epithelial and mesenchymal phenotype of HT-29 CRC cells was determined. Oxidative stress was generated and oxidative damage was detected; correlation between the oxidative damage and GST isoenzymes was determined at gene and protein levels in the epithelial and mesenchymal phenotypes of HT-29 CRC cells. Both phenotypes of HT-29 CRC cells were treated with ethacrynic acid (ETA) that is a FDA approved GST inhibitor. Expressions of the GST isoenzymes and their protein levels were determined following ETA treatment. Assays were repeated for oxidatively damaged epithelial and mesenchymal phenotypes of HT-29 cells in order to investigate the effect of GST inhibitor on EMT in CRC. Epithelial and mesenchymal phenotypes were treated with adjuvant therapy combination and also with the adjuvant therapy combination plus ETA to investigate the efficacy of the new therapeutic protocol. Blank and ETA loaded PLGA-*b*-PEG nanoparticles and mPLGA-PEG-SS-ETA nanoconjugates were prepared by nanoprecipitation technique. These nanoformulations were characterized in terms of mean particle size, PDI, zeta potential and morphology. ETA loading capacity and loading efficiency of nanoformulations were determined by validated HPLC method. The optimized nanoformulations were coupled with Vimentin (Vim) monoclonal antibody specific to mesenchymal phenotype of HT-29 CRC cells for targeted delivery. *In vitro* cytotoxicity of nanoformulations were determined on L929 cells. Epithelial and mesenchymal phenotypes were treated with adjuvant therapy combination plus ETA loaded and mesenchymal phenotype targeted nanoformulations to investigate the efficacy of the new targeted therapeutic protocol. *In vivo* EMT model was created in the immunosuppressed Wistar rats. Animals were treated with adjuvant therapy combination and adjuvant therapy

combination plus ETA loaded and mesenchymal phenotype targeted nanoformulations to investigate the *in vivo* efficacy of the new targeted therapeutic protocol.

*In vitro* EMT model was successfully established in HT-29 CRC cells. In mesenchymal phenotype of HT-29 cells, elevated expression and protein levels of GST- $\pi$  were observed, however, no remarkable difference in GST- $\mu$  expression patterns was observed. GST inhibitor ETA was successfully loaded in PLGA-*b*-PEG nanoparticles. ETA was also conjugated to PLGA-*b*-PEG copolymer via disulphide bond and resulting polymer self-assembled into nanosized particles. ETA loaded nanoformulations in the range of 115 to 130 nm with a narrow size distribution were obtained. Both nanoformulations were successfully targeted to mesenchymal phenotype with Vim mAb conjugation. Targeted formulations had higher cell uptake rates and showed inhibition effect on GST- $\pi$  isoenzyme activity even at lower concentrations.

*In vivo* EMT model were successfully induced by the injection of HT-29 CRC cells in immuno-suppressed Wistar rats. Increased levels of GST- $\pi$  isoenzyme expression in animals with EMT formation were observed. ETA-loaded and mesenchymal phenotype targeted nanoformulations increased adjuvant therapy efficacy and reduced formed granuloma sizes.

**Keywords:** Colorectal cancer, epithelial mesenchymal transition, GST isoenzymes, ethacrynic acid, immunonanoparticles, immunonanoconjugates, adjuvan therapy

## ACKNOWLEDGEMENT

Firstly, I would like to express my sincere gratitude to my advisor Prof. Dr. Alper B. İSKİT for the continuous support of my Ph.D study and related research, for his patience, motivation, and immense knowledge. His guidance helped me in all the time of research and writing of this thesis.

Besides my advisor, I would like to thank Prof. Dr. Gülberk UÇAR, for her unending patience, enlightening guidance and inspiring instruction to the successful completion of this study.

I also thank Assoc. Prof. Dr. İpek EROĞLU for her invaluable contributions. It was truly an honor to receive her insights and inspiring instructions into this project. Without her precious support it would not be possible to conduct this research.

I would like to express my deepest and sincere gratitude to Dr. Açelya ERİKÇİ for her unending patience, enlightening guidance and inspiring instruction to the successful completion of this study. She always encouraged me to do my best and her belief in me kept me focused during those difficult times.

My sincere thanks also goes to Assoc. Prof. Dr. Kemal KÖSEMEHMETOĞLU who provided me an opportunity to access to the laboratory and research facilities.

I would like to thank The Scientific and Technological Research Council of Turkey for financial support through project no:116S347.

I would like to thank Hacettepe University Scientific Research Projects Coordination Unit for financial support through project no: TSA-2017-15520.

I would like to thank my friends, Laçın KAPUCUOĞLU KELEŞ, Fatih DOKUMACI, Aslı KARA, Bediha AKMEŞE and Gamze ÇAĞATAY, for all the good times, for their insightful comments, encouragement and support.

A special gratitude and love goes to my family: my parents, Nadire & Mustafa ÖZÇELİK, and to my sisters, Büşra ÖZÇELİK and Bahar PALABIYIK, for their unfailing support, absolute belief in my abilities and for their abiding love.

Burçin ÖZÇELİK

Ekim 2018, Ankara

# INDEX

ÖZET .....	i
ABSTRACT .....	iv
ACKNOWLEDGEMENT .....	vii
INDEX .....	viii
INDEX OF TABLES.....	xiii
INDEX OF FIGURES .....	xiv
SYMBOLS AND ABBREVIATIONS.....	xviii
1. INTRODUCTION .....	1
2. GENERAL INFORMATION .....	4
2.1. Cancer .....	4
2.2.1. Intratumoral Heterogeneity .....	8
2.2.2. Enhanced Drug Efflux.....	8
2.2.3. Enhanced DNA Repair .....	9
2.2.4. Altered Expression of Drug Metabolizing Enzymes .....	10
2.2.5. Dysregulated Apoptosis.....	10
2.3. Epithelial-Mesenchymal Transition (EMT) .....	11
2.3.1. Epithelial Cells versus Mesenchymal Cells.....	11
2.3.2. EMT Effectors.....	12
2.3.3. Subtypes of EMT .....	13
2.3.4. EMT Inducers .....	15
2.3.5. EMT and Cancer Treatment Resistance.....	16
2.4. Glutathione S-Transferases (GSTs) .....	17
2.4.1. Structure of the GSTs .....	18
2.4.2. Classification of GSTs .....	19

2.4.3.	Role of GSTs in Drug Resistance .....	20
2.5.	Colorectal Cancer (CRC).....	21
2.5.1.	Treatment of CRC .....	21
2.5.2.	CRC, EMT and Drug Resistance.....	22
2.6.	Nano-sized Drug Delivery Systems in Cancer Treatment.....	23
2.6.1.	Polymeric Nanoparticles .....	24
2.6.1.1.	Polymers Used for Preparation of Polymeric Nanoparticles .....	24
2.6.1.2.	Nanoparticle Preparation Methods .....	25
2.6.1.2.1.	Polymerization Method .....	25
2.6.1.2.2.	Interfacial Polymerization Method.....	26
2.6.1.2.3.	Micelle Polymerization .....	26
2.6.1.2.4.	Emulsification-Solvent Evaporation Method .....	26
2.6.1.2.5.	Nanoprecipitation.....	26
2.6.1.3.	Characterization of Nanoparticles.....	27
2.6.1.3.1.	Particle Size.....	27
2.6.1.3.2.	Zeta Potential.....	27
2.6.1.3.3.	<i>In vitro</i> release .....	28
2.7.	GST Inhibitor ETA .....	29
3.	MATERIALS and METHODS .....	30
3.1.	MATERIALS .....	30
3.2.	METHODS.....	31
3.2.1.	<i>In vitro</i> EMT Modelling and Demonstrating EMT .....	31
3.2.1.1.	Cell culture.....	31
3.2.1.2.	<i>In vitro</i> EMT Modelling in HT-29 CRC Cell Line.....	32
3.2.1.3.	Evaluation of the Molecular Markers of EMT .....	33
3.2.1.4.	Immunofluorescence Staining .....	35

3.2.2.	Determination of the Expression Levels for GST- $\pi$ and GST- $\mu$ Isoenzymes in Epithelial and Mesenchymal Phenotypes of HT-29 Cells, Activity Assay and Inhibition of GST Isoenzymes.....	36
3.2.2.1.	Determination of Expression Levels for GST Isoenzymes in Epithelial and Mesenchymal Phenotypes of HT-29 Cells (qRT-PCR).....	37
3.2.2.2.	Determination of GST- $\pi$ and GST- $\mu$ Protein Levels .....	37
3.2.2.3.	Treatment of Epithelial and Mesenchymal Phenotypes of HT-29 Cells with GST Inhibitor ETA .....	37
3.2.2.4.	Formation and Determination of Oxidative Stress in Epithelial and Mesenchymal Phenotypes of HT-29 cells.....	38
3.2.2.5.	Treatment of Oxidative Stressed Epithelial and Mesenchymal Phenotypes of HT-29 Cells with GST Inhibitor ETA .....	39
3.2.3.	Preparation of GST Inhibitor ETA Loaded and Mesenchymal Phenotype Targeted Nanosized Formulations.....	39
3.2.3.1.	Quantification of ETA by HPLC .....	39
3.2.3.2.	Synthesis of PLGA- <i>b</i> -PEG Copolymer .....	41
3.2.3.3.	Synthesis of mPEG-PLGA-SS-ETA .....	42
3.2.3.4.	Preparation of Blank Nanoparticles .....	43
3.2.3.5.	Preparation of ETA Loaded Nanoparticles .....	45
3.2.3.6.	Preparation of MPEG-PLGA-SS-ETA Nanoconjugates.....	45
3.2.3.7.	Characterization of Nanoformulations .....	45
3.2.3.8.	Entrapment Efficiency and Loading Capacity .....	46
3.2.3.9.	<i>In vitro</i> Release Studies.....	47
3.2.3.10.	Stability of Nanoformulations .....	47
3.2.3.11.	Sterilization of Nanoformulations .....	48
3.2.3.12.	Sterility Control of Nanoformulations .....	48
3.2.3.13.	Antibody Conjugation of Nanoformulations.....	48
3.2.4.	<i>In vitro</i> Studies.....	49



3.2.4.1.	Treatment of Oxidative Stress Generated Epithelial and Mesenchymal Phenotypes of HT-29 Cells with Nanoparticulated ETA .....	50
3.2.4.2.	Treatment of Oxidative Stress Generated Epithelial and Mesenchymal Phenotypes of HT-29 Cells with FOLFOX .....	50
3.2.4.3.	Treatment of Oxidative Stress Generated Epithelial and Mesenchymal Phenotypes of HT-29 Cells with ETA+FOLFOX .....	50
3.2.4.4.	Treatment of Oxidative Stress Generated Epithelial and Mesenchymal Phenotypes of HT-29 Cells with Nanoparticulated ETA +FOLFOX .....	51
3.2.5.	<i>In vivo</i> Studies .....	51
3.2.5.1.	Establishment of <i>in vivo</i> CRC Model .....	51
3.2.5.2.	Study Groups.....	52
3.2.5.3.	Histopathology.....	54
3.2.5.4.	RNA extraction, cDNA synthesis and qRT-PCR .....	54
3.2.5.5.	Immunohistochemistry.....	54
3.2.6.	Statistical Analysis.....	54
4.	RESULTS and DISCUSSION.....	55
4.1.	TGF- $\beta$ 1 Induced EMT in HT-29 CRC Cells .....	55
4.1.1.	Morphological Alterations in HT-29 Cells Induced with TGF- $\beta$ 1 .....	56
4.1.2.	Molecular Markers of Epithelial and Mesenchymal Phenotypes.....	56
4.1.3.	Immunofluorescence Staining .....	62
4.2.	Determination of Expression Levels for GST- $\pi$ and GST- $\mu$ Isoenzymes in Epithelial and Mesenchymal Phenotypes of HT-29 Cells, Activity Assay and Inhibition of GST Isoenzymes.....	65
4.2.1.	Elevated Expression and Protein Levels of GST- $\pi$ in Mesenchymal Phenotype of HT-29 Cells.....	65
4.2.4.	Treatment of Oxidative Stress Generated Epithelial and Mesenchymal Phenotypes of HT-29 Cells with GST Inhibitor ETA .....	73

4.3.	Preparation of GST Inhibitor ETA Loaded And Mesenchymal Phenotype Targeted Nanoparticles .....	74
4.3.1.	Quantification of ETA and HPLC Method Validation.....	74
4.3.1.1.	Construction of Calibration Curve .....	75
4.3.2.	Synthesis and Characterization of mPEG–PLGA–SS–ETA .....	78
4.3.3.	Preparation of Blank Nanoparticles .....	79
4.3.4.	Preparation of Drug Loaded Nanoparticles.....	82
4.3.11.	Antibody Conjugation of Nanoformulations.....	91
4.3.12.	<i>In vitro</i> Cytotoxicity .....	92
4.4.	<i>In vitro</i> studies .....	94
4.4.1.	Treatment of OxidativeStress Generated Epithelial and Mesenchymal Phenotypes of HT-29 Cells with Nanoparticulated ETA .....	94
4.4.2.	Treatment of Oxidative Stress Generated Epithelial and Mesenchymal Phenotypes of HT-29 Cells with FOLFOX .....	98
4.4.3.	Treatment of Oxidative Stress Generated Epithelial and Mesenchymal Phenotypes of HT-29 cells with ETA plus FOLFOX .....	99
4.4.4.	Treatment of Oxidative Stress Generated Epithelial and Mesenchymal Phenotypes with Nanoparticulated ETA plus FOLFOX .....	100
4.5.	<i>In vivo</i> Studies .....	104
5.	CONCLUSION.....	113
	REFERENCES.....	115
	CURRICULUM VITAE .....	140

## INDEX OF TABLES

<b>TABLE 3.1.</b>	Reagents for the first step of cDNA synthesis .....	34
<b>TABLE 3.2.</b>	Reagents for the second step of cDNA synthesis.....	34
<b>TABLE 3.3.</b>	The sequences of human specific primers for EMT-associated markers ...	35
<b>TABLE 3.4.</b>	Protocol for immunofluorescence staining .....	36
<b>TABLE 3.5.</b>	List of antibodies used for immunofluorescence studies.....	35
<b>TABLE 3.6.</b>	The sequences of human specific primers of GTSs .....	37
<b>TABLE 3.7.</b>	MTT assay protocol .....	38
<b>TABLE 4. 1.</b>	Linear regression data obtained from HPLC analysis for ETA.....	75
<b>TABLE 4. 2.</b>	Accuracy data for ETA .....	77
<b>TABLE 4.3.</b>	Data of repeatability for ETA .....	77
<b>TABLE 4. 4.</b>	The effect of polymer concentration on particle size, polydispersity index and $\zeta$ -potential of PLGA and PLGA- <i>b</i> -PEG nanoparticles.....	80
<b>TABLE 4. 5.</b>	Effect of surfactant concentration on particle size, polydispersity index and $\zeta$ -potential of PLGA and PLGA- <i>b</i> -PEG nanoparticles. ....	81
<b>TABLE 4.6.</b>	The effect of organic phase to aqueous phase ratio (v/v) on particle size, polydispersity index and $\zeta$ -potential of PLGA and PLGA- <i>b</i> -PEG nanoparticles. 82	
<b>TABLE 4.7.</b>	The effect of drug concentration (w/v) on particle size, polydispersity index and $\zeta$ -potential of PLGA and PLGA- <i>b</i> -PEG nanoparticles. ....	83
<b>TABLE 4.8.</b>	Effect of polymer concentration (w/v) on physicochemical properties of mPEG-PLGA-SS-ETA nanoconjugates.. ....	85
<b>TABLE 4.9.</b>	The effect of drug concentration (w/v) on physicochemical properties of nanoformulations.....	86
<b>TABLE 4.10.</b>	Stability of ETA-loaded PLGA- <i>b</i> -PEG nanoparticles at room temperature and at +4°C.....	90
<b>TABLE 4.11.</b>	Stability of mPEG-PLGA-SS-ETA nanoconjugates at room temperature and at +4°C.....	91

## INDEX OF FIGURES

<b>Figure 2.1.</b>	Three stages of carcinogenesis.....	<b>4</b>
<b>Figure 2.2.</b>	Mechanisms of chemotherapeutic drug resistance in cancer cells .....	<b>7</b>
<b>Figure 2.3.</b>	Schematic representations of epithelial and mesenchymal cells .....	<b>12</b>
<b>Figure 2.4.</b>	Molecular structure of ETA .....	<b>29</b>
<b>Figure 3.1.</b>	Schematic representations of the synthesis route PLGA- <i>b</i> -PEG.....	<b>42</b>
<b>Figure 3.2.</b>	Synthesis of the polymer conjugates of ETA .....	<b>43</b>
<b>Figure 3.3.</b>	Schematic representations nanoprecipitation (solvent displacement) method .....	<b>44</b>
<b>Figure 4.1.</b>	Untreated and TGF- $\beta$ 1 treated HT-29 cells under inverted light microscope .....	<b>55</b>
<b>Figure 4.2.</b>	Immunofluorescence staining of untreated and TGF- $\beta$ 1 treated HT-29 cells .....	<b>55</b>
<b>Figure 4.3.</b>	Relative mRNA levels of epithelial markers after TGF- $\beta$ 1 induction for 24 hours .....	<b>57</b>
<b>Figure 4.4.</b>	Relative mRNA levels of epithelial markers after TGF- $\beta$ 1 induction for 48 hours .....	<b>58</b>
<b>Figure 4.5.</b>	Relative mRNA levels of transcription factors, after TGF- $\beta$ 1 induction for 24 hours.....	<b>59</b>
<b>Figure 4.6.</b>	Relative mRNA levels of transcription factors, after TGF- $\beta$ 1 induction for 48 hours .....	<b>60</b>
<b>Figure 4.7.</b>	Relative mRNA levels of mesenchymal markers after TGF- $\beta$ 1 induction for 24 hours .....	<b>61</b>
<b>Figure 4.8.</b>	Relative mRNA levels of mesenchymal markers after TGF- $\beta$ 1 induction for 48 hours .....	<b>63</b>
<b>Figure 4.9.</b>	Immunofluorescence staining identified EMT-related genes in epithelial and mesenchymal phenotype.....	<b>64</b>
<b>Figure 4.10.</b>	Immunofluorescence staining identified the upregulation of SNAIL-I and translocation of $\beta$ -catenin and SNAIL to nucleus in the mesenchymal phenotype.....	<b>65</b>
<b>Figure 4.11.</b>	A) Relative mRNA levels of GST isoenzymes after treatment with TGF- $\beta$ 1 .....	<b>66</b>
<b>Figure 4.12.</b>	Determination of % activity of GST- $\pi$ activity after treatment with different concentrations of ETA for epithelial phenotype.....	<b>69</b>

<b>Figure 4.13.</b>	Determination of % activity of GST- $\pi$ activity after treatment with different concentrations of ETA for mesenchymal phenotype .....	<b>68</b>
<b>Figure 4.14.</b>	GST- $\pi$ protein levels after treatment with different concentrations of ETA .....	<b>69</b>
<b>Figure 4.15.</b>	% cell viability of epithelial and mesenchymal phenotype of HT-29 cells following treatment with various concentrations of H <sub>2</sub> O <sub>2</sub> for 1 hour .....	<b>70</b>
<b>Figure 4.16.</b>	% cell viability of epithelial and mesenchymal phenotypes after treatment with various concentrations of H <sub>2</sub> O <sub>2</sub> for 2 hours .....	<b>71</b>
<b>Figure 4.17.</b>	MDA levels of epithelial and mesenchymal phenotypes after treatment with various concentrations of H <sub>2</sub> O <sub>2</sub> for 2 hours .....	<b>72</b>
<b>Figure 4.18.</b>	Relative mRNA levels of GST- $\pi$ after treatment with different concentrations of H <sub>2</sub> O <sub>2</sub> .....	<b>73</b>
<b>Figure 4.19.</b>	Determination of % GST- $\pi$ activity after treatment with different concentrations of ETA for oxidative stress generated epithelial phenotypes .....	<b>74</b>
<b>Figure 4.20.</b>	Determination of % GST- $\pi$ activity after treatment with different concentrations of ETA for oxidative stress generated mesenchymal phenotype .....	<b>74</b>
<b>Figure 4.21.</b>	Calibration curve of ETA .....	<b>76</b>
<b>Figure 4.22.</b>	NMR analysis of mPEG-PLGA-SS-ETA .....	<b>78</b>
<b>Figure 4.23.</b>	FT-IR spectrum of mPEG-PLGA-SS-ETA .....	<b>79</b>
<b>Figure 4.24.</b>	Scanning electron microphotographs of ETA loaded PLGA- <i>b</i> -PEG nanoparticles and mPEG-PLGA-SS-ETA nanoconjugates .....	<b>85</b>
<b>Figure 4.25.</b>	<i>In vitro</i> release profile of nanoparticles at pH 6.8 .....	<b>88</b>
<b>Figure 4.26.</b>	<i>In vitro</i> release profile of nanoparticles at pH 7.4 .....	<b>88</b>
<b>Figure 4.27.</b>	<i>In vitro</i> release profile of nanoconjugates at pH 6.8 .....	<b>89</b>
<b>Figure 4.28.</b>	<i>In vitro</i> release profile of nanoconjugates at pH 7.4 .....	<b>89</b>
<b>Figure 4.29.</b>	BSA validation curve .....	<b>92</b>
<b>Figure 4.30.</b>	Cytotoxicity of PLGA- <i>b</i> -PEG nanoparticles on L929 cells .....	<b>93</b>
<b>Figure 4.31.</b>	Cytotoxicity of mPLGA-PEG-SS-ETA nanoconjugates on L929 cells .....	<b>93</b>
<b>Figure 4.32.</b>	Cytotoxicity of ETA-loaded PLGA- <i>b</i> -PEG nanoparticles on L929 cells .....	<b>94</b>
<b>Figure 4.33.</b>	Determination of % GST- $\pi$ activity after treatment with different concentrations of A) ETA loaded PLGA- <i>b</i> -PEG nanoparticles B) mPLGA-PEG-SS-ETA nanoconjugates for epithelial phenotypes .....	<b>96</b>

<b>Figure 4.34.</b>	Determination of % GST- $\pi$ activity after treatment with different concentrations of A) ETA loaded PLGA- <i>b</i> -PEG immunonanoparticles B) mPLGA-PEG-SS-ETA immunonanoconjugates for epithelial phenotypes.....	<b>96</b>
<b>Figure 4.35.</b>	Determination of % GST- $\pi$ activity after treatment with different concentrations of A) ETA loaded PLGA- <i>b</i> -PEG nanoparticles B) mPLGA-PEG-SS-ETA nanoconjugates for mesenchymal phenotypes .....	<b>97</b>
<b>Figure 4.36.</b>	Determination of % GST- $\pi$ activity after treatment with different concentrations of A) ETA loaded PLGA- <i>b</i> -PEG immunonanoparticles B) mPLGA-PEG-SS-ETA immunonanoconjugates for mesenchymal phenotypes .....	<b>97</b>
<b>Figure 4.37.</b>	Determination of % cell viability of epithelial and mesenchymal phenotypes after treatment with A) FOLFOX and B) ETA plus FOLFOX .....	<b>98</b>
<b>Figure 4.38.</b>	Determination of % cell viability of A) epithelial and B) mesenchymal phenotypes after treatment with FOLFOX and ETA plus FOLFOX .....	<b>100</b>
<b>Figure 4.39.</b>	% cell viability of epithelial and mesenchymal phenotypes after treatment with ETA loaded nanoparticles and ETA loaded immunonanoparticles .....	<b>101</b>
<b>Figure 4.40.</b>	% cell viability of epithelial and mesenchymal phenotypes after treatment with mPLGA-PEG-SS-ETA nanoconjugates and mPLGA-PEG-SS-ETA Immunonanoconjugates .....	<b>102</b>
<b>Figure 4.41.</b>	Determination of % cell viability of epithelial phenotypes after treatment with FOLFOX, ETA plus FOLFOX and different nanoformulations plus FOLFOX .....	<b>103</b>
<b>Figure 4.42.</b>	Determination of % cell viability of mesenchymal phenotypes after treatment with FOLFOX, ETA plus FOLFOX and different nanoformulations plus FOLFOX .....	<b>103</b>
<b>Figure 4.43.</b>	<i>In vivo</i> images of the colorectal tissues of rats on the day 0-95 <sup>th</sup> .....	<b>105</b>
<b>Figure 4.44.</b>	Photomicrograph showing granuloma formation <b>A)</b> H&E stain, X100, <b>B)</b> H&E stain, X400 .....	<b>106</b>
<b>Figure 4.45.</b>	Relative colonic COX-2 mRNA levels between 15-95 <sup>th</sup> days .....	<b>106</b>
<b>Figure 4.46.</b>	Relative mRNA levels of epithelial markers on the 95-115 <sup>th</sup> days after injection of HT-29 CRC cells into rats .....	<b>107</b>
<b>Figure 4.47.</b>	Relative mRNA levels of mesenchymal markers on the 95-115 <sup>th</sup> days after injection of HT-29 CRC cells into rats .....	<b>108</b>

<b>Figure 4.48.</b> Immunohistochemical staining of granulomas for expression of mesenchymal markers .....	<b>109</b>
<b>Figure 4.49.</b> Relative mRNA levels of COX-2 in rats after different treatment regimens .....	<b>110</b>
<b>Figure 4.50.</b> Protein levels of GST- $\pi$ in rats after different treatment regimens .....	<b>111</b>
<b>Figure 4.51.</b> Protein levels of MDA in the rats after different treatment regimens .....	<b>112</b>

## SYMBOLS AND ABBREVIATIONS

### Symbols

$\mu$	micro
$\pi$	Pi
$\beta$	Beta
$\zeta$	Zeta
$\alpha$	alfa

### Abbreviations

<b>CRC</b>	Colorectal cancer
<b>TGF-<math>\beta</math></b>	Transforming Grow Factor-beta
<b>EMT</b>	Epithelial-Mesenchymal Transition
<b>MET</b>	Mesenchymal-Epithelial Transition
<b>ETA</b>	Ethacrynic acid
<b>GSTs</b>	Glutathione S-Transferases
<b>MDA</b>	Malondialdehyde
<b>ROS</b>	Reactive Oxygen Species
<b>NCI</b>	National Cancer Institute
<b>FDA</b>	US Food and Drugs Administration
<b>EMA</b>	European Medicine Agency
<b>PLA</b>	Poly (lactic acid)
<b>PLGA</b>	Poly (lactic-co-glycolic acid)
<b>PEG</b>	Poly (ethylene glycol)
<b>Vim</b>	Vimentin
<b><math>\alpha</math>-SMA</b>	Alfa-Smooth Muscle Actin
<b>DNA</b>	Deoxyribo Nucleic Acid
<b>RNA</b>	Ribo Nucleic Acid
<b>qRT-PCR</b>	Quantitative Real Time Polymerase Chain Reaction
<b>ELISA</b>	Enzyme-Linked Immuno Sorbent Assay
<b>HPLC</b>	High Performance Liquid Chromatography



<b>DAPI</b>	4',6-Diamidino-2-Phenylindole
<b>MTT</b>	Thiazolyl Blue Tetrazolium Bromide
<b>DME</b>	Drug Metabolizing Enzymes
<b>DMSO</b>	Dimethyl Sulfoxide
<b>COX</b>	Cyclooxygenase
<b>MDR</b>	Multi Drug Resistance
<b>ABC</b>	ATP-Binding Casette
<b>BER</b>	Base Excision Repair
<b>NER</b>	Nucleotide Excisin Repair
<b>MMR</b>	Mismatch Repair
<b>GSH</b>	Glutathione
<b>MSI</b>	Microsatellite Instability
<b>CIN</b>	Chromosomal Instability
<b>5-FU</b>	5-Fluorouracil
<b>LCV</b>	Leucovorin
<b>EPR</b>	Enhanced Permeation And Retention

# 1. INTRODUCTION

Colorectal cancer (CRC), constitutes 10-15% of all cancers, is the most frequently type of malignancy in the gastrointestinal system. It may begin in the rectum or intestine and is referred to colon or rectal cancer individually depending on where to begin. Hereditary and environmental variables have been found to be correlated with CRC risk. Underlying mechanism accountable for the advancement of CRC is suggested to include the transformation of benign polyps into adenocarcinoma. The disorders in some signalling pathways of P13K/AKT,  $\beta$ -cadherine, TGF- $\beta$  and P53 are reported to contribute in the development of CRC. Surgery is the first option for the treatment of CRC, however, chemotherapy (neoadjuvan, adjuvan and advanced-stage chemotherapy) is still widely used. Standard neoadjuvan (5-fluorouracil) based treatments and substantially extended adjuvant therapies such as oxaliplatin (antitumor mechanism activator), leucovorin (antifolate), irinotecan (topoisomerase I inhibitor), oxaliplatin (antitumor mechanism activator) are most commonly used regimens in the treatment of CRC. Adjuvant monoclonal antibody immunotherapy targeted to vascular endothelial develop factor (VEGF) and epidermal development variable (EGRF) receptors are recently used for the treatment of metastatic CRC. However, these chemotherapeutics have serious adverse side effects; recurrence is frequently observed and metastases and drug-resistance are developed during chemotherapy. Resistance to chemotherapeutic agents used for cancer therapy results from several variables including a decrease in intracellular drug accumulation, reduced drug-target relationship, change in anti-oxidant mechanisms and alterations in drug distribution.

Epithelial-Mesenchymal Transition (EMT) is a developmental process which is significant in embryogenesis and cancer metastasis. Cancer-associated EMT is a complicated process in that the cells lose their epithelial properties including intercellular junctions and apico-basal polarity and acquire mesenchymal phenotype properties like mobility, invasive ability and significantly most of the characteristics of stem cells. Recently, EMT has a significant role in resistance to chemotherapeutics and apoptosis, but the reason of these intrinsic relationship remains unclear. Anti-EMT therapies that reverse the EMT status by regulating the key targets are in progress, however, limited number of satisfactory results are

reported. It is proposed that transformed phenotypes improve opposition to the oxidative tension and tend to gain resistance for chemotherapeutic drug treatment regimen based on the creating oxidative tension to become self-advocates. Oxidative stress is identified as an imbalance between the free radicals generated by normal anabolic and metabolic processes and biological antioxidant systems. The free radicals which are often referred to as reactive oxygen species (ROS) can promote the tumor development and progression. Glutathione S-Transferases (GSTs) are a superfamily of isozymes that play a significant role that are responsible for the cellular detoxification of electrophilic xenobiotics. GSTs possess catalytic activity through the conjugation of glutathione (GSH) to xenobiotic molecules. Among the sixteen members of GSTs, the pi ( $\pi$ ) and mu ( $\mu$ ) classes take more attention because of their significant role in cellular protection and also in tumor progression. GSTs have long been implicated in the development of resistance to the current chemotherapeutic drugs. Direct detoxification of chemotherapeutics and inhibitory effect of GSTs on the MAP kinase cascade caused GST-associated drug resistance. Overexpression of GSTs has been observed in a wide variety of both cancer cells and tumor samples and a correlation between increased GST levels and resistance against alkylating agents is also reported. Although there are some studies in which EMT model is applied to CRC and different resistance profiles between epithelial and mesenchymal phenotypes are identified, relationship between the drug resistance mechanism in mesenchymal phenotype of CRC cells and GST has not yet been elucidated.

Nanoparticles attract much notice as drug and gene delivery systems due to their small particle size and their penetration capability into cell capillaries. PLGA-PEG, a non-toxic and FDA approved polymer, is basically used to prepare polymeric nanoparticles presenting stealth properties.

In the light of this information, the purpose of this work was;

- To create *in vitro* EMT model in HT-29 CRC cell line and to demonstrate EMT using immunohistochemical and biochemical methods
- To determine expression and protein levels of GST isoenzymes in the epithelial and mesenchymal phenotypes of HT-29 CRC cells

- To formulate and characterize GST inhibitor ETA loaded and mesenchymal phenotype targeted nanoformulations
- To investigate the efficacy of the nanoformulations to enhance the adjuvant therapy efficacy
- To create *in vivo* EMT model in immunosuppressed Wistar rats
- To assess the efficacy of the nanoformulations to enhance the *in vivo* adjuvant therapy efficacy.

## 2. GENERAL INFORMATION

### 2.1. Cancer

National Cancer Institute (NCI) defines cancer as a collection of related diseases in which cells divide in an uncontrolled manner and invade into surrounding tissues [1]. Accelerating cell division is created by either the sequential collection of random transformation in critical genes that check cell cycle, regulate susceptibility to programmed cell death, and maintain genetic stability or altered gene expression profile due to epigenetic modifications of DNA [2-4]. Just as Darwinian evolution indicate, presence of specific transformations give rise to a selective advantage to cancer cells.

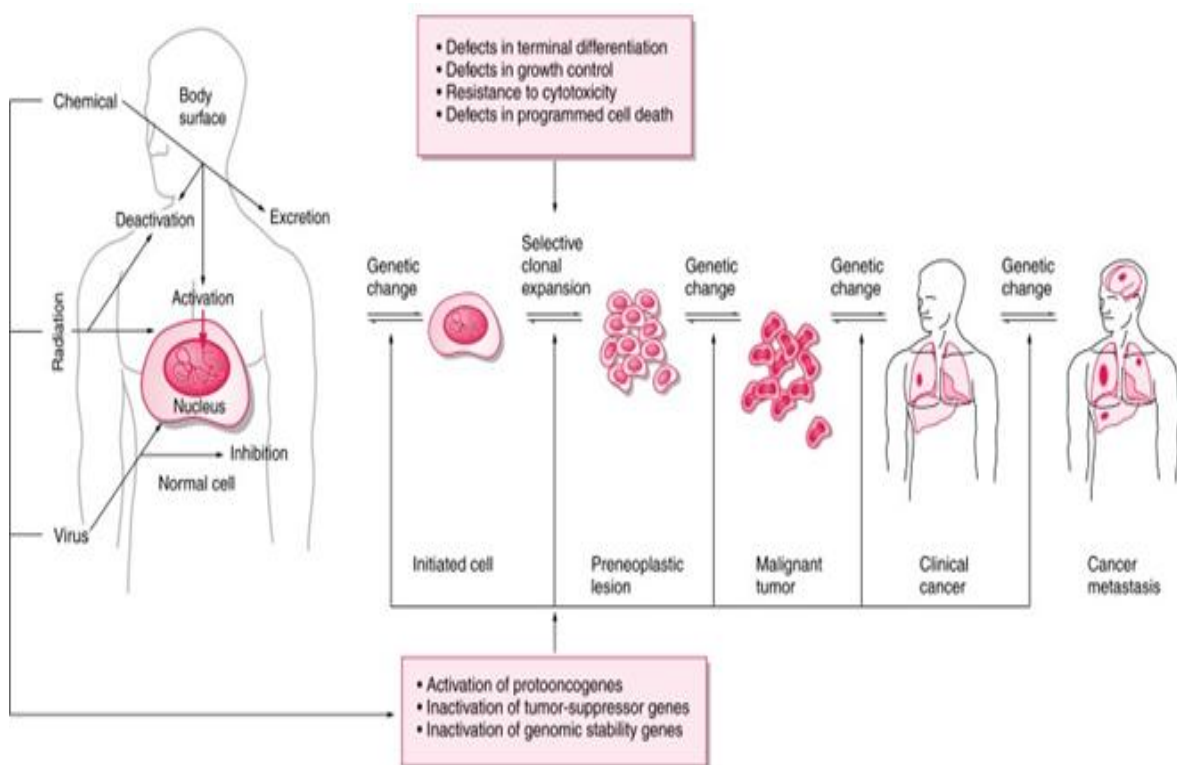


**Figure 2.1.** Stages of carcinogenesis

At the cellular level, transformation of healthy cells into cancerous cells with increased capacity of proliferation, invasion, and metastasis is fundamentally a multifactorial and multistep process [5, 6]. Exposure to the environmental agents such as chemical carcinogens, radiation, viruses and inherited genetic factors can

initiate the malignant transformation. Malignant cells are self-sufficient in growth signals and insensitive to growth-inhibitory signals. According to the three-stage theory of carcinogenesis, initiation where the inherited or sporadic mutations lead to changes in cellular function is the first step (Figure 2.1). This irreversible genetic change drives normal cells toward cancer cells. Acquisition of mutations lead increased proliferation of initiated cells and the promotion of tumor phenotype by the selection of variants with best survival, growth and invasion of the colonies of cancer cells.

Following initiation and promotion, cells go through a process referred to as progression. During progression, genetically vulnerable precancerous cells, which already possess significant growth advantages over normal cells, are become preinvasive state. Progression is the final stage of neoplastic transformation, where genetic and phenotypic changes and cell proliferation occur. This involves a fast increase in the tumor size, where the cells may undergo further mutations with invasive and metastatic potential.

Thousands of genes whose mutation contributes to the initiation and the progression of cancer are identified and generally grouped into two broad classes according to whether the cancer development arises from gain-of-function or loss-of-function mutations in these genes [7-10]. Genes of the first class, whose mutation stimulate cell growth, proliferation and survival, are called proto-oncogenes. Gain-of-function mutations convert protooncogenes into their mutant, overactive forms named as oncogenes. Activation of oncogenes may arise through point mutations in a protooncogene resulting in activation of an enzyme or amplification of a DNA segment that includes a protooncogene leading to increased transcription of the encoded protein. Oncogene activation may also result from chromosomal translocation events that lead to generation of fusion proteins with abnormal activities [11, 12]. ERBB2, members of the RAS family, and MYC are the most commonly activated oncogenes in human cancers. The most common example for oncogenic mutations is the *ras* family of protooncogenes. Experimental studies both in cultured cells and in animals and molecular studies in clinical samples have shown that K-*ras* mutations occur in approximately 30% of lung adenocarcinomas, 50% of colon carcinomas, and 90% of carcinomas of the pancreas [13]. The MYC gene is also an important oncogene

implicated in the pathogenesis of many different types of human cancers including neuroblastoma, colorectal adenocarcinomas and squamous cell carcinomas [14-17].

Genes of the second class, whose mutation during carcinogenesis let the cancer cells escape from cell cycle checkpoints, are called tumor suppressor genes [18-21]. Functional loss of tumour suppressor genes results from small deletions or insertions, frame-shift mutations, or missense mutations [19, 22, 23]. One of the most frequently inactivated gene in human cancers is the tumor suppressor p53 that controls cell cycle and stress signals such as apoptosis, DNA damage, ribonucleotide depletion, nutritional starvation, and hypoxia. It was demonstrated that the loss of function mutations in p53 gene are found in over 50% of human cancers [18].

### **Drug Resistance in Cancer Treatment**

Among the different treatment options such as surgery, radiotherapy and hormone therapy, chemotherapy is still one of the most effective strategy for the treatment of different types of tumors even after the development of metastasis. However, the ability of tumors to eliminate the cytotoxic effects of anti-cancer agents results in therapeutic failure in the majority of the most common forms of cancers. This phenomenon, known as drug resistance, constitutes a lack of response to drug-induced tumour growth inhibition and renders the disease uncontrollable, causing in high mortality [24].

The resistance against the chemotherapeutic agents may be inherent in a subpopulation of heterogeneous cancer cells (intrinsic drug resistance) as well as it could be acquired during the course of therapy in response to the sequential or simultaneous exposure of tumor to cytotoxic drugs (acquired resistance). Genotypic and/or phenotypic alterations in cancer cells within the same tumor which modulate therapeutic resistance are required for acquired resistance. These naturally selected drug-tolerant subpopulations cause the failure of therapy. Acquisition of resistance could be towards to the previously used drug or it has also developed to new agents with different structures and mechanisms of action. The development of resistance to a variety of unrelated chemotherapeutic agents is called multiple drug resistance (MDR) [25].

Diverse variety of mechanisms including drug inactivation, somatic transformations within targets of therapeutics and drug transporters, enhanced DNA repair systems, and dysregulated apoptosis caused both inherent and acquired drug resistance in cancer therapy.

Diverse variety of mechanisms that promote or enable both inherent and acquired drug resistance have been proposed, including drug inactivation, somatic mutations within drug targets and drug efflux, DNA damage repair, dysregulated apoptosis, and the epithelial-mesenchymal transition.

In this chapter, different mechanisms involved in cancer drug resistance are outlined. Roles of Epithelial-Mesenchymal Transition (EMT) and Glutathione S-Transferases (GSTs) in cancer cell resistance against chemotherapeutics will be discussed in Chapter 2.3. and 2.4., respectively.

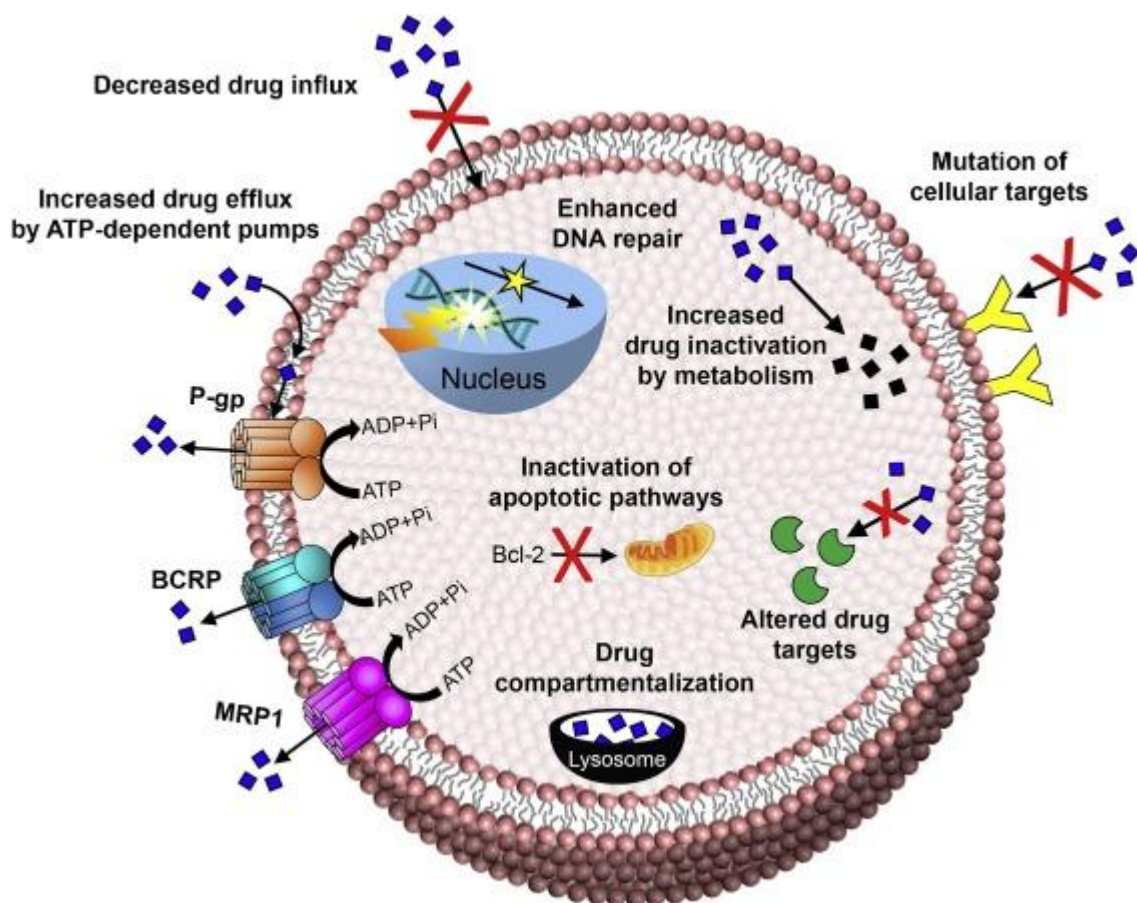


**Figure 2.2.** Mechanisms of chemotherapeutic drug resistance in cancer cells [24].



### **2.2.1. Intratumoral Heterogeneity**

Differences in morphology, genetic and/or epigenetic profile, motility and proliferation rate may be observed in malignant cells within the same tumor as a consequence of genotypic alterations and micro-environmental heterogeneity [24] and these different cell subpopulations are named as tumor clones [25]. The genotypic alterations such as mutations, gene amplifications, deletions, chromosomal rearrangements, translocations and differences in microRNA types lead to genomic instability, resulting in intratumoral genetic heterogeneity [26]. As well as molecular variabilities, cell-extrinsic factors such as interactions with heterogeneous cellular populations, nutrient availability, waste and pH gradients, oxygen (O<sub>2</sub>) tension, extracellular matrix (ECM) deposition, physical and oxidative pressures generate intratumoral heterogeneity. These interactions among tumor cells and surrounding matrix impact the signaling molecules that tumor cells receive, thereby modulating phenotypic features such as metabolism, motility, proliferative and metastatic potential and drug responsiveness. Chemotherapeutic drugs can efficiently eliminate drug-responsive clones whereas the drug-resistant clones can still proliferate, form drug-resistant tumors and leading to failure in treatment [27].

### **2.2.2. Enhanced Drug Efflux**

One of the most significant form of resistance against the variety of clinically used chemotherapy agents is by the action of a group of transmembrane proteins which extrude cytotoxic molecules, maintaining the drug concentration within the cells below a cell-killing threshold. These transporters act either to promote drug efflux from the cell or to sequester it to cellular vesicles that are later eliminated by exocytosis. Efflux pump-mediated mechanisms have been extensively studied for their association with drug resistance due to overexpression in cancer cells. Increased expression of efflux systems confers resistance by preventing sufficient intracellular accumulation of chemotherapeutics, thereby avoiding their cytotoxic or apoptotic effects [28, 29].

To date, more than 400 genes encoding membrane transporters have been annotated in the human genome, and they are divided into two major superfamilies: ATP-binding cassette (ABC) and solute carrier (SLC) transporters [30].

Members of the ABC transporter family proteins are the most important regulators for enhanced drug efflux. ABC transport molecules are generally expressed on the plasma membrane and on the membranes of cellular vesicles, and they play vital physiologic functions and also affect the pharmacokinetic properties of chemotherapeutics in humans. Among the 49 known ABC transporters in humans, overexpression of three members, P-gp, the product of the ABCB1 (MDR1) gene, multidrug resistance-associated protein 1 (MRP1) and mitoxantrone resistance protein [MXR; also known as breast cancer resistance protein (BCRP) or placenta ABC protein (ABC-P)], have been correlated with cancer chemoresistance to various drugs [31-33].

Expression of P-gp was detected in more than 50% of the NCI-60 tumor cell lines including all melanomas and central nervous system tumors and with high levels in renal and colorectal carcinomas. The elevated P-gp expression in cancer cells has been linked to reduced chemotherapeutic responses and poor clinical outcome in various cancer types including both blood cancers and solid tumors. Some tumors with low levels of P-gp expression at baseline, such as leukemia and breast cancer, have shown upregulation of P-gp after disease progression following chemotherapy. A plethora of anticancer drugs that are central to many chemotherapeutic regimens are susceptible to P-gp-mediated efflux such as the microtubule-targeting vinca alkaloids (e.g., vinblastine and vincristine) and taxanes (paclitaxel and docetaxel), the DNA-chelating anthracyclines (doxorubicin and daunorubicin), the topoisomerase inhibitors (topotecan and etoposide), and the tyrosine kinase inhibitors (dasatinib and gefitinib), among many others [34-36].

### **2.2.3. Enhanced DNA Repair**

Many chemotherapeutic agents such as alkylating agents and platinum-based agents target directly and/or indirectly the DNA of cancer cells resulting in DNA damage. Upon recognizing the damage, cancer cells activate a variety of signaling pathways according to the types of DNA damage induced. Extensive studies indicate that high levels of proteins involved in repair systems reflect elevated DNA repair capacity and are associated with clinical resistance to chemotherapy. Drug-induced damage of DNA is corrected by the DNA repair systems such as base excision repair (BER), nucleotide excision repair (NER) and mismatch repair (MMR) [37, 38].

BER is known as a major pathway for the repair of base damage and is responsible for repairing one or a small number of bases with smaller modifications such as alkylating and oxidative lesions caused by drugs such as nitrosoureas [39, 40].

NER is a highly conserved DNA repair mechanism necessary for repairing bulky DNA lesions which alter the helical structure of the DNA molecule and interfere with DNA replication and transcription. Several proteins encoded by NER genes are responsible for detecting and repairing bulky DNA damage [41, 42].

MMR is an important post-replicative repair system that plays an important role in the correction of DNA polymerase errors, either by preventing error-prone bypass replication or by correcting the formed mismatches. Mismatch repair has also recently been shown to be involved in repairing oxidative and methylated DNA damage [43-45].

#### **2.2.4. Altered Expression of Drug Metabolizing Enzymes**

In recent years, it has been reported that intratumoral expression of drug metabolizing enzymes (DME) play important role in patients' responses to treatment and the onset of resistance to therapy. The expression of these enzymes in malignant tumours is one possible mechanism of anti-cancer drug resistance. Expression of DME within tumor cells is significantly affects absorption, distribution, metabolism, and excretion (ADME) of drugs. In cancer subclones, there tends to be a strong genomic instability that leads to highly variable expression of DME. Cancer cell drug resistance or sensitivity is critically impacted by expression of DME within tumors, and understanding which specific DME contribute to response to particular drugs will lead to better precision medicine [46, 47].

#### **2.2.5. Dysregulated Apoptosis**

Anticancer treatment using cytotoxic drugs is considered to induce stress pathways such as p38 kinase or suppress signalling pathways such as those coordinated by phosphatidylinositol-3-phosphate kinase (PI3K) to reactivate key elements of apoptosis program. However, defects in apoptotic pathways and redundant survival mechanisms in cancer cells allows them to escape apoptosis leading to uncontrolled proliferation resulting in tumor survival, therapeutic resistance and

recurrence of cancer. There are many potential mechanisms associated with resistance to apoptosis in cancer cells such as increased expression of anti-apoptotic genes and proteins, as well as decreased expression or defective function of pro-apoptotic molecules [48-50].

### **2.3. Epithelial-Mesenchymal Transition (EMT)**

Mammals are composed of mainly of two cell types, epithelial and mesenchymal, which differ in morphology as well as function and these cell types are not always permanent [51]. As was discovered more recently, it is possible to move back and forth between epithelial and mesenchymal phenotypes via the processes termed epithelial-mesenchymal transition (EMT) and the reverse mesenchymal-epithelial transition (MET) [52, 53]. Both of these processes are biologic mechanisms that govern alterations in morphology, cytoskeletal networks, adhesion and migration capacity of cells [54]. EMT allows highly differentiated, polarized and well-organized epithelial cells to convert into mobile and extracellular matrix secreting mesenchymal cells [52, 54-57]. The MET process whereby mesenchymal cells polarize into apical and basolateral domains and express the multiprotein complexes associated with adherens junctions is the reverse of EMT [58-60].

#### **2.3.1. Epithelial Cells versus Mesenchymal Cells**

Epithelial cells are tightly attached by specialized membrane structures, such as tight junctions, desmosomes, adherens junctions and gap junctions, resulting in organized cell layer called epithelium [61-63]. E-cadherin (encoded by CDH1), a transmembrane  $\text{Ca}^{2+}$ -dependent homophilic intercellular adhesion molecule, is one of the most crucial and ubiquitous mediators of epithelial junctions. The extracellular domain of E-cadherin forms a  $\text{Ca}^{2+}$ -dependent bridge from one cell to its neighbor, stabilizing cell-cell interactions [64, 65]. This transmembrane protein provides linkage to the cytoskeleton through a group of molecules,  $\alpha$ -catenin,  $\beta$ -catenin and p120-catenin which interact with intracellular actin filaments [66-68]. These cell adhesion molecules are not only responsible for assembling cells together, but also regulate the cytoskeleton and cell shape, play important roles in cell recognition, coordinate the translation of basic genetic information from microenvironment to the cell, and control epithelial cell plasticity [69-72].

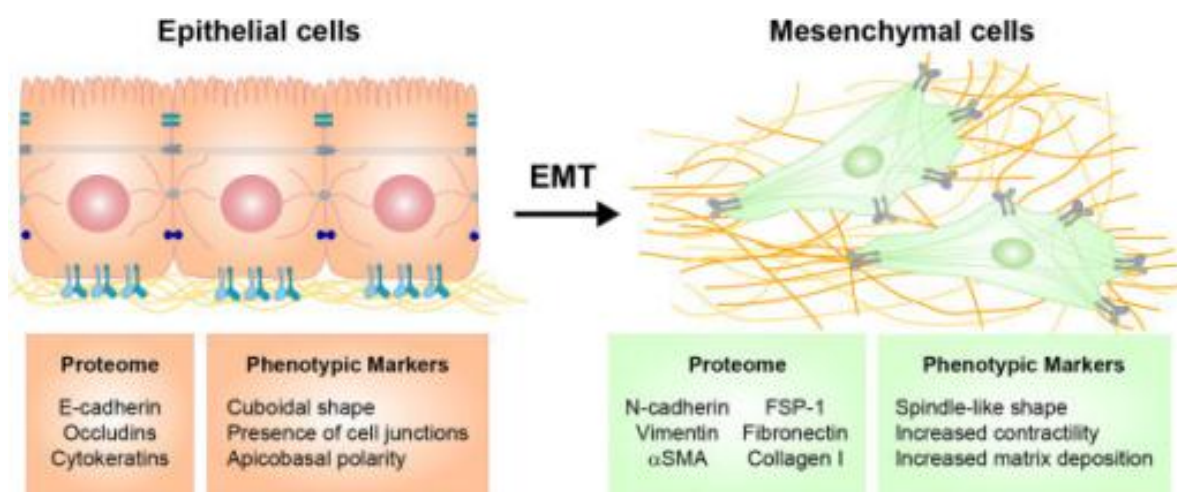


**Figure 2.3.** Schematic representations of epithelial and mesenchymal cells [73].

In addition, the cytoplasm and the plasma membrane of epithelial cells is polarized along an apical and basal axis, which considerably differ in molecular composition [74, 75]. This polarization is characterized by the polarized organization of the actin cytoskeleton and the presence of a basement membrane at the basal surface [76, 77]. Under normal conditions, invasion of epithelial cells into the underlying extracellular matrix is forestalled by basement membrane, thereby maintaining the integrity of epithelial sheet [77].

Fibroblast-like, spindle shaped mesenchymal cells, on the contrary, exhibit front-rear polarity. Mesenchymal cells, rarely establish direct contacts with neighboring cells, are loosely attached to the surrounding extracellular matrix through focal adhesions and are not associated with the basement membrane, resulting in more mobility to increase cell migration and anchorage distantly [52, 78-80].

### 2.3.2. EMT Effectors

Profound morphological, structural and functional alterations in epithelial cells occur during the EMT process. During EMT, epithelial cells progressively lose junctional molecules, including both adherens junctions and tight junctions, allowing epithelial cells to become detached [81, 82]. The central structural component of epithelial adherens junctions, E-cadherin, is downregulated at the mRNA and protein levels [83-85] and replaced by mesenchymal cell specific N-cadherin by a process termed as cadherin switch [86-88]. E-cadherin to N-cadherin switch, which occurs during embryonic development and cancer progression, is used to

monitor EMT. Indeed, reorganization of cortical actin into stress fibers and the replacement of cyokeratin intermediate filaments by vimentin are associated by EMT [52, 54, 89, 90]. Vimentin induces alterations in cell shape, motility, and adhesion during EMT [91]. Fibronectin, an extracellular protein, is also overexpressed upon activation of EMT and plays an important role in mesenchymal cell migration [80]. These junctional and cytoskeletal changes enable the transition into a spindle-shaped cell morphology from a cuboidal/columnar precursor, correspond with a more flexible and migratory phenotype. Such alterations in junctional complexes and in the cytoskeleton are necessary but not sufficient to initiate the mobility of epithelial cells. Epithelial cells must reorganise into front-rare polarity to achieve morphological movements and migrate through extracellular matrix. Front-rare polarity is initiated in response to activation of integrins and cadherins. Front-rare polarization of cytoskeletal components and migration of signaling molecules on the plasma membrane are essential for the initiation of cell motility [92]. Regulation of actin polymerisation controlled by GTPases of Rho family are of crucial importance in the formation of active membrane protrusion at the front side [93, 94]. The cell rear also actively participates in cell displacement by controlling detachment from the ECM and acto-myosin contraction. Indeed, production of matrix metalloproteinases (MMPs) provide an increased ability to degrade of underlying basement membrane [95] Complete detachment from the basement membrane is the signal for the completion of EMT and the formation of a complete mesenchymal phenotype with migration capacity [52, 80]. Importantly, the changes observed in cell phenotype are often reversible modulations and the process of MET enables the cells that arrive at a suitable location for colonization to reconstitute the original epithelial phenotype [58, 60].

### **2.3.3. Subtypes of EMT**

Transdifferentiation between epithelial-mesenchymal phenotypes is critical during developmental stages such as gastrulation, nephrogenesis, myogenesis, and heart valve formation [96, 97]. Besides being critical during embryonic development, EMT can also be reactivated under pathological conditions such as chronic inflammation, rheumatoid arthritis, fibrosis, invasion of neoplastic cells, and ultimately metastasis [52, 80, 81, 98]. Despite genetic and biochemical similarities between developmental and pathological EMT, there are also key

differences in the functional consequences and factors participate in the regulation of EMT-associated pathways, leading to classification of different EMT subtypes. EMT is proposed to classify three separate subtypes, based on the physiological conditions [52, 99].

Type I EMT is observed during implantation of a developing embryo into uterine wall, embryogenesis and organ development. Through the process of embryonic implantation, the cells of the trophoectoderm infiltrate the endometrium through EMT and form placenta. In the embryo itself, the first set of mesenchymal cells are generated at the gastrulation stage, where the blastula is transformed to three germ layers by the inward migration of cells. Organogenesis also involves subsequent cycles of EMT and MET, such as seen in heart valve development [52, 100, 101].

Type II EMT is associated with wound healing, tissue regeneration, and organ fibrosis. Type II EMT is activated as a physiological response to injuries in tissues. Tissue repair process require the reconstruction of tissue integrity through re-epithelialization. Generation of inflammatory cytokines by injured tissue, together with mechanical stress, promote EMT-mediated formation of fibroblasts and/or myofibroblasts from epithelial cells. In the case of acute injury, EMT is associated with reparative fibrosis whereas chronic inflammation forms abnormal myofibroblasts, thereby excessive extracellular matrix leads to organ destruction [52, 101-103].

The third proposed subtype of EMT is type III EMT and has significant importance in tumorigenesis from early stages of tumor development to metastasis as well as in resistant profile of cancer cells. In contrast to developmental EMT, EMT is not complete in cancer cells. Cells in a tumor can be in multiple transitional states and express both epithelial and mesenchymal genes. The cells undergone partial EMT can migrate collectively as cell clusters or as individual cells and metastasize through the circulatory system and attach at a new location. At distant tissues, MET activation enables the mesenchymal cells to transform completely back into secondary epithelium and secondary tumor is formed [52, 102, 104]. EMT has been demonstrated in several tumors originate from epithelial cells such as colorectal, breast, lung and prostate cancer. Besides becoming motile, neoplastic

cells transformed to mesenchymal phenotype acquire aggressive behaviors including resistance to chemotherapeutics, stress conditions such as nutrient depletion and hypoxic environment, and apoptosis. Inhibition of senescence, immune evasion and acquisition of stem cell-like features are also the results of EMT. Additionally, EMT enhances the expression of pro-inflammatory and immunosuppressive cytokines in cancer cells, thereby triggering tumour-promoting effects on the composition of the tumour microenvironment, including the infiltrating immune system.

#### **2.3.4. EMT Inducers**

Transformation of epithelial phenotype into mesenchymal phenotype in normal cells and neoplastic cells is triggered and orchestrated by different molecular mechanisms including the activation of transcription factors which suppress the epithelial state associated genes responsible for cellular junction, cell polarity and reorganization of cytoskeleton and activate mesenchymal phenotype genes [105, 106].

Among the many transcription factors that trigger EMT, the members of the Snail family (Snail1 and Snail2), the Zeb family (Zeb1 and Zeb2) and the Twist family (Twist1 and Twist2) are the master transcriptional regulators of epithelial morphogenesis [107-109]. The expression of these transcription factors, and their downstream targets are proposed as a reliable prognostic biomarkers to reflect tumor aggressiveness and predict poor prognosis.

E-cadherin gene (CDH1) expression is modulated by transcription factors. Snail is capable of binding to specific E-box sequences in the CDH1 promoter and directly repressing its expression, consequently inducing EMT. Additional expression analysis of cancer cell lines showed that Snail is mainly overexpressed in epithelial cancer cell lines and that overexpression of SNAIL is associated with the downregulation of E-cadherin. Besides two members of Snail family, the two Zeb proteins are also CDH1 repressors [110]. ZEB2 mediated repression occurs by binding to an E-box sequence both in Xbra2 promoter and in delta-crystallin enhancer.



### **2.3.5. EMT and Cancer Treatment Resistance**

Chemotherapy and radiotherapy with or without surgical operation are used either alone or together in the cancer treatment. Resistance against these therapy strategies is clinically significant problem, with global effects [111, 112]. According to the recent findings obtained both in the experimental models (*in vitro* and *in vivo*) and in clinical trials, EMT program is closely related with development of cancer treatment resistance [113, 114]. The persistent accumulation of mesenchymal and stem-like cells in the patients with recurrent cancers following primary treatment strongly supports the role of EMT in the reduction of therapy efficacy [114-116].

Several key transcription factors such as SNAIL and TWIST and miRNAs that regulate the expression of EMT-associated genes are investigated in both transitioned cells and cancer treatment resistant cells [112, 116]. Sarkar et al. [117] reported that strong expression of epithelial marker E-cadherin in the various gemcitabine-sensitive pancreatic cancer cell lines was observed whereas gemcitabine-resistant pancreatic cancer cell lines exhibited strong expression of mesenchymal makers including vimentin and ZEB-1 at mRNA and protein levels. Similarly, it was reported that paclitaxel, docetaxel, or doxorubicin resistant MCF-7 breast cancer cell lines exhibited overexpression of Slug, resulting in the elevation of mesenchymal markers such as N-cadherin and vimentin and repression of epithelial markers E-cadherin and occludin [118, 119]. In models of drug resistant breast and ovarian cancers, EMT gene signatures have been found to correlate with the presence of drug resistance [30, 31] and manipulation of EMT transcriptional regulators modulates resistance to chemotherapeutic drugs in lung and bladder cancers [32, 33]. Additional evidence suggests that EMT may contribute to the acquisition of drug resistance by altering expression of key genes involved in cell cycle regulation, drug transport and apoptosis.

There are also clinical studies in which EMT-associated genes profiling is analyzed in therapy resistant cancer patients. Assessment of correlation between gene-expression patterns of tumour samples obtained from patients with various cancer types and treatment outcome of these patients have resulted in close association between upregulation of EMT-associated genes and treatment resistance [120].

## 2.4. Glutathione S-Transferases (GSTs)

Glutathione S-Transferases (GSTs; EC:2.5.1.18) are a super family of multifunctional isoenzymes that are involved in the cellular detoxification of electrophiles, of both endogenous and exogenous origins [121]. They play an important role in clearance of cytotoxic and genotoxic compounds and in cellular protection against redox cycling and oxidative stress [122-124].

The GSTs are belonging to phase II detoxification enzymes that catalyze the formation of thioether conjugates between sulfhydryl group of the tripeptide glutathione ( $\gamma$ -L-glutamyl-L-cysteinyl glycine) and electrophilic carbon, sulfur or nitrogen atoms of nonpolar compounds [125, 126]. This conjugation neutralizes the highly reactive nucleophile sites of the parent compound and enhances its water solubility. Due to the enhanced water solubility and action of specific transporters, GSH conjugates are removed from the cell, thereby preventing nucleic acids and crucial cellular cell constituents from the harmful effects of reactive electrophilic compounds [127, 128].

GSTs show wide substrate spectrum, different types of GSTs can deal with a wide variety of biological and non-biological electrophiles. GSTs have an important role in metabolism of endogenous molecules generated during oxidative stress. Endogenously formed quinones, epoxides, and hydroperoxides are the important substrates of GSTs. Besides metabolising endogenous substrates, these enzymes may detoxify electrophilic xenobiotics, like chemical carcinogens, environmental contaminants, and antitumoral agents. The further natural GST substrates contains steroids, leukotrienes, anthocyanines, and organic isothiocyanates [129, 130].

Many different types of reaction are catalyzed by GSTs. The transferases form thioether bond between GSH and molecules containing electrophilic center by a process named as substitution reaction. These enzymes are also involved in nucleophilic addition reactions [131]. This reaction can be exemplified by addition of glutathione thiolate to carbon-carbon bond in an unsaturated carbonyl molecule. Reduction of organic hydroperoxides and steroid isomeration are the other types of GST-catalyzed reactions [62].

Besides serving as a catalyst for conjugation reactions, GSTs also have several non-catalytic functions. Several GSTs have selenium-independent peroxidase action. Selenium-independent activity of GSTs provide protection from phospholipid oxidation, degradation of nucleic acids by hydroperoxide activity. The conversion of lipid hydroperoxides to alcohols prevents their participation in free radical propagation reactions during oxidative stress. Human GSTO1-1 with a non-detoxification function modulates ryanodine receptors (RyR), a group of calcium channels in the endoplasmic reticulum of cardiac and skeletal muscle cells. Human omega class GSTs also possess dehydroascorbate reductase and thioltransferase activity [132-134], and prostaglandin D synthase activity was demonstrated for human sigma GST [135].

GSTs can also act as regulators in various cellular events through protein-protein interactions. The most important of these are signal transduction pathways. The subunit of the monomeric GSTP1 interacts directly with c-Jun N-terminal kinase 1 (JNK1), suppressing the activity of JNK1. In the case of oxidative stress, the GSTP1 subunits are oligomerized and release active JNK1 into the environment, and thus GSTP1 regulates the response of the cell to oxidative stress. Another GST isoenzyme, GSTM1-1, functions as a regulator of MAP kinase pathway by binding to various kinases in this pathway [125, 132]. A group of isoenzymes have a role in ion channel modulation [130].

Furthermore, cytosolic GSTs have the ability to bind hydrophobic molecules without non-catalytic reactions. This property is known as ligand function. Ligand site binds compounds including steroid and thyroid hormones like bilirubin, hemes, bile salts and penicillin. It is thought that GSTs can provide protection against harmful effects of hydrophobic molecules on the cell by binding compounds which may affect normal cell functions [130].

#### **2.4.1. Structure of the GSTs**

GSTs consist of two sub-units existing as homodimers and heterodimers that each sub-unit in the dimeric protein functions independently [133-135]. GSTs are dimeric enzymes and contains two different domains in each monomer that are approximately 26 kDa in size. Kinetic and binding assays show that each subunit has independent active regions. The polypeptide chain of each GST subunit comprises two domains combined by short linker regions [136-142].

N-terminal domain consists of 80 amino acids arranged in a  $\beta$ -sheet and three  $\alpha$ -helix structure. This domain is responsible for connection of GSH and includes much of the G-site. C-terminal domain consists of amino acid arranged in the remaining 5 or 6  $\alpha$ -helix structure and includes whole of the H site that binds various range of hydrophobic substrate [142-147]

#### **2.4.2. Classification of GSTs**

GSTs are common in all living organisms, from proteobacteria, cyanobacteria and fungi to plants and animals. Plural isoforms of GSTs are stated in organism. The GST superfamily have been fundamentally sub-divided into an ever-rising number of classes trust on a numerous of factor, containing substrate selectivity, position of introns within the genes, inhibitor sensibility, immunologic cross reactions, tertiary and quaternary structure of their respective complexes [148-151].

Based on the amino acid sequence, three-dimensional structure, function, and subcellular localization, proteins with glutathione transferase activity are distinguished into 3 subfamilies. Cytosolic and mitochondrial GSTs are similar in three-dimensional folds, and these groups are called soluble GSTs. The GSTs in this group have a variety of isoenzymes. Expression levels of these isoenzymes differ in tissues. Soluble GST isoenzymes are distinct with regards to differences between amino acid sequences and isoelectric points. Another subfamily comprises microsomal GST which is also called as membrane-associated proteins in eicosanoid and glutathione (MAPEG) metabolism. Microsomal GSTs have no structural similarity with soluble groups, their primary structure is different from cytosolic and mitochondrial GST forms [149].

Cytosolic GSTs represent the major family of such transferases. According to the primary structure, cytosolic GSTs have been further sub-divided into various species-independent classes, and numerous of them are particular to phyla. Up to date, 13 various cytosolic GST classes have been identified. 7 classes of cytosolic GSTs include minimum 16 genes are recognized in human and other mammalian species, designated as Alpha ( $\alpha$ ), Mu ( $\mu$ ), Pi ( $\pi$ ), Sigma ( $\sigma$ ), Theta ( $\theta$ ), Zeta ( $\zeta$ ), Omega ( $\omega$ ). Other classes of this superfamily, called Beta ( $\beta$ ), Delta ( $\delta$ ), Phi ( $\phi$ ), Epsilon ( $\epsilon$ ) and Lambda ( $\lambda$ ) are represented in prokaryotes, invertebrates, and plants. Cytosolic GSTs at a similar class have more than about 40% identity in terms of primary structure while those in different classes have less than 25%

identity. Amino acid sequence at the amino end of cytosolic GSTs take attention because this region that is an important part of catalytic site tends to be more conserved than others within the classes [139,152-154].

### **2.4.3. Role of GSTs in Drug Resistance**

Chemotherapeutic resistance continues to be the major obstruction in the medical oncology. Cancer cells can change metabolic and signaling pathways responsible for drug metabolism. Among these mechanisms, alterations in expression profile and enzymatic activity of several DME have a significant role in resistance to chemotherapeutic agents. GST-mediated detoxification of electrophilic alkylating drugs, and elevated levels of GSH and GSTs in drug-resistant cell lines led researchers to modulate GSH pathways [156].

In cancer cells within the same tumor, there tends to be a strong genomic instability that leads to highly variable expression of GSTs. It is well known that overexpression of GSTs have a significant role in chemotherapeutic resistance or sensitivity. GSTs encourage the development of resistance to anticancer drugs via suppressing apoptosis through its ROS-scavenging activity as well as displaying inhibitory effect on the MAP kinase cascade. Diverse array of cancer chemotherapeutics such as chlorambucil, cyclophosphamide, melphalan are metabolized by GST-mediated detoxification reactions. GSH metabolism can detoxify many chemotherapeutic agents that decompose to produce electrophilic species. The importance of GSTs in detoxification of some chemotherapeutics including busulfan, chlorambucil, adriamycin, cisplatin or melphalan and the correlation between overexpression of GST and chemotherapeutic resistance have been evaluated [157-159].

Alpha, pi and mu classes of GST are the most expressed isozymes in drug-resistant cancer cells. The functions of GSTs in signal transduction pathways are thought to contribute to the development of resistance. For example, overproduction of GST-pi in tumor cells is thought to suppress the activity of JNK1, which directs the cell to apoptosis, thereby inhibiting apoptosis and inactivating treatment. For this reason, in order to overcome drug resistance and increase the effectiveness of cancer treatment, new GST inhibitors are investigated [154,156].

## **2.5. Colorectal Cancer (CRC)**

It is the third most common cancer in men (746.000 new cases per year) and second most common cancer in women (614.000 new cases per year) worldwide, and the third leading cause of cancer-associated mortality, with approximately 700.000 deaths each year. The 5-year survival rate for patients with metastatic colon cancer at the time of diagnosis is less than 10% the median survival time without chemotherapy is approximately 5 months. CRC prevalence is expected to increase appreciably in most developed countries as a result of population growth and aging, because CRC incidence increases with age [160-163].

CRC can be subdivided into several categories due to the mechanisms responsible for genomic instability. Among the three categories of genetic disruption, prevalence of microsatellite instability (MSI) and chromosomal instability (CIN) in patients with CRC is very high. MSI is characterized by the accumulation of satellite repeats as a result of defects in any of the DNA mismatch repair (MMR) genes. Another type of genomic instability is the CIN which develops due to the alterations in the chromosome number and/or structure [163].

CRC presents in one of three patterns: inherited, familial, and sporadic. Inherited and familial CRC derive, at least in part, from germline mutations. Inherited CRC accounts for 10 % of cases and presents as well-characterized cancer predisposition syndromes including Lynch syndrome and familial adenomatous polyposis (FAP). Familial CRC accounts for 25 % of CRCs and presents without precisely defined Mendelian inheritance or genetic etiology. Sporadic CRC derives from somatic mutation, accounts for approximately 70 % of CRCs, and is not associated with family history [161].

### **2.5.1. Treatment of CRC**

Medical treatment, radiotherapy and surgical treatment constitute the treatment modalities in patients with CRC. Surgery is the main treatment modality for locoregional CRCs. Adjuvant chemotherapy reduces the risk of recurrence in colon cancers. Neoadjuvant chemo or radiotherapy in rectal cancers is used to increase resectability, to protect the sphincter and to prevent localized metastases [161]. Adjuvant chemotherapy is used to prevent distant metastases. Chemotherapy is applied in stage IV diseases. For liver metastases, there is a consensus that all patients who can be resectable should be taken to surgery.

Neoadjuvant and adjuvant therapies are applied in patients who cannot be operated [163].

- **Chemotherapeutic drug combinations used in neoadjuvant therapies:**

1. 5-Fluorouracil (5-FU) + Radiation therapy [1000 mg/m<sup>2</sup>/day (i.v) 1-5 days/week (5-FU) +180 cGy / 1-5 days/week]
2. Capecitabine + Radiation therapy [825 mg/m<sup>2</sup>/day (PO) 1-5 days/week (Capecitabine) + 180 cGy/ 1-5 days/ week]

- **Chemotherapeutic drug combinations used in adjuvant therapies:**

1. 5-Fluorouracil (5-FU) + Leucovorin (LCV) [425 mg/m<sup>2</sup>/day (i.v) 1-5 days/week (5-FU) + 20 mg/m<sup>2</sup> /day (i.v) 1-5 days/week (LCV)]
2. Oxaliplatin + 5-Fluorouracil (5-FU) + Leucovorin (LCV) (FOLFOX4) [85 mg/m<sup>2</sup> (iv) 1<sup>st</sup> day (Oxaliplatin) +400 mg/m<sup>2</sup> (iv) 1<sup>st</sup> and 2<sup>nd</sup> day (5-Fluorouracil) +200 mg/m<sup>2</sup> (iv) 1<sup>st</sup> and 2<sup>nd</sup> day (LCV)]
3. Oxaliplatin + Capecitabine (XELOX) [130 mg 1 day (Oxaliplatin) + 1000 mg/m<sup>2</sup> PO 1-14 days (capecitabine)]

- **Chemotherapeutic drug combinations used in metastatic conditions:**

1. Irinotecan + 5-Fluorouracil (5-FU) + Leucovorin (LCV) [125 mg/m<sup>2</sup> (i.v) 4 weeks (Irinotecan) + 500 mg/m<sup>2</sup> (i.v) 4 weeks (5-FU) + 20 mg/m<sup>2</sup> (i.v) 4 weeks (LCV)]
2. Irinotecan + 5-Fluorouracil (5-FU) + Leucovorin (LCV) + Bevacizumab (BV) [125 mg/m<sup>2</sup> (i.v) 4 weeks (Irinotecan) + 500 mg/m<sup>2</sup> (i.v) 4 weeks (5-FU) +20 mg/m<sup>2</sup> (i.v) 4 weeks (LCV) + 5 mg/kg (i.v) 2 weeks (BV)]

### 2.5.2. CRC, EMT and Drug Resistance

Chemotherapy is still one of the most important adjuvant therapy options in CRC treatment. However, the resistance of CRC cells to conventional chemotherapeutics is the most important problem in CRC treatment. Researchs show that EMT is responsible for cancer formation, metastasis and drug resistance in CRC as well as in many tumor types. In a study, a 5-FU resistant HT-29 CRC cell line was developed by treating the cells with increased concentration of 5-FU. Elevated expression levels of EMT-associated regulators including Twist and Zeb family with the increased doses of the drug is reported. In addition, EMT

markers were screened in the drug-resistant cell line and reduction in epithelial biomarkers such as E-cadherin and overexpression of fibronectin, an important mesenchymal marker, were reported [160].

In another study, it has been reported that the cellular changes associated with EMT such as polarity loss and intercellular cleavage have been observed in KM12L4 and HT-29 CRC cells that are resistant to oxaliplatin. In the same study, reduction in expression of E-cadherin was observed. Translocation of  $\beta$ -catenin to nucleus was also observed [Yang, 2006]. Although there are studies showing the relationship between chemotherapeutic resistance and EMT in CRC, the mechanism of EMT and resistance relationship has not been elucidated yet [163].

## **2.6. Nano-sized Drug Delivery Systems in Cancer Treatment**

The engineering, synthesis, and use of materials and devices at the nanoscale is called nanotechnology [164]. Most of scientific branches including biology, chemistry, mathematics, physics, electrical engineering, material science, and pharmaceutical science all are involved in the field of nanoscale technology, hence nanotechnology designates as interdisciplinary field. Physicochemical properties and functionalities of nanosized materials are remarkably different from those in the bulk owing to surface and quantum size effects. These unusual physical and chemical properties offer nanomaterials great potential for biomedical applications, given the range of biological processes that occur at the molecular or nanoscale level. Nanotechnology has also led innovative applications in medicine. Influence of nanotechnology in medicine can mainly be seen in drug delivery systems as well as regenerative medicine [165, 166].

According to the NCI, nanosized drug delivery systems are the carriers that are typically 300 nm or smaller in size. Nanosized drug delivery systems not only transport the drugs or other therapeutic agents, also lead to improved pharmacokinetic and pharmacodynamic profiles of therapeutics. Nano-sized delivery systems are innovative approaches to deliver a therapeutic agent to the target cellular compartment or tissue with the improved pharmacological responses. Furthermore, in the past two decades continued progress in processing nanosized drug delivery systems has led to the innovative and promising applications in health-care systems. From diagnose the disease with nanotechnology-based sensors to treatment in molecular level, nanosized delivery



systems in various forms such as liposomes, polymeric nanoparticles, nanocapsules, quantum dots, carbon nanotubes have attracted attention [167-169].

One of the potential applications of nanotechnology is in the treatment of cancer. Conventional methods for cancer treatments including chemotherapy, surgery, or radiation have some challenges such as non-specificity and toxicity. Innovative technologies are needed to overcome multidrug resistance, and increase drug localization and efficacy. The challenge of current drug therapy is the optimization of the pharmacological action of the drug, and the minimization of its toxic side effect. Local concentration of the drug at the cancer sites needs to be high, while at other tissues low to prevent any negative reactions. Application of nanotechnology in cancer treatment has the potential to solve these limitations and new horizons have been opened in the treatment of cancer with targeted nano-sized drug delivery systems. Chemotherapeutics encapsulated in these nano-sized carrier systems do not interfere with healthy cells in the blood. In addition, since the size of the carrier is larger than the capillary holes in the healthy tissue and the drug is not free, the drug cannot pass from the blood circulation to healthy tissues and have no side effects. The drug remaining in circulation is removed from the circulation when it comes to cancerous tissue with holes in the size of the carrier, and allows the collection of the drug in cancerous tissue. This phenomenon is called the enhanced permeability and retention (EPR) [170-173].

## **2.6.1. Polymeric Nanoparticles**

### **2.6.1.1. Polymers Used for Preparation of Polymeric Nanoparticles**

Polymeric nanoparticles are known as colloidal solid particles of natural polymers such as chitosan and collagen or biodegradable polymers such as poly (lactic acid) (PLA) and poly (lactic co-glycolic acid) (PLGA). Thanks to their size these particles can easily pass through capillaries and allow for re-entanglement in areas affected by chemotherapeutic agents. An important part of these components is naturally formulated during the coupling by means of block polymers of at least two polymeric chains of different hydrophilicity [174-177].

Polyester PLGA is a copolymer of poly lactic acid (PLA) and poly glycolic acid (PGA). It is the best defined biomaterial available for drug delivery with respect to design and performance. PLGA has been certified by FDA and the European

Agency for Medical Medicine (EMA) for parenteral studies due to its high biocompatibility. The presence of PLGA in commercial activities, positive deterioration in physiological conditions, low side effects, regulation of surface and physicochemical characteristics, continuity, high biocompatibility and predictable biodegradability have shown PLGA as the most remarkable polymeric drug carrier in many clinical studies. PLGA can be easily metabolized through hydrolysis of ester bonds *in vitro* and *in vivo*. The polymer bonds can undergo a total deterioration, and this deterioration is usually carried out in a similar manner throughout the PLGA matrix. The carboxylic ends in the PLGA bonds, with the separation of the polymer bonds, continue to biodegrade and increase their number. These conditions are considered to catalyze the stages of biological dissolution however, it is known that significant fragments are internally deformed more and the amorphous regions are more degraded than in the crystalline regions. The biological degradation states of PLGA polymers are associated with lactic and glycolic acid ratio, molecular weight, crystallinity ratios of the polymer and the Tg of the polymer [178-182].

It has a significant role in determining release profile and doses. PLGA delivery systems have a known biphasic curve in drug release. The forms of encapsulated drugs, the properties of the drugs and the hydrophobicity of the polymer determine the rate of reaction during the first explosion. In the next step, the water matrix performs hydrolysis, and then the drug is systematically removed from the thicker layers of the PLGA matrix [183, 184].

#### **2.6.1.2. Nanoparticle Preparation Methods**

Preparation method is determined according to chemical properties of the polymer used and solubility of pharmaceutical agent. As nanoparticle preparation methods, methods based on *in situ* polymerization of monomers in various environments were used [173, 174].

##### **2.6.1.2.1. Polymerization Method**

In this method, monomers are polymerized to provide nanoparticles in aqueous solution. The drug is loaded by dissolving it in the polymerization medium or by adsorption onto the surface of the nanoparticles after the polymerization is complete. The nanoparticles are then purified to remove stabilizing agents and resuspenden in a non-surfactant-containing isotonic medium [174].

#### **2.6.1.2.2. Interfacial Polymerization Method**

In this method, the polymerization of the monomer at the interface results in formation of nanoparticles. Emulsion containing surfactant and organic solvent is used as an outer phase. The monomer solution is added to this emulsion to form the polymer. The formed nanoparticles are separated by centrifugation, washed and lyophilized [182].

#### **2.6.1.2.3. Micelle Polymerization**

In this process, the continuous phase of which is organic phase, monomers with high solubility in water cannot be diffused from micelles to organic phase due to their low fractional coefficients. The water-soluble monomer solution is dispersed in the hydrophobic phase by the help of surfactants and the micelles are obtained. A solid granular colloidal system is obtained by the help of an energy such as x-ray, IR beam, which is used as the polymerization initiator, and the nanoparticles are separated from the medium by ultracentrifugation [182].

#### **2.6.1.2.4. Emulsification-Solvent Evaporation Method**

In the method of forming a double emulsion in which the peptide, protein and other macromolecules are entrapped, the aqueous solution of the active ingredient is dispersed in the polymer solution and an aqueous solution of the oil/water emulsifier is added to the mixture. Subsequently, the water/oil/ water emulsion forms droplets of the polymer solution containing the drug solution, and after the solvent is evaporated, the nanoparticle suspension containing the aqueous solution of the active substance is obtained [178].

#### **2.6.1.2.5. Nanoprecipitation**

Nanoprecipitation, also known as solvent displacement, is a method for developing nanoparticles and microparticles. The polymer dissolved in water-miscible organic solvent is added dropwise to the aqueous phase under moderate magnetic stirring and homogenized. The organic solvent is then removed and the nanoparticles are obtained. The nanoprecipitation method has several advantage that it allows the formation of nanoparticles immediately and in a single step and is simple and fast to apply. In this method, two dissolving solvents are required. The organic phase has to dissolve polymer and the active ingredient. Polymer should not be dissolved in the aqueous phase. When the polymer solution is added to the non-soluble phase, nano-precipitation occurs by rapid addition of the polymer. The polymer is

degraded by diffusion of the solvent containing the polymer into the mixed phase. Nanoprecipitation generally allows the preparation of nanoparticles in a narrow range of dispersion and in the size of 10-300 nm with polymers such as PLGA cellulose derivatives, polycaprolactone (PCL) [182, 183].

### **2.6.1.3. Characterization of Nanoparticles**

#### **2.6.1.3.1. Particle Size**

In nanoparticles having a particle size of 10 to 1000 nm, the particle size distribution is determined by Coulter Nanosizer and Malvern devices. The Coulter Counter device has a capillary flow cell. When the dispersion medium of nanoparticles is passed between the two electrodes, the resistance of the liquid is continuously measured. Particle volume depending on electrical resistance alterations. The Malvern device is operated by light scattering. The dynamic light scattering method is based on the measurement of the intensity and change of light scattering from small particles in the solution. The change in scattered light intensity depends on the particle movement and thus the particle size, the viscosity of the environment and the temperature. Colloidal suspensions are characterized by two basic light scattering methods. Static light scattering method is used to determine the molecular weight of the polymers, the turning radius and the second virial coefficient. Dynamic light scattering method is used to obtain hydrodynamic magnitude, diffusion coefficient, distribution index and particle size distribution. Combining two techniques gives information to determine the particle structure in solution. Transmission Electron Microscopy (TEM) is an another method that is used to determine the particle size and morphological properties of nanoparticles, which provides higher resolution and magnification imaging when compared to Scanning Electron Microscopy (SEM) [171-174,182,183].

#### **2.6.1.3.2. Zeta Potential**

The DLVO (Derjaguin-Landau-Verwey-Overbeek) theory explains the energy of the interaction between the suspended and emulsified particles and gives information about the stability of the colloidal systems. According to the DLVO theory, the force on the particles in a colloidal distribution comes from electrostatic repulsion and Van der Waals tensile forces. At short distances there is a strong attraction between the particles, but as the distance between the particles increases, the electrostatic repulsion energy falls more rapidly than Van der Waals

gravitational energy, and the net effect is seen as weak shots. At medium distances, electrostatic repulsion is dominant and the net interaction has maximum potential. The pull-through force between the particles depends on the characteristic and size of the particle. The electrostatic thrust depends on the surface potential, surface load density and is directly related to the zeta potential. Zeta potential is defined as the sum of the loads that the particles have in a given environment. The value of the zeta potential gives information about the possible stability of the colloidal system. If all the particles have a high negative or positive zeta potential, they push each other and the dispersion becomes resistant. If the particles have a low zeta potential, then there is no force to prevent the combination of particles and the dispersion is not resistant. Generally, the formation of aggregate is seen less with high zeta potential. Zeta potential value, approximately +/- 30 mV and above is indicative of stable nanoparticle suspension [181,183].

#### **2.6.1.3.3. *In vitro* release**

Release from the nanoparticles is due to the dissolution of the drug from the particle surface, solubility, leakage, matrix erosion and diffusion mechanisms. The drug is released by polymer degradation from the nanoparticles prepared with biodegradable polymers. The degradation rates are based on the alkyl chain length. The degradation from the polymer surface can be chemical or enzymatic. If the drug diffusion exceeds the matrix erosion, the release is controlled by the diffusion mechanism. Since the diffusion distance is very short due to the particle size, the systems that release by this mechanism do not show controlled and sustained release.

The weak binding of the drug to the nanoparticles or the adsorption on the wide surface of the nanoparticles results in a sudden release of the drug that is called burst effect. The release rate of the drug can be reduced and the extended release properties can be increased according to the nanoparticle preparation method. If the nanoparticle is coated by a polymer, the rate of release is determined by diffusion from the polymeric membrane. In addition, the release rate can be altered by the ionic interaction between the drug and the added excipients. If the drug and the adjuvant form a complex that is less soluble in water, the drug release rate may decrease and no immediate release effect is observed [173,182,183].

## 2.7. GST Inhibitor ETA

Many GST inhibitors have been developed to date to overcome the drug resistance. Compounds analogous to GSH are known as competitive inhibitors of the GSH binding site. The purpose of using these compounds is to increase isozyme selectivity or stability of the drug. One of the most studied GST inhibitor is ETA. This molecule, which is the reversible inhibitor of GST- $\pi$ , binds to the H region of the enzyme with low affinity, and conjugated with GSH, it is easily excreted from the cell. Some pathways and mechanisms were discovered for the inhibition of the GST enzymes by ETA. ETA has been shown to be a substrate of reduced GSH, on the other hand nonenzymatic GSH conjugation of ETA also exist. Additionally it was shown that the ETA glutathione conjugate was an inhibitor of GSTs as well due to its stronger affinity for the enzymes. So ETA itself inhibits GSTs through reversible covalent binding and the ETA glutathione conjugate is another strong inhibitor of GSTs [157, 158].

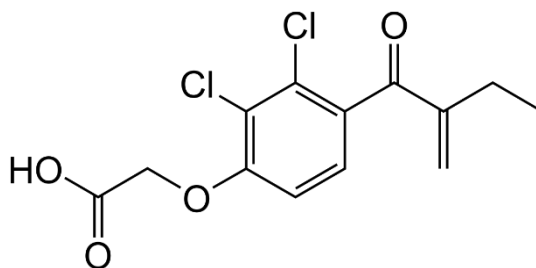


**Figure 2.4.** Chemical structure of ETA

### 3. MATERIALS and METHODS

#### 3.1. MATERIALS

HT-29 CRC cells (ATCC HTB-38) and L929 (NCTC clone 929) were purchased from ATCC (Virginia, USA). Cell culture media, supplements and reagents were purchased from Capricorn (Germany) and Thermo Fisher Scientific (USA). Recombinant TGF- $\beta$ 1 was purchased from eBioscience (USA). Antibodies to SNAIL, SLUG, Vimentin,  $\beta$ -catenin, and N-cadherin were purchased from Elabscience (USA). Mouse monoclonal antibody against human E-cadherin and  $\alpha$ -SMA were from R&D systems (Abingdon, UK). Alexa Fluor secondary antibodies were purchased from Elabscience (USA). Total RNA extraction kit, cDNA synthesis kit and SYBR Green PCR Master mix kit were purchased from Capricorn (Germany). Gene-specific primers for RT-PCR were purchased from Sentegen Biyotek (Ankara, Turkey). GST- $\pi$ , GST- $\mu$  and MDA ELISA kits were purchased from Elabscience (USA).

PLGA (50:50) (RG 502H) (Molecular Weight: 24,000 - 38,000 Da) was purchased from Evonik (Germany). CA (PEG) was purchased from Sigma-Aldrich (Germany). The active ingredient, Ethacrynic acid (ETA) was purchased from Santa Cruz (USA). All organic solvent used were analytical grade and purchased from Sigma (Germany). Dialysis Tubing Cellulose Membrane (average flat width 25mm, MW cut-off 12.000 Da) was purchased from Sigma-Aldrich (Germany). Tryptic Soy Broth, Fluid Thioglycollate Medium and Malt Extract Broth for nanoparticles' sterility control test were purchased from Merck (Darmstadt, Germany). Syringe filters with 0.22 and 0.45  $\mu$ m pore sizes were purchased from Sigma-Aldrich (Germany).

Oxaliplatin, 5-Fluorouracil and Leucovorin were purchased from Sigma-Aldrich (Germany) for combination therapy studies. Thiazolyl Blue Tetrazolium Bromide (MTT) was purchased from Sigma-Aldrich (Germany) for cytotoxicity tests.

Male Wistar rats for *in vivo* CRC and EMT model establishment were purchased from Kobay A.S. Experimental Animals Laboratory (Ankara, Turkey). Cyclosporin A for suppression of immunosystem of animals was purchased from Sigma-Aldrich (Germany). Primer and sekonder antibodies for immunohistochemistry analysis were purchased from Elabscience (USA).

## 3.2. METHODS

This thesis work was carried out in 5 different stages:

- *In vitro* EMT Modelling and Demonstrating EMT
- Determination of Expression Levels of GST- $\pi$  and GST- $\mu$  Isoenzymes in Epithelial and Mesenchymal Phenotypes of HT-29 cells, Activity Assay and Inhibition of GST Isoenzymes
- Preparation of ETA (GST inhibitor) Loaded and Mesenchymal Phenotype Targeted Nanosized Formulations
- *In Vitro* Studies
- *In Vivo* Studies

### 3.2.1. *In vitro* EMT Modelling and Demonstrating EMT

#### 3.2.1.1. Cell culture

HT-29 CRC cells were cultured in McCoy's 5A medium supplemented with 10% heat inactivated fetal bovine serum (FBS), and 1% Penicillin-Streptomycin solution at 37°C in a humidified incubator with 5% CO<sub>2</sub>. The growth medium was changed every 2-3 days. The cells were passaged upon reaching 70-80% of confluency.

#### ***Subculturing procedure***

- Prior to passaging the cells, medium was removed and discarded.
- The cell layer was rinsed twice with 5 ml of phosphate buffer saline (PBS) to remove all traces of serum which contains trypsin inhibitor.
- Pre-warmed Trypsin-EDTA solution (3 to 4 ml) was added to the flask in order to degrade the anchoring proteins and allowed the content to cover the cell layer. Flasks were incubated at 37°C for about 5-10 minutes.
- The cells were examined with an inverted microscope to ensure all the cells were detached and in suspension.
- Upon detachment, trypsin was inactivated by the adding of two volume of complete medium to the flask.
- After gentle pipetting up and down several times, cell suspension was transferred to a centrifuge tube and centrifuged at 250 g for 5 minutes to pellet cells.



- The supernatant was carefully discarded and the pellet was resuspended in complete medium. The required amount of cell suspension was added to 10 ml of fresh medium in a new 75 cm<sup>2</sup> flask.

### ***Counting and determining the viability of cells***

The cell viability and viable cell yield in cell suspension were determined with the trypan blue exclusion method as described at the below:

- 100 µl of 0.4% Trypan Blue Stain and 400 µl of cell suspension were added to a 1.5 ml microcentrifuge tube and mixed vigorously by pipeting.
- 100 µl of Trypan Blue-treated cell suspension was applied to each chamber of the haemocytometer by pipetting and allowing the chamber to be filled by capillary action.
- Under the light microscope, using the 10X objective and focusing on the gridlines of the chamber, the unstained cells (live cells do not take up Trypan Blue) in one set of 16 squares were counted.
- Cells that were on the lines were counted only if they lied on the bottom and right-hand lines of each square.
- Cells stained with Trypan Blue were also be counted to determine viable cell yield.
- To calculate the number of viable cells in 1 ml cell suspension, following formula was used:

$$\text{cell number in ml} = \text{Average number of cells} \times \text{dilution factor} \times 10.000$$

#### **3.2.1.2. *In vitro* EMT Modelling in HT-29 CRC Cell Line**

As an *in vitro* model for EMT, HT-29 CRC cells were induced by TGF-β1. For this purpose, 1x10<sup>5</sup> HT-29 CRC cells were plated in 6-well plate. 70-80% confluent cultures of cells were serum-starved overnight prior to stimulation with TGF-β1. The cells were incubated with various concentrations of TGF-β1 (0.5 ng/ml, 5 ng/ml, 10 ng/ml, 20 ng/ml and 40 ng/ml) for different time intervals (24 hours and 48 hours) at 37°C in a humidified incubator with 5% CO<sub>2</sub>. All experiments were performed in triplicate wells for each condition and repeated at least three times.

### **3.2.1.3. Evaluation of the Molecular Markers of EMT**

#### ***Total RNA isolation***

Total RNA was purified by Hybrid-R™ RNA extraction kit (GeneAll) following manufacturer's instructions.

- The growth medium was collected and stored at -80°C for further studies.
- The attached cells were homogenised with RiboEx™ at room temperature for 5 minutes.
- 200 µl of chloroform was added to the homogenised cell lysate and incubated at room temperature for 2 minutes.
- To separate the cell debris and RNA, the mixture was centrifuged at 12.000 x g for 15 minutes at 4°C and the aqueous phase was transferred to a fresh tube.
- One volume of RBI buffer was added to supernatant and the mixture was transferred to mini column. The column was centrifuged at 12.000 x g for 30 seconds at room temperature in order to bind RNA.
- The column membrane was washed one time with SWI and one time with RNW buffer to avoid residual chloroform.
- RNA was eluted by adding 100 µl of RNase-free water and centrifuged for 1 minute at 12,000 x g.
- RNA concentration and purity ratios were then evaluated by measuring the absorbance of UV light and calculating the 260/280 ratio using NanoDrop™ 1000 spectrophotometer (Thermo Scientific).
- Subsequently, samples were used for complementary DNA (cDNA) synthesis and stored at -80°C until required.

#### ***Complementary DNA (cDNA) synthesis***

cDNA was synthesised by HyperScript™ first strand synthesis kit (GeneAll) following instructions of manufacturer.

- Following reagents (Table 3.1) were mixed on ice and mixture was incubated at 65°C for 5 min.

**Table 3.1.** Reagents for the first step of cDNA synthesis

Template RNA	Total RNA	1 µg
Primer	random hexamer primers	0.75 µL
	oligo dT	0.75 µL
10 mM dNTPs		1 µL
DEPC-treated water		to 14 µl

- Samples chilled on ice at least 1 minutes, and then following reagents (Table 3.2) were mixed on ice.

**Table 3.2.** Reagents for the second step of cDNA synthesis

10X RTase reaction buffer	2 µL
0.1 M DTT	2 µL
HyperScript™ Reverse Transcriptase	1 µL
ZymAll™ RNase Inhibitor	2 µL

- Sample were centrifuged briefly and incubated at 25°C for 5 min, followed by 55°C for 50 min.
- Termination of the reaction was occurred at 85°C for 5 min.

### ***Quantitative polymerase chain reaction analysis (qRT-PCR)***

EMT markers both in nontreated and TGF-β1 treated HT-29 CRC cells were determined by qRT-PCR. SYBR Green were used for performing qRT-PCR analyzes following instructions of manufacturer.

Primer-BLAST program (NCBI) was used for generating candidate primer pairs for associated genes. Table 3.1 showed human specific primers' sequences.

Applied Biosystems 7500 Real-time PCR system (Applied Biosystems, Foster City, CA, USA) was used for the qRT-PCR analysis by following the recommended protocol. The  $\Delta\Delta C_t$  method was used for performing relative gene expression analysis to determine the expression level of each target gene. The results from the qRT-PCR were analyzed using the 7500 Software version 2.0.5 (Applied Biosystems, Foster City, CA, USA). In each sample, the mean quantity of each

gene was normalized with mean quantity of endogenous control (housekeeping gene). Human GAPDH was the gene.

qRT-PCR reactions were conducted in triplicate wells for every gene and at least three independent experiments were performed. Water was added to three wells instead of cDNA as a negative controls.

**Table 3.3.** The sequences of human specific primers for EMT-associated markers

	FORWARD (5'-> 3')	REVERSE (5'-> 3')
<b>GAPDH</b>	CATCAATGGAAATCCCATCA	TTCTCCATGGTGGTGAAGAC
<b>E-cadherin</b>	TTCTGCTGC TCTTGCTGTTT	TGGCTCAAGTCAAA GTCCTG
<b>Vimentin</b>	ATCTGGATTCACCTCCCTCTGGTT	GTGATGCTGAGAAGTTTCGTTGATA
<b>N-cadherin</b>	CCATCAAGCCTGTGGGAATC	GCAGATCGGACCGGATACTG
<b>SNAIL</b>	CCTCCCTGTCAGATGAGGAC	CCAGGCTGAGGTATTCCTTG
<b>SLUG</b>	ACCGAGTGAGAGGCAACC	TGAGAAAGGAGACCCAGCAG
<b>Fibronectin</b>	ACCAACCTACGGATGACTCG	GCTCATCATCTGGCCATTTT
<b><math>\alpha</math>-SMA</b>	CTGGCATCGTGCTGGACTCT	GATCTCGGCCAGCCAGATC
<b>Occludin</b>	CAGCCACTGAAAGGAAAGGC	CCTCCTGGGTGCCTCTAGAAT

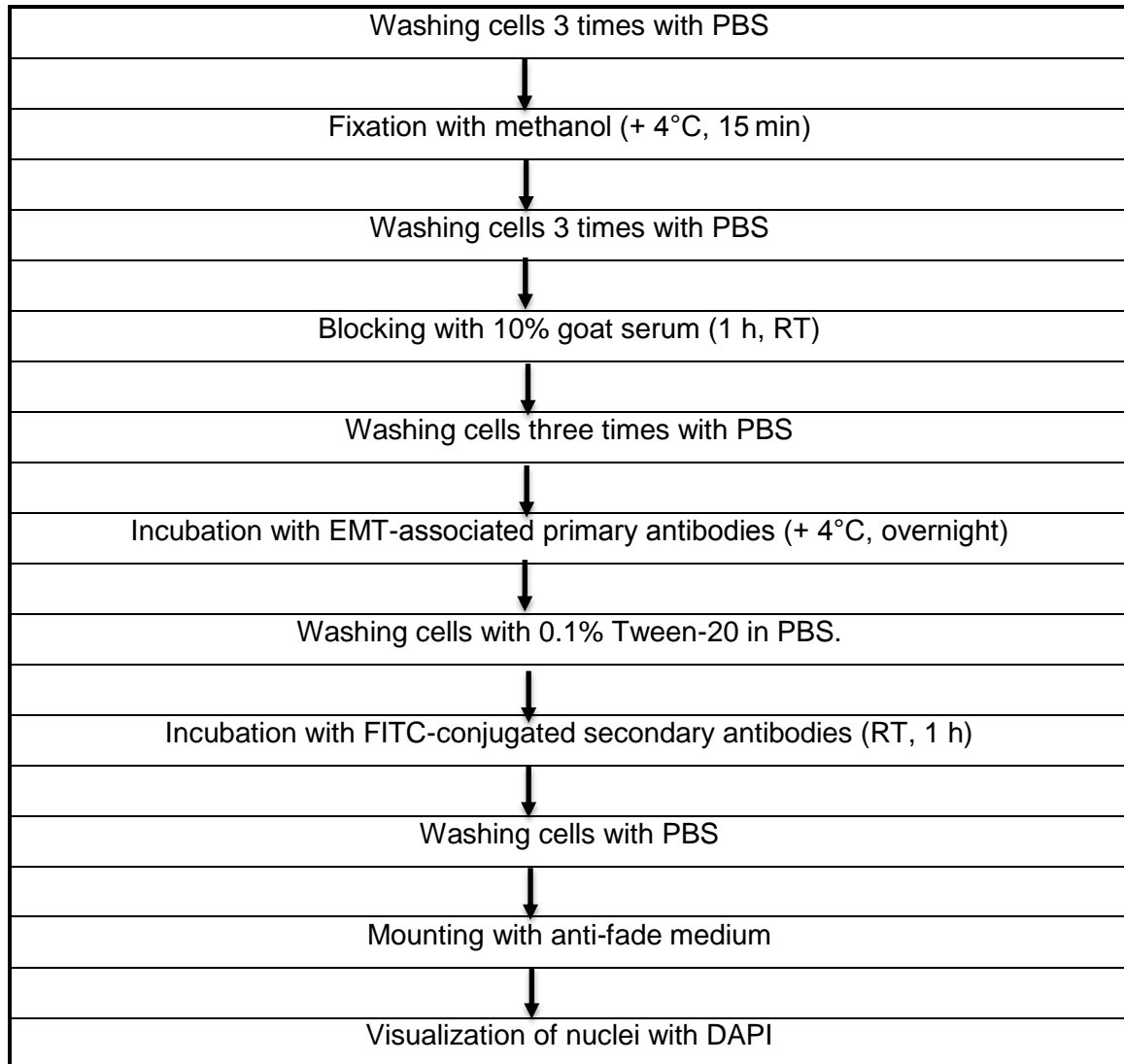
#### 3.2.1.4. Immunofluorescence Staining

- $10^4$  HT-29 CRC cells per well were cultured in 8-well chamber slides.
- Cells were allowed to attach overnight prior to TGF- $\beta$ 1 induction. EMT was induced as described in the *Section 3.3.1.2*.
- List of antibodies and the protocol used for immunofluorescence studies at the end of the induction period was schematized in Table 3.4. and Table 3.5., respectively.

**Table 3.4.** List of antibodies used for immunofluorescence studies

Primary antibodies	Species	Type	Dilution	Supplier
Vimentin	Mouse	Monoclonal	1:100	Elabscience
SNAI	Mouse	Monoclonal	1:100	Elabscience
N-cadherin	Mouse	Monoclonal	1:100	Elabscience
$\beta$ -catenin	Mouse	Monoclonal	1:100	Elabscience
E-cadherin	Human	Monoclonal	1.200	Abcam
Vimentin	Rabbit	Monoclonal	1.200	Abcam

**Table 3.5.** Protocol for immunofluorescence staining



- All treated and untreated samples were photographed using immunofluorescence microscope and identical exposure times.

### **3.2.2. Determination of the Expression Levels for GST- $\pi$ and GST- $\mu$ Isoenzymes in Epithelial and Mesenchymal Phenotypes of HT-29 Cells, Activity Assay and Inhibition of GST Isoenzymes**

In all subsections of this part,  $1 \times 10^5$  and  $2 \times 10^4$  HT-29 CRC cells/well were cultured either in six-well plate or in 24-well plate, respectively. Upon reaching 70-80% confluency, medium was replaced with serum-free media and incubated at 37°C in a humidified incubator with 5% CO<sub>2</sub> overnight. After serum-starving, medium was

replaced with serum-free media for epithelial phenotypes but in the case of mesenchymal phenotype induction, medium was replaced with serum-free media containing 10 ng/ml TGF- $\beta$ 1. Both epithelial phenotypes and mesenchymal phenotypes of HT-29 cells were incubated at 37°C in a humidified incubator with 5% CO<sub>2</sub> for 48 hours.

### 3.2.2.1. Determination of Expression Levels for GST Isoenzymes in Epithelial and Mesenchymal Phenotypes of HT-29 Cells (qRT-PCR)

48 hours after induction, the growth medium was collected for further studies and RNA extraction, cDNA synthesis and qRT-PCR techniques for both phenotypes of HT-29 cells were carried out as previously described in the *Section 3.3.1.3*. The primer sequences for GST isoenzymes were given in Table 3.3.

**Table 3.6.** The sequences of human specific primers of GSTs

	Forward (5'--->3')	Reverse (5'--->3')
<b>GST-<math>\pi</math></b>	CTAGGAGCAGCTTTGAAACGCAC	CGTTGTTGGAGAATGTTGTACCGACG
<b>GST-<math>\mu</math></b>	TGCCATAATGCGCTACCTTG	AAGCATGATGAGCTGCATGC

### 3.2.2.2. Determination of GST- $\pi$ and GST- $\mu$ Protein Levels

GST- $\pi$  and GST- $\mu$  protein levels of epithelial and mesenchymal phenotypes of HT-29 cells were determined by ELISA technique using a commercial kit (Elabscience, USA). The measurements were carried out in accordance with the manufacturer's protocol. Three independent experiments with triplicate measurements were performed for each sample.

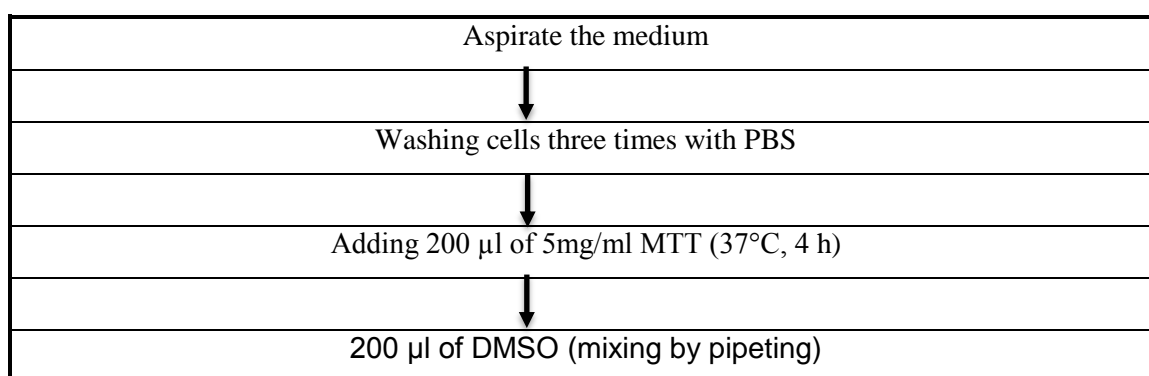
### 3.2.2.3. Treatment of Epithelial and Mesenchymal Phenotypes of HT-29 Cells with GST Inhibitor ETA

Inhibition potential of ETA towards GST isoenzymes for both epithelial and mesenchymal phenotypes of HT-29 cells was determined by IC<sub>50</sub> curve analysis by plotting various concentrations of ETA versus the percentage inhibition of GST- $\pi$  activity. The IC<sub>50</sub> values were calculated as the concentration of inhibitor required for inhibiting the enzyme activity by 50% compared with the controls. For this

purpose, 10 mM stock solution of ETA in 20% ethanol were prepared initially, and subsequent concentrations were diluted from this stock solution.

HT-29 CRC cells were cultured in 96-well plate, upon completion of transition (48 hours after TGF- $\beta$ 1 induction), both epithelial and mesenchymal phenotypes of HT-29 cells were treated by different concentrations of ETA for 24 hours. The inhibition was determined by GST- $\pi$  and GST- $\mu$  protein level analysis in both phenotypes. Triplicate measurements were performed for each concentration. The cytotoxic effect of different concentrations of ETA on HT-29 CRC cells was determined by examining the cell viability assay by MTT. Table 3.7. shows the MTT assay protocol.

**Table 3.7.** MTT assay protocol



- Presence of viable cells was visualized by the development of purple color due to formation of formazan crystals and the absorbance intensity of formazan crystals was measured by a microplate reader at 490 nm with a reference wavelength of 620 nm.
- All experiments were performed in quadruplicate, and the relative cell viability (%) was expressed as a percentage relative to the untreated control cells (185).

#### **3.2.2.4. Formation and Determination of Oxidative Stress in Epithelial and Mesenchymal Phenotypes of HT-29 cells**

Both of two phenotypes of HT-29 CRC cells were treated by different concentrations of hydrogen peroxide ( $H_2O_2$ ) (10-160  $\mu$ M) for different time intervals (60-120 minutes) to compare oxidative stress responses between two phenotypes of HT-29 cells. Oxidative damage was detected by the determination of MDA levels by ELISA kit due to the manufacturer's instructions. Response to oxidative

stress in both phenotypes of HT-29 CRC cells was determined by the change in protein levels of GST isoenzymes. Protein level determinations of GST isoenzymes were performed as previously described in *Section 3.3.2.2*. The cytotoxic effect of different concentrations of H<sub>2</sub>O<sub>2</sub> on HT-29 CRC cells was determined by examining the cell viability assay by MTT.

#### **3.2.2.5. Treatment of Oxidative Stressed Epithelial and Mesenchymal Phenotypes of HT-29 Cells with GST Inhibitor ETA**

Oxidative stress was formed in epithelial and mesenchymal phenotypes of HT-29 cells as previously described in *Section 3.2.2.4* and cells were exposed to various concentrations of ETA for 24 hours and 48 hours. The inhibition was detected as previously described in *Section 3.2.2.2*.

#### **3.2.3. Preparation of GST Inhibitor ETA Loaded and Mesenchymal Phenotype Targeted Nanosized Formulations**

In this thesis, two different strategies were used to formulate ETA-loaded nanosized delivery systems. Firstly, ETA was encapsulated into PLGA-*b*-PEG nanoparticles via nanoprecipitation technique. Secondly, ETA was conjugated with PLGA-*b*-PEG polymer and resulting polymer was used to prepare nanoconjugate.

##### **3.2.3.1. Quantification of ETA by HPLC**

The amount of ETA was detected by a high pressure liquid chromatography (HPLC) method as described Lin *et al.* [186] with slight modifications.

The chromatographic separation was performed using a Inertsil<sup>®</sup> ODS-3V column (5 µm; 4.6 mm × 250 mm). HPLC analysis was performed by isocratic elution with a flow rate of 1 ml/min and the injection volume was 10 µl.

The mobile phase consisted of %41 water, 57% acetonitrile and 2% acetic acid. Then, mixture of mobile phase components in different ratios was elevated to achieve acceptable retention time.

The ETA was quantified by a UV detector set at  $\lambda = 230$  nm at 25 °C. All measurement were performed within the linear ranges of calibration curves. The method was validated through the parameters of linearity, accuracy, precision, selectivity, sensitivity and stability.



### ***Linearity***

Linearity denotes the ability of the method to provide results directly proportional to the concentration of substance in question within a given application range.

The method linearity was assessed by using calibration curve to calculate regression equation, coefficient of correlation, and intercept values. For this purpose, a 25 mg amount of ETA was accurately weighed, dissolved in acetone and diluted to volume in a 50 ml volumetric flask to obtain 500  $\mu\text{g/ml}$  stock solution. Dilutions with mobile phase were performed in order to obtain solutions with concentrations between 2.5  $\mu\text{g/ml}$  and 200  $\mu\text{g/ml}$ , where an average concentration is 50  $\mu\text{g/ml}$ . The calibration curve was plotted using peak areas of ETA versus ETA concentrations.

### ***Accuracy***

The accuracy of an analytical procedure expresses the closeness of agreement between the value which is accepted either as a conventional true value or an accepted reference value and the value found.

Three samples at three different concentration levels 5  $\mu\text{g/ml}$ , 50  $\mu\text{g/ml}$  and 100  $\mu\text{g/ml}$  were prepared by dissolving it in acetone and diluting in 50 ml mobile phase as in sample solution preparation. The tests were conducted in sextuplicate for each concentration level and were assessed using Student's t test by comparing results obtained against theoretical values defined for each analyzed concentration.

### ***Precision***

Precision is the variability in the data from replicate determinations of the same homogeneous sample under the normal assay conditions. Precision may be considered at three levels: repeatability, intermediate precision and reproducibility and usually expressed as the variance, standard deviation or coefficient of variation of a series of measurements.

Repeatability expresses the precision under the same operating conditions over a short interval of time. For assessing the repeatability, one of the concentrations of prepared ETA solutions (50 ppm) was chosen and analysed with 6 replicates time

after time. Mean values, standard deviation or coefficient of variation of a series were then calculated.

Intermediate precision expresses within-laboratories variations: different days, different analysts, different equipment, etc. For assessing the inter-days, the chosen concentration (50 µg/ml) that was prepared in 3 consecutive days, was measured and mean values, standard deviation or coefficient of variation were then calculated. Reproducibility expresses the precision between laboratories. For assessing the reproducibility, 6 samples of ETA solution which are prepared at the same concentrations (50 µg/ml) were analysed and mean values, standard deviation or coefficient of variation were then calculated.

### ***Sensitivity***

Sensitivity of the method was determined by finding the limit of detection and limit of quantitation. Limit of detection (LOD) is the lowest concentration of analyte in a sample that can be detected, but not necessarily quantitated, under the stated experimental conditions. The minimum concentration (1µg/mL) at which a signal to noise ratio is 3:1 was accepted as detection limit. Limit of Quantification (LOQ) is the lowest concentration of analyte in a sample that can be quantified with acceptable precision and accuracy under the stated experimental conditions. The minimum concentration (1µg/mL) at which a signal to noise ratio is 10:1 was accepted as quantification limit.

### ***Specificity***

Specificity is the ability to determine the desired analyte in a sample that contains of all different potential components. The specificity of analytical methods is typically assessed by examining system interference with the detection and quantification of analytes.

#### **3.2.3.2. Synthesis of PLGA-*b*-PEG Copolymer**

PLGA-*b*-PEG co-polymer with carboxyl ended functional group was synthesized through formation of thioester bond between PLGA-COOH and COOH-PEG-NH<sub>2</sub> by the method described by Devulapally et al [187]. Figure 3.1. showed the schematic representation of the conjugation of PLGA with PEG.

300 mg Resomer 502H (PLGA-COOH) was solubilized in dry dichloromethane (DCM), and 20.7 mg of NHS (0.17mmol) and 34.5 mg of EDC were added for the

activation of carboxylic acid group in PLGA. The organic mixture was stirred continuously for 24 hours. The resulting PLGA-NHS was precipitated with ice cold ethyl ether. The precipitated PLGA-NHS was centrifuged three times; washed with ethyl ether-metanol mixture, and precipitate was dried under vacuum.

300 mg PLGA-NHS was dissolved in chloroform. Heterobifunctional  $\text{NH}_2\text{-PEG-COOH}$  ( $\text{MW}_{\text{PEG}}=1146.35 \text{ g/mol}$ ) and  $\text{N,N}$ -diisopropylethylamine were added to the organic solution of PLGA-NHS at a molar ratio 1:1 and 1:3, respectively. The reaction was continued for 24 hours with continuous stirring. Resulting polymer was precipitated with 5 ml cold ethyl ether and washed with ethyl ether-metanol mixture (70:30, v/v) three times to remove unreacted PEG. Precipitated polymer was dried under vacuum and detected by nuclear magnetic resonance.

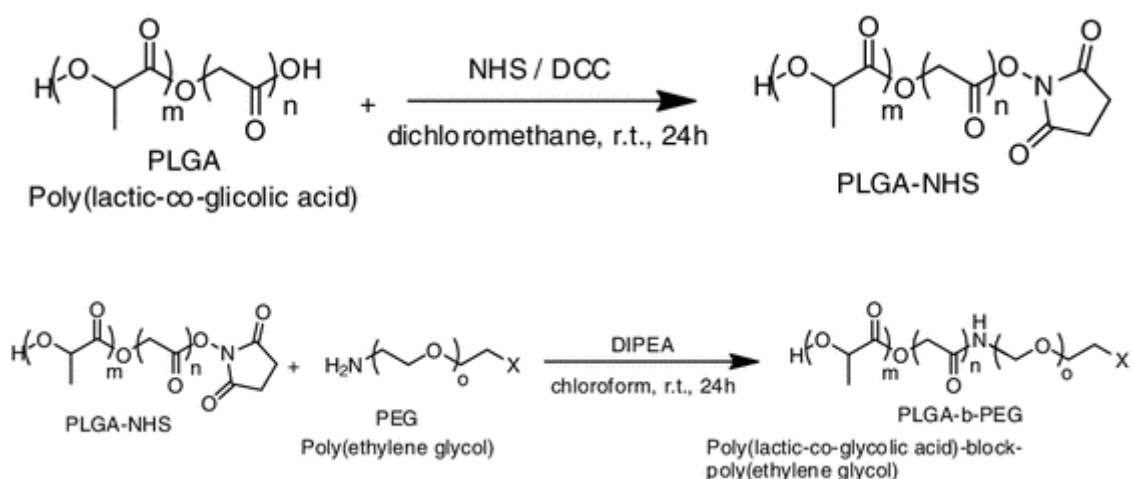


**Figure 3.1.** Schematic of the synthesis of the polymer poly-DL-lactic-co-glycolic (PLGA) polyethylene glycol (PEG) (188).

### 3.2.3.3. Synthesis of mPEG-PLGA-SS-ETA

mPEG-PLGA-SS-ETA was synthesized according to the procedure described in Han et al [189] with slight modifications. Figure 3.2. showed the schematic of the synthesis route of the conjugation between mPEG-PLGA and ETA.

300 mg mPEG-PLGA was solubilized in DCM, and 28 ml triethanol amine (TEA) was added to polymer solution. 12% 4-dimethylaminopyridine (DMAP) and 0.25 mol tosyl chloride (TsCl) were solubilized together in DCM. This mixture was added dropwisely into the previously prepared polymer solution throughout 6

hours. Then the resulting mixture was stirred overnight and precipitated with cold diethyl ether.

Following solubilization in dimethyl sulfoxide (DMSO), cystamine hydrochloride, TEA and DMAP were added and stirred magnetically. After the completion of reaction, solution was dropwised into cold ethyl ether to obtain precipitate. Precipitate was vacuum dried and lyophilized. The lyophilized product was detected by  $^1\text{H-NMR}$ .

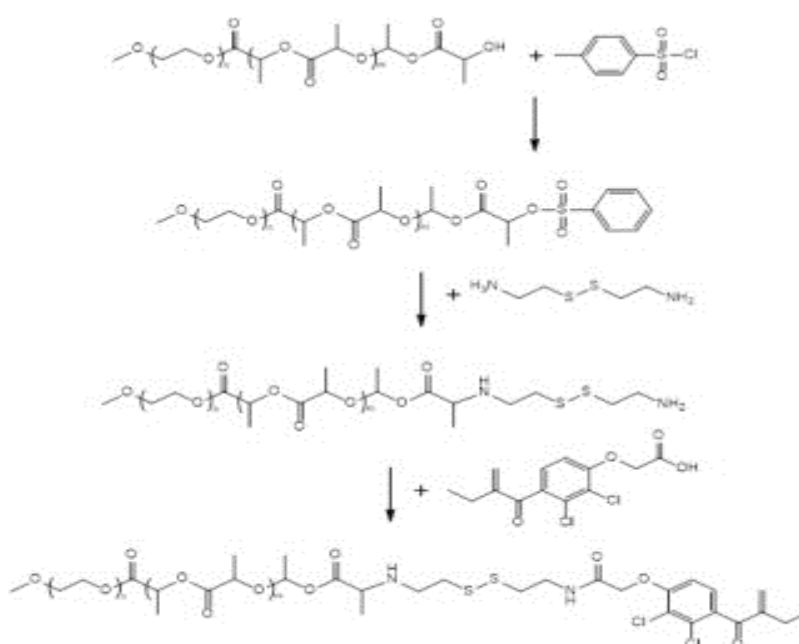


**Figure 3.2.** Synthesis of the polymer conjugates of ETA (190)

200 mg of polymer with disulfide bond was solubilized in DCM, and DMAP and an equal volume of ETA and carbonyl diimidazole (CDI) were added, which was stirred for 36 hours. The mixture was dropwised into cold ethyl ether for the precipitation and freeze-dried. The lyophilized product was detected by  $^1\text{H-NMR}$ .

#### **3.2.3.4. Preparation of Blank Nanoparticles**

PLGA and PLGA-*b*-PEG nanoparticles were prepared by the nanoprecipitation (solvent displacement) method aspreviously described by Fessi *et al.* [191] with

slight modifications. Figure 3.3. showed the schematic representation of preparation of polymeric nanoparticles.

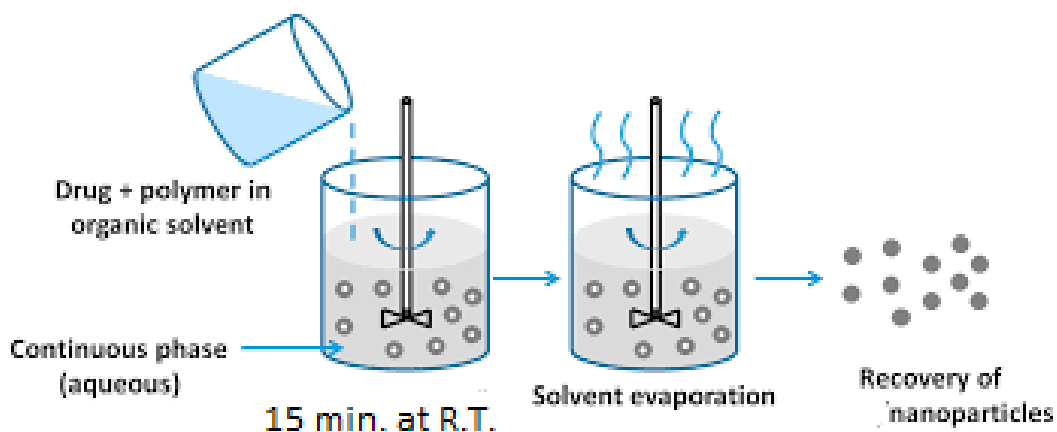


**Figure 3.3.** Schematic preparation of polymeric nanoparticles by nanoprecipitation (solvent displacement) method [192].

Briefly, polymer was dissolved in water miscible organic solvent and organic solution of polymer was then added dropwisely into an aqueous surfactant solution under continuous stirring. The resulting colloidal suspension was stirred at 1000 rpm for 15 minutes at room temperature. The nanosuspension was then stirred for 3 hours to evaporate the organic solvent and to obtain nanoparticle dispersion at the final desired volume 25 mL. After the evaporation of solvent, nanoparticles obtained as a suspension were centrifuged at 4.000 rpm to separate nanoparticles from macroaggregates. Finally, nanoparticles were collected additional centrifugation at 14.000 rpm for 30 minutes at +4°C, washed three times with distilled water to remove unloaded ETA and surfactant residues. The supernatant was kept at +4°C to further determine the amount of drug non-entrapped in nanoparticles. After centrifugation, nanoparticles were kept at -20 °C overnight and freeze-dried at -55 °C and 0.5 kPa for 24 hours. Lyophilized nanoparticles were stored at +4°C until further studies.

The influence of various formulation parameters such as polymer concentration, polymer molecular weight, ratio of organic to aqueous phase, amount of surfactant on the physicochemical properties of nanoparticles were evaluated. Therefore, blank nanoparticles were formulated by changing the polymer concentration

(concentration range 0.5% to 2% w/v), organic phase to aqueous phase volume ratio (1:1, 1:2, 1:5 v/v). In addition to these parameters, surfactant concentration (concentration range from 0.1% to 1% w/v) were also evaluated to optimize the formulations.

#### **3.2.3.5. Preparation of ETA Loaded Nanoparticles**

ETA loaded PLGA and PLGA-*b*-PEG nanoparticles were formulated in a similar manner to that of blank nanoparticles stated in *Section 3.3.3.4.* by adding ETA in the organic phase. ETA loaded formulations were prepared according to the pre-formulation results of blank PLGA and PLGA-*b*-PEG nanoparticles. Briefly, ETA was dissolved in the organic phase consisting of 50 mg polymer in 5 ml acetone following dissolution of the polymer. The solution was added drop wise into 25 ml ultra-pure water containing 1% Pluronic F68 (PF-68) under magnetic stirring. The nanoprecipitation and purification procedure were repeated as described previously.

#### **3.2.3.6. Preparation of MPEG-PLGA-SS-ETA Nanoconjugates**

For the preparation of mPEG-PLGA-SS-ETA nanoconjugates, mPEG-PLGA co-polymer was synthesised and following co-polymer synthesis, ETA was conjugated with the mPEG-PLGA through disulfide bonds as previously described in *Section 3.2.3.2.*

Single emulsion-solvent evaporation technique was used to prepare mPEG-PLGA-SS-ETA nanoconjugates as described by Han *et al* [189]. 250 mg of mPEG-PLGA-SS-ETA were solubilized in DCM at room temperature using a magnetic stirrer for 1 hour. After the completion of solubilization, the conjugate solution was added dropwisely into aqueous solution of 0.1% PF-68 and the mixture was sonicated by an ultrasonic probe at 30 W for 3 minutes (15 seconds pulses). The organic solution was evaporated for 4 hours. Nanoparticles were collected and lyophilized as previously described in *Section 3.2.3.4.*

#### **3.2.3.7. Characterization of Nanoformulations**

The average particle size and polydispersity index of the nanoformulations were determined by the dynamic laser light scattering method (Nanosizer Coulter N4 Plus®) (Malvern Instruments, UK) before and after lyophilisation. Aqueous dispersion of lyophilised formulations at a concentration of 0.1 mg/ml and 1 ml of

fresh nanoformulation suspension were used to evaluate the average particle size and size polydispersity. The measurements were conducted at 25°C. The viscosity and refraction index of the continuous phase were set equal to those specific to water. Triplicate measurements were performed for each sample with each measurement consisting of 12 runs.

The  $\zeta$  potential of nanoformulations was measured in aqueous dispersion with a Zetasizer 4 (Malvern Instruments, UK) at 25°C. Experimental values were the average of six different formulations.

The morphological analysis of nanoparticles were performed by transmission electron microscopy (TEM). 100  $\mu$ l of the aqueous dispersion was placed over a copper grid of 400 mesh with carbon film. The droplet was reduced after 5 minutes with a filter paper to eliminate the excess of nanoparticles. Finally, the sample was air dried prior to placing it in the TEM.

#### **3.2.3.8. Entrapment Efficiency and Loading Capacity**

Entrapment efficiency and loading capacity of formulations were determined using both direct and indirect procedures and the results of the indirect and direct assay were compared.

In the direct method, 10 mg of lyophilized samples were dissolved in 1 mL of acetonitrile and shaken slightly followed by sonication for 5 minutes. Then, 2 mL of methanol was added to precipitate the polymer. The solution was then centrifuged at 4.000 rpm for 10 minutes at 4°C to remove the polymeric debris and polymeric debris was washed twice with fresh solvent to extract any adhered inhibitor. The supernatant containing inhibitor was assessed for drug content by validated HPLC method.

In the indirect method, the amount of inhibitor encapsulated within the nanoformulations was determined by measuring the amount of unencapsulated drug in supernatant recovered after centrifugation and washing of formulations.

The encapsulation efficiency and loading capacity were calculated mean  $\pm$  SD of three readings from three batches. The encapsulation efficiency (1) and the percent loading of ETA (2) were then calculated as follows:

$$\text{Encapsulation efficiency} = \frac{\text{Total amount of ETA-Free ETA}}{\text{Total amount of ETA}} \times 100 \quad (1)$$

$$\text{Loading capacity} = \frac{\text{Total amount of ETA-Free ETA}}{\text{Nanoparticles weight}} \times 100 \quad (2)$$

### 3.2.3.9. *In vitro* Release Studies

*In vitro* release profiles of nanoformulations were evaluated by dialysis method. 10 mg of freeze-dried nanoformulations suspended in 10 mL of isotonic pH 7.4 solution of PBS, were transferred into a dialysis bag. The dialysis bag (12 kDa, surface area = 18 cm<sup>2</sup>) containing 10 mL nanoformulation suspension were placed in a tube containing 100 ml of release medium. The whole assembly was kept in a horizontal laboratory shaker (200 rpm) and maintained at 37±0.5 °C.

*In vitro* release studies of ETA from nanoformulations were carried out in ethanol-phosphate buffered saline of pH 7.4 and pH 5 buffer solutions at 37°C. In the case of mPEG–PLGA–SS–ETA nanoconjugates, 10 mM GSH containing buffer solution were also used to examine the impact of GSH on disulfide bonds' dissociation in mPEG–PLGA–SS–ETA nanoconjugates. At designated time points, 2 ml of the external medium were withdrawn from the beaker and replaced with fresh medium to ensure the sink condition. The samples were filtered through a 0.45-µm PVDF membrane, and the amount of drug present in the release media were analyzed directly by HPLC according to the method described before in *Section 3.2.3.1*. The concentration of ETA released from the formulations was expressed as a percentage of the total ETA loaded into the formulation and was plotted as a function of time.

### 3.2.3.10. Stability of Nanoformulations

The optimized formulation of either PLGA-*b*-PEG nanoparticles or mPEG–PLGA–SS–ETA nanoconjugates was tested for their stability. Freshly prepared freeze-dried three samples of optimized formulations were stored as aqueous dispersions in ultrapure water at 4°C and at room temperature for 4 months. With a sampling frequency of one month, formulations were analyzed for mean size.



### **3.2.3.11. Sterilization of Nanoformulations**

Two different sterilization techniques were used for the removal of microbial contamination from nanoformulations. Filter sterilization was implemented through 0.22  $\mu\text{m}$  filters. Nanoformulations were also sterilized by UV-irradiation at room temperature for 12 hours. Weight field was determined after sterilization. The particle size distribution and toxicity of formulations before and after filtration were also examined.

### **3.2.3.12. Sterility Control of Nanoformulations**

Sterility control of nanoformulations was evaluated for both aerobic and anaerobic bacteria production. Tryptic Soy Broth and Fluid Thioglycollate Medium were used for the detection of aerobic and anaerobic bacteria, respectively. Malt Extract Broth was also used as medium for the detection of yeasts and fungi. Non-sterile formulations were used as positive controls. The plates were incubated at  $37\pm 0.5^\circ\text{C}$  or at  $25\pm 0.5^\circ\text{C}$  for bacterial and fungal growth, respectively. The turbidity of the media was then observed over a basic period of 14 days in comparison to positive controls. The experiments were repeated three times.

### **3.2.3.13. Antibody Conjugation of Nanoformulations**

Drug loaded and optimized nanoformulations were conjugated to FITC tagged anti-vimentin mAbs by the carbodiimide process as previously described by Arruebo *et al* [193] with slight modifications. The conjugation process was described below:

- The lyophilized nanoformulation dispersed in PBS at a concentration of 10 mg/ml was mixed with 2 mM N-Hydroxysuccinimide (NHS) and 2 mM carbodiimide (CDI) under continuous stirring to activate the carboxyl groups of nanoformulation. The resulting mixture was stirred for 1 hour.
- After the completion of activation process, the activated nanoformulation was centrifuged at 10,000 rpm and suspended in PBS.
- Nanoformulation dispersion was mixed with 10  $\mu\text{l}$  FITC tagged anti-Vimentin mAbs and stirred for 4 hours in the dark.
- The mixture was centrifuged at 12,000 rpm and rinsed three times with PBS to remove residual reagents and antibodies.

- Antibody conjugated nanoformulation was dispersed in glycine solution for the saturation of free coupling sites, washed with distilled water and lyophilised as described in *Section 3.2.3.4*.
- The amount of antibody conjugated to the nanoformulation was assessed by BCA assay and conjugation efficiency was calculated.
- Nanoformulation with the highest conjugation efficiency was also determined by <sup>1</sup>H-NMR.
- Both of antibody conjugated nanoparticles or antibody conjugated nanoconjugates were henceforth referred to as immunonanoformulations.

#### **3.2.3.14. *In vitro* Cytotoxicity**

Cytotoxicity of nanoformulations was evaluated by MTT assay against L929 mouse fibroblast cells. L929 cells were cultured in Dulbecco's modified Eagle's medium supplemented with 10% FBS, 2 mM L-glutamine, as well as 1% penicillin-streptomycin solution.

The cells were seeded in 96-well plates at the density of  $1 \times 10^4$  viable cells/well and incubated for 24 hours to allow cell attachment. The following day, the medium was replaced by 100  $\mu$ L medium containing the nanoformulations at concentrations of 20-100  $\mu$ g/ml for 24 and 48 hours. MTT assay was applied to determine cell viability.

#### **3.2.4. *In vitro* Studies**

During *in vitro* studies, oxidative stress generated epithelial and mesenchymal phenotypes of HT-29 cells were used to evaluate the effect of both free ETA and nanoparticulated ETA on the GST- $\pi$  protein levels of the cells. Anti-Vimentin conjugated immunonanoformulations were also evaluated for their inhibition capabilities. Effectiveness of adjuvant therapy in the drug resistant mesenchymal phenotypes of HT-29 cells as a response of GST- $\pi$  inactivation with free ETA and nanoparticulated ETA was also assessed.

In all subsections of this part, oxidative stress was generated in both epithelial and mesenchymal phenotypes of HT-29 cells by the induction of cells with 20  $\mu$ M H<sub>2</sub>O<sub>2</sub> for 1 hour.

Adjuvant therapy used in this study was the combination of 5 mM 5-Fluorouracil (5-FU), 500  $\mu$ M Folinic acid (FA) and 90  $\mu$ M oxaliplatin, henceforth referred to as FOLFOX regimen. The selected concentrations of drugs were in accordance with the studies reported in the literature [194]. All assays were performed with 6 replicates.

A 600 mM stock of 5-FU was prepared in absolute DMSO and stored at  $-20$  °C. For treatment, stock solutions of all drugs were diluted in cell culture medium to achieve the desired concentration. The final concentration of DMSO was less than 1%.

#### **3.2.4.1. Treatment of Oxidative Stress Generated Epithelial and Mesenchymal Phenotypes of HT-29 Cells with Nanoparticulated ETA**

After oxidative stress induction, the cells were incubated for 4 hours in the presence of free ETA, ETA loaded PLGA-*b*-PEG nanoparticles, mPEG–PLGA–SS–ETA nanoconjugates at concentrations ranging from 0.2  $\mu$ g/mL to 2  $\mu$ g/mL. Effectiveness of nanoformulations were compared according to the variabilities in the GST- $\pi$  activities. IC<sub>50</sub> values of ETA loaded nanoformulations for epithelial and mesenchymal phenotypes of HT-29 cells was determined.

#### **3.2.4.2. Treatment of Oxidative Stress Generated Epithelial and Mesenchymal Phenotypes of HT-29 Cells with FOLFOX**

Oxidative stress generated epithelial and mesenchymal phenotypes of HT-29 CRC cells were subjected to treatment with FOLFOX. For this purpose, the cells were incubated in the presence of 5 mM 5-FU, 500  $\mu$ M FA and 90  $\mu$ M oxaliplatin for 24 hours. Inhibition of cell growth in response to adjuvant therapy was assessed by MTT spectrophotometric assay. The cells incubated without FOLFOX 24 hours were used as control. Treated and untreated cells were compared according to the cell viability ratio.

#### **3.2.4.3. Treatment of Oxidative Stress Generated Epithelial and Mesenchymal Phenotypes of HT-29 Cells with ETA+FOLFOX**

Cells were pre-treated with 3.2  $\mu$ M ETA for 2 hours and then co-incubated with 15 mM 5-FU, 2 mM FA and 500  $\mu$ M oxaliplatin for 24 hours. Medium was changed very two days and freshly prepared inhibitor and drug solutions were added into wells as described previously. Cell viability was determined by MTT. Results of

groups those were treated only with FOLFOX and those were pre-treated with ETA upon FOLFOX treatment were compared according to the cell viability.

#### **3.2.4.4. Treatment of Oxidative Stress Generated Epithelial and Mesenchymal Phenotypes of HT-29 Cells with Nanoparticulated ETA +FOLFOX**

Cells were pre-treated with 2 mg/ml ETA loaded PLGA-*b*-PEG nanoparticles and 0.4 mg/ml mPEG–PLGA–SS–ETA nanoconjugates for 24 hours. Then, the cells were treated with the indicated drug concentrations as previously described in *Section 3.2.4.2*.

#### **3.2.5. *In vivo* Studies**

4-6 weeks old male Wistar rats (200-250 g) were purchased from Kobay Experimental Animals Incorporated Company and were housed under controlled conditions at 21± 2°C and 30–70% relative humidity with a 12-hours dark/light illumination sequence and ad libitum access to tap water and standard pellet rodent chow. All animals were deprived of food 12 hours prior to experimentation but had free access to water. All experiments on animals were performed with strict adherence to European Community guidelines and the Declarations of Helsinki and Tokyo, and they were approved by the Institutional Experimental Animal Care and Use Ethics Committee of Hacettepe University before the commencement of any interventions (Approval number: 2017/26-10).

##### **3.2.5.1. Establishment of *in vivo* CRC Model**

*In vivo* CRC model was established in Wistar rats by introducing HT-29 CRC cells intraperitoneally as previously described by Akhter *et al.* (195) with slight modifications. Prior to tumour cell implantation, cyclosporine was given i.p. at a concentration of 35 mg/kg/day to suppress the immune system of animals. Thereafter, the same dose was given i.p. daily. 50 x10<sup>6</sup> HT-29 cells resuspended in 500 µl PBS was injected in Wistar rats. The animals were then housed as described above for 15 to 35 days in order to obtain colorectal adenocarcinoma. On the 15<sup>th</sup>, 30<sup>th</sup> and 45<sup>th</sup> days following the HT-29 cells implantation, 6 animals from each group were sacrificed with high-dose chloral hydrate treatment to determine the CRC formation period. Tumor formation was described by examining the tumor tissue morphologically and histopathologically. Moreover, E-

cadherin, vimentin, N-cadherin, Slug, transgelin,  $\alpha$ -SMA and GST- $\pi$  levels were determined in the tumor tissue samples.

### **3.2.5.2. Study Groups**

**Control group:** Colon and rectal tissues were removed in the control group and E-cadherin, vimentin, N-cadherin, Slug,  $\alpha$ -SMA, and transgelin expression levels were determined by RT-PCR analysis. Moreover, GST- $\pi$  protein level was determined to determine the basal values of these parameters.

**CRC group-1:** In this group animals were divided in seven groups with three rats per group.  $50 \times 10^6$  HT-29 cells resuspended in 500  $\mu$ l PBS was injected in Wistar rats. The animals were then housed as described above for 15 to 95 days in order to obtain colorectal adenocarcinoma. On the 15<sup>th</sup>-95<sup>th</sup> days following the HT-29 implantation, 3 animals from each group were sacrificed with high-dose chloral hydrate treatment to determine the CRC formation period. Tumor formation was demonstrated by examining the tumor tissue morphologically and histopathologically. Moreover, E-cadherin, vimentin, N-cadherin, Oct-4 and transgelin, GST- $\pi$  protein levels were determined in the tumor tissue samples.

**CRC group-2:** In this group animals were divided in three groups with six rats per group. CRC model model was established in all groups according to the results obtained from CRC group-1. The day of tumor volume reached  $1\text{m}^3$  was accepted as day 0. Then, the animals were housed as described above for additional 10 to 20 days in order to determine the EMT formation period. On the 0, 10<sup>th</sup> and 20<sup>th</sup> days following the formation of cancer, animals were sacrificed and tumor tissue samples were removed. EMT was demonstrated by biochemical markers and immunohistochemical techniques. Immunohistochemical analysis was performed to determine the metastatic formation in the liver tissue samples of these 3 groups.

Following the determination of tumor and EMT formation periods, 36 animals were injected with HT-29 CRC adenocarcinoma cell line intraperitoneally. At the end of the EMT formation period determined in CRC group 2, animals were divided into 6 groups (n=6 for each group) to construct experimental groups.

**Study group-1:** The animals in this group were administered with FOLFOX chemotherapy. The FOLFOX chemotherapy regimen consisted of weekly cycles of

intraperitoneal (i.p.) FOLFOX consisting of 6 mg/kg Oxaliplatin followed 2 hours later by 50 mg/kg 5-FU and 90 mg/kg leucovorin. This drug-dosing schedule was based upon a careful review of the literature (196, 197). The treatment protocol was terminated one week after the second treatment. At the end of the second week, animals were sacrificed with high dose chloral hydrate, tumor tissue was removed and morphological and histopathological examinations were performed.

**Study group-2:** The animals in this group were administered with ETA intravenously every day for 1 week. ETA dosage was determined according to *in vitro* study results. At the end of 1 week, animals were sacrificed with high dose chloral hydrate, biochemical markers, GST- $\pi$  activity and lipid peroxidation levels were determined in the tumor tissues.

**Study group-3:** The animals in this group were administered with ETA prior to FOLFOX chemotherapy. At the end of the second week, animals were sacrificed with high dose chloral hydrate, tumor tissue was removed and morphological and histopathological examinations were performed.

**Study group-4:** The animals in this group were administered with immunonanoparticles. At the end of the second week, animals were sacrificed with high dose chloral hydrate, tumor tissue was removed and morphological and histopathological examinations were performed. Biochemical markers, GST- $\pi$  activity and lipid peroxidation levels were also detected in the tumor tissues.

**Study group-5:** The animals in this group were administered with ETA loaded immunonanoparticles. At the end of the second week, animals were sacrificed with high dose chloral hydrate, tumor tissue was removed and morphological and histopathological examinations were performed. Biochemical markers, GST- $\pi$  activity and lipid peroxidation levels were also determined in the tumor tissues.

**Study group-6:** The animals in this group were administered with ETA loaded immunonanoparticles prior to FOLFOX chemotherapy. At the end of the second week, animals were sacrificed with high dose chloral hydrate, tumor tissue was removed and morphological and histopathological examinations were performed. Biochemical markers, GST- $\pi$  activity and lipid peroxidation levels were also determined in the tumor tissues.

### **3.2.5.3. Histopathology**

Tissues were fixed in 10% formaldehyde and automatically processed by routine procedure. After processing, paraffin blocks were obtained from these samples. 5  $\mu$ M thick tissue sections were stained with routine hematoxylin-eosin. Tissues were macroscopically and microscopically examined for the presence of neoplasm.

Histopathological changes were classified as mild, moderate and severe dysplasia. Tissues with prolonged, crowded, and pseudo-layered nuclei with a slightly decreased number of goblet cells in which the polarization was maintained were classified as mild dysplasia. Tissue specimens with increased number of immune cells in the connective tissue, defectorization and hyperchromatic features in the cell nuclei were characterized as moderate dysplasia. Colorectal carcinoma formation was characterized by complete disappearance of the morphological features of the origin tissue and presence of signal ring cells.

### **3.2.5.4. RNA extraction, cDNA synthesis and qRT-PCR**

Total RNA was extracted using the HyridR isolation kit according to the manufacturer's instructions. One microgram of total RNA was used to generate cDNA using cDNA synthesis kit and a random hexamer primer. qRT-PCR was performed using SYBR-Green reagents. GAPDH was used as the internal control.

### **3.2.5.5. Immunohistochemistry**

5  $\mu$ M thick sections were deparaffinised and stained for primary antibodies using Leica Bond Max autostainer following manufacturer's instructions. Appropriate antigen retrieval and concentration of antibodies were calibrated using positive and negative controls.

### **3.2.6. Statistical Analysis**

All statistical analysis were performed using GraphPad Prism 7.0 (GraphPad Software, Inc., San Diego, CA). The significance of differences was assessed by Student's t-test. P value less than 0.05 ( $p < 0.05$ ) was considered to denote a statistically significant difference. All data in this thesis study are represented as mean  $\pm$  SEM

## 4. RESULTS and DISCUSSION

### 4.1. TGF- $\beta$ 1 Induced EMT in HT-29 CRC Cells

TGF- $\beta$ 1 stands out as an important mediator of EMT. Extensive studies demonstrated that treatment with TGF- $\beta$ 1 led to a progressive stimulation of EMT in numerous malignant cell lines [198-202]. In this study, the transformation of epithelial phenotype into the mesenchymal phenotype of HT-29 CRC cells was induced by TGF- $\beta$ 1. Optimum concentration and exposure time of TGF- $\beta$ 1 for the induction of EMT were determined by morphological and biochemical analysis.

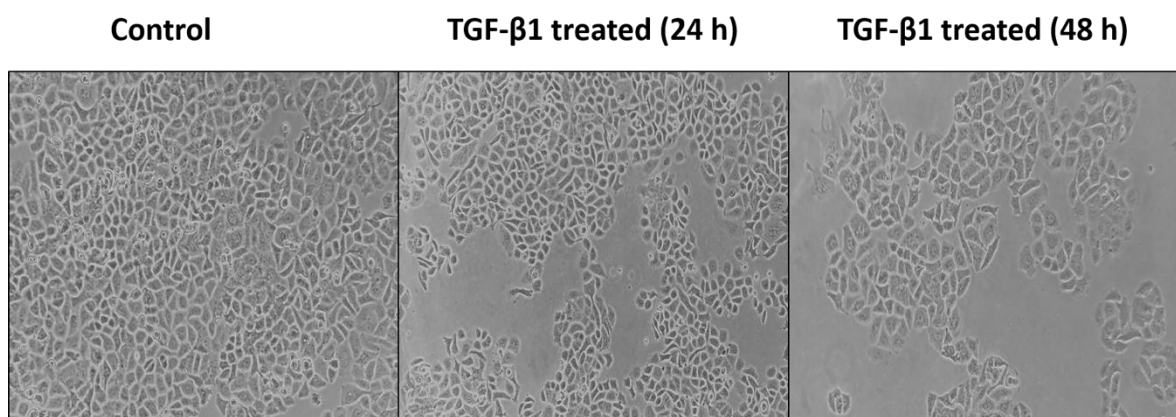


**Figure 4.1.** Untreated and 10 ng/ml TGF- $\beta$ 1 treated HT-29 cells under inverted light microscope.

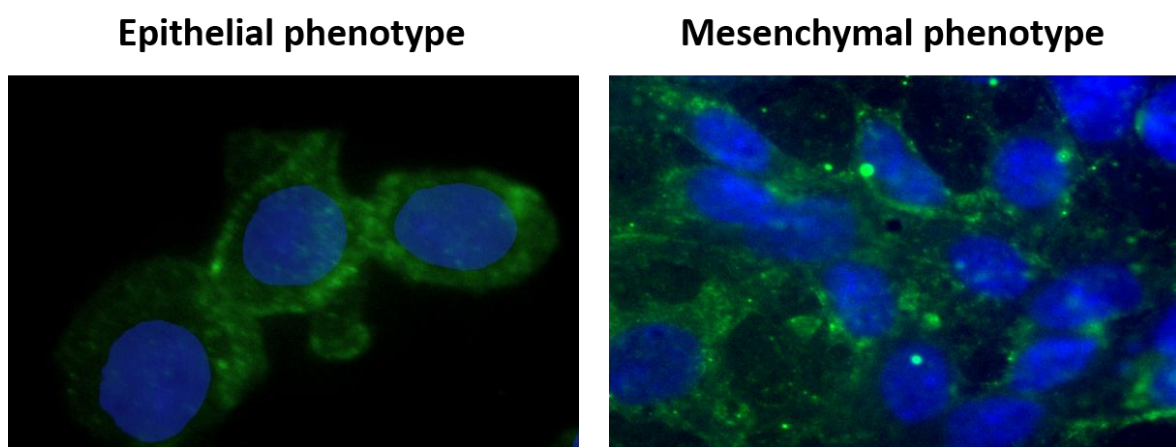


**Figure 4.2.** Immunofluorescence staining of untreated and 10 ng/ml TGF- $\beta$ 1 treated HT-29 cells.



#### **4.1.1. Morphological Alterations in HT-29 Cells Induced with TGF- $\beta$ 1**

Morphological changes following treatment of HT-29 CRC cells with various concentrations (2.5–40 ng/ml) of TGF- $\beta$ 1 for 24 and 48 hours were observed with inverted light microscopy and immunofluorescence staining. Different cellular morphology can be easily observed using inverted microscope at the indicated time intervals. As depicted in Figure 4.1., untreated HT-29 cells were present in colonies and form a monolayer with tight junctions between adjacent cells, while TGF- $\beta$ 1 treated cells appeared detached and showed a spindle-shaped, fibroblast-like phenotype, consistent with a mesenchymal phenotype. Differences in morphology could also be observed from the images of immunofluorescence staining (Figure 4.2). TGF- $\beta$ 1 exposed cells displayed more elongated cytoplasm with extending outward protrusions.

#### **4.1.2. Molecular Markers of Epithelial and Mesenchymal Phenotypes**

In addition to morphological changes after TGF- $\beta$ 1 stimulation, the effect of concentration and induction time of TGF- $\beta$ 1 on the expression patterns of EMT associated genes were determined by qRT-PCR analysis. For this purpose, expressions of the epithelial phenotype markers (E-cadherin, ZO-1 and  $\beta$ -catenin) and mesenchymal phenotype markers (vimentin,  $\alpha$ -SMA, fibronectin and N-cadherin) were evaluated at mRNA level. EMT-inducing transcription factors, including SNAIL and Slug were also determined to qRT-PCR analyses.

Membrane E-cadherin is an important adhesion molecule related to epithelial phenotype. Extensive experimental and clinical studies revealed that the suppression of E-cadherin disrupted the cell adhesion followed by loss of epithelial integrity and facilitated cell migratory capacity via EMT [203, 204]. As E-cadherin downregulation is a significant hallmark of EMT, mRNA levels of E-cadherin both in untreated and TGF- $\beta$ 1 treated cells were investigated. As expected, E-cadherin expression was downregulated in response to TGF- $\beta$ 1 treatment. As it can be clearly seen in the Figure 4.3. and Figure 4.4., TGF- $\beta$ 1 exposure significantly reduced E-cadherin expression in a concentration and time dependent manner. After stimulation with TGF- $\beta$ 1 at the concentration of 2.5 ng/ml for 24 hours, a slight reduction was observed in E-cadherin expression (20%). Treatment of HT-29 cells with 5 ng/ml and 10 ng/ml TGF- $\beta$ 1 for 24 h resulted in 36% and 54% reduction in E-cadherin expression, respectively. Furthermore, exposure of HT-29

cells to 10 ng/ml TGF- $\beta$ 1 for 48 hours resulted induced 80% loss of E-cadherin expression. In addition to E-cadherin, the expression of Zonula occludens (ZO-1) was also downregulated. According to the results stated in Figure 4.3. and Figure 4.4., the highest suppression of ZO-1 was obtained after 10 ng/ml TGF- $\beta$ 1 treatment for 48 hours consistent with the literature [205-207]. These findings suggested that HT-29 CRC cells exhibited a dose and time-dependent loss of epithelial markers. These alterations in the expression of epithelial markers are similar to previous reports of TGF- $\beta$ 1 induced EMT in HT-29 cells [201, 208, 209].

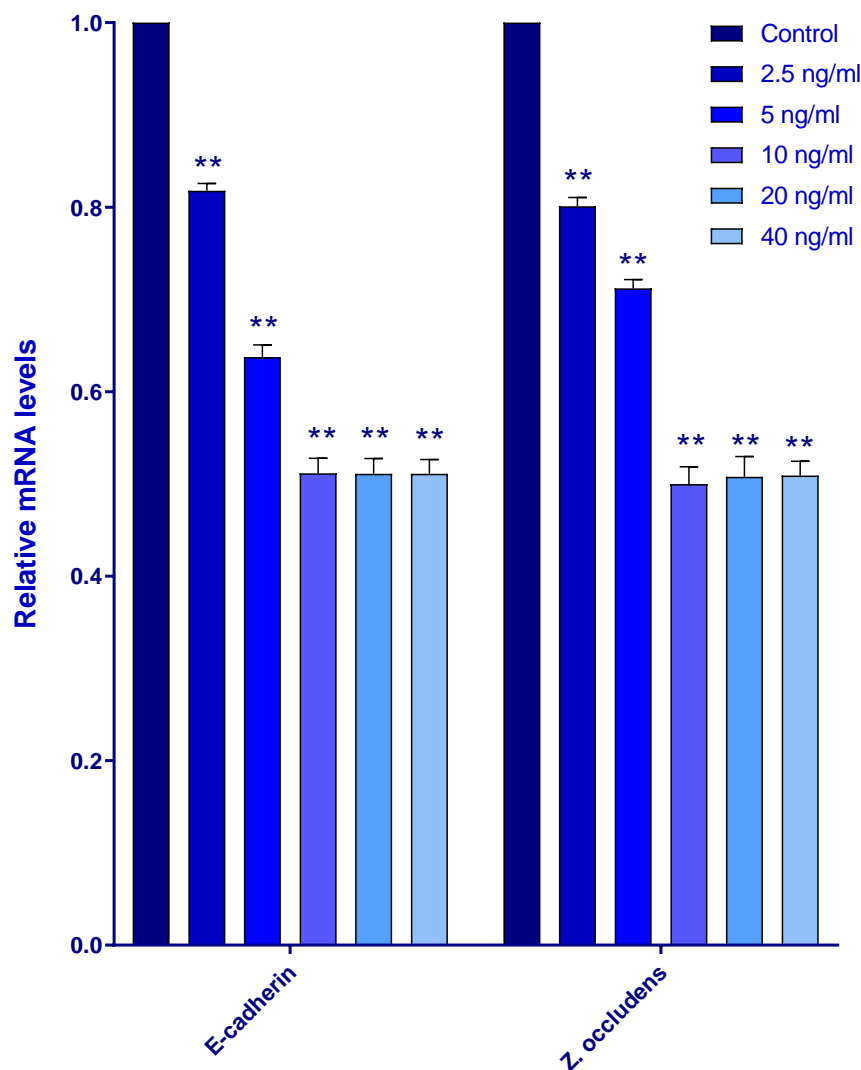


**Figure 4.3.** Relative mRNA levels of epithelial markers following TGF- $\beta$ 1 treatment for 24 hours. Levels of mRNA expression were normalized to GAPDH. Each bar represents mean  $\pm$  SEM of six independent experiments (\*\*  $p < 0.01$  vs control).

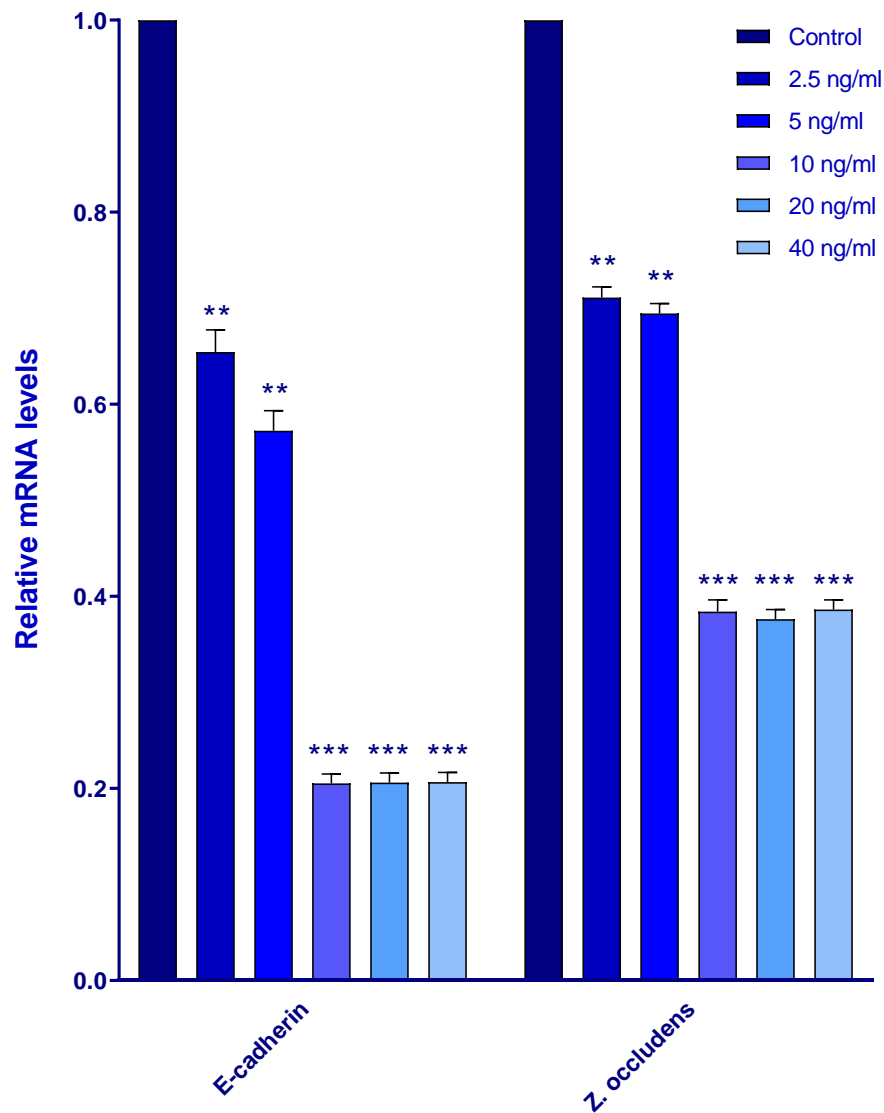


**Figure 4.4.** Relative mRNA levels of epithelial markers following TGF- $\beta$ 1 treatment for 48 hours. Levels of mRNA expression were normalized to GAPDH. Each bar represents mean  $\pm$  SEM of six independent experiments (\*\* $p < 0.01$  and \*\*\* $p < 0.001$  vs control).

Under normal physiological conditions, E-cadherin forms an adhesion complex with  $\beta$ -catenin at the membrane. Dysregulations in the signaling pathways like TGF- $\beta$  and EGF may cause disassociation of this complex and formation of free  $\beta$ -catenin [204, 210, 211]. This free cytoplasmic  $\beta$ -catenin interacts mainly with T-cell Factor/Lymphoid Enhancer Factor (TCF/LEF) to translocate to the nucleus. Nuclear localization of  $\beta$ -catenin activate the Wnt signaling followed by the activation of transcription factors leading to cancer cell proliferation, invasion and metastasis [212]. As the one potential mechanism by which TGF- $\beta$ 1 induces EMT is  $\beta$ -catenin dependent [213, 214],  $\beta$ -catenin mRNA levels were examined. In

contrast to E-cadherin and ZO-1,  $\beta$ -catenin was found to be significantly ( $p < 0.001$ ) upregulated in TGF- $\beta$ 1 stimulated HT-29 cells. These results were accordance with several studies in the literature [215] while reports from several laboratories indicates that  $\beta$ -catenin expression was downregulated in conjunction with E-cadherin repression.

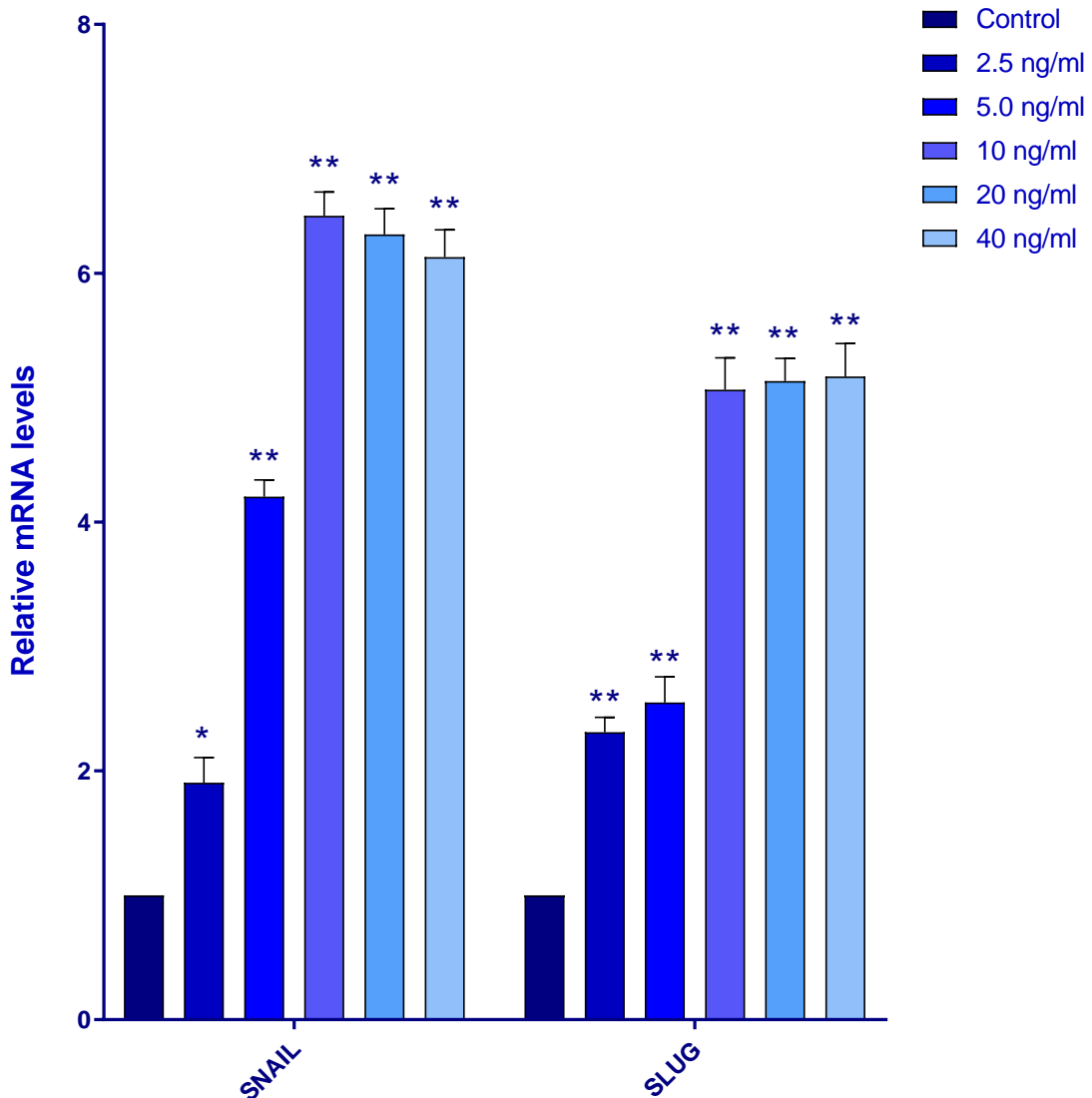


**Figure 4.5.** Relative mRNA levels of transcription factors, SNAIL and SLUG, following TGF- $\beta$ 1 treatment for 24 hours. Levels of mRNA expression were normalized to GAPDH. Each bar represents mean  $\pm$  SEM of six independent experiments (\* $p < 0.05$  and \*\*  $p < 0.01$  vs control)

Repression of epithelial markers can be mediated by several master transcription factors, including Snail, Slug, and Twist [83, 84, 216, 217]. It has been reported

that TGF- $\beta$ 1 induces the overexpression of these transcription factors [218-220]. To determine whether these genes were upregulated in HT-29 cells following TGF- $\beta$ 1 exposure, mRNA levels of SNAIL and SLUG were determined. The expression of SNAIL and SLUG was significantly induced by various concentrations of TGF- $\beta$ 1 in HT-29 CRC cell lines (Figure 4.5 and Figure 4.6). Strongly elevated mRNA levels of these transcription factors coincided with E-cadherin suppression.

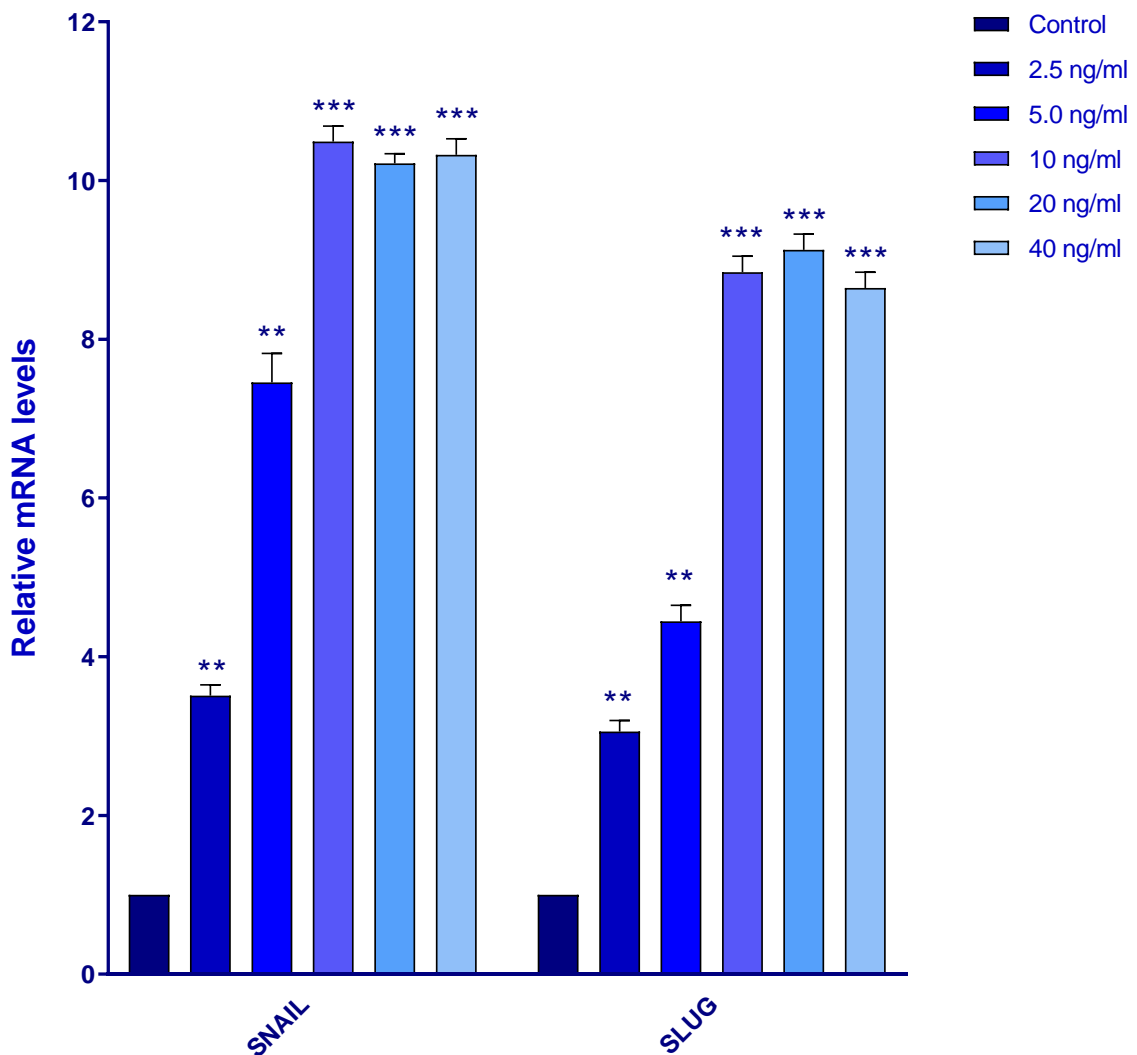


**Figure 4.6.** Relative mRNA levels of transcription factors, SNAIL and SLUG, following TGF- $\beta$ 1 treatment for 48 hours. Levels of mRNA expression were normalized to GAPDH. Each bar represents mean  $\pm$  SEM of six independent experiments (\*\* $p$ <0.01 and \*\*\* $p$ <0.001 vs control).

De novo expression of vimentin is one of the most important hallmarks for EMT [56, 90, 201, 221]. Furthermore, vimentin expression is associated with the cell motility and the invasive phenotype of cancer cells [222, 223]. Upregulation of N-cadherin is another important event occurs in EMT. Gain of N-cadherin following E-cadherin suppression resulted in increased motility and invasion rate [224, 225].

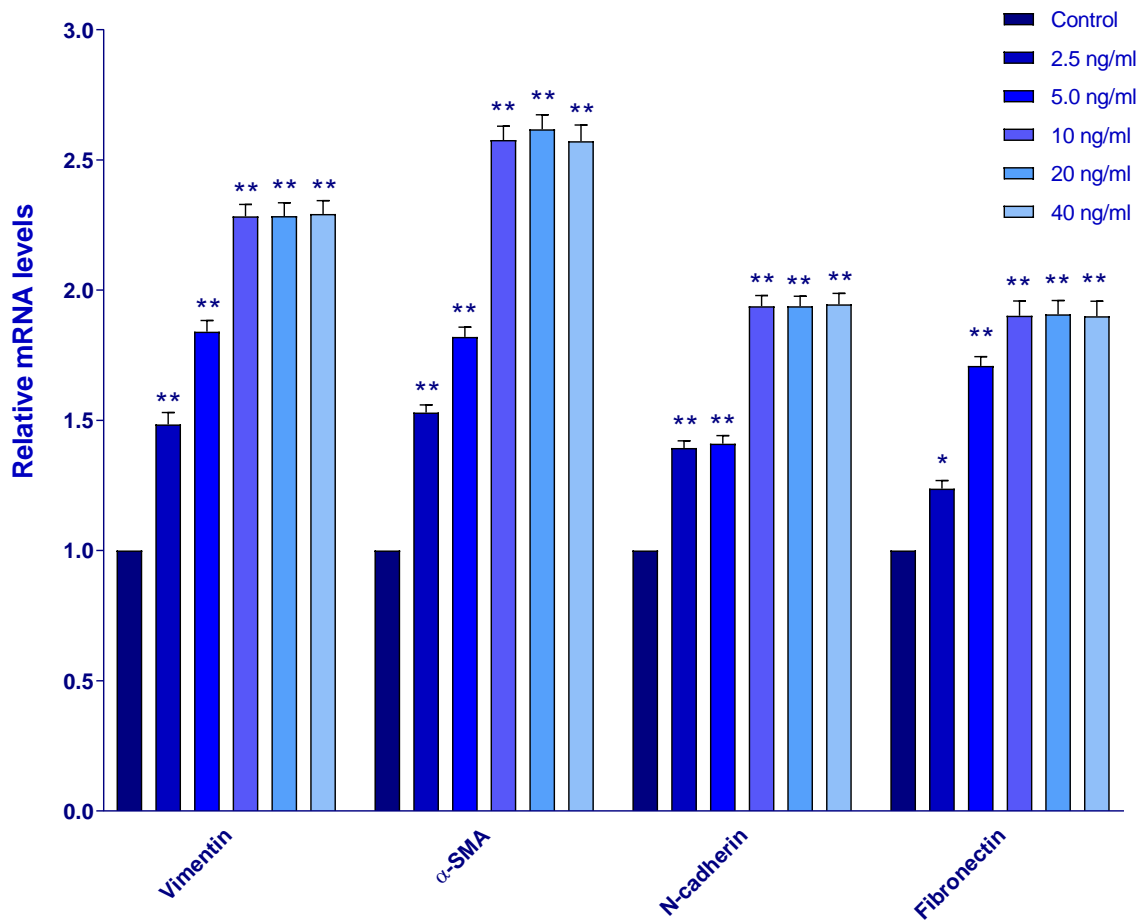


**Figure 4.7.** Relative mRNA levels of mesenchymal markers following TGF-β1 treatment for 24 hours. Levels of mRNA expression were normalized to GAPDH. Each bar represents mean ± SEM of six independent experiments (\*p<0.05, \*\*p<0.01 and \*\*\*p<0.001 vs control).

Overexpression of α-SMA and fibronectin are also reported for the mesenchymal phenotypes of some cancer cell lines including neuroblastoma and colorectal adenocarcinoma [226-228].

In consistent the significant decrease in the epithelial markers, expression changes of the mesenchymal markers following treatment with TGF- $\beta$ 1 were concentration and time dependent. Exposure to lower doses of TGF- $\beta$ 1 seems to induce a marked increase in vimentin,  $\alpha$ -SMA and N-cadherin expressions, while a modest but still significant increase in fibronectin was observed. 10 ng/ml TGF- $\beta$ 1 treatment for 24 hours enhanced the expression of all indicated markers with a maximal induction of 2.58 folds of  $\alpha$ -SMA (Figure 4.7). Treatment with 10 ng/ml TGF- $\beta$ 1 induced up to 80% and 90% increase of vimentin (3.69 fold) and  $\alpha$ -SMA (4.29 fold) expression, respectively within 48 hours (Figure 4.8). N-cadherin expression increased to ~ 2 fold upon 48 hours treatment. This result, in conjunction with the E-cadherin repression, demonstrated that cadherin switch was induced in response to TGF- $\beta$ 1 treatment. There was no significant difference in the expression patterns of EMT-associated markers between cells treated with 10 ng/ml TGF- $\beta$ 1 and >10 ng/ml TGF- $\beta$ 1. Therefore, HT-29 CRC cells were treated with 10 ng/ml TGF- $\beta$ 1 for 48 hours to induce EMT for subsequent assays.

#### **4.1.3. Immunofluorescence Staining**

To examine the transition of epithelial phenotype to mesenchymal phenotype in TGF- $\beta$ 1 induced HT-29 cells, immunofluorescence staining for E-cadherin, a marker of epithelial phenotype, and for vimentin, N-cadherin and  $\alpha$ -SMA, markers of mesenchymal phenotype, was performed. Expression of EMT-inducing transcription factor SNAIL-I was also evaluated by immunofluorescence staining. As shown in Figure 4.9., immunofluorescence staining revealed that TGF- $\beta$ 1 induction for 48 hours markedly increased the expression of mesenchymal markers vimentin, N-cadherin and  $\alpha$ -SMA whereas reduced the expression of epithelial marker E-cadherin. Protein expression levels of related genes were consistent with their mRNA levels. Moreover, it was clearly seen in the Figure 4.9.,  $\beta$ -catenin was translocated into the nucleus. Consistent with these molecular changes in surface proteins, expression of EMT-inducing transcription factor SNAIL-I was significantly upregulated (Figure 4.10) and as expected, SNAIL-I was accumulated in the nucleus of TGF- $\beta$ 1 induced HT-29 cells. These results demonstrated that TGF- $\beta$ 1 induced the upregulation of SNAIL-I and expression of SNAIL-I can induce EMT in HT-29 cells, which is accompanied with the downregulation of epithelial markers and upregulation of mesenchymal markers.

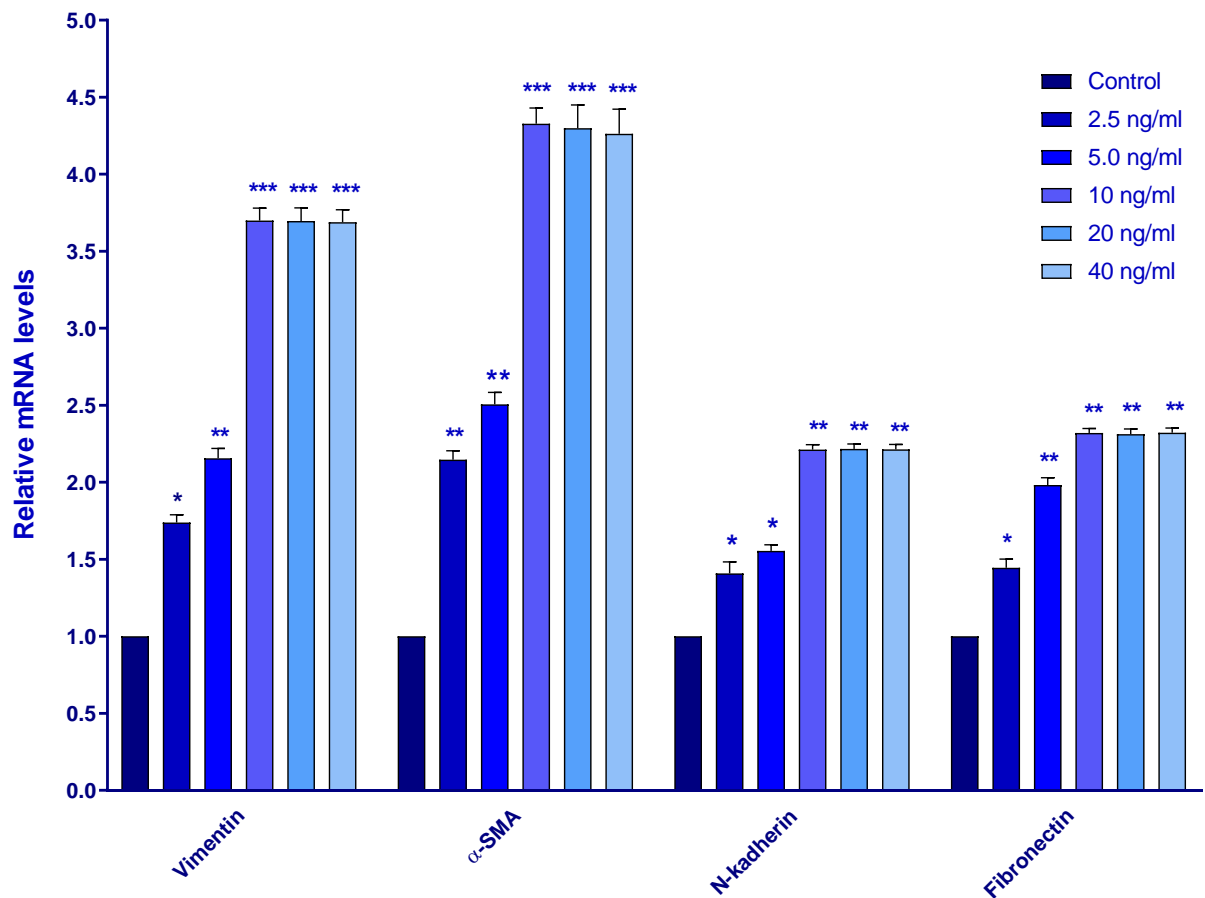


**Figure 4.8.** Relative mRNA levels of mesenchymal markers following TGF- $\beta$ 1 treatment for 48 hours. Levels of mRNA expression were normalized to GAPDH. Each bar represents mean  $\pm$  SEM of six independent experiments (\* $p$ <0.05, \*\* $p$ <0.01 and \*\*\* $p$ <0.001 vs control).

Moreover, it was clearly seen in the Figure 4.9.,  $\beta$ -catenin was translocated into the nucleus. Consistent with these molecular changes in surface proteins, expression of EMT-inducing transcription factor SNAIL-I was significantly upregulated (Figure 4.10) and as expected, SNAIL-I was accumulated in the nucleus of TGF- $\beta$ 1 induced HT-29 cells. These results demonstrated that TGF- $\beta$ 1 induced the upregulation of SNAIL-I and expression of SNAIL-I can induce EMT in HT-29 cells, which is accompanied with the downregulation of epithelial markers and upregulation of mesenchymal markers.



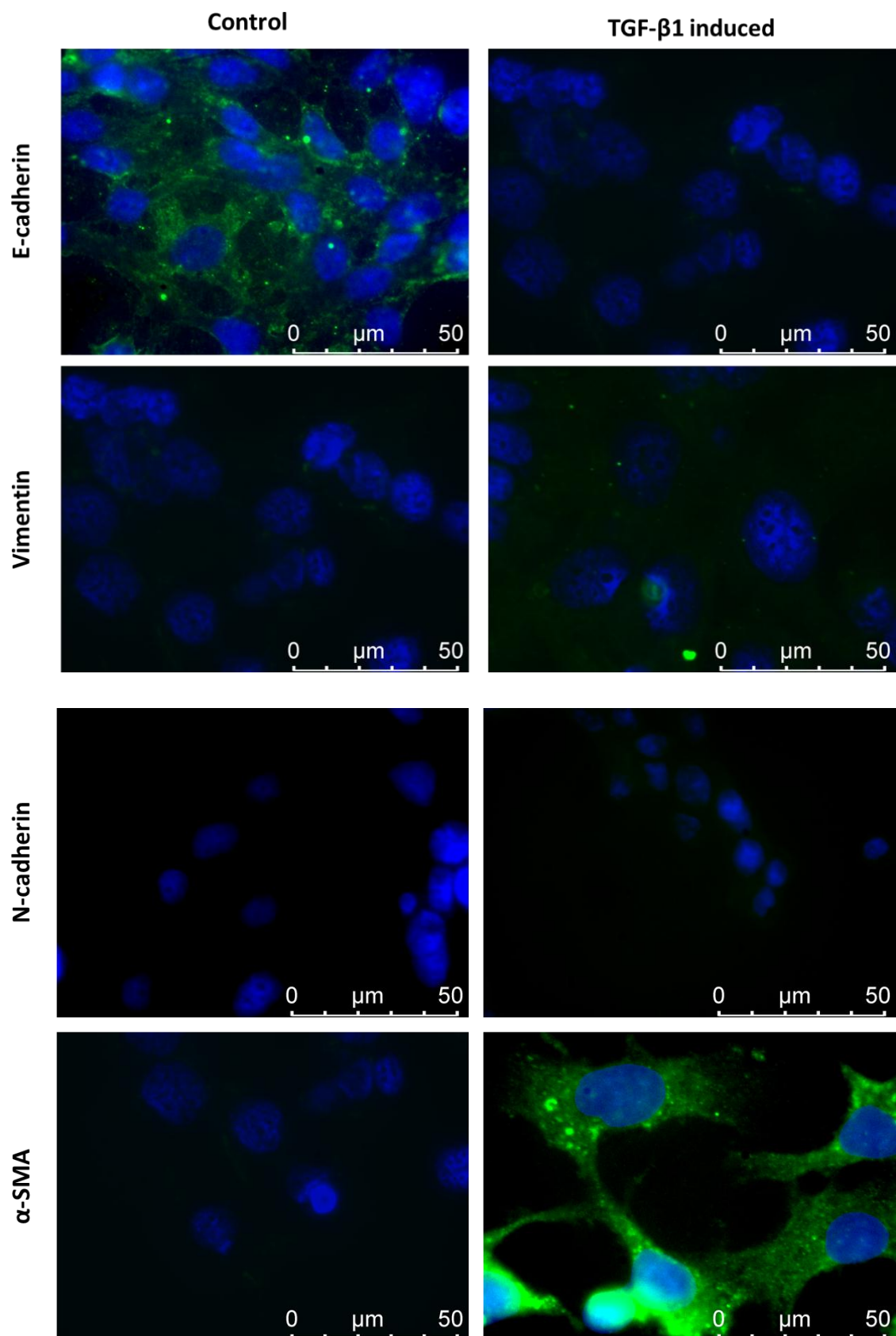


**Figure 4.9.** Immunofluorescence staining identified the expression of EMT-related genes in epithelial phenotype and mesenchymal phenotype of HT-29 cells.

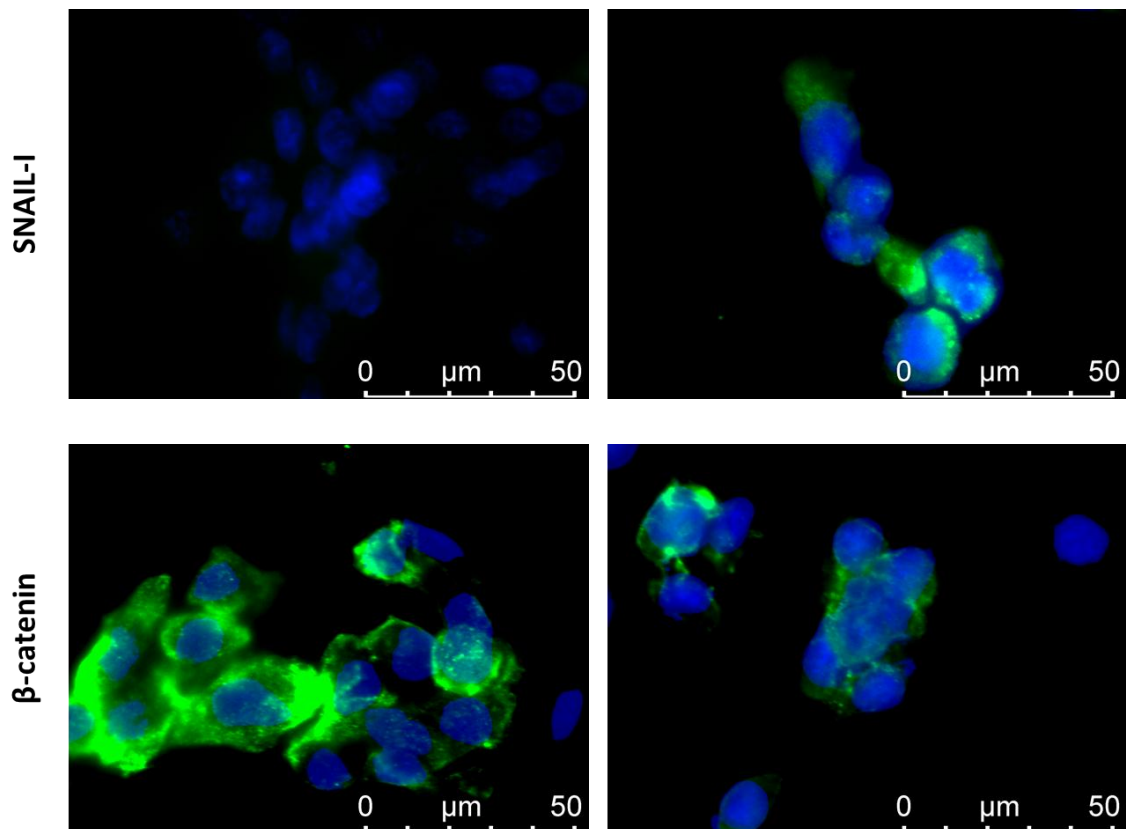


**Figure 4.10.** Immunofluorescence staining identified the upregulation of SNAIL-I and translocation of  $\beta$ -catenin and SNAIL to nucleus in the mesenchymal phenotype of HT-29 cells.

#### 4.2. Determination of Expression Levels for GST- $\pi$ and GST- $\mu$ Isoenzymes in Epithelial and Mesenchymal Phenotypes of HT-29 Cells, Activity Assay and Inhibition of GST Isoenzymes

##### 4.2.1. Elevated Expression and Protein Levels of GST- $\pi$ in Mesenchymal Phenotype of HT-29 Cells

Enhancement of detoxifying enzymes either in cancer cells or in clinical tumor samples had been implicated in resistance to chemotherapeutics [229-232]. Since drug resistance in cancer treatment is also associated with EMT [111, 233-235], expression levels of GST- $\pi$  and GST- $\mu$  isoenzymes were assessed both in epithelial and mesenchymal phenotypes of HT-29 cells to investigate whether the overexpression of these isoenzymes is responsible for chemoresistance in mesenchymal phenotype of HT-29 cells. It can be clearly seen from the results in Figure 4.11-A that higher mRNA levels of GST- $\pi$  were observed in TGF- $\beta$ 1 induced mesenchymal phenotypes of HT-29 cells. Indeed, the significance difference in GST- $\pi$  expression levels between 24 hours treated and 48 hours

treated cells was observed ( $p < 0.01$ ). However, no significant change in the expression of GST- $\mu$  was observed following stimulation of the cells with TGF- $\beta$ 1 ( $p > 0.05$ ).

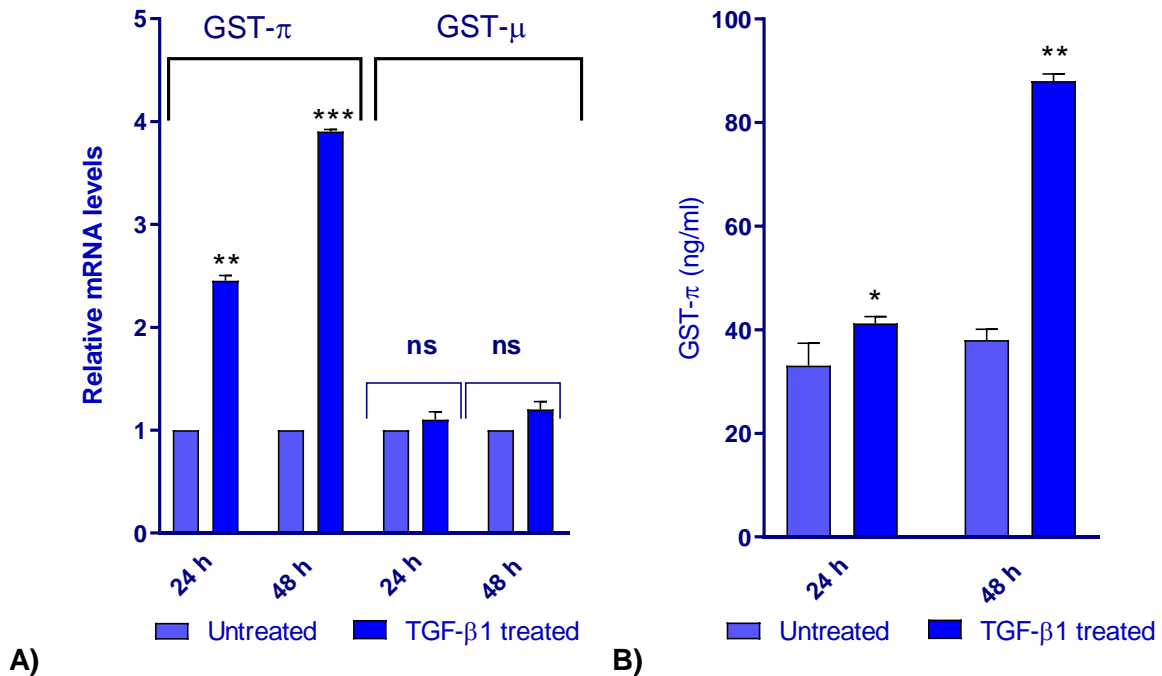


**Figure 4.11.** A) Relative mRNA levels of GST isoenzymes following treatment with TGF- $\beta$ 1. Relative expression was adjusted to the reference gene GAPDH. B) Protein level of GST- $\pi$  following treatment with TGF- $\beta$ 1. Data are represented as the mean  $\pm$  SEM. (\* $p < 0.05$ , \*\* $p < 0.01$  and \*\*\*\* $p < 0.0001$  vs control).

Protein levels of GST isoenzymes were also determined in both culture medium and cell lysates of TGF- $\beta$ 1 treated and non-treated cells. In accordance with the qRT-PCR analysis results, GST- $\pi$  protein levels were elevated ~2.5 fold upon treatment with TGF- $\beta$ 1 for 48 hours, while no significant changes in protein level of GST- $\mu$  was observed (Figure 4.11-A). As seen in Figure 4.11-B, GST- $\pi$  protein level slightly increased in non-treated cells, but this increase was not statistically significant ( $p > 0.05$ ). In HT-29 cells, GST- $\mu$  protein was not detectable, although HT-29 cells do not bear the null-genotype for GST- $\mu$  [236]. These results were in agreement with the study that evaluated GST- $\pi$  and GST- $\mu$  at the mRNA and protein levels in doxorubicin resistant colorectal adenocarcinoma cell lines (HT-29, LoVo, SW620, and Caco-2). According to the results, GST- $\pi$  was expressed at protein and mRNA levels whilst GST- $\mu$  expression was not detectable at the

protein and mRNA levels [237]. However, to our knowledge, this was the first study that assessed the correlation between expression and protein levels of GST- $\pi$  and GST- $\mu$  isoenzymes and EMT-associated drug resistance in colorectal cancer cells. TGF- $\beta$ 1 may activate multiple signaling pathways including p38MAPK, Erk1/2 and PI3-kinase and activation of these signaling pathways cause formation of stress conditions in the cells [238] Yang *et al.* [239] was reported that TNF- $\alpha$  induced F-actin stress fiber formation was inhibited by GST- $\pi$  by inhibition of F-actin reconstruction and TNF- $\alpha$  induction upregulated GST- $\pi$  expression. According to these results, it could be concluded that GST- $\pi$  expression may be upregulated to inhibit the TGF- $\beta$ 1 induced actin remodelling and F-actin stress fiber formation in mesenchymal phenotypes of HT-29 cells. However, GST- $\pi$  expression levels could not be sufficient to inhibit stress fiber formation due to long term exposure of TGF- $\beta$ 1.

#### 4.2.2. Treatment of Epithelial and Mesenchymal Phenotypes of HT-29 Cells with ETA

The calibration curves of ETA for both epithelial and mesenchymal phenotypes of HT-29 cells were constructed and IC<sub>50</sub> values were calculated as described in Section 3.2.2.3. IC<sub>50</sub> values were determined for only GST- $\pi$  due to lack of GST- $\mu$  activity. The calibration curves of % inhibition of GST- $\pi$  activity of epithelial phenotypes of HT-29 cells versus ETA concentration and % inhibition of GST- $\pi$  activity of mesenchymal phenotypes of HT-29 cells versus ETA concentration were shown in Figure 4.12. and 4.13., respectively.

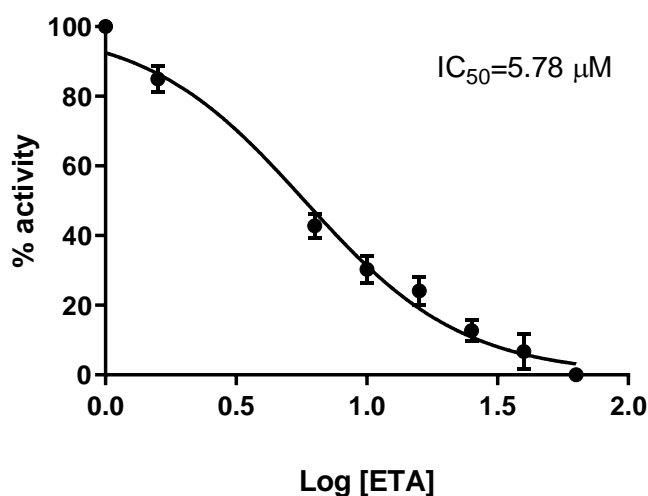


**Figure 4.12.** Determination of % activity of GST- $\pi$  activity following treatment with various concentrations of ETA for epithelial phenotype of HT-29 cells.

According to the results stated in Figure 4.12. and Figure 4.13.,  $IC_{50}$  values of ETA were 5.78  $\mu$ M and 7.08  $\mu$ M for GST- $\pi$  of epithelial phenotype and mesenchymal phenotype of HT-29 cells, respectively.  $IC_{50}$  value of ETA for GST- $\pi$  of mesenchymal phenotype was significantly higher than for GST- $\pi$  of epithelial phenotype of HT-29 cells ( $p < 0.01$ ). ~ 33% of increment in  $IC_{50}$  value for GST- $\pi$  of mesenchymal cells were observed. GST- $\pi$  protein levels were also evaluated after ETA treatment. Results suggested that ETA not only inhibited GST- $\pi$  catalytic activity but also affected GST- $\pi$  expression at posttranscriptional level (Figure 4.14). Protein levels of GST- $\pi$  in epithelial and mesenchymal phenotypes of HT-29 cells decreased 58% and 62%, respectively.

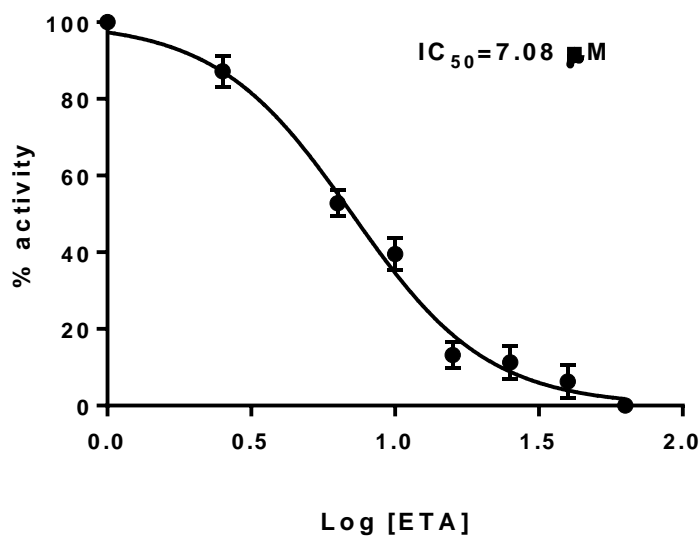


**Figure 4.13.** Determination of % activity of GST- $\pi$  activity following treatment with various concentrations of ETA for mesenchymal phenotype of HT-29 cells.

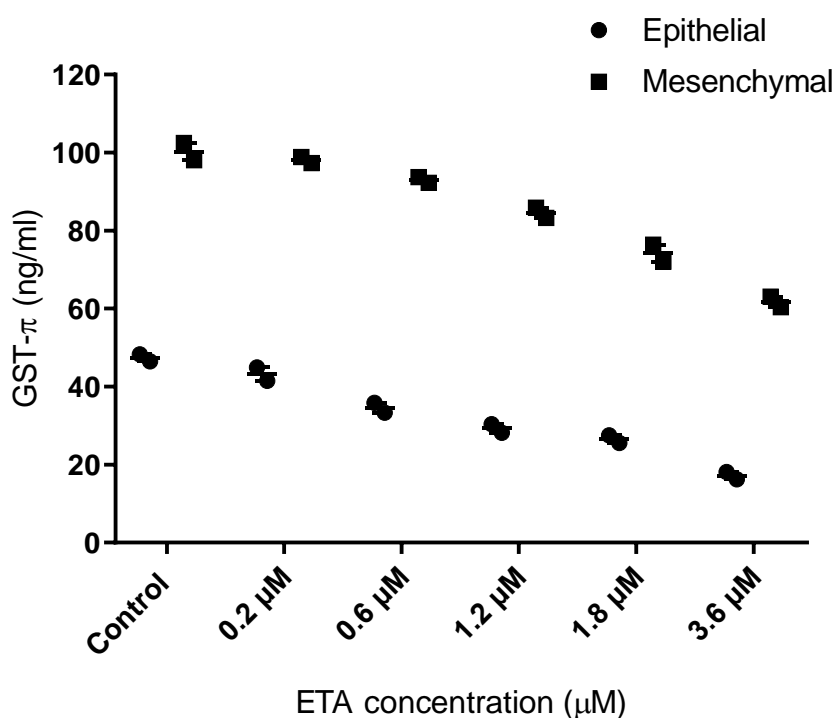


**Figure 4.14.** GST- $\pi$  protein levels after treatment with ETA at various concentrations. Data are represented as the mean $\pm$ SEM.

#### 4.2.3. Formation and Determination of Oxidative Stress in Epithelial and Mesenchymal Phenotype of HT-29 Cells

Cancer cells underwent EMT exhibit resistance to ROS-induced oxidative stress. Possible mechanisms for ROS-induced oxidative stress resistance in various cancer cell types are established in literature. However, there is no study that determines correlation between oxidative stress resistance and GST- $\pi$  expression in mesenchymal cells. To evaluate whether elevated GST- $\pi$  activity is responsible for resistance to ROS-induced oxidative stress in the mesenchymal phenotypes of HT-29 cells, oxidative stress was generated by H<sub>2</sub>O<sub>2</sub> exposure in both epithelial and mesenchymal phenotype of HT-29 cells and their responses to oxidative stress were evaluated in terms of GST- $\pi$  protein level as stated in the *Section 3.2.2.4*. For this purpose, epithelial and mesenchymal phenotype of HT-29 cells were exposed to varying concentrations of H<sub>2</sub>O<sub>2</sub> to assess the effect of different concentrations of H<sub>2</sub>O<sub>2</sub> on the cell viabilities of cells. The results demonstrated that epithelial phenotypes of HT-29 cells were more sensitive to H<sub>2</sub>O<sub>2</sub> cytotoxicity than mesenchymal forms of HT-29 cells. According to the results stated in Figure 4.15., a significant decrease in cell viability of epithelial phenotype of HT-29 cells at

concentrations  $>25 \mu\text{M}$  upon 1 hour treatment was observed. However, mesenchymal cells showed higher resistance with the detectable cytotoxic effect at higher concentrations of  $\text{H}_2\text{O}_2$ . The non-cytotoxic range of  $\text{H}_2\text{O}_2$  was 5-10  $\mu\text{M}$  and 5-50  $\mu\text{M}$  for epithelial and mesenchymal cells, respectively. Indeed, the cytotoxic effects of  $\text{H}_2\text{O}_2$  were relatively stable at higher levels of  $\text{H}_2\text{O}_2$  for mesenchymal cells. Extending the treatment time to 2 hours cause the significant reduction in epithelial cell viability ( $p<0.001$ ). Therefore, epithelial cell viability drastically decreased upon treatment with  $\text{H}_2\text{O}_2$  gradually above 25  $\mu\text{M}$ . Taken together, these results suggested that  $\text{H}_2\text{O}_2$  exert cytotoxic effect on epithelial HT-29 cells in a dose and time dependent manner. Similar results were reported for epithelial colorectal cancer cells [240, 241]. In contrast to significant reduction in cell viability as observed in epithelial phenotype of HT-29, statistically significant ( $p<0.05$ ) increase in viability of mesenchymal phenotypes upon exposure to  $\text{H}_2\text{O}_2$  for 2 hours, even in high doses, was observed (Figure 4.16). These results confirmed the adaptation potential of mesenchymal phenotypes of HT-29 cells to oxidative stress agents.

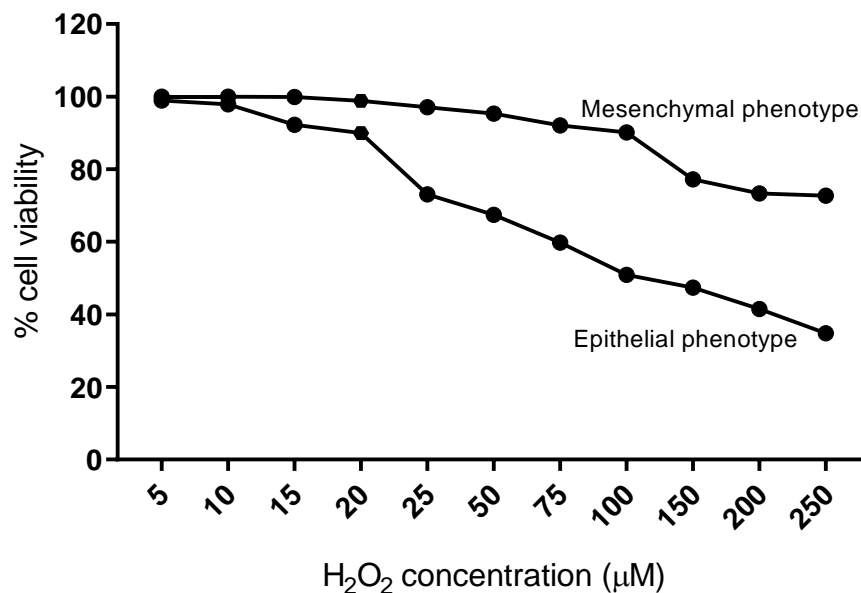


**Figure 4.15.** % cell viability of epithelial and mesenchymal phenotype of HT-29 cells following treatment with various concentrations of  $\text{H}_2\text{O}_2$  for 1 hour. Values for MTT assay were converted into percentage of control (control=100%).

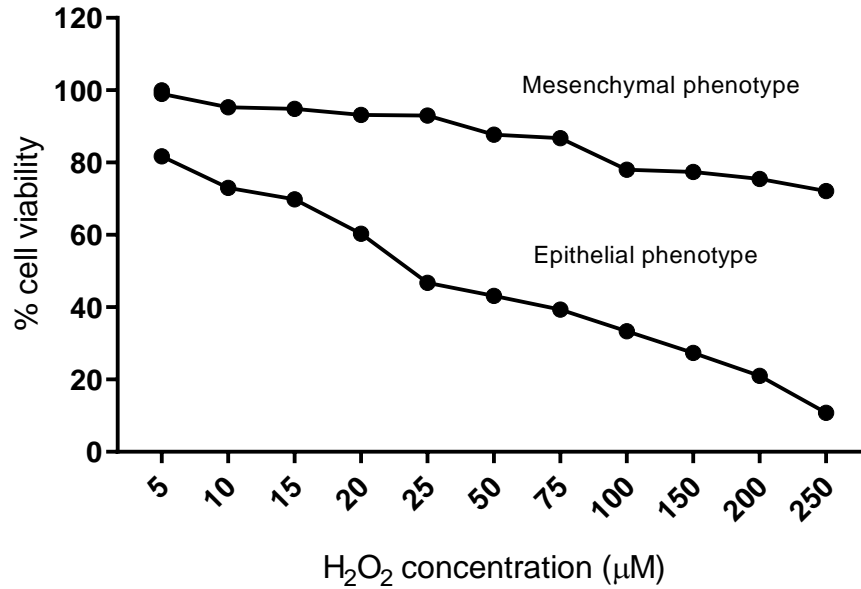


**Figure 4.16.** % cell viability of epithelial and mesenchymal phenotypes of HT-29 cells following treatment with various concentrations of H<sub>2</sub>O<sub>2</sub> for 2 hours. Values for MTT assay were converted into percentage of control (control=100%).

After the detection of cytotoxic doses of H<sub>2</sub>O<sub>2</sub>, oxidative stress was induced in both epithelial and mesenchymal HT-29 cells by the treatment with H<sub>2</sub>O<sub>2</sub> at concentrations <25 μM for 1 hour. H<sub>2</sub>O<sub>2</sub> treatment results in lipid peroxidation and malondialdehyde (MDA) can be formed as an end product during peroxidation process [242, 243]. Since MDA has been widely used for many years as a stable and convenient biomarker for lipid peroxidation [244, 245], oxidative damage induced by H<sub>2</sub>O<sub>2</sub> was assessed by quantifying MDA in this study. Figure 4.17. showed the MDA levels in the epithelial and mesenchymal phenotype of HT-29 cells. MDA levels in both epithelial phenotype and mesenchymal phenotypes of HT-29 cells were significantly elevated upon treatment with hydrogen peroxide (p<0.01). The results also revealed a clear dose dependent increase in the production of MDA in both phenotypes of HT-29 cells. As compared to control, exposure to 20 μM H<sub>2</sub>O<sub>2</sub> resulted in ~ 95% increase in MDA levels in epithelial phenotypes of HT-29 cells. However, MDA levels of mesenchymal phenotype were significantly lower compared to epithelial phenotype (Ψ<0.001). These results indicated that transition from epithelial phenotype to mesenchymal phenotype resulted in resistance to oxidative stress.



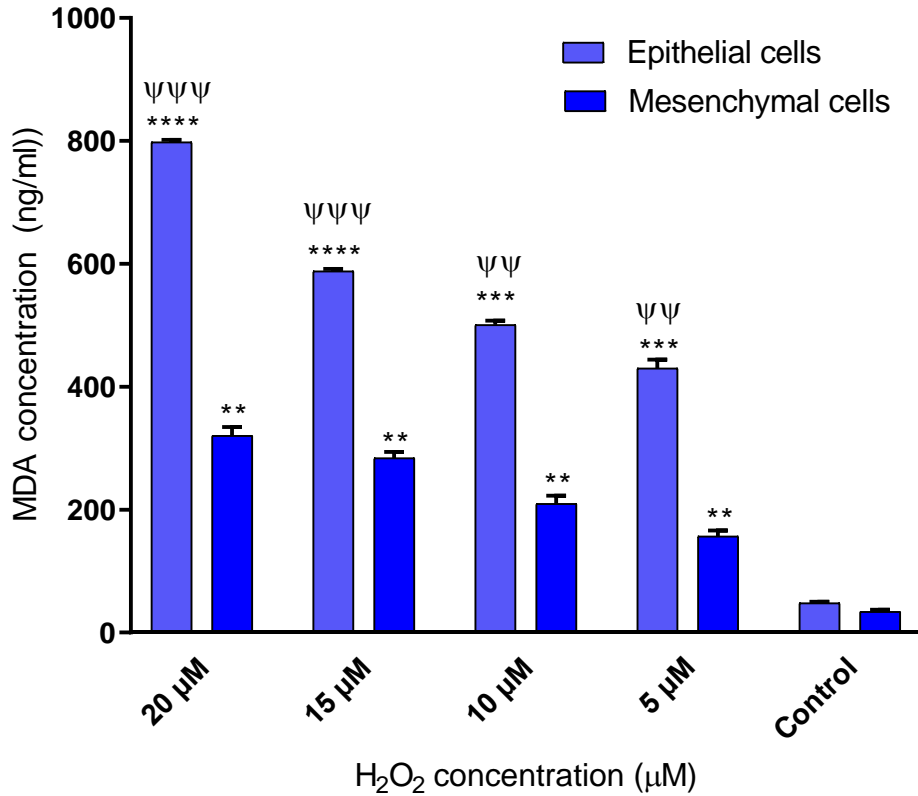


**Figure 4.17.** MDA levels of epithelial and mesenchymal phenotypes of HT-29 cells following treatment with various concentrations of H<sub>2</sub>O<sub>2</sub> for 2 hours. Data are represented as the mean±SEM. (\*p<0.05, \*\*p<0.01 and \*\*\*\*p<0.0001 vs control; ΨΨ p<0.01 and ΨΨΨ p<0.001 vs mesenchymal phenotypes).

To further determine whether GST-π is related with increased adaptability of mesenchymal phenotypes of HT-29 cells to ROS-induced oxidative stress, GST-π expression and protein levels were investigated. It was clearly seen from the results that GST-π expression was exponentially increased following H<sub>2</sub>O<sub>2</sub> treatment in mesenchymal phenotypes of HT-29 cells (Figure 4.18). mRNA levels of GST-π in epithelial phenotypes of HT-29 cells increased at a lower grade. Statistically important difference in GST-π expression patterns of epithelial and mesenchymal phenotypes of HT-29 cells was observed even at the lowest concentration of H<sub>2</sub>O<sub>2</sub>.

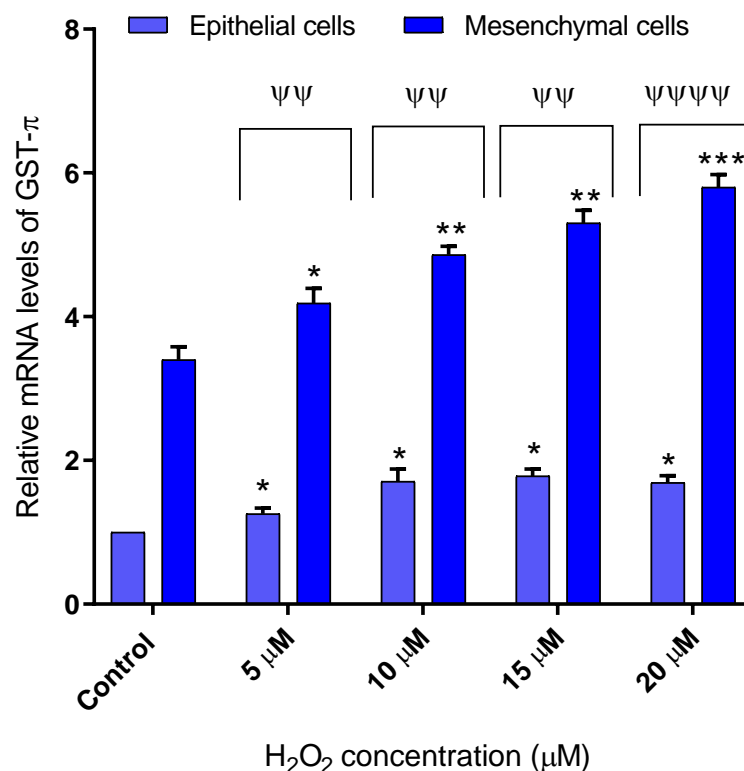


**Figure 4.18.** Relative mRNA levels of GST- $\pi$  following treatment with different concentrations of H<sub>2</sub>O<sub>2</sub>. Data are represented as the mean $\pm$ SEM. (\*p<0.05, \*\*p<0.01, p<0.001 and \*\*\*\*p<0.0001 vs control.  $\Psi\Psi$ p<0.01,  $\Psi\Psi\Psi$ p<0.001 and  $\Psi\Psi\Psi\Psi$ p<0.0001 mesenchymal cells vs epithelial cells).

#### 4.2.4. Treatment of Oxidative Stress Generated Epithelial and Mesenchymal Phenotypes of HT-29 Cells with GST Inhibitor ETA

Epithelial and mesenchymal phenotypes of HT-29 cells were treated with various concentrations of ETA to determine if any difference between IC<sub>50</sub> values of ETA in phenotypes of HT-29 cells. Figure 4.19. and Figure 4.20. showed the calibration curve of ETA for epithelial and mesenchymal phenotypes of HT-29 cells, respectively. According to calibration curve equations, IC<sub>50</sub> values of ETA for epithelial and mesenchymal phenotypes of HT-29 cells were 2.09  $\mu$ M and 2.99  $\mu$ M, respectively. When these results were compared to results obtained from Section 4.2.2., it is clearly seen IC<sub>50</sub> values of ETA is higher in oxidative stress generated phenotypes of HT-29 cells than nontreated cells, suggesting that GST- $\pi$  protein levels of both phenotypes cells increased due to ROS-induced oxidative stress. However, mesenchymal phenotypes of HT-29 cells showed much more increased GST- $\pi$  activity.

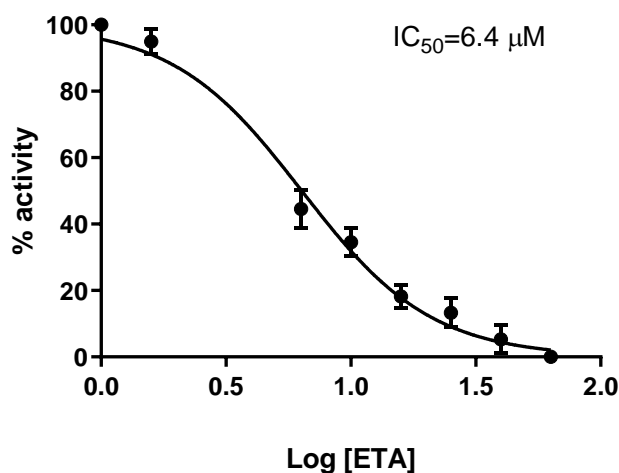


**Figure 4.19.** Determination of % GST- $\pi$  activity following treatment with various concentrations of ETA for oxidative stress generated epithelial phenotypes of HT-29 cells.

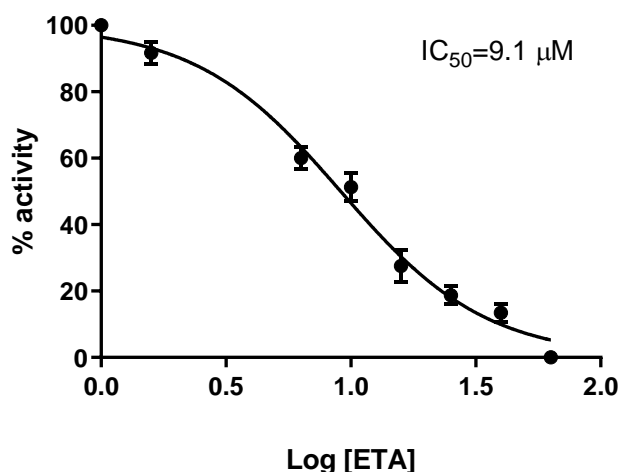


**Figure 4.20.** Determination of % GST- $\pi$  activity following treatment with various concentrations of ETA for oxidative stress generated mesenchymal phenotype of HT-29 cells.

#### 4.3. Preparation of GST Inhibitor ETA Loaded And Mesenchymal Phenotype Targeted Nanoparticles

##### 4.3.1. Quantification of ETA and HPLC Method Validation

Quantitative determination of ETA was performed as described in *Section 3.2.3.1*. Figure 4.21. represents the chromatogram for ETA. Under chromatographic conditions used for the analysis of ETA, the retention time was 7.4 minutes.

#### 4.3.1.1. Construction of Calibration Curve

ETA calibration curve was constructed according to the method described in *Section 3.2.3.1*. The calibration curve was given in Figure 4.21. The slope of this curve was derived from different series which were calculated along with intercept and correlation coefficient as can be seen in Table 4.1.

**Table 4.1.** Linear regression data obtained from HPLC analysis for ETA

<b>Parameters</b>	
Concentration Range	2.5 µg/ml - 200 µg/ml
Slope	0.3963
Intercept	0.0069
Correlation Coefficient	0.999

#### **Linearity**

Linearity was evaluated with standard solutions of ETA (2.5 to 200 µg/µL) as described in *Section 3.2.3.1*. Linearity of the assay procedure was determined by calculation of a regression line. Concentrations of ETA standard solutions were calculated from the resulting peak heights and the regression equation of the calibration curve [220].

Linear relation between ETA concentration and peak area was confirmed by the regression analysis from Table 4.1. The calibration curves constructed for ETA showed that the analytical method was linear from 2.5 to 200 µg/mL. ETA standard solutions displayed good linearity in this range. Coefficient also proves the linearity. A linearity correlation coefficient above 0.999 is acceptable for HPLC methods of major component analysis. The square correlation coefficient ( $R^2$ ) was found 0.999 which was found to very close to 1, representing absolute linearity.

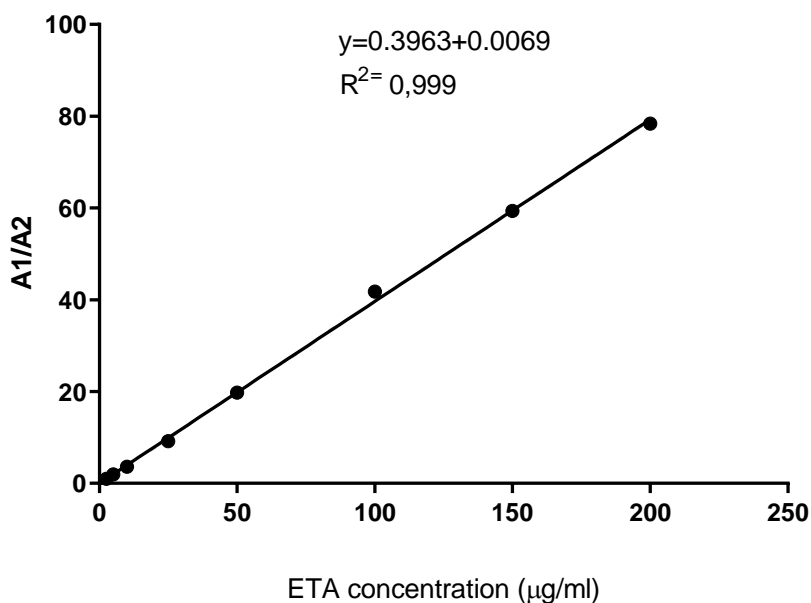


**Figure 4.21.** Calibration Curve of ETA.

### **Accuracy**

Accuracy is defined as the consistency between the found value and the true concentration value which is independently determined. As described in *Section 3.2.3.1.*, accuracy is determined by replicate analysis of samples containing known amounts (5, 50 and 150 µg/mL) of ETA covering the specified range and representing low, medium and high concentrations in that specific range. The accuracy of the method was evaluated considering the recovery. Based on the calculated ETA concentrations and the known composition of ETA, the percent recovery of ETA was calculated. Considering each point concentration of ETA, the average recovery was found within the range 99.86 – 100.5% (Table 4.2).

### **Precision**

As stated in *Section 3.2.3.1.* precision of an analytical procedure expresses the closeness of agreement between a series of measurements and was measured as repeatability, reproducibility and intermediate precision. The precision of an analytical method is usually expressed as coefficient of variation of a series of measurements [223].

Repeatability, which is also termed intra-assay precision, was determined by assaying replicates of the same concentration of ETA (20 µg/mL) in a single run.

Assay precision was calculated as Coefficient of Variation (CV) expressed as a percentage of the mean observed concentrations and the observed data were given in Table 4.3.

**Table 4. 2.** Accuracy data for ETA

<b>Samples</b>	<b>5 µg/mL Recovery (%)</b>	<b>50 µg/mL Recovery (%)</b>	<b>150 µg/mL Recovery (%)</b>
<b>1</b>	100.6167	100.0042	100.1462
<b>2</b>	100.4004	99.7921	100.2713
<b>3</b>	99.8453	99.8161	99.7239
<b>4</b>	101.0338	99.7728	99.8222
<b>5</b>	100.4942	99.9216	100.5354
<b>Mean</b>	100.4781	99.8614	100.0998
<b>Standart deviation</b>	0.0492	0.4970	0.0424
<b>CV</b>	0.0489	0.4970	0.0420

**Table 4.3.** Data of repeatability for ETA

<b>Sample</b>	<b>Calculated Concentration (µg/ml)</b>
<b>1</b>	19.7844
<b>2</b>	19.8037
<b>3</b>	19.6892
<b>4</b>	19.8604
<b>5</b>	19.7321
<b>6</b>	19.8356
<b>Mean</b>	19.7842
<b>SD</b>	0.0585
<b>CV</b>	0.0034

#### 4.3.2. Synthesis and Characterization of mPEG–PLGA–SS–ETA

mPEG–PLGA–SS–ETA was synthesized as described in Section 3.2.3.3. mPEG–PLGA–SS was conjugated to ETA covalently via carbon-nitrogen bond. The resulting polymer was characterized by  $^1\text{H-NMR}$  and FT-IR analysis. Figure 4.22. showed  $^1\text{H-NMR}$  spectra of mPEG–PLGA–SS–ETA. According to NMR data, the peaks at 7.14 and 7.28 ppm in  $^1\text{H-NMR}$  spectrum correspond to aromatic protons of ETA, H on the phenyl ring. Moreover, peaks at 5.8 and 6.2 are related to protons of the phenyl ring, respectively. These results indicated that ETA was successfully conjugated to mPEG–PLGA. Figure 4.23. showed the FT-IR spectra of mPEG–PLGA–SS–ETA. The absorption around  $1640\text{ cm}^{-1}$  indicated the presence of phenyl ring. Therefore, the peak at around  $3350\text{ cm}^{-1}$  showed  $-\text{NH}$  stretch. Furthermore, the results showed the successful conjugation between ETA and mPEG–PLGA.

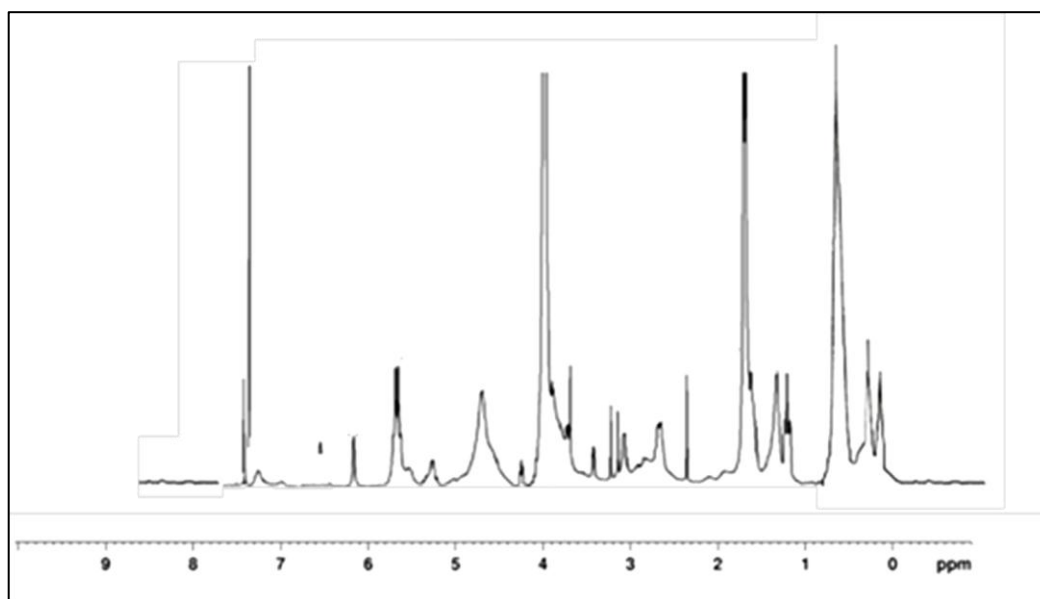


**Figure 4.22.** NMR analysis of mPEG–PLGA–SS–ETA.

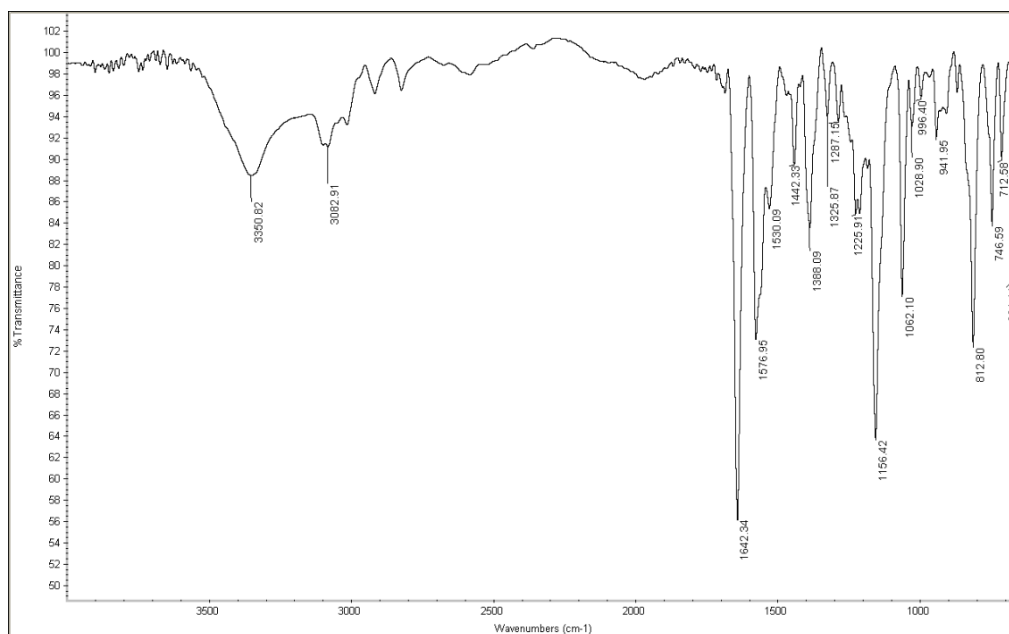


**Figure 4.23.** FT-IR spectrum of mPEG-PLGA-SS-ETA.

### 4.3.3. Preparation of Blank Nanoparticles

In the field of nanobiology, mean particle size is a currently important attribute of nanoparticulate drug delivery systems [246-248]. Mean particle size impacts both physicochemical characteristics of nano-sized systems such as encapsulation efficiency, drug release profile and stability, and *in vivo* pharmacokinetics in terms of cellular uptake and biodistribution throughout the body [249, 250]. Furthermore, as mean particle size affects the half-life of nanoparticles in the blood circulation, it can also influence its ability to permeate through tissue. In addition to mean particle size, PDI and surface charge have also important influence on both *in vitro* profile and *in vivo* behaviour of nanoparticles [251-253].

In this study, various formulation parameters were evaluated in order to modulate physicochemical characteristics of nanoparticles and to establish an optimal formulation of PLGA and PLGA-*b*-PEG nanoparticles. Firstly, the effect of polymer concentration on physicochemical characteristics of PLGA and PLGA-*b*-PEG nanoparticles were evaluated. Range of concentrations was recognized from studies previously reported. As represented in the Table 4.4., the mean particle size significantly increased as a result of increasing polymer concentration ( $p < 0.01$ ) whereas no significant change was observed for PDI ( $p > 0.05$ ) for both PLGA and PLGA-*b*-PEG nanoparticles. The increase in the mean particle size can be



explained by increasing viscosity of organic phase. Organic phase with higher polymer concentrations resulted in more viscous solution. As a result of higher viscosity, net shear stress reduces and polymer-polymer interactions increases, which causes the formation of larger particles. Reduction in polymer concentration decreases the organic phase viscosity as well as mean particle size [254-258]. The results were well corroborated with studies reported by Morales-Cruz *et al.* [259], Cheng *et al.* [260], Halayqa *et al.* [261] and Sharma *et al.* [262].

Results also revealed that all formulations had a negative  $\zeta$  potential value, due to the PLGA and PLGA-*b*-PEG features, indicating good particle stability in solution. This was due to the presence of carboxylic groups deprotonated at the experimental conditions. The  $\zeta$  potential values of the NPs obtained by nanoprecipitation ranges between  $-20$  and  $-30$  mV.

**Table 4. 4.** The effect of polymer concentration on particle size, polydispersity index and  $\zeta$ -potential of PLGA and PLGA-*b*-PEG nanoparticles. Data was represented as mean  $\pm$  SEM values of three independent batches.

Polymer concentration	Formulations	Particle Size (nm)	Polydispersity Index (PI)	Zeta Potential (mV)
2%	PLGA nanoparticles	365.69 $\pm$ 4.74	0.31 $\pm$ 0.19	-27.3 $\pm$ 4.27
	PLGA-PEG nanoparticles	240.1 $\pm$ 6.88	0.23 $\pm$ 0.032	-19.6 $\pm$ 4.71
1%	PLGA nanoparticles	310.3 $\pm$ 6.44	0.29 $\pm$ 0.13	-25.8 $\pm$ 1.38
	PLGA-PEG nanoparticles	195.99 $\pm$ 1.21	0.19 $\pm$ 0.023	-16.09 $\pm$ 2.29
%0.5	PLGA nanoparticles	280.43 $\pm$ 3.32	0.28 $\pm$ 0.05	-25.2 $\pm$ 3.10
	PLGA-PEG nanoparticles	180.32 $\pm$ 0.82	0.14 $\pm$ 0.041	-14.62 $\pm$ 2.63

In addition to the effect of polymer concentration, impact of surfactant concentration was also evaluated. Surfactants are not required for preparation of nanoparticles but addition of surfactants helps to preserve the nanoparticle suspensions from agglomeration, especially in long storage periods [263]. As represented in Table 4.5., mean particle size was significantly decreased by the

addition of appropriate amount of surfactant. This might be due to the concentration of PF-68 concentration resulted in reducing the surface tension and facilitating particle partition. However, nanoparticles' size increased while increasing surfactant concentration from 0.1% to 1%. Stabilizing agents in the aqueous medium interacts with nanoparticle surface and their adsorption to the surface generally results in increasing in the size. But, PF-68 is a neutral stabilizing agent with a low molecular weight and its interaction with nanoparticles' surface were relatively lower than positively or negatively charged stabilizers [264]. It could be concluded that increase in the surfactant concentration can lead to more viscous aqueous phase, resulting a poorer dispersibility of the organic phase into the aqueous phase. The results were in agreement with those reported by Tekko *et al.* [263] for the preparation of polymeric nanoparticles by nanoprecipitation method using polyvinyl alcohol (PVA) as a surfactant. Nanoparticles were also evaluated in terms of zeta potential. Because of its neutral nature, PF-68 had no significant influence on the surface charges of nanoparticles.

**Table 4. 5.** Effect of surfactant concentration on particle size, polydispersity index and  $\zeta$ -potential of PLGA and PLGA-*b*-PEG nanoparticles. Data was represented as mean $\pm$ SEM values of three independent batches.

Surfactant concentration	Formulations	Particle Size (nm)	Polydispersity Index (PI)	Zeta Potential (mV)
-	PLGA nanoparticles	285.64 $\pm$ 3.12	0.33 $\pm$ 0.25	-26.5 $\pm$ 3.41
	PLGA-PEG nanoparticles	190.76 $\pm$ 1.54	0.18 $\pm$ 0.14	-12.5 $\pm$ 3.81
0.1%	PLGA nanoparticles	278.49 $\pm$ 2.61	0.15 $\pm$ 0.10	-27.1 $\pm$ 0.46
	PLGA-PEG nanoparticles	165.28 $\pm$ 0.83	0.11 $\pm$ 0.04	-14.6 $\pm$ 3.93
0.5%	PLGA nanoparticles	297.0 $\pm$ 6.63	0.25 $\pm$ 0.18	-26.9 $\pm$ 4.2
	PLGA-PEG nanoparticles	196.78 $\pm$ 5.27	0.18 $\pm$ 0.062	-14.9 $\pm$ 3.05
1%	PLGA nanoparticles	310 $\pm$ 11.75	0.28 $\pm$ 0.09	-28 $\pm$ 4.54
	PLGA-PEG nanoparticles	201.6 $\pm$ 4.10	0.18 $\pm$ 0.053	-14.3 $\pm$ 0.13

The effect of organic phase to aqueous phase volume ratio was examined at a constant polymer and surfactant concentration (0.5 % and 0.1 %, respectively). The determined volume ratios were in accordance with the previously reported studies [265, 266]. When organic phase to aqueous phase volume ratio was varied during formulation process, inversely proportional increase in mean size of nanoparticles was observed (Table 4.6). The increase in aqueous phase volume led to reduction in particle size due to increase of dispersion ability of the water-soluble organic solvent and polymer in the aqueous phase, resulting smaller particles. Thus, larger particle size was obtained for formulations containing less aqueous phase. The obtained results are in accordance with the results of studies reported by Fonseca et al [265], Lancheros et al [266], Peltonen et al [267] and Higuchi et al [268].

**Table 4.6.** The effect of organic phase to aqueous phase ratio (v/v) on particle size, polydispersity index and  $\zeta$ -potential of PLGA and PLGA-*b*-PEG nanoparticles. Data was represented as the mean $\pm$ SEM of three independent batches.

Organic phase:aqueous phase (v/v)	Formulations	Particle Size (nm)	Polydispersity Index (PI)	Zeta Potential (mV)
1:1	PLGA nanoparticles	306.25 $\pm$ 4.73	0.32 $\pm$ 0.12	-26.3 $\pm$ 0.65
	PLGA-PEG nanoparticles	179.82 $\pm$ 6.09	0.19 $\pm$ 0.06	-13.8 $\pm$ 4.23
1:2	PLGA nanoparticles	281.26 $\pm$ 3.93	0.21 $\pm$ 0.09	-26.03 $\pm$ 0.41
	PLGA-PEG nanoparticles	161.34 $\pm$ 2.37	0.16 $\pm$ 0.05	-14.08 $\pm$ 2.56
1:5	PLGA nanoparticles	224.6 $\pm$ 2.79	0.18 $\pm$ 0.04	-25.7 $\pm$ 2.9
	PLGA-PEG nanoparticles	116.23 $\pm$ 2.78	0.12 $\pm$ 0.021	-13.7 $\pm$ 2.0

#### 4.3.4. Preparation of Drug Loaded Nanoparticles

According to results obtained from pre-formulation studies of blank PLGA and PLGA-*b*-PEG nanoparticles, 0.5 % w/v polymer, 0.1 % v/v surfactant and 1:5 organic to aqueous phase volume ratio were selected as parameters for ETA loaded formulations. Various concentrations of ETA (10 mg, 25 mg and 50 mg)

were loaded to optimized formulations and the effect of ETA concentration on physicochemical properties of PLGA and PLGA-*b*-PEG nanoparticles were evaluated in terms of particle size, polydispersity index and  $\zeta$ -potential. As shown in Table 4.7., particle size increased with the drug concentration.

**Table 4. 7.** The effect of drug concentration (w/v) on particle size, polydispersity index and  $\zeta$ -potential of PLGA and PLGA-*b*-PEG nanoparticles. Data was represented as the mean $\pm$ SEM values of three independent batches.

Drug concentration	Formulations	Particle Size (nm)	Polydispersity Index (PI)	Zeta Potential (mV)
2 mg/ml	PLGA nanoparticles	292.55 $\pm$ 3.22	0.29 $\pm$ 0.004	-25.7 $\pm$ 1.73
	PLGA-PEG nanoparticles	127.19 $\pm$ 2.18	0.18 $\pm$ 0.03	-13.2 $\pm$ 3.50
5 mg/ml	PLGA nanoparticles	295.50 $\pm$ 4.07	0.28 $\pm$ 0.05	-22.31 $\pm$ 1.52
	PLGA-PEG nanoparticles	128.51 $\pm$ 1.63	0.17 $\pm$ 0.09	-13.11 $\pm$ 3.26
10 mg/ml	PLGA nanoparticles	321.42 $\pm$ 7.42	0.32 $\pm$ 0.10	-19.2 $\pm$ 1.3
	PLGA-PEG nanoparticles	163.72 $\pm$ 5.82	0.20 $\pm$ 0.01	-10.6 $\pm$ 3.7

The mean particle size of PLGA and PLGA-*b*-PEG nanoparticles increased from 292.55 $\pm$ 3.22 to 321.42 $\pm$ 7.42 and from 127.19 $\pm$ 2.18 to 163.72 $\pm$ 5.82, respectively by increasing the drug concentration from 2 mg/ml to 10 mg/ml. Shifts in the PDI of nanoparticles were also observed with the increase of drug concentration. Nanoparticles with different initial drug concentration were compared to blank nanoparticles in terms of PDI values. In PLGA-*b*-PEG nanoparticles, PDI of formulation increase from 0.154 for the 1% loading to 0.203 for the 5% loading and 0.212 for the 10% loading. However, no significant difference in either particle size or PDI between 2 mg/ml and 5 mg/ml of drug concentration was observed ( $p > 0.05$ ). The drug concentration in nanoparticles should be kept as high as possible in order to achieve desirable concentration for *in vitro* inhibition studies. Therefore, 5 mg/ml of drug concentration was selected for further studies. These

findings are consistent with the research showing that docetaxel encapsulated PLGA-*b*-PEG nanoparticles' size and PDI increased with increased concentration of docetaxel [260]. Reduction in the  $\zeta$ -potential of both ETA loaded PLGA and PLGA-*b*-PEG nanoparticles compared to blank nanoparticles was observed because of slight positive charge of ETA at neutral pH ranges. The results were directly in line with previous finding [269].

#### **4.3.5. Preparation and Characterization of mPEG–PLGA–SS–ETA Nanoconjugates**

Drug-polymer nanoconjugates are remarkable delivery systems in nanomedicine. Their functional capabilities to deliver multiple agents with different chemical features *in vitro* or *in vivo* provide much more benefits than nanoparticles.

Nanoconjugates were prepared from mPEG–PLGA–SS–ETA by single emulsion-solvent evaporation method as describe in the *Section 3.2.3.6*. Influence of polymer concentration on the physicochemical properties of nanoconjugates was evaluated in terms of particle size, polydispersity index and  $\zeta$ -potential. Table 4.8 showed the physicochemical properties of nanoconjugates. As it can be clearly seen from the results, mean particle size of nanoconjugates was highly dependent on polymer concentration. Reduction in the polymer concentration resulted in smaller formulations. The smallest formulation was obtained with 2% (w/v) of polymer concentration. As mentioned in the *Section 4.3.3.*, it would be explained by viscosity of the organic phase. Increase in the polymer concentration also increased the viscosity of organic phase followed by reduction in the dispersion rate, resulting in precipitation of larger particles. Polymer concentration had significant impact also on PDI of nanoconjugates ( $p < 0.01$ ). Decrease in the polymer concentration led to formation of highly monodispersed nanoparticles. No significant effect on the  $\zeta$ -potential was observed ( $p > 0.05$ ). Hence, nanoconjugates were prepared by 2% (w/v) of initial polymer concentration for further studies.

**Table 4. 8.** Effect of polymer concentration (w/v) on particle size, polydispersity index and  $\zeta$ -potential of PLGA and PLGA-*b*-PEG nanoparticles. Data was represented as the mean $\pm$ SEM values of three independent batches.

Polymer concentration	Formulations	Particle Size (nm)	Polydispersity Index (PI)	Zeta Potential (mV)
2%	mPEG-PLGA-SS-ETA Nanoconjugate	116.55 $\pm$ 1.02	0.114 $\pm$ 0.008	-8.78 $\pm$ 0.30
2.5%	mPEG-PLGA-SS-ETA Nanoconjugate	198.47 $\pm$ 3.21	0.26 $\pm$ 0.051	-7.43 $\pm$ 0.49
3%	mPEG-PLGA-SS-ETA Nanoconjugate	252.23 $\pm$ 1.78	0.31 $\pm$ 0.006	-7.12 $\pm$ 0.9

#### 4.3.6. Morphological Analysis of Nanoformulations

The morphologies of nanoformulations were investigated by scanning electron microscopy (SEM). Mean particle size results obtained by Zetasizer analysis were also confirmed by SEM. Figure 4.24. showed SEM images of the nanoformulations. It could be clearly seen that nanoformulations exhibited spherical morphology, with particle size ranging between 150-200 nm. These results were in agreement with DLS results.

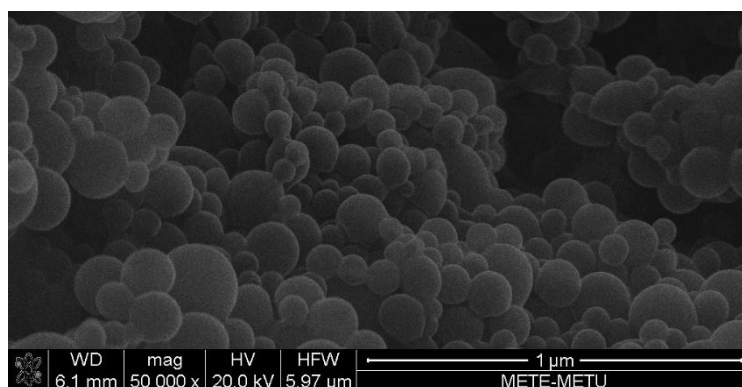


**Figure 4.24.** Scanning electron microphotographs of ETA loaded PLGA-*b*-PEG nanoparticles and mPEG-PLGA-SS-ETA nanoconjugates.

#### 4.3.7. Entrapment Efficiency and Loading Capacity of Nanoformulations

Entrapment efficiency and loading capacity were evaluated for both nanoformulations. As seen in Table 4.9., increased entrapment efficiency and loading capacity were observed for mPEG–PLGA–SS–ETA nanoconjugates than PLGA-*b*-PEG nanoparticles. In other words, conjugation of ETA with the polymer enhanced the loading capacity as well as the entrapment efficiency. This could be due to self-assembly ability of the nanoconjugate. Since the therapeutic agent is present during the formation of self-assembled formulations, loss of drug is minimized and drug loading capacity increases [270, 271]. mPEG–PLGA–SS–ETA is an amphiphilic polymer. mPEG segment of the conjugate functions as the hydrophilic part while PLGA–SS–ETA block acts as the hydrophobic part. Under aqueous conditions, this conjugate could self-assembled into nanosized micelle due to its amphiphilic nature [269]. Conjugation of polymers with therapeutic agents offers advantages compared to the physical encapsulation of therapeutics in an inert carrier in terms of high drug-loading nanomedicines as well as their capabilities to deliver multiple agents because of self-assembly ability [271]. These results were in great accordance with the studies reported by Shen *et al.* [272], Gou *et al.* [273] and Zhang *et al.* [274]. Similarly, Zhou *et al.* [275] conjugated the polyacrylate amphiphiles with the camptothecin, a hydrophobic drug, to enhance the loading capacity. The resulting amphiphilic conjugate self-assembled into micelles and a high drug-loading content of 60 % for camptothecin was obtained.

**Table 4. 9.** The effect of drug concentration (w/v) on particle size, polydispersity index and  $\zeta$ -potential of nanoformulations. Data was represented as the mean $\pm$ SEM values of three independent batches.

Formulations	Encapsulation efficiency (%)	Loading capacity (%)
PLGA-PEG nanoparticles	33.6 $\pm$ 2.2	24 $\pm$ 3
mPEG–PLGA–SS–ETA Nanoconjugate	63.4 $\pm$ 6.1	53 $\pm$ 5

#### 4.3.8. *In vitro* Release Studies

*In vitro* release studies are crucial to evaluate the therapeutic efficacy and *in vivo* behaviour of nanomedicines [276, 277]. In release studies, solubility of the therapeutic agent is an important parameter for its diffusion across the dialysis membrane [278, 279]. Hence, *in vitro* release profiles of both PLGA-*b*-PEG nanoparticles and PEG-PLGA-SS-ETA nanoconjugates were investigated by dialysis method in two different release medium. Since ETA is soluble in ethanol, ethanol:PBS buffer was selected as the release medium. As extended studies indicated elevated GSH levels in cancer cells [190, 280, 281], the effect of GSH on release kinetics of nanoformulations were assessed. Therefore, ethanol:PBS buffer with 10 mM GSH was also evaluated. The measured acidic pH of extracellular fluid of solid tumors has extensively been documented for a few decades, combined with biological backgrounds of this observation. The acidic pH is now regarded as a phenotype of solid tumors for their growth and invasiveness. This finding has prompted investigators to fabricate pH-sensitive carriers by decorating the surface with carboxylic groups. Based on their findings, at pH 6.8 and 6.4 the pH-sensitive nanoparticles aggressively bounded to tumor cells. So, release medium with different pH values were also evaluated. Figure 4.25.-4.28. show cumulative ETA release from nanoformulations as a function of time. As expected, a biphasic release pattern was observed for all formulations with an initial burst effect followed by extended release phase. Results also suggested that the release rate of ETA from nanoconjugates were increased with the presence of GSH. 55.50% of ETA was released from mPEG-PLGA-SS-ETA nanoconjugates in the first 8 hours in the medium with GSH at pH 6.8. However, almost the same amount of ETA was released during 18 hours in the medium with GSH. These results were attributed to cleavage of the disulfide bonds in the nanoconjugate by GSH [282]. However, GSH had no significant effect on the PLGA-*b*-PEG nanoparticles' release pattern. PLGA-*b*-PEG nanoparticles released ~ 60% of ETA within 24 hours either with or without GSH and its release remained up to 5 days at pH 7.4. This initial burst effect of PLGA-*b*-PEG nanoparticles might be due to the drug that was adsorbed or close to the surface of the nanoparticles [283]. Moreover, PLGA-*b*-PEG nanoparticles could be degraded due to the hydrophilic character of PEG chain [284]. Similar results were reported by Davaran *et al.* [285], Hines *et al.* [286] and Amin *et al.* [287].



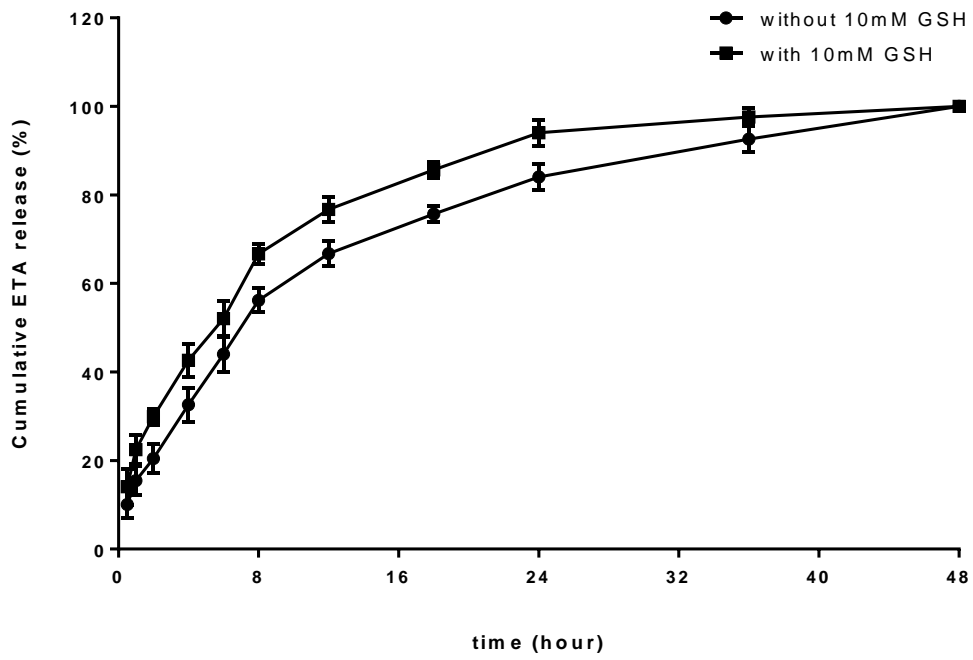


Figure 4.25. *In vitro* release profile of nanoparticles at pH 6.8.

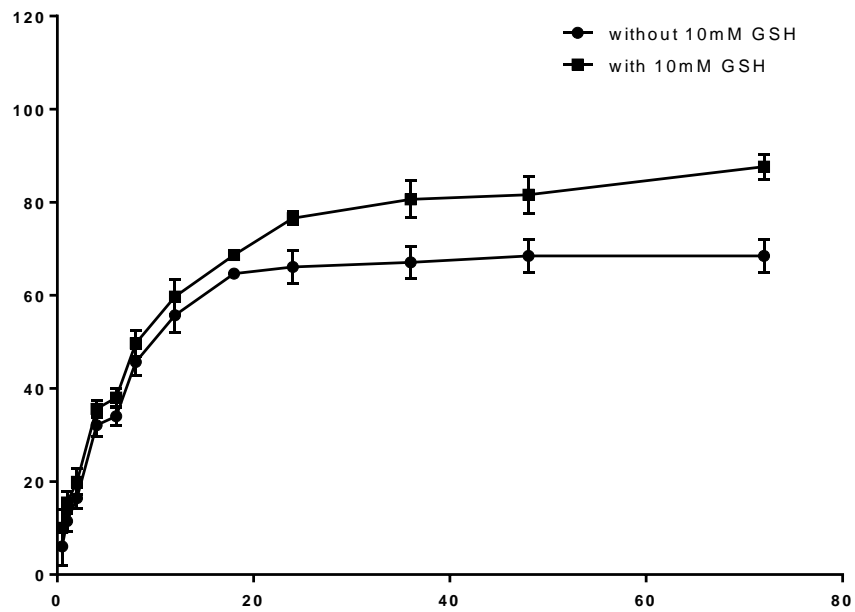
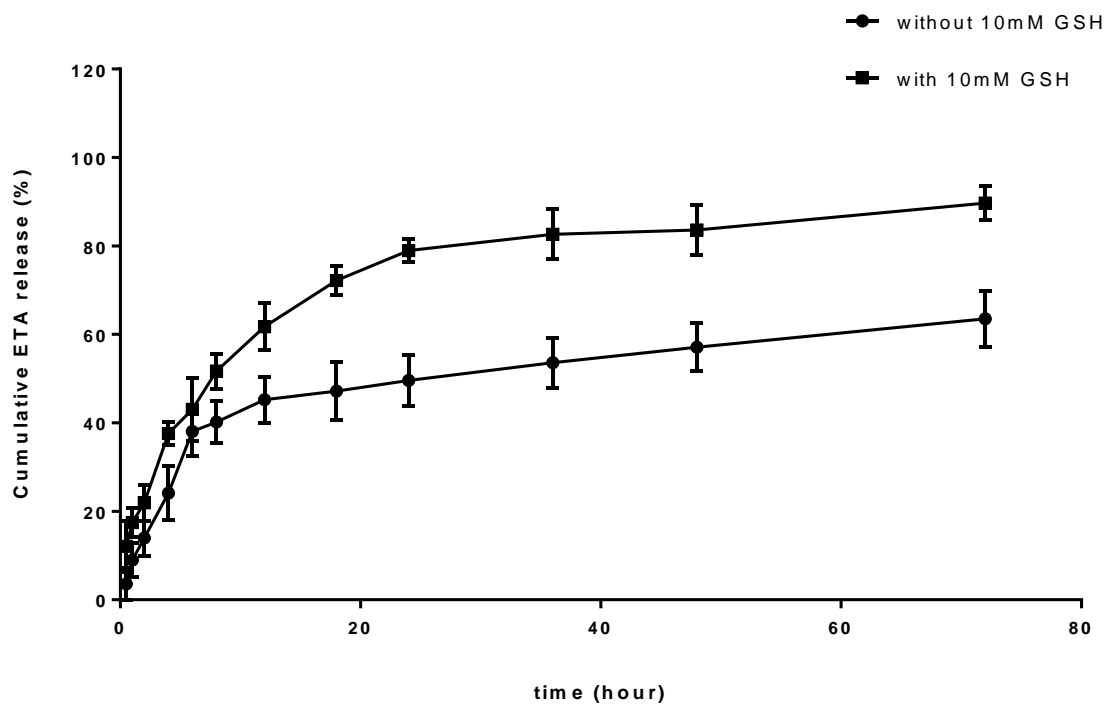
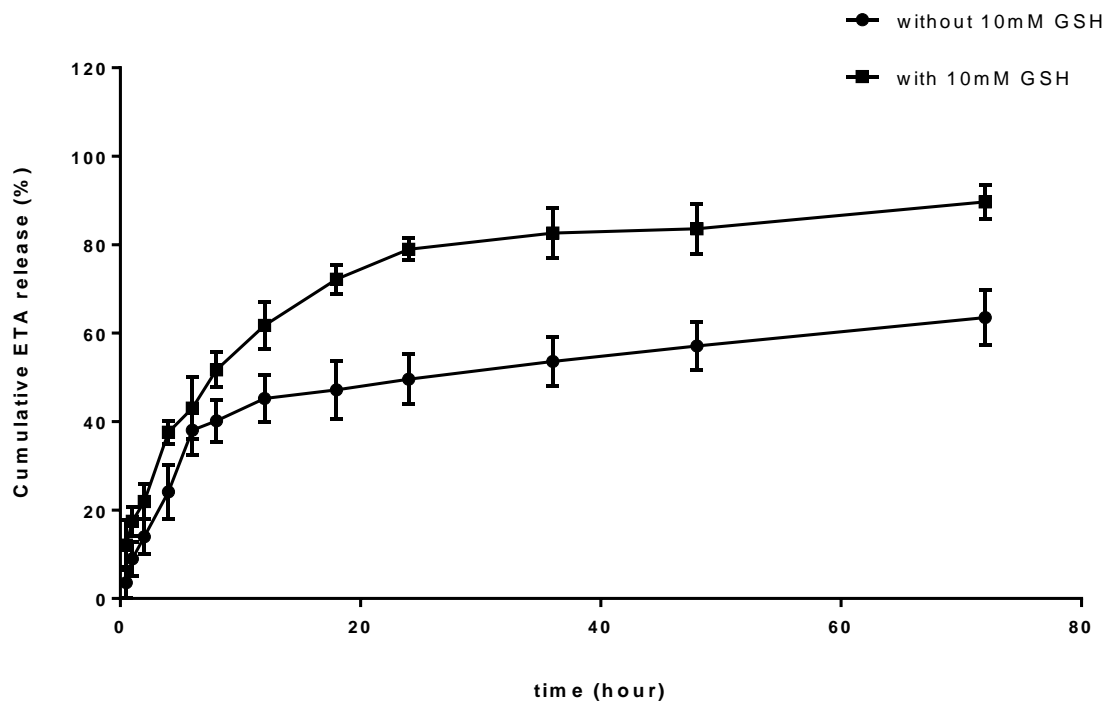


Figure 4.26. *In vitro* release profile of nanoparticles at pH 7.4.



**Figure 4.27.** *In vitro* release profile of nanoconjugates at pH 6.8.



**Figure 4.28.** *In vitro* release profile of nanoconjugates at pH 7.4.

### 4.3.9. Stability of Nanoparticles

The stability of nanoformulations were investigated during storage either at room temperature or at +4°C and their physicochemical properties were determined at various time intervals. As it can be seen from Table 4.10., no significant change in physicochemical properties of PLGA-*b*-PEG nanoparticles was observed until storage of 2 months. After 2 months, aggregation in PLGA-*b*-PEG nanoparticles stored at room temperature was observed while nanoparticles stored at +4°C were still stable. However, aggregation in mPEG-PLGA-SS-ETA nanoconjugates started after 1 month of storage. Mean particle size and PDI of the nanoconjugates significantly increased due to aggregation (Table 4.11). mPEG-PLGA-SS-ETA nanoconjugates are the non-covalently conjugated self-assemblies. In long storage periods, hydrophilic mPEG chain can disassemble from micelle and critical micelle concentration can decrease below the threshold resulting in disassociation of self-assembly.

**Table 4.10.** Stability of ETA-loaded PLGA-*b*-PEG nanoparticles at room temperature and at +4°C.

	Room Temperature			
	1 month	2 months	3 months	4 months
Particle size (nm)	131.22 ± 2.05	133.56 ± 3.67	237.72 ± 5.98	294.72 ± 4.31
PDI	0.18 ± 0.06	0.19 ± 0.02	0.26 ± 0.07	0.34 ± 0.1
Zeta potential (mV)	-12.40 ± 2.1	-13.23 ± 1.0	-10.05 ± 1.1	-10.38 ± 0.9
	+4°C			
	1 month	2 months	3months	4months
Particle size (nm)	129.43 ± 3.01	132.61 ± 4.6	133.79 ± 5.7	130.02 ± 5.6
PDI	0.17 ± 0.02	0.17 ± 0.08	0.18 ± 0.02	0.19 ± 0.04
Zeta potential (mV)	-12.84 ± 3.6	-11.03 ± 2.8	-12.20 ± 1.8	-12.35 ± 4.6

**Table 4.11.** Stability of mPEG-PLGA-SS-ETA nanoconjugates at room temperature and at +4°C.

	Room Temperature			
	1 month	2 months	3 months	4 months
Particle size (nm)	138.49 ± 6.52	145.69 ± 4.51	161.93 ± 2.20	179.42 ± 2.82
PDI	0.15 ± 0.01	0.18 ± 0.06	0.20 ± 0.08	0.28 ± 0.04
Zeta potential (mV)	-9.23 ± 1.6	-12.83 ± 3.2	-11.42 ± 4.0	-13.28 ± 2.5
	+4°C			
	1 month	2 months	3months	4months
Particle size (nm)	134.25 ± 6.21	139.26 ± 2.3	178.21 ± 2.9	176.62 ± 7.9
PDI	0.15 ± 0.03	0.17 ± 0.04	0.21 ± 0.07	0.23 ± 0.12
Zeta potential (mV)	-10.92 ± 4.3	-10.26 ± 3.1	-11.54 ± 5.7	-13.62 ± 5.1

#### 4.3.10. Sterilization of Nanoformulations and Sterility Control

As nanomedicines are important tools for delivering therapeutic agents to cells and/or to the organisms, their sterility has great importance to avoid contamination. Two different strategies were used to sterilize the nanoformulations; filter sterilization and UV-irradiation. Neither bacterial nor fungal growth was observed after the incubation period. Both methods can be used to sterilize formulations.

#### 4.3.11. Antibody Conjugation of Nanoformulations

Nanoformulations were prepared with various concentrations of FITC-conjugated Vimetin mAb and the conjugation of the mAb Vimentin on the surface of nanoformulations was confirmed by Bradford assay. Amount of antibody conjugated to nanoformulations was quantified by BSA calibration curve (Figure 4.29). Covalent conjugation of the antibody was validated with conjugation efficiency 54,8%, 72,3% and 81.4% for PLGA nanoparticles, PLGA-*b*-PEG nanoparticles and mPEG-PLGA-SS-ETA nanoconjugates, respectively. Increasing the antibody concentration from 10 µg to 50 µg increased the conjugation efficiency with no significant increase in particle size. Antibodies which have a hydroxyl as the end functional group, preferentially bound to the PEG backbone. Hence, PLGA-*b*-PEG nanoparticles had higher antibody conjugation efficiency than PLGA nanoparticles. Therefore, antibodies bound to methoxy functionalized PEG conjugates with higher affinity than binding to non-functionalized PEG.

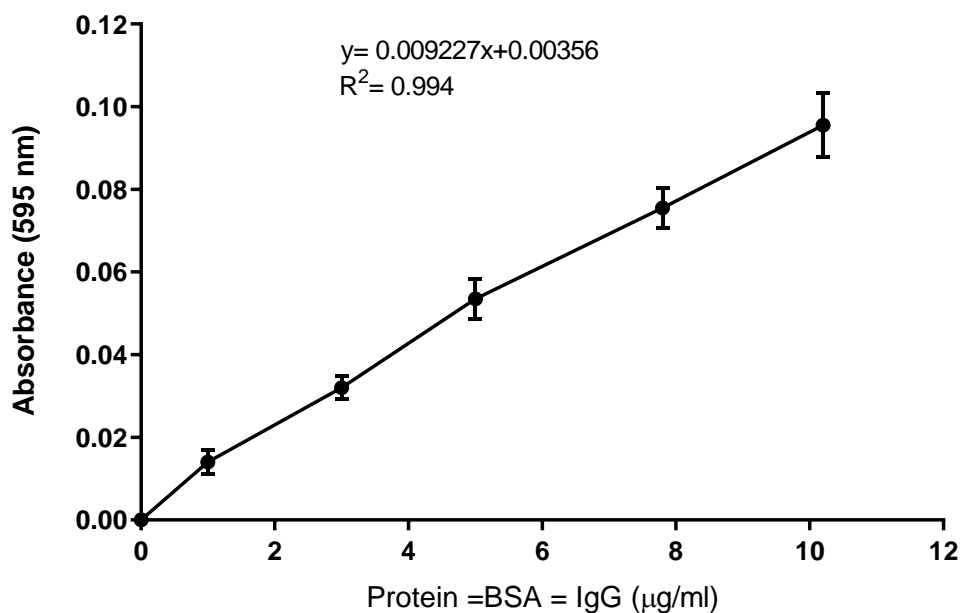


**Figure 4.29.** BSA validation curve.

#### 4.3.12. *In vitro* Cytotoxicity

Cytotoxicity studies are important initial steps to evaluate the biocompatibility of the material used for medical applications [288]. The L929 mouse fibroblasts is a well established and commonly used cell line for cytotoxicity evaluation of nanomaterials [289-291]. In this study, possible cytotoxic effects of nanoformulations were evaluated on L929 cell line. The effect of different concentrations of nanoformulations on L929 cell viability was determined with MTT assay. Figure 4.30., Figure 4.31. and Figure 4.32 showed the percentage viability of L929 cells following 24 and 48 hours incubation with nanoparticles, nanoconjugates and ETA-loaded nanoparticles, respectively. The results clearly demonstrated that nanoformulations showed concentration dependent toxicity. There was no significant difference in cell viability between 24 hours and 48 hours incubation periods ( $p > 0.05$ ). These results suggested that the nanoformulations were not toxic in the range of 20-60 µg/ml and could be used in safety.

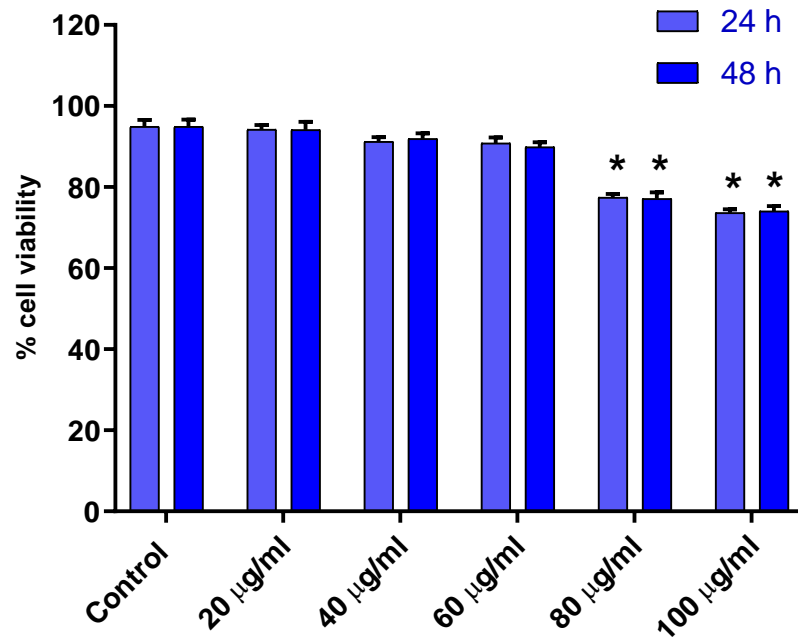


**Figure 4.30.** Cytotoxicity of PLGA-*b*-PEG nanoparticles on L929 cells. (\* $p < 0.05$  vs control).

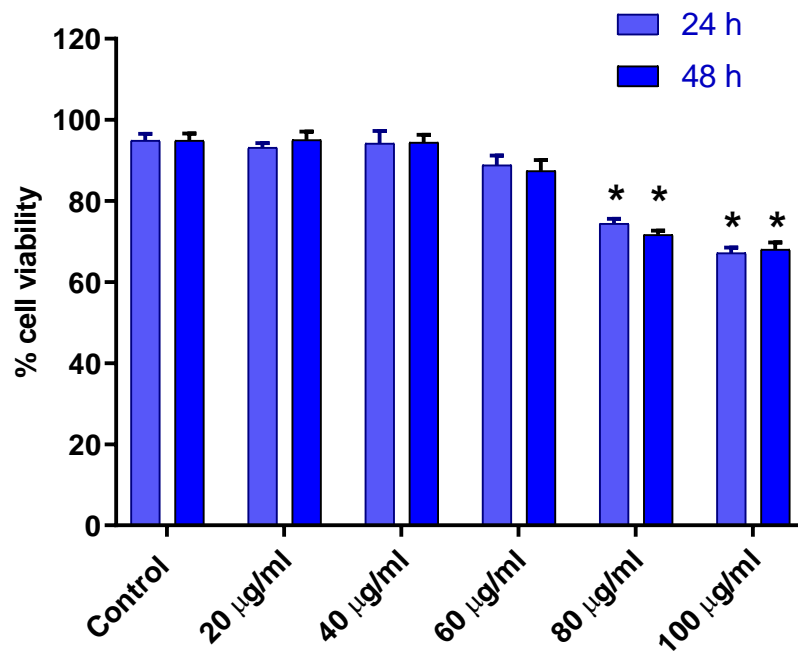


**Figure 4.31.** Cytotoxicity of mPLGA-PEG-SS-ETA nanonanoconjugates on L929 cells. (\* $p < 0.05$  vs control).

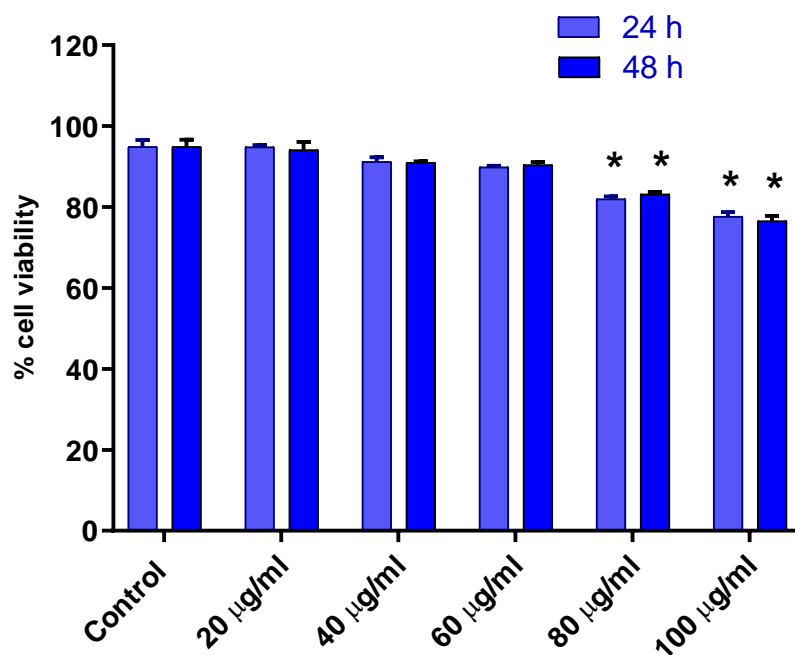


**Figure 4.32.** Cytotoxicity of ETA-loaded PLGA-*b*-PEG nanoparticles on L929 cells. (\* $p < 0.05$  vs control).

#### 4.4. *In vitro* studies

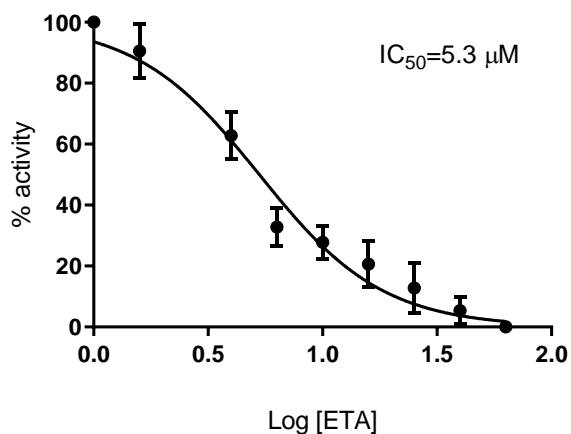
##### 4.4.1. Treatment of Oxidative Stress Generated Epithelial and Mesenchymal Phenotypes of HT-29 Cells with Nanoparticulated ETA

Oxidative stress generated epithelial and mesenchymal phenotypes of HT-29 cells were treated with free ETA, ETA loaded nanoformulations and immunonanoformulations at ETA concentrations ranging from 0.1 µg/ml to 1.6 µg/ml. The concentration of ETA in nanoformulations was estimated by drug content studies.  $IC_{50}$  values of all formulations both for epithelial and mesenchymal phenotypes of HT-29 cells were determined as described in *Section 3.2.4.1*. Figures 4.33.- 4.36. show the  $IC_{50}$  values of nanoformulations.  $IC_{50}$  values of free ETA, ETA-loaded PLGA-*b*-PEG nanoparticles, mPEG-PLGA-SS-ETA nanoconjugates, Vim-conjugated-PLGA-*b*-PEG nanoparticles and Vim-conjugated-mPEG-PLGA-SS-ETA nanoconjugates were 9.10 µM, 8.60 µM, 8.30 µM, 7.70 µM and 6.01 µM, respectively for mesenchymal phenotypes of HT-29 cells. It can be clearly seen that the Vim-free and Vim-conjugated nanoformulations accumulated in mesenchymal cells to a greater extent than free ETA. This result can be attributed to enhanced permeation and retention effect of nanoformulations. Moreover,  $IC_{50}$  values determined for Vim-free formulations were significantly higher than those obtained for immunonanoformulations. Thus,

immunonanoformulations markedly enhanced the GST- $\pi$  inhibition with lower IC<sub>50</sub> values. These results indicated that the vimentin conjugation enhanced the cellular uptake of nanoformulations in mesenchymal phenotypes of HT-29 cells via receptor-mediated endocytosis. The combined effect of active targeting and enhanced cellular uptake of Vim-conjugated nanoformulations would be the main reason for the lower IC<sub>50</sub> values of immunonanoformulations than for the Vim-free nanoformulations. Therefore, Vim-conjugated-mPEG-PLGA-SS-ETA nanoconjugates inhibited GST- $\pi$  activity at lower concentrations than at Vim-conjugated-PLGA-*b*-PEG nanoparticles. These results confirmed that the nanoconjugates have greater capacity for loading ETA than PLGA-*b*-PEG nanoparticles have. In contrast, Vim-conjugation did not affect the uptake of nanoformulations in epithelial phenotypes of HT-29 cells. IC<sub>50</sub> values of free ETA, ETA loaded PLGA-*b*-PEG nanoparticles, mPEG-PLGA-SS-ETA nanoconjugates, Vim-conjugated-PLGA-*b*-PEG nanoparticles and Vim-conjugated-mPEG-PLGA-SS-ETA nanoconjugates were 6.4  $\mu$ M, 5.30  $\mu$ M, 4.70  $\mu$ M, 5.20  $\mu$ M and 4.2  $\mu$ M, respectively, for epithelial phenotypes of HT-29 cells. IC<sub>50</sub> values of either ETA-loaded nanoparticles and Vim-conjugated ETA-loaded nanoparticles or mPEG-PLGA-SS-ETA nanoconjugates and Vim-conjugated-nanoconjugates were not statistically significant ( $p > 0.05$ ). These results confirmed that epithelial phenotypes of HT-29 cells did not express vimentin. Therefore, IC<sub>50</sub> values of nanoconjugated ETA was lower than of nanoparticulated ETA, also confirming that nanoconjugates had greater capacity for loading ETA than did PLGA-*b*-PEG nanoparticles.



A)



B)

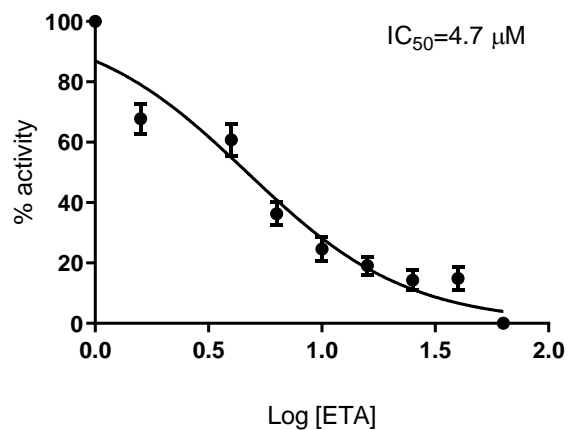
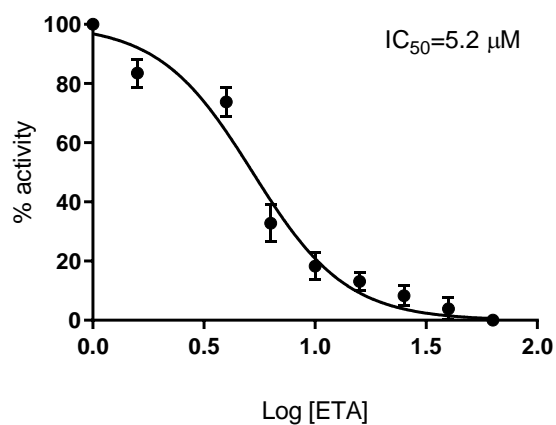


**Figure 4.33.** Determination of % GST- $\pi$  activity following treatment with various concentrations of A) ETA loaded PLGA-*b*-PEG nanoparticles B) PLGA-PEG-SS-ETA nanoconjugates for epithelial phenotypes of HT-29 cells.

A)



B)

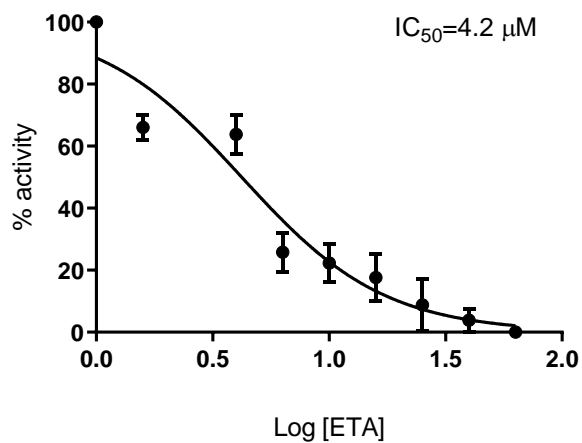


**Figure 4.34.** Determination of % GST- $\pi$  activity following treatment with various concentrations of A) ETA loaded PLGA-*b*-PEG immunonanoparticles B) PLGA-PEG-SS-ETA immunonanoconjugates for epithelial phenotypes of HT-29 cells.

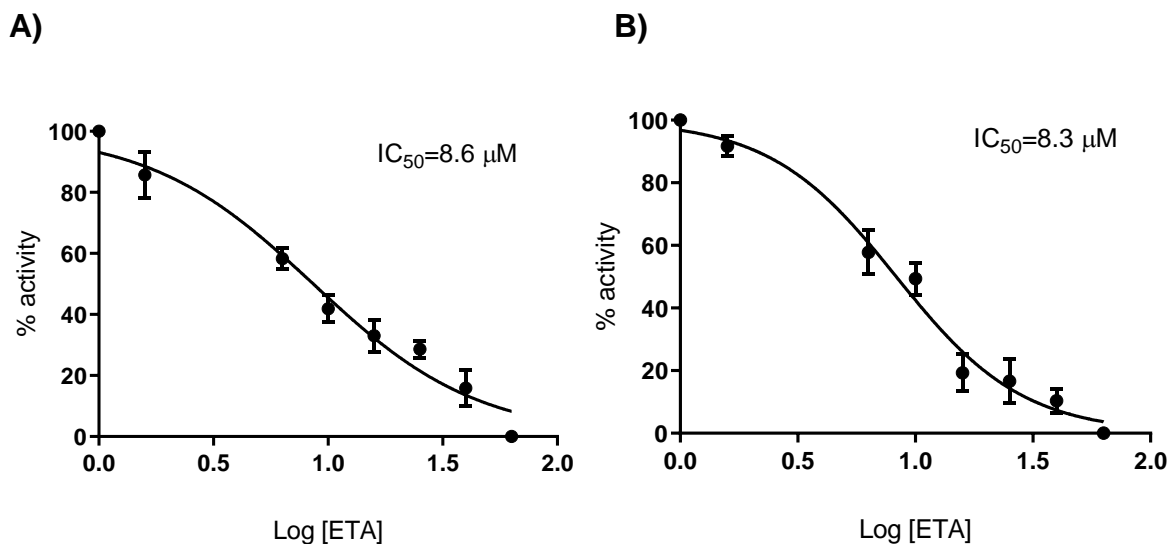


**Figure 4.35.** Determination of % GST- $\pi$  activity following treatment with various concentrations of A) ETA loaded PLGA-*b*-PEG nanoparticles B) PLGA-PEG-SS-ETA nanoconjugates for mesenchymal phenotypes of HT-29 cells.

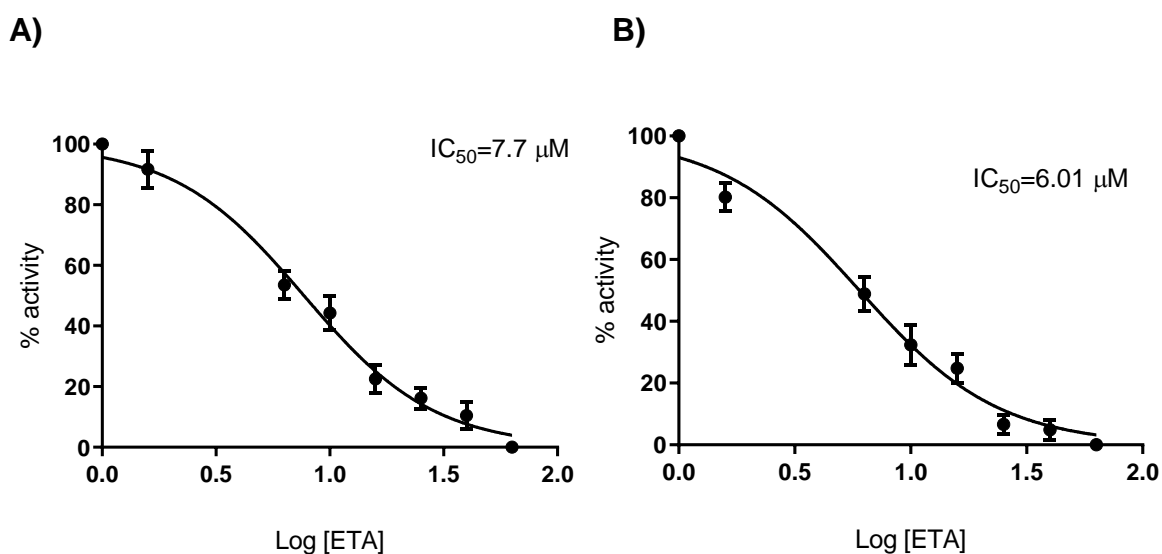


**Figure 4.36.** Determination of % GST- $\pi$  activity following treatment with various concentrations of A) ETA loaded PLGA-*b*-PEG immunonanoparticles B) PLGA-PEG-SS-ETA immunonanoconjugates for mesenchymal phenotypes of HT-29 cells.

#### 4.4.2. Treatment of Oxidative Stress Generated Epithelial and Mesenchymal Phenotypes of HT-29 Cells with FOLFOX

The viability of the epithelial and mesenchymal phenotypes of HT-29 cells exposed to FOLFOX was determined by MTT assay following 24 hours of treatment. As shown in Figure 4.37-A., the viability of the epithelial and mesenchymal phenotypes of HT-29 cells decreased significantly following 24 hours of incubation with FOLFOX as compared to untreated controls. However, the reduction in the cell viability of epithelial phenotype was significantly greater than in the mesenchymal phenotype of HT-29 cells following treatment ( $\Psi < 0.01$ ). These results demonstrated that mesenchymal phenotypes of HT-29 cells exhibited resistance to FOLFOX regimen (Figure 4.37-B).

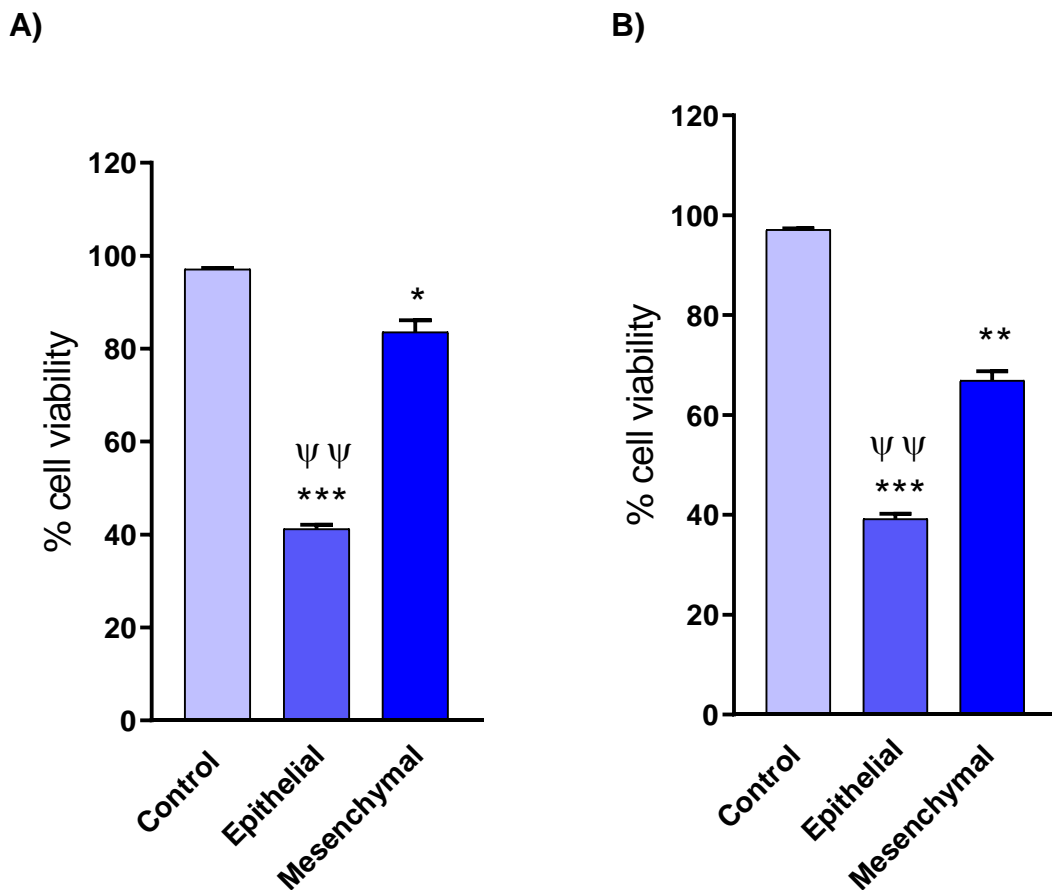


**Figure 4.37.** Determination of % cell viability of epithelial and mesenchymal phenotypes of HT-29 cells following treatment with A) FOLFOX and B) ETA plus FOLFOX. Data are represented as the mean  $\pm$  SEM (\* $p < 0.05$ , \*\* $p < 0.01$  and \*\*\* $p < 0.001$  vs control;  $\Psi\Psi$   $p < 0.01$  vs epithelial phenotypes of HT-29 cells).

As indicated in *Section 4.2.1.*, GST- $\pi$  expression and protein levels were remarkably increased in mesenchymal phenotypes of HT-29 cells. The combined results of lower reduction rate in cell viability and enhanced GST- $\pi$  protein levels also indicate the importance of GST- $\pi$  activity in the resistance of mesenchymal phenotype of HT-29 cells to FOLFOX regimen, making it a potential target to overcome drug resistance in CRC cells undergo EMT.

#### **4.4.3. Treatment of Oxidative Stress Generated Epithelial and Mesenchymal Phenotypes of HT-29 cells with ETA plus FOLFOX**

Both phenotypes of HT-29 cells were treated with 4.2  $\mu$ M ETA (the dosage that inhibited at least 70% of GST- $\pi$  activity both in two phenotypes of HT-29 cells) followed by FOLFOX treatment. It could be clearly seen from Figure 4.38. that inhibition of GST- $\pi$  activity with ETA further decreased the cell viability in mesenchymal cells. In other words, the sensitivity of the mesenchymal phenotypes of HT-29 cells to FOLFOX regimen was significantly increased in the presence of ETA, suggesting that over-activity of this detoxifying enzyme was responsible for the resistance to chemotherapeutics in mesenchymal phenotypes of HT-29 cells. MTT assay results demonstrated that pretreatment with ETA significantly decreased the mesenchymal cell viability as compared to untreated controls ( $p < 0.01$ ). Moreover, a significant decrease in the viability of mesenchymal phenotypes of HT-29 cells pretreated with ETA was observed as compared to those treated with only FOLFOX regimen ( $\Psi < 0.05$ ). As shown in Figure 4.38., epithelial cell viability also decreased significantly as compared to untreated control following ETA+FOLFOX treatment ( $p < 0.001$ ). However, the difference between cell viability rates of FOLFOX-treated and ETA+FOLFOX treated epithelial cells was not statistically significant. These results were in great accordance with the results indicated in *Section 4.2.2.* that showed the inhibitory effect of ETA on the GST- $\pi$  activity. All of these data also suggested that inhibition of GST- $\pi$  activity following ETA treatment reversed the resistant phenotype of mesenchymal cells and enhanced the adjuvant therapy efficacy in mesenchymal phenotypes of HT-29 cells.

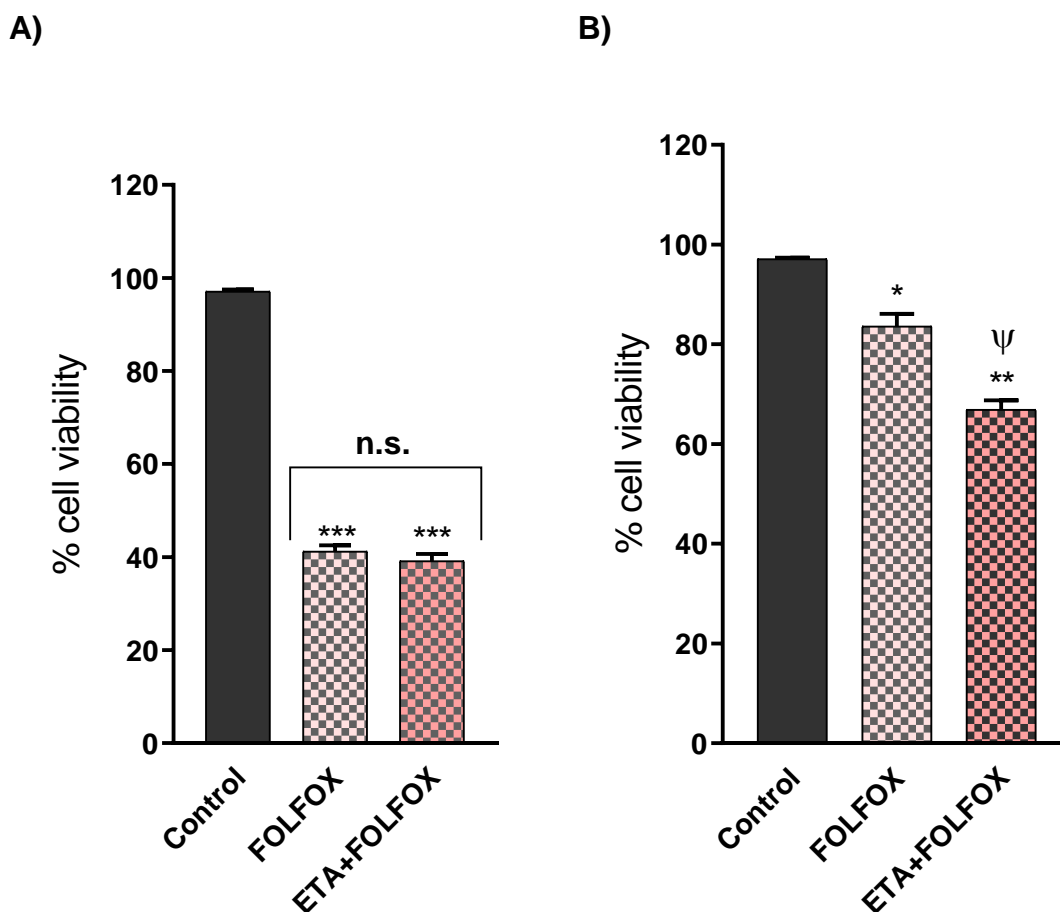


**Figure 4.38.** Determination of % cell viability of **A)** epithelial and **B)** mesenchymal phenotypes of HT-29 cells following treatment with FOLFOX and ETA plus FOLFOX. Data are represented as the mean $\pm$ SEM (\* $p$ <0.05, \*\* $p$ <0.01 and \*\*\* $p$ <0.001 vs control;  $\psi$  $p$ <0.05 vs epithelial phenotypes of HT-29 cells).

#### 4.4.4. Treatment of Oxidative Stress Generated Epithelial and Mesenchymal Phenotypes with Nanoparticulated ETA plus FOLFOX

Epithelial and mesenchymal phenotypes of HT-29 cells were pretreated with ETA loaded nanoformulations and immunonanoformulations at 4.2  $\mu$ M ETA concentration for 24 hours and then exposed to FOLFOX regimen for additional 24 hours. Figure 4.39. show the relative viability of epithelial and mesenchymal phenotypes of HT-29 cells as reported by the MTT assay when incubated with ETA loaded nanoparticles or ETA-loaded immunonanoparticles. As shown in Figure 4.39., inclusion of ETA-loaded PLGA-*b*-PEG nanoparticles and ETA-loaded immunonanoparticles increased cytotoxicity of FOLFOX regimen in epithelial phenotypes of HT-29 cells. As expected, ETA-loaded immunonanoparticles showed no discernable effect on the epithelial cell viability as compared to ETA-loaded nanoparticles, suggesting that epithelial phenotypes of HT-29 cells did not

express vimentin. However, ETA-loaded immunonanoparticles decreased the mesenchymal cell viability at a greater extent as compared to ETA-loaded nanoparticles. This greater reduction in the cell viability of mesenchymal cells suggested that these immunonanoparticles successfully accumulated in the vimentin overexpressed cells. Epithelial and mesenchymal phenotypes of HT-29 cells were also pretreated with PLGA-PEG-SS-ETA nanoconjugates or PLGA-PEG-SS-ETA immunonanoconjugates.

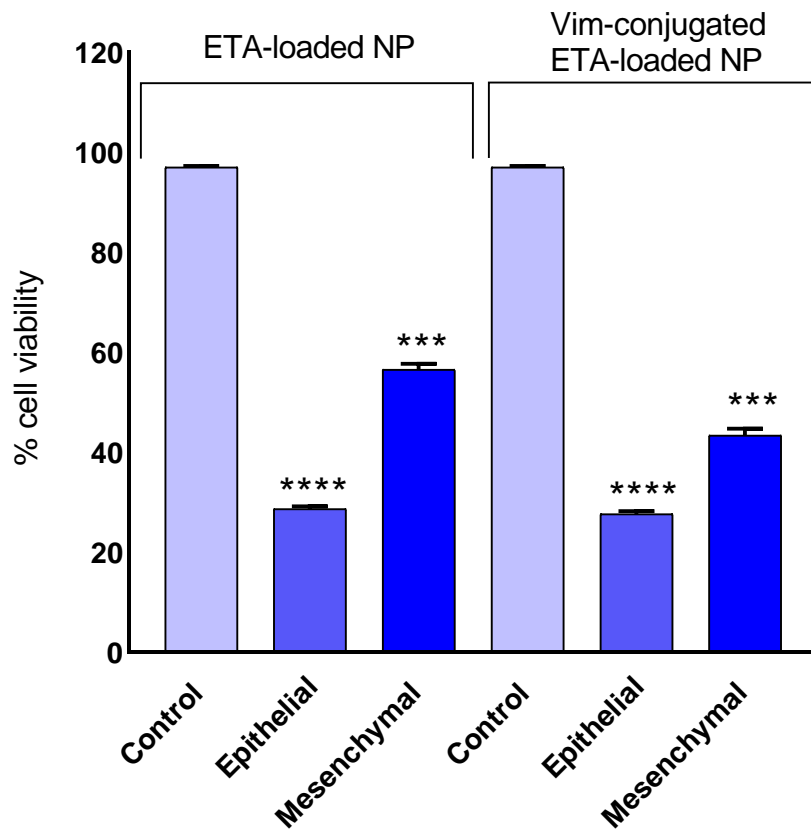


**Figure 4.39.** % cell viability of epithelial and mesenchymal phenotypes of HT-29 cells following treatment with ETA loaded nanoparticles and ETA loaded immunonanoparticles. Data are represented as mean±SEM (\*\*\*) $p < 0.001$  and \*\*\*\*) $p < 0.0001$  vs control).

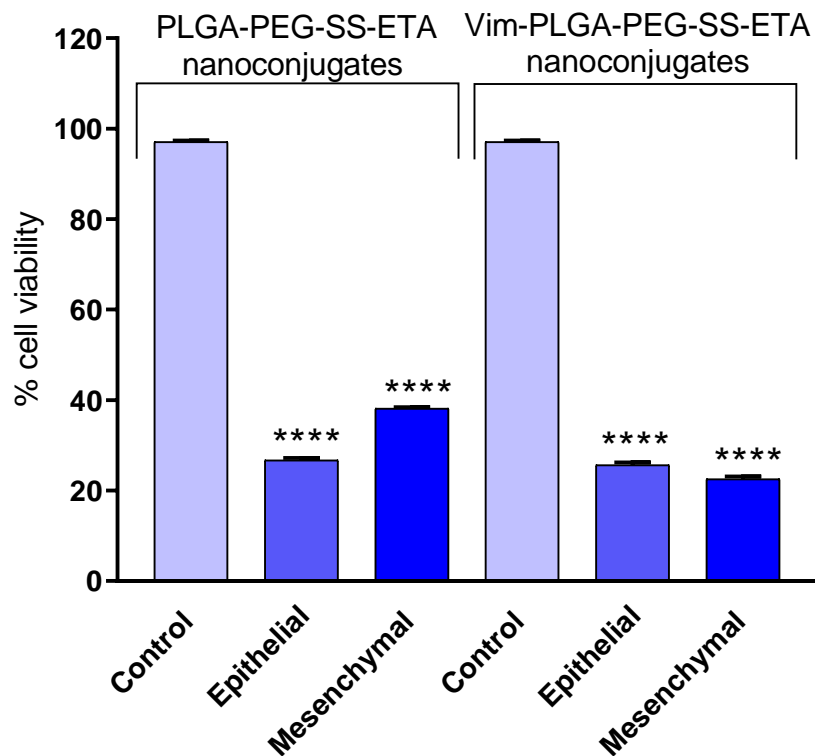


**Figure 4.40.** % cell viability of epithelial and mesenchymal phenotypes of HT-29 cells following treatment with PLGA-PEG-SS-ETA nanoconjugates and PLGA-PEG-SS-ETA immunonanoconjugates. Data are represented as mean±SEM (\*\*\*\*p<0.0001 vs control).

Neither nanoconjugates nor immunonanoconjugates showed further sensitization to FOLFOX regimen in epithelial phenotypes of HT-29 cells whereas mesenchymal cell viability significantly decreased by addition of either ETA loaded nanoconjugates or ETA-loaded immunonanoconjugates. Moreover, FOLFOX regimen was more effective in mesenchymal phenotype of HT-29 cells following immunonanoconjugate treatment (Figure 4.40). All of these data indicated that both increased accumulation of ETA in the mesenchymal cells as well as enhanced adjuvant therapy efficacy were achieved when immunonanoformulations were used. Figure 4.41 and Figure 4.42 showed the effectiveness of different treatment options for epithelial and mesenchymal phenotypes of HT-29 cells

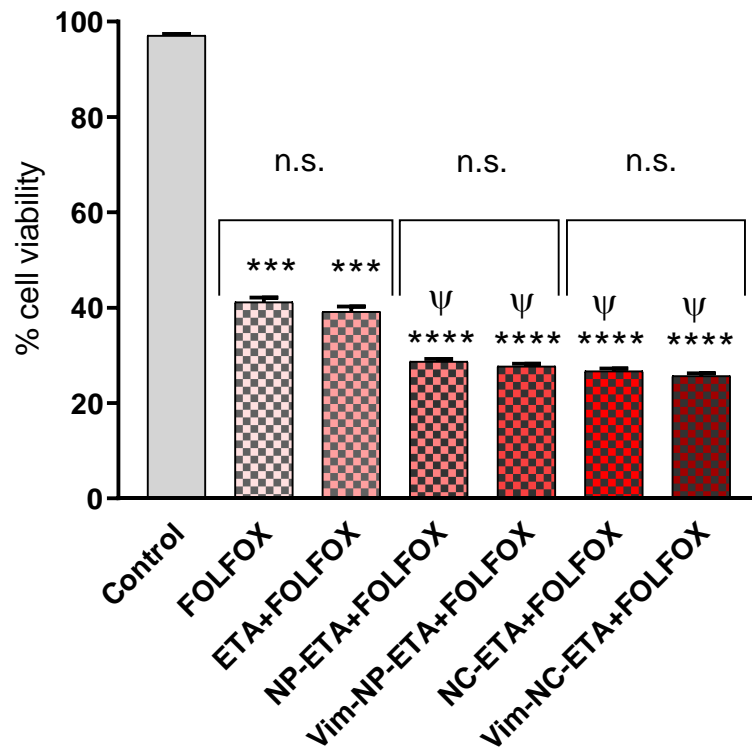


**Figure 4.41.** Determination of % cell viability of epithelial phenotypes of HT-29 cells following treatment with FOLFOX, ETA plus FOLFOX and different nanoformulations plus FOLFOX. Data are represented as mean±SEM (\*\*\*p<0.001 and \*\*\*\*p<0.0001 vs control; Ψp<0.05 vs group treated with FOLFOX).

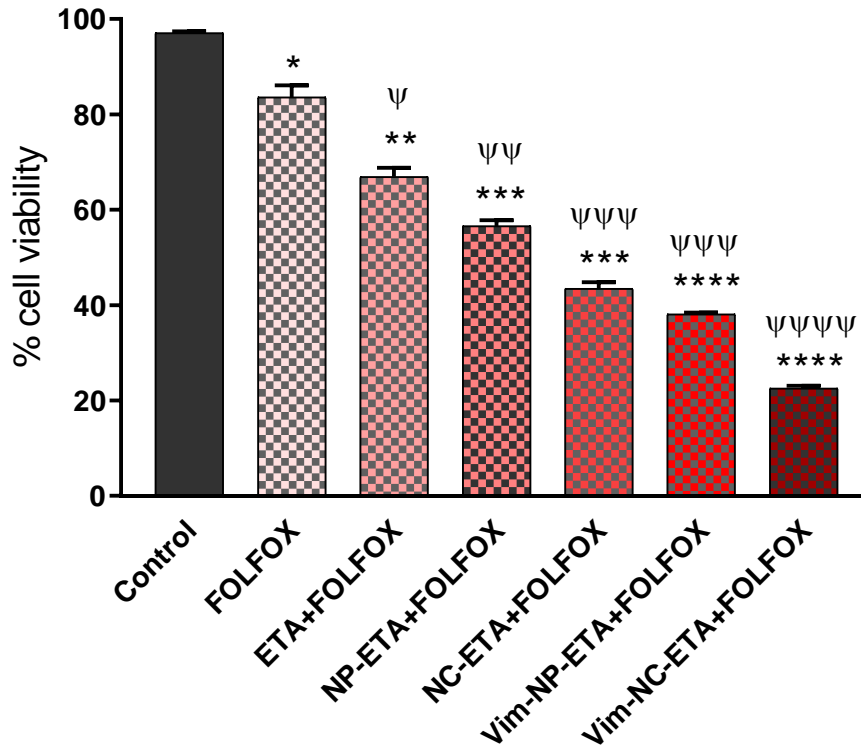


**Figure 4.42.** Determination of % cell viability of mesenchymal phenotypes of HT-29 cells following treatment with FOLFOX, ETA plus FOLFOX and different nanoformulations plus FOLFOX. (\*p<0.05, \*\*p<0.01, \*\*\*p<0.001 and \*\*\*\*p<0.0001 vs control; Ψp<0.05, ΨΨp<0.01, ΨΨΨp<0.001 and ΨΨΨΨp<0.0001 vs group treated with FOLFOX).



#### 4.5. *In vivo* Studies

*In vivo* studies were conducted to determine whether the ETA-loaded immunonanoformulations were effective to inhibit GST- $\pi$  activity and able to enhance the adjuvant therapy efficacy. For this purpose, forty-two rats previously injected with  $50 \times 10^6$  cells were randomly divided into 7 groups and sacrificed at 15, 30, 45, 60, 75, 85 and 95 days respectively after cell injection. For each group, colorectal tissues of 6 animals were collected following sacrifice. As shown in Figure 4.46., animals presented no signs of morphological changes up to 60 days. At 10 weeks of injection, all of the animals developed intestinal inflammation characterized by the presence of granulomas (Figure 4.43 and Figure 4.44). Granulomatous inflammation has been described in association with micro-invasive breast carcinomas and in relation to microscopic foci of colonic carcinoma within perivascular mesenteric fat [292]. However, no necrotic malignant cells were observed in these granulomas. These granulomas observed frequently in the middle and distal colon reached 5-10 mm in diameter at 95<sup>th</sup> day.

Cyclooxygenase (COX) is one of the rate-limiting enzymes in synthesis of prostaglandins which play a key role in the generation of the inflammatory response. Among two isoforms of COX, COX-1 and COX-2, COX-1 is expressed in normal intestine whereas COX-2 is responsible for inflammation and induced by mitogens, cytokines and growth factors. Indeed, overexpression of COX-2 both in human and rat colorectal carcinogenesis has been reported. Therefore, in addition to morphological examination, the expression of COX-2 either in colorectal tissues of all animals or in granulomas was evaluated. Mean COX-2 mRNA level of animals in the control group was evaluated as baseline level. Figure 4.45. demonstrates the relative colonic COX-2 mRNA levels of animals both in control group and CRC-1 group. Coincident with the morphological changes, elevated COX-2 expression levels were observed either in colorectal tissue or in granulomas. COX-2 expression in HT-29 CRC cell injected rats markedly increased in a time dependent manner. The increase in COX-2 expression was slightly but not significantly higher in the colorectal tissue dissected 15 days after injection than in healthy colorectal tissue. 30 days after HT-29 CRC cell injection, a significant increase in colonic COX-2 mRNA levels was observed ( $p < 0.05$ ). Maximal change in mRNA levels of COX-2 occurred at the 95th day after HT-29

CRC cell injection. Therefore, 95th day was accepted as day 0 for EMT studies considering the increase in COX-2 expression and morphological changes.

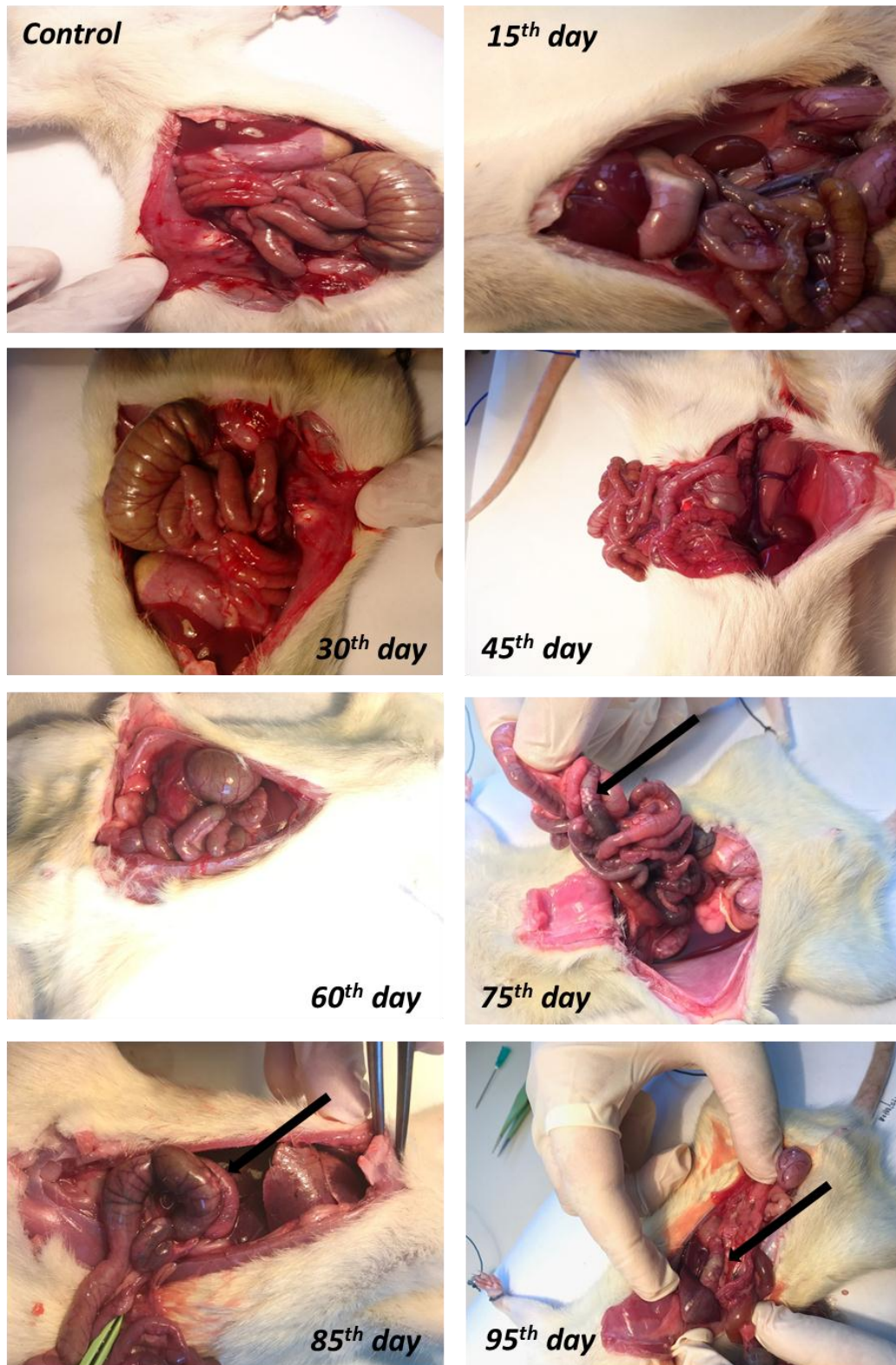


**Figure 4.43.** *In vivo* images of the colorectal tissues of rats on the day 0-95<sup>th</sup>.

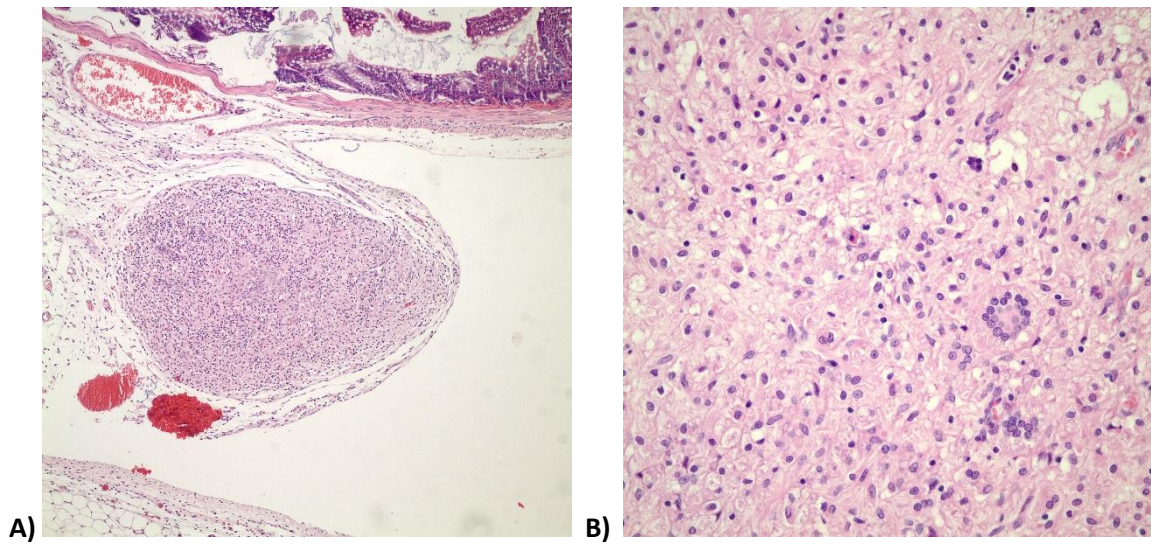


**Figure 4.44.** Photomicrograph showing granuloma formation **A)** H&E stain, x100 **B)** H&E stain, x400.

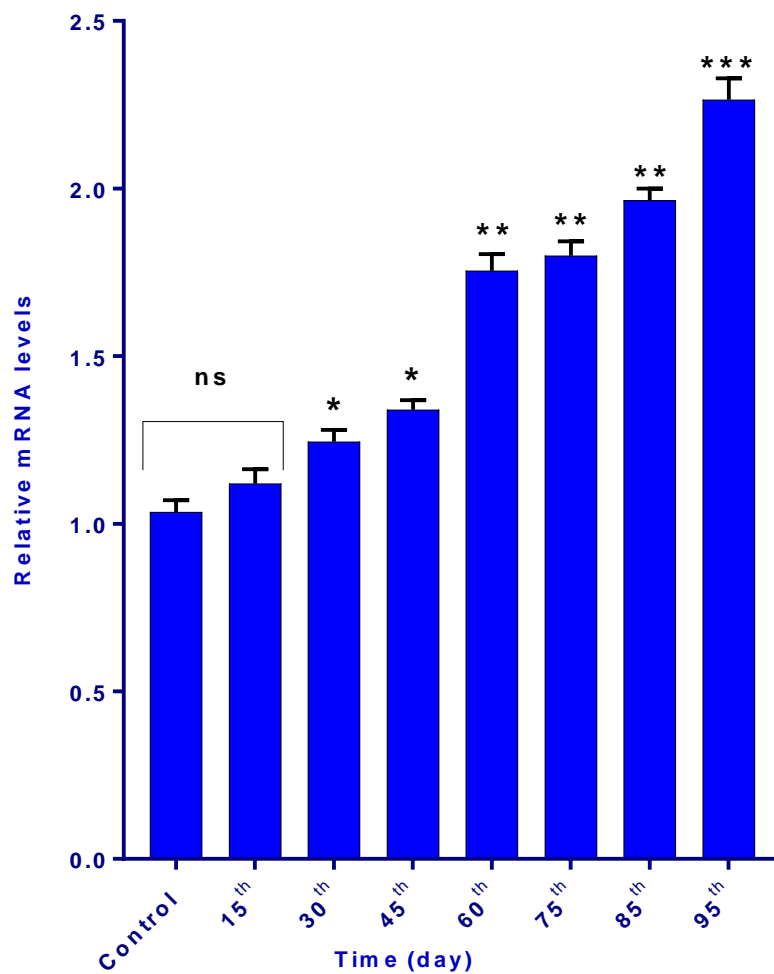


**Figure 4.45.** Relative colonic COX-2 mRNA levels between 15-95<sup>th</sup> days. (\* $p < 0.05$ , \*\* $p < 0.01$  and \*\*\* $p < 0.001$  vs control).

After formation of granulomas, EMT development period was also determined in the animals. To demonstrate the existence of EMT in *in vivo*, the granulomas and adjacent colorectal tissue were dissected from the sacrificed rats at the indicated days (0-20 days). Homogenates both of granulomas and colorectal tissue were subjected to qRT-PCR analysis to evaluate the changes in gene expression associated with EMT. The observed patterns in mRNA expression were consistent with EMT. As expected, the epithelial markers E-cadherin and Zonula occludens expressions were downregulated in a time dependent manner. No heterogeneity of expression within granulomas in the same group was observed (Figure 4.46).

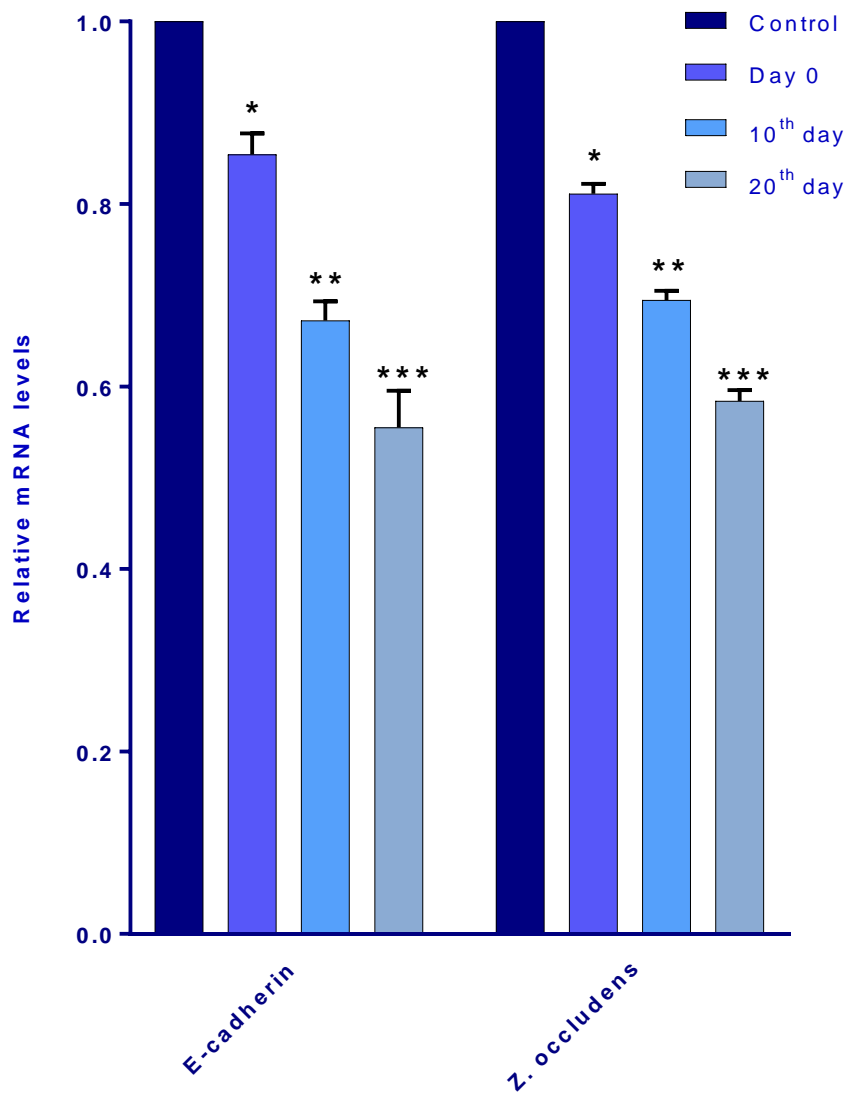


**Figure 4.46.** Relative mRNA levels of epithelial markers on the 95-115<sup>th</sup> days after injection of HT-29 CRC cells into rats. (\* $p < 0.05$ , \*\* $p < 0.01$  and \*\*\* $p < 0.001$  vs control).

Coincident with these changes in epithelial markers, expression of mesenchymal markers increased in a time-dependent manner. As it can be clearly seen from Figure 4.47., mRNA levels of mesenchymal markers following 115 days (95 days for formation of granulomas and 20 days for EMT development) were significantly higher than those following 95 days ( $p < 0.0001$ ). Decreased expression of epithelial markers and the upregulation of mesenchymal markers supported the transition of epithelial cells into mesenchymal phenotype. However, heterogeneity of expression patterns of mesenchymal markers, especially in fibronectin, was observed in the same group. This can be due to the presence of different subpopulations in EMT. Granulomas generally consist of connective tissue, blood vessels and inflammatory cells. Cells transformed to mesenchymal phenotype are adjacent to the blood vessel-enriched stroma [293].

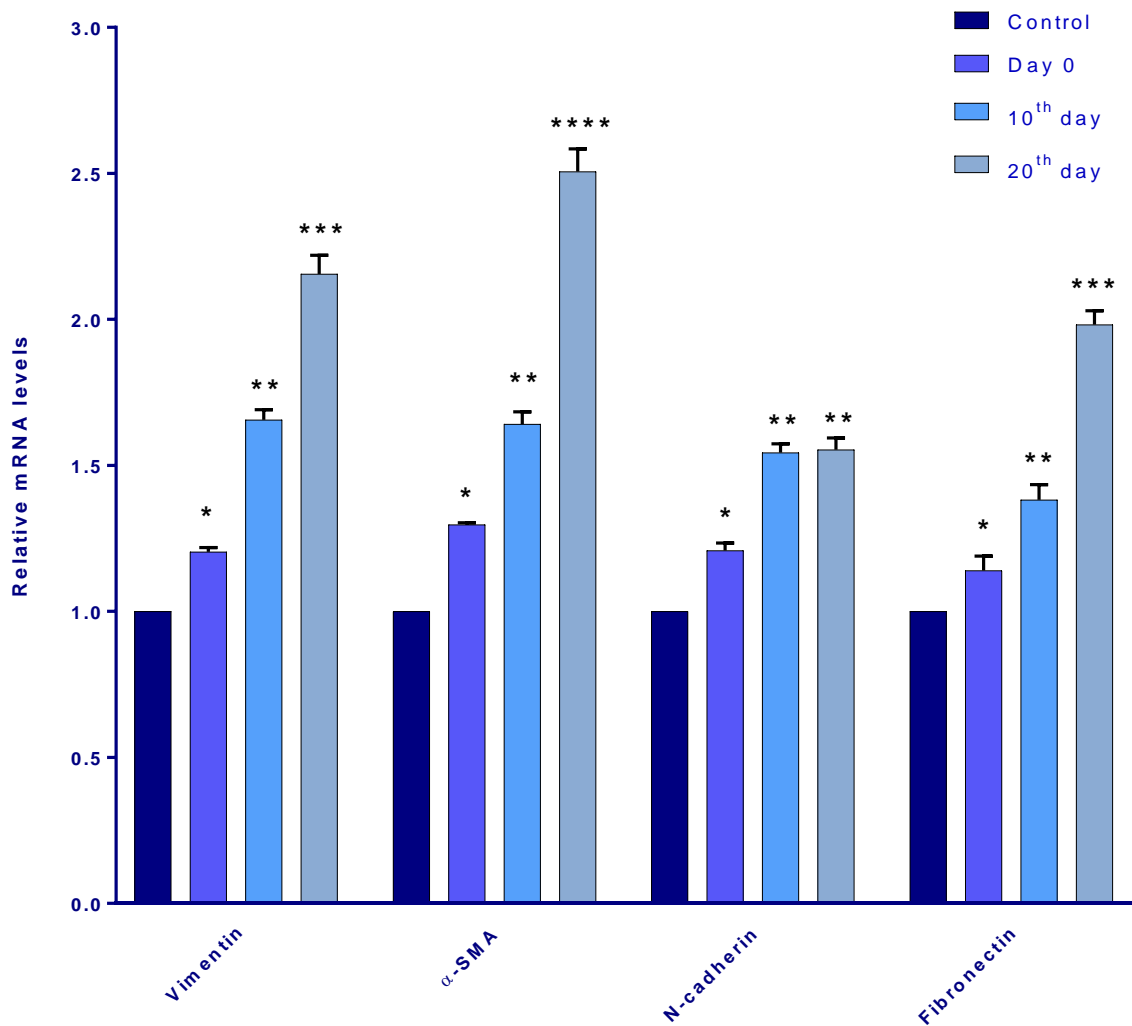


**Figure 4.47.** Relative mRNA levels of mesenchymal markers on the 95-115<sup>th</sup> days after injection of HT-29 CRC cells into rats. (\* $p < 0.05$ , \*\* $p < 0.01$ , \*\*\* $p < 0.001$  and \*\*\*\* $p < 0.0001$  vs control).



Development of EMT in the granulomas was also evaluated by immunohistochemical analysis. However, immunohistochemical results were not correlated with qRT-PCR analysis data that supported the transformation of the cells (Figure 4.48).

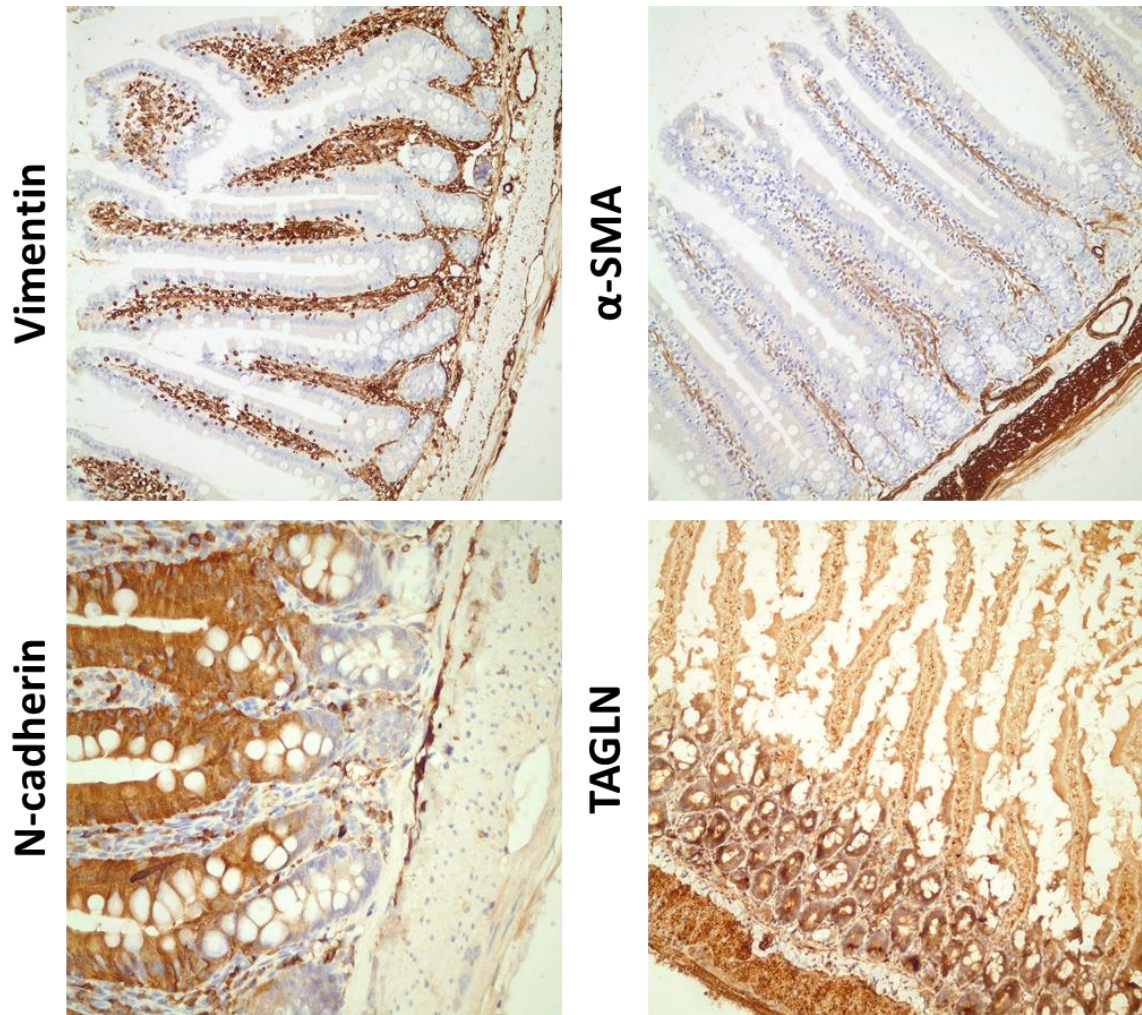


**Figure 4.48.** Immunohistochemical staining of granulomas for expression of mesenchymal markers.

After observation of granulomas formation and EMT development, rats bearing granulomas were received different treatment regimens. GST- $\pi$  and COX-2 expression levels were determined for each group at the end of treatment protocol. As depicted in the Figure 4.49., Group 2, Group 4 and Group 5 exhibited evidently higher COX-2 expression levels than FOLFOX regimen treated groups. No significant difference was observed between these three groups and control group.

Furthermore, much more reduction in the COX-2 expression levels was observed in the animals pretreated ETA or nanoformulated ETA than those treated with only FOLFOX regimen. In other words, increased responsiveness to FOLFOX regimen was observed in the groups pretreated with ETA or nanoformulated ETA, indicating a reduction of GST- $\pi$  expression levels in the granulomas by the cotreatment of rats with FOLFOX and ETA. Group 6 showed the lowest COX-2 mRNA level among all groups, suggesting that pretreatment with immunonanoconjugates was more effective to increase adjuvan therapy efficacy.

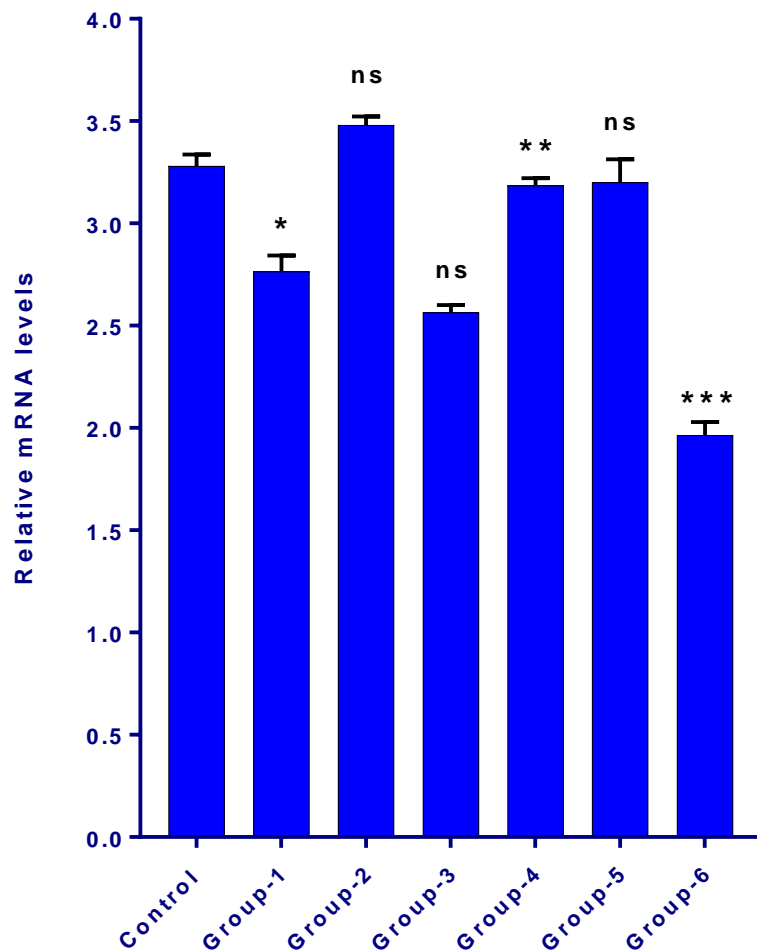


**Figure 4.49.** Relative mRNA levels of COX-2 in rats after different treatment regimens. (\* $p < 0.05$ , \*\* $p < 0.01$  and \*\*\* $p < 0.001$  vs control).

GST- $\pi$  protein levels were further analysed to determine whether the reduction in COX-2 expression levels was due to the inhibition of GST- $\pi$  with ETA. Protein expression levels of GST- $\pi$  in the granulomas treated with only FOLFOX regimen

were significantly higher compared with granulomas treated with FOLFOX regimen plus ETA or plus nanoformulated ETA (Figure 4.50.). Furthermore, Group 6 exhibited the highest inhibitory effect on GST- $\pi$  protein level of the granulomas among all groups, suggesting immunonanoconjugates was more effective to deliver ETA than ETA-loaded immunonanoparticles because of its release profile and targeting efficiency.

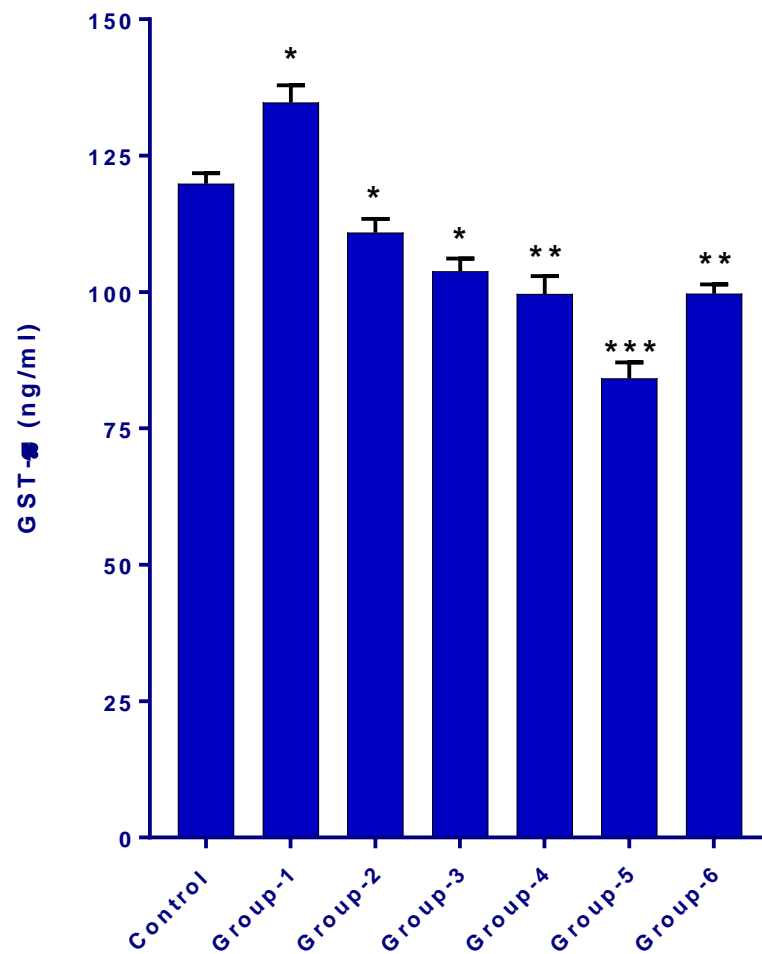


**Figure 4.50.** Protein levels of GST- $\pi$  in rats after different treatment regimens. (\* $p < 0.05$ , \*\* $p < 0.01$  and \*\*\* $p < 0.001$  vs control).



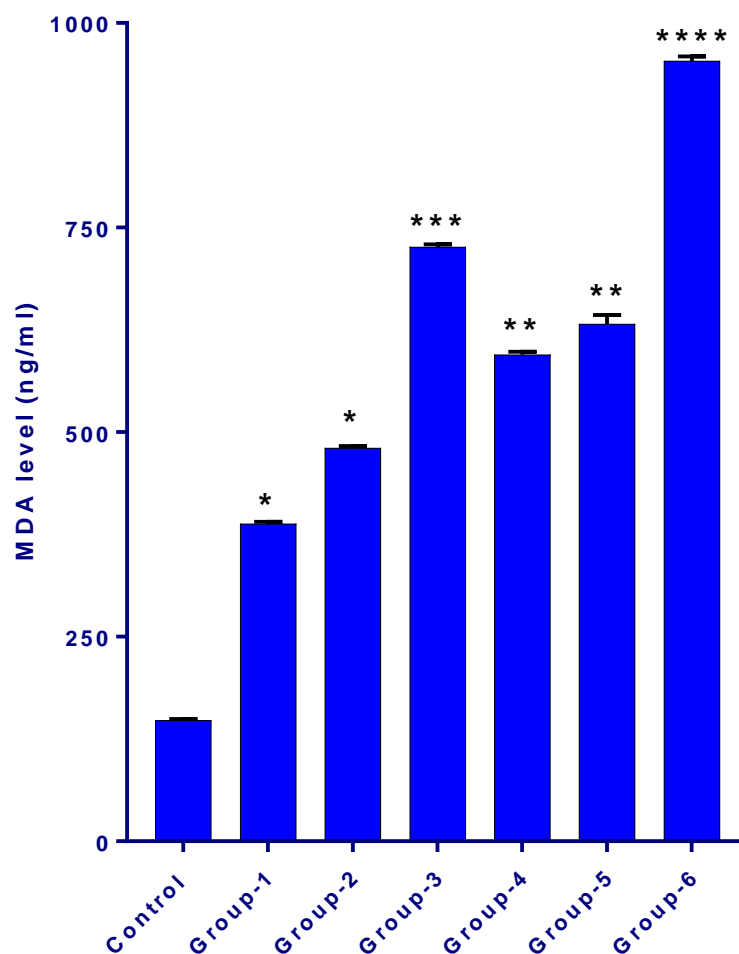


**Figure 4.51.** Protein levels of MDA in the rats after different treatment regimens regimens. (\* $p < 0.05$ , \*\* $p < 0.01$ , \*\*\* $p < 0.001$  and \*\*\*\* $p < 0.0001$  vs control).

MDA levels were also determined to evaluate the lipid peroxidation levels. The drugs in the adjuvant combination, especially oxaliplatin, induced oxidative damage. Oxaliplatin exerts its cytotoxic effects via formation of platinum-DNA adducts that trigger immobilization of the mitotic cell cycle and stimulate apoptosis of dividing cells. This effect on the cancer cells was increased lipid peroxidation As it can be clearly seen in the control group, drugs had no peroxidation effect (Figure 4.51.). It can be clearly mentioned that resistance towards FOLFOX therapy developed in the animals due to overexpression of GST- $\pi$ . ETA+adjuvant combinations. Following inhibition of GST- $\pi$  with ETA (Group 2), lipid peroxidation levels increased. Furthermore, as expected MDA level was the highest in the group treated with nanoparticulated. Mesenchymal phenotype-targeted nanoformulations deliver ETA *in vivo* successfully.

## 5. CONCLUSION

This thesis is focused on role of GSTs in drug resistance profile of colorectal cancer cells that undergo EMT and design and development of a GST inhibitor targeting system which is directed to EMT to enhance the efficacy of adjuvant therapy clinically used in CRC treatment.

Conclusions obtained in the light of data from this thesis are as follows:

1. *In vitro* EMT model was created successfully in HT-29 CRC cells by induction with 10 ng/ml TGF- $\beta$ 1 for 48 hours.
2. Elevated GST- $\pi$  expression and protein levels were observed in the mesenchymal phenotype of HT-29 cells.
3. Mesenchymal phenotype of HT-29 cells became oxidative stress resistant because of elevated GST- $\pi$  activity.
4. IC<sub>50</sub> value of free ETA was found to be higher in mesenchymal phenotype than the one of epithelial phenotype. IC<sub>50</sub> value of ETA in ETA-loaded PLGA-*b*-PEG nanoparticles was found to be decreased in mesenchymal phenotype of HT-29 cells. IC<sub>50</sub> value of ETA in mPEG-PLGA-SS-ETA nanoconjugates was found to be lowered almost to the level of ETA in epithelial phenotype.
5. PLGA-*b*-PEG nanoparticles and mPEG-PLGA-SS-ETA nanoconjugates were observed with appropriate mean particle size (<150nm), PDI (<0.2) and zeta potential values.
6. HPLC method we modified and applied for the quantitative determination of ETA was found to be linear, precise, accurate, specific with low limits of detection and quantification for ETA. This analytical method was proved to be valid for the quantitative determination of ETA.
7. The encapsulation efficiency and loading capacity of mPEG-PLGA-SS-ETA nanoconjugates were found to be higher than PLGA-*b*-PEG nanoparticles.
8. Drug release experiments highlighted a sustained release of ETA from all nanoformulations. Elevated glutathione levels in release medium appeared to be accelerated the release of ETA from mPEG-PLGA-SS-ETA

nanoconjugates due to the disulfide bridge of the mPEG-PLGA polymer and ETA.

9. Vimentin mAb conjugated mPEG-PLGA-SS-ETA nanoconjugates successfully targeted the ETA to the mesenchymal phenotype of HT-29 cells.
10. Pretreatment with Vimentin-conjugated and ETA-loaded nanoformulations enhanced the efficacy of adjuvant therapy in mesenchymal phenotype of HT-29 cells.
11. HT-29 CRC cell injection was successfully formed granulomas in Wistar rats.
12. After formation of granulomas, EMT was observed in rats and elevated GST- $\pi$  activity was observed in the homogenates of granulomas.
13. Pretreatment with Vimentin-conjugated and ETA-loaded nanoformulations enhance the efficacy of adjuvant therapy *in vivo*.

Future studies with ETA-loaded nano-sized formulations are planned. Different polymeric delivery systems will be formulated for targeting ETA. Indeed, it is planned to investigate and develop selective GST- $\pi$  inhibitors that are more efficient than ETA. In particular, the preparation of siRNA delivery systems directed to mesenchymal phenotypes of different colorectal cancer cell lines is envisaged.

## REFERENCES

- [1] National Cancer Institute, What Is Cancer, <https://www.cancer.gov/about-cancer/understanding/what-is-cancer> (Access date: **February 9, 2015**).
- [2] S.S. Knox, From 'omics' to complex disease: a systems biology approach to gene-environment interactions in cancer, *Cancer Cell International*, 10 (**2010**) 11.
- [3] D.S. Wishard, Is Cancer a Genetic Disease or a Metabolic Disease?, *EbioMedicine*, 2 (**2015**) 12.
- [4] A. Balmain, Cancer as a Complex Genetic Trait: Tumor Susceptibility in Humans and Mouse Models, *Cell*, 108 (**2002**) 145.
- [5] B. Kalyanaraman, Teaching the basics of cancer metabolism: Developing antitumor strategies by exploiting the differences between normal and cancer cell metabolism, *Redox Biology*, 12 (**2017**) 833.
- [6] R.J. Deberardinir, N. Sayed, D. Ditsworth and C. B. Thompson, Brick by brick: metabolism and tumor cell growth, *Current Opinion in Genetics and Development*, 18 (**2008**) 1.
- [7] N. Komorova, L.J. Josp, Loss- and Gain-of-Function Mutations in Cancer: Mass-action, Spatial and Hierarchical Models, *Journal of Statistical Physics*, 128 (**2007**) 1.
- [8] Y.H.P. Lee and W.J. Müller, Oncogenes and Tumor Suppressor Genes, *Cold Spring Harbor Perspectives in Biology*, 2 (**2010**) 10.
- [9] H. Wang, H. Han, S. Mousses and D.D. Von Hoff, Targeting loss-of-function mutations in tumor-suppressor genes as a strategy for development of cancer therapeutic agents, *Seminars in Oncology*, 33 (**2006**) 4.
- [10] B. Mair, T. Konopoka, C. Kerzendorfer, K. Sleiman, S. Salic and V. Serra, Gain- and Loss-of-Function Mutations in the Breast Cancer Gene GATA3 Result in Differential Drug Sensitivity, *PLOS Genetics*, 12 (**2016**) 9.
- [11] J. Zheng, Oncogenic chromosomal translocations and human cancer *Oncology Reports*, 30 (**2013**) 5.
- [12] I.A. Prior, P.D. Lewis and C. Mattos, A comprehensive survey of Ras mutations in cancer, *Cancer Research*, 72 (**2012**) 10.
- [13] T. Minamoto, M. Mai and Z. Ronai, K-ras mutation: early detection in molecular diagnosis and risk assessment of colorectal, pancreas, and lung cancers, *Cancer Detection and Prevention*, 24 (**2000**) 1.
- [14] O. Brison, Gene amplification and tumor progression, *Biochimica et Biophysica Acta*, 1155 (**1993**) 1.

- [15] M. Schwab, K. Alitalo, K.H. Klempnauer, H.E. Varmus, J.M. Bishop and F. Gilbert, Amplified DNA with limited homology to myc cellular oncogene is shared by human neuroblastoma cell lines and a neuroblastoma tumour, *Nature*, 305 (**1983**) 5931.
- [16] M. Huang and W.A. Weiss, Neuroblastoma and MYCN, *Cold Spring Harbor Perspectives in Medicine*, 3 (**2013**) 10.
- [17] K.S. Lee, Y. Kwak, K.H. Nam, D.W. Kim, S.B. Kang and G. Choe Favorable prognosis in colorectal cancer patients with co-expression of c-MYC and  $\beta$ -catenin, *BioMed Central Cancer*, 16 (**2016**) 1.
- [18] A. Giordano and W.H. Lee, Preface, *Oncogene*, 25 (**2006**) 5189.
- [19] J. Liu, C. Zhang and Z. Feng, Tumor suppressor p53 and its gain-of-function mutants in cancer, *Acta Biochimica et Biophysica Sinica*, 46 (**2014**) 3.
- [20] A.J. Levine, W. Hu and Z. Feng, Tumor Suppressor Genes. J. Mendelsohn, P. M. Howley, M. A. Israel, J. W. Gray and C. B. Thompson (Eds). *The Molecular Basis of Cancer (Third Edition)*, W.B. Saunders, Philadelphia, 31-38, **2008**.
- [21] D.K. Lam, and B.L. Schmidt, in: *Current Therapy In Oral and Maxillofacial Surgery*, S. C. Bagheri, R. B. Bell and H. A. Khan (Eds), W.B. Saunders, Saint Louis, Chapter 10, **2012**.
- [22] T. Ozaki and A. Nakagawara, Role of p53 in Cell Death and Human Cancers, *Cancers*, 3 (**2011**) 1.
- [23] A. Muller Patricia and H. Vousden Karen, Mutant p53 in Cancer: New Functions and Therapeutic Opportunities, *Cancer Cell*, 25 (**2014**) 3.
- [24] C.E. Meacham and S.J. Meacham, Tumour heterogeneity and cancer cell plasticity, *Nature*, 501 (**2013**) 7467.
- [25] C.M. Lovly, A.K. Salama and R. Salgia, Tumor Heterogeneity and Therapeutic Resistance, *American Society of Clinical Oncology Educational Book*, **2016**.
- [26] B. Mansoori, A. Mohammadi, S. Davudian, S. Shirjang and B. Baradaran, The Different Mechanisms of Cancer Drug Resistance: A Brief Review, *Advanced Pharmaceutical Bulletin*, 7 (**2017**) 3.
- [27] D.L. Dexter and J.T. Leith, Tumor heterogeneity and drug resistance, *Journal of Clinical Oncology*, 4 (**1986**) 2.
- [28] X. Xue and X.J. Liang, XUE X., Overcoming drug efflux-based multidrug resistance in cancer with nanotechnology, *Chinese Journal of Cancer*, 31 (**2012**) 1.
- [29] X. Dong and R.J. Mumper, Nanomedicinal strategies to treat multidrug-resistant tumors: current progress, *Nanomedicine*, 5 (**2010**) 1.

- [30] Y. Liang, S. Li and L. Chen, Physiological role of drug transporters, *Protein and Cell*, 6 (2015) 3.
- [31] S. Wilkens, Structure and mechanism of ABC transporters, *Prime Reports*, 7 (2015) 14.
- [32] R.W. Robey, S. Shukla, E.M. Finley, R.K. Oldham and D. Barnett, Inhibition of P-glycoprotein (ABCB1)- and multidrug resistance-associated protein 1 (ABCC1)-mediated transport by the orally administered inhibitor, CBT-1, *Biochemical Pharmacology*, 75 (2008) 1.
- [33] Y.L. Sun, A. Patel, P. Kumar and Z.S. Chen, Role of ABC transporters in cancer chemotherapy, *Chinese Journal of Cancer*, 31 (2012) 51.
- [34] E.L. Bradshaw-Pierce, T. M. Pitts, A.C. Tan, K. McPhillips, M. West, D. L. Gustafson, Tumor p-Glycoprotein Correlates with Efficacy of PF-3758309 in *in vitro* and *in vivo* Models of Colorectal Cancer, *Frontiers in Pharmacology* 4 (2013) 22.
- [35] J. F. Deeken, R. W. Robey, S. Shukla, K. Steadman, A. R. Chakraborty and B. Poonkuzhali, Identification of Compounds that Correlate with ABCG2 Transporter Function in the National Cancer Institute Anticancer Drug Screen, *Molecular Pharmacology*, 76 (2009) 956.
- [36] G. Szakács, J.P. Annereau, S. Lababidi, U. Shankavaram, A. Arciello and K. J. Bussey, Predicting drug sensitivity and resistance: Profiling ABC transporter genes in cancer cells, *Cancer Cell*, 6 (2004) 2.
- [37] N. S. Gavande, P. S. Vander, H. D. Vere-Carozza Hinshaw, S. I. Jalal, C. R. Sears and K. S. Pawelczak, DNA repair targeted therapy: The past or future of cancer treatment?, *Pharmacology and Therapeutics*, 160 (2016) 65.
- [38] M. R. Salehan and H. R. Morse, DNA damage repair and tolerance: a role in chemotherapeutic drug resistance, *British journal of Biomedical Science*, 70 (2013) 1.
- [39] S. Maynard, S. H. Schurman, C. Harboe, N. C. de Souza-Pinto and V. A. Bohr, Base excision repair of oxidative DNA damage and association with cancer and aging, *Carcinogenesis*, 30 (2009) 2.
- [40] Y.J. Kim and D. M. Wilson, Overview of Base Excision Repair Biochemistry, *Current Molecular Pharmacology*, 5 (2012) 3.
- [41] T. Budden and N. A. Bowden, The Role of Altered Nucleotide Excision Repair and UVB-Induced DNA Damage in Melanomagenesis, *International Journal of Molecular Sciences*, 14 (2013) 2.
- [42] G. Spivak, Nucleotide excision repair in humans, *DNA repair*, 36 (2015) 1.
- [43] D. Fink, S. Aebi and S. B. Howell The role of DNA mismatch repair in drug resistance, *Clinical Cancer Research*, 4 (1998) 1.

- [44] K. Pors and L. H. Patterson, DNA mismatch repair deficiency, resistance to cancer chemotherapy and the development of hypersensitive agents, *Current Topics in Medicinal Chemistry*, 5 (2005) 1.
- [45] M. M. de las Alas, S. Aebi, D. Fink, S. B. Howell and G. Los, Loss of DNA mismatch repair: effects on the rate of mutation to drug resistance, *Journal of Natinal Cancer Institute*, 89 (1997) 1.
- [46] S. Ahmed, Z. Zhou, J. Zhou and S.Q. Chen, Pharmacogenomics of Drug Metabolizing Enzymes and Transporters: Relevance to Precision Medicine, *Genomics, Proteomics and Bioinformatics*, 14 (2016) 2.
- [47] T. N. Johnson, The development of drug metabolising enzymes and their influence on the susceptibility to adverse drug reactions in children, *Toxicology*, 192 (2003) 2.
- [48] R.M. Mohammad, I. Muqbil, L. Lowe, C. Yedjou, H.Y. Hsu and L.T. Lin, Broad targeting of resistance to apoptosis in cancer, *Seminars in Cancer Biology*, 35 (2015) 2.
- [49] R.S.Y. Wong, Apoptosis in cancer: from pathogenesis to treatment, *Journal of Experimental and Clinical Cancer Research*, 30 (2011) 1.
- [50] R. Gerl and D.L. Vaux, Apoptosis in the development and treatment of cancer, *Carcinogenesis*, 26 (2005) 2.
- [51] H. Acloque, M.S. Adam, K. Fishwick, M. Bronner-Fraser and M.A. Nieto, Epithelial-mesenchymal transitions: the importance of changing cell state in development and disease, *The Journal of Clinical Investigation*, 119 (2009) 1.
- [52] R. Kalluri and R.A. Weinberg, The basics of epithelial-mesenchymal transition, *The Journal of Clinical Investigation*, 119 (2009) 1.
- [53] A. Ferrer-Vaquer, M. Viotti and A.K. Hadjantonakis, Transitions between epithelial and mesenchymal states and the morphogenesis of the early mouse embryo, *Cell Adhesion and Migration*, 4 (2010) 1.
- [54] J.M. Lee, S. Dedhar, K. Kalluri and E.W. Thompson, The epithelial-mesenchymal transition: new insights in signaling, development, and disease, *Journal of Cell Biology*, 172 (2006) 1.
- [55] S. Lamouille, J. Xu and R. Derynck, Molecular mechanisms of epithelial–mesenchymal transition, *Nature Reviews Molecular Cell Biology*, 15 (2014) 2.
- [56] M. K. Wendt, T. M. Allington and W.P. Schiemann, Mechanisms of Epithelial-Mesenchymal Transition by TGF- $\beta$ , *Future Oncology*, 5 (2009) 1.
- [57] J. Yang and R.A. Weinberg, Epithelial-Mesenchymal Transition: At the Crossroads of Development and Tumor Metastasis, *Developmental Cell*, 14 (2008) 2.

- [58] E. Rodriguez-Boulan and I.G. Macara, Organization and execution of the epithelial polarity programme, *Nature Reviews Molecular Cell Biology*, 15 (2014) 2.
- [59] K. Campbell, J. Casanova and H. Skaer, Mesenchymal-to-epithelial transition of intercalating cells in *Drosophila* renal tubules depends on polarity cues from epithelial neighbours, *Mechanisms of Development*, 127 (2010) 3.
- [60] I.G. Macara and L. McCaffrey, Cell polarity in morphogenesis and metastasis, *Philosophical Transactions of the Royal Society B: Biological Sciences*, 368 (2013) 2.
- [61] B.N.G. Giepmans and S.C.D. Van-Ljzendoorn, Epithelial cell–cell junctions and plasma membrane domains, *Biochimica et Biophysica Acta-Biomembranes*, 1788 (2009) 831.
- [62] B.J.A. Alberts and J. Lewis, *Cell Junctions. Molecular Biology of the Cell* 4<sup>th</sup> edition, Garland Science, New York, 2002.
- [63] K.W. Jeon, *International Review of Cytology*, Vol. 129, Elsevier Science, Amsterdam, (2000).
- [64] N. Pećina-Šlaus, Tumor suppressor gene E-cadherin and its role in normal and malignant cells, *Cancer Cell International*, 3 (2003) 17.
- [65] S. Baranwal and S.K. Alahari, Molecular mechanisms controlling E-cadherin expression in breast cancer, *Biochemical and Biophysical Research Communications*, 384 (2009) 6.
- [66] Y. Sun, J. Zhang and L. Ma,  $\alpha$ -catenin: A tumor suppressor beyond adherens junctions, *Cell Cycle*, 13 (2014) 2334.
- [67] L. Shapiro and W.I. Weis, Structure and Biochemistry of Cadherins and Catenins, *Cold Spring Harbor Perspectives in Biology*, 1 (2009) 1.
- [68] A. Hartsock and W.J. Nelson, Adherens and Tight Junctions: Structure, Function and Connections to the Actin Cytoskeleton, *Biochimica et Biophysica Acta*, 1778 (2008) 9.
- [69] A. Ahmad Khalili and M.R.A. Ahmad, Review of Cell Adhesion Studies for Biomedical and Biological Applications, *International Journal of Molecular Sciences*, 16 (2015) 4.
- [70] J. Miyoshi and Y. Takai, Structural and functional associations of apical junctions with cytoskeleton, *Biochimica et Biophysica Acta Biomembranes*, 1778 (2008) 1.
- [71] E. Stepniak, G.L. Radice and V. Vasioukhin, Adhesive and Signaling Functions of Cadherins and Catenins in Vertebrate Development, *Cold Spring Harbor Perspectives in Biology* 1 (2009) 1.



- [72] R. Aguilar-Cuenca, C. Llorente-Gonzalez, C. Vicente and M. Vicente-Manzanares, Microfilament-coordinated adhesion dynamics drives single cell migration and shapes whole tissues, *F1000 Research*, 6 (2017) 1.
- [73] J. W. O'Connor and E.W. Gomez, Biomechanics of TGF $\beta$ -induced epithelial-mesenchymal transition: implications for fibrosis and cancer, *Clinical and Translational Medicine*, 3 (2014) 23.
- [74] H.A.J. Müller and O. Bossinger, Molecular networks controlling epithelial cell polarity in development, *Mechanisms of Development*, 120 (2003) 6.
- [75] J.P. Campanale, T.Y. Sun and D.J. Montell, Development and dynamics of cell polarity at a glance, *Journal of Cell Science*, 130 (2017) 7.
- [76] A. Manninen, Epithelial polarity – Generating and integrating signals from the ECM with integrins, *Experimental Cell Research*, 334 (2015) 9.
- [77] J. Roignot, X. Peng and K. Mostov, Polarity in Mammalian Epithelial Morphogenesis, *Cold Spring Harbor Perspectives in Biology*, 5 (2013) 1.
- [78] D. Pradella, C. Naro, C. Sette and C. Ghigna, EMT and stemness: flexible processes tuned by alternative splicing in development and cancer progression, *Molecular Cancer*, 16 (2017) 8.
- [79] R.M. Bavle and K. Paremala, Cancer Conundrum, *Journal of Oral and Maxillofacial Pathology*, 19 (2015) 9.
- [80] J.H. Tsai and J. Yang, Epithelial–mesenchymal plasticity in carcinoma metastasis, *Genes and Development*, 27 (2013) 6.
- [81] J.P. Thiery, H. Acloque, R.Y.J. Huang and M.A. Nieto, Epithelial-Mesenchymal Transitions in Development and Disease, *Cell*, 139 (2009) 1.
- [82] J. Jim and J.P. Thiery, Epithelial-mesenchymal transitions: insights from development, *Development*, 139 (2012) 19.
- [83] E. Batlle, E. Sancho, C. Franci, D. Dominguez, M Monfar and J. Baulida, The transcription factor snail is a repressor of E-cadherin gene expression in epithelial tumour cells, *Nature Cell Biology*, 2 (2000) 9.
- [84] A. Cano, M.A. Perez-Moreno, I. Rodrigo, A. Locascio and M.J. Blanco, The transcription factor snail controls epithelial-mesenchymal transitions by repressing E-cadherin expression, *Nature Cell Biology*, 2 (2000) 3.
- [85] K.M. Hajra, D.Y. Chen and E.R. Fearon, The SLUG zinc-finger protein represses E-cadherin in breast cancer, *Cancer Research*, 62 (2002) 8.
86. A. Gheldof and G. Berx, Cadherins and epithelial-to-mesenchymal transition, *Progress in Molecular Biology and Translational Science*, 116 (2013) 6.
- [87] G.J. Zhu, P.P. Song, H. Zhou, X.H. Shen, J.G. Wang and X.F. Ma, Role of epithelial-mesenchymal transition markers E-cadherin, N-cadherin,  $\beta$ -

- catenin and ZEB2 in laryngeal squamous cell carcinoma, *Oncology Letters*, 15 (2018) 1.
- [88] K. Gravdal, O.J. Halvorsen, S.A. Haukaas, L.A. Akslen, A switch from E-cadherin to N-cadherin expression indicates epithelial to mesenchymal transition and is of strong and independent importance for the progress of prostate cancer, *Clinical Cancer Research*, 13 (2007) 1.
- [89] A.W. Holle, M. Kalafat, A.S. Ramos, T. Seufferlein, R. Kemkemer and J.P. Spatz, Intermediate filament reorganization dynamically influences cancer cell alignment and migration, *Scientific Reports*, 7 (2017) 2.
- [90] C.Y. Liu, H.H. Lin, M.J. Tang and Y.K. Wang, Vimentin contributes to epithelial-mesenchymal transition cancer cell mechanics by mediating cytoskeletal organization and focal adhesion maturation, *Oncotarget*, 6 (2015) 3.
- [91] M.G. Mendez, S.I. Kojima and R.D. Goldman, Vimentin induces changes in cell shape, motility, and adhesion during the epithelial to mesenchymal transition, *The FASEB Journal*, 24 (2010) 1
- [92] V.G. Brunton, I.R.J. MacPherson and M.C. Frame, Cell adhesion receptors, tyrosine kinases and actin modulators: a complex three-way circuitry, *Biochimica et Biophysica Acta Molecular Cell Research*, 1692 (2004) 4.
- [93] U. Cavallaro and G. Christofori, Cell adhesion and signalling by cadherins and Ig-CAMs in cancer, *Nature Review Cancer*, 4 (2004) 2.
- [94] G. Christofori, New signals from the invasive front, *Nature*, 441 (2006) 5.
- [95] E.S. Radisky and D.C. Radisky, Matrix Metalloproteinase-Induced Epithelial-Mesenchymal Transition in Breast Cancer, *Journal of Mammary Gland Biology and Neoplasia*, 15 (2010) 2.
- [96] D.S. Micalizzi, S.M. Farabaugh and H.L. Ford, Epithelial-Mesenchymal Transition in Cancer: Parallels Between Normal Development and Tumor Progression, *Journal of Mammary Gland Biology and Neoplasia*, 15 (2010) 2.
- [97] J.M. Pérez-Pomares and R. Muñoz-Chápuli, Epithelial–mesenchymal transitions: A mesodermal cell strategy for evolutive innovation in Metazoans, *The Anatomical Record*, 268 (2002) 351.
- [98] J.M. López-Novoa and M.A. Niete, Inflammation and EMT: an alliance towards organ fibrosis and cancer progression, *EMBO Molecular Medicine* 1 (2009) 1.
- [99] Y.M. Yang and W.X. Yang, Epithelial-to-mesenchymal transition in the development of endometriosis, *Oncotarget*, 8 (2017) 9.
- [100] S. Ghanta, N. Nayan, N. Raj Kumar and S. Pasupuleti, Epithelial-mesenchymal transition: Understanding the basic concept, 4 (2012) 6.

- [101] A. Fatatis, Signaling Pathways and Molecular Mediators in Metastasis: Vol. 1, Springer, Netherlands, **2012**.
- [102] R.C. Stone, I. Pastar, N. Ojeh, V. Chen, S. Liu and K.I. Garzon, Epithelial-Mesenchymal Transition in Tissue Repair and Fibrosis, Cell and Tissue Research, 365 (**2016**) 6.
- [103] X.F. Xu and H.P. Dai, Type 2 epithelial mesenchymal transition *in vivo*: truth or pitfalls?, Chinese Medicinal Journal, 125 (**2012**) 7.
- [104] S. Heerboth, G. Housman, M. Leary, M. Longacre, S. Byler and K. Lapinska, EMT and tumor metastasis, Clinical and Translational Medicine, 4 (**2015**) 6.
- [105] S. Ansieau, G. Collin and L. Hill, EMT or EMT-Promoting Transcription Factors, Where to Focus the Light, Frontiers in Oncology, 4 (**2014**) 3.
- [106] E. Sanchez-Tillo, Y. Liu, O. de Barrios Siles and L. Fanlo, EMT-activating transcription factors in cancer: beyond EMT and tumor invasiveness, Cellular Molecular Life Science, 69 (**2012**) 6.
- [107] V.M. Díaz, R. Viñas-Castells and A. García de Herreros, Regulation of the protein stability of EMT transcription factors, Cell Adhesion and Migration 8 (**2014**) 8.
- [108] S. Goossens, N. Vandamm, P. Van Vlierberghe and G. Berx, EMT transcription factors in cancer development re-evaluated: Beyond EMT and MET, Biochimica et Biophysica Acta Reviews on Cancer, 1868 (**2017**) 1.
- [109] M. Garg, Epithelial-mesenchymal transition - activating transcription factors - multifunctional regulators in cancer, World Journal of Stem Cells, 5 (**2013**) 6.
- [110] A.G., De Herreros, S. Peiró, M. Nassour and P. Savagner, Snail family regulation and epithelial mesenchymal transitions in breast cancer progression, Journal of Mammary Gland Biology and Neoplasia, 15 (**2010**) 7.
- [111] B. Du and J.S. Shim, Targeting Epithelial-Mesenchymal Transition (EMT) to Overcome Drug Resistance in Cancer, Molecules, 12 (**2016**) 21.
- [112] T. Shibue and R.A. Weinberg, EMT, CSCs, and drug resistance: the mechanistic link and clinical implications, Nature Review of Clinical Oncology, 14 (**2017**) 9.
- [113] J. Wang, Q. Wei, X. Wang, S. Tang, H. Liu and F. Zhang, Transition to resistance: An unexpected role of the EMT in cancer chemoresistance, Genes and Diseases, 3 (**2016**) 6.
- [114] P. Zhou, B. Li, F. Liu, M. Zhang, Q. Wang and Y. Liu, The epithelial to mesenchymal transition (EMT) and cancer stem cells: implication for treatment resistance in pancreatic cancer, Molecular Cancer, 16 (**2017**) 52.

- [115] B.N. Smith and N.A. Bhowmick, Role of EMT in Metastasis and Therapy Resistance, *Journal of Clinical Medicine*, 5 (2016) 17.
- [116] T.W. Stark, P.J. Hensley, A. Spear, H. Pu, S.S., Strup and N. Kyprianou, Predictive value of epithelial-mesenchymal-transition (EMT) signature and PARP-1 in prostate cancer radioresistance, *Prostate*, 77 (2017) 17.
- [117] F.H. Sarkar, Y. Li, Z. Wang and D. Kong, Pancreatic cancer stem cells and EMT in drug resistance and metastasis, *Minerva Chirurgica*, 64 (2009) 5.
- [118] Ö.D. Işeri, M.D. Kars, F. Arpaci, C. Atalay, I. Pak and U. Gündüz, Drug resistant MCF-7 cells exhibit epithelial-mesenchymal transition gene expression pattern, *Biomedicine and Pharmacotherapy*, 65 (2011) 5.
- [119] C.P. Prasad, G. Rath, S. Mathur, D. Bhatnaga, R. Parshad and R. Ralhan Expression analysis of E-cadherin, Slug and GSK3beta in invasive ductal carcinoma of breast, *BioMed Cancer*, 9 (2009) 5.
- [120] P. Farmer, H. Bonnefoi, P. Anderle, D. Cameron, P. Wirapati and V. Bécette, A stroma-related gene signature predicts resistance to neoadjuvant chemotherapy in breast cancer, *Nature Medicine*, 15 (2009) 4.
- [121] H. Raza, Dual Localization of Glutathione S-Transferase in the Cytosol and Mitochondria: Implications in Oxidative Stress, Toxicity and Disease, *The FEBS journal*, 278 (2011) 1.
- [122] T. Pandey, S.K. Singh, G. Chhetri, T. Tripathi and A.K. Singh, Characterization of a Highly pH Stable Chi-Class Glutathione S-Transferase from *Synechocystis* PCC 6803, *PLoS ONE*, 10 (2015) 1.
- [123] A. Vararattanavech, P. Prommeenate and J. Ketterman Albert, The structural roles of a conserved small hydrophobic core in the active site and an ionic bridge in domain I of Delta class glutathione S-transferase, *Biochemical Journal*, 393 (2006) 95.
- [124] R. Udomsinprasert, A. Bogoyevitch Marie and J. Ketterman Albert, Reciprocal regulation of glutathione S-transferase spliceforms and the *Drosophila* c-Jun N-terminal kinase pathway components, *Biochemical Journal*, 383 (2004) 490.
- [125] O. Modén and B. Mannervik, in *Glutathione Transferases in the Bioactivation of Azathioprine*, D.M. Townsend and K.D. Tew (Eds), Chapter Six, Academic Press San Diego, 2014.
- [126] K. Bachmann, in: *Drug Metabolism*, M. Hacker, W. Messer and K. Bachman (Eds), Chapter Eight, Academic Press San Diego, 2009.
- [127] C. Espinosa-Diez, V. Miguel, D. Mennerich, T. Kietzman, P. Sánchez-Pérez and S. Cadenas, Antioxidant responses and cellular adjustments to oxidative stress, *Redox Biology*, 6 (2015) 3.

- [128] R.N. Armstrong, Glutathione S-transferases: reaction mechanism, structure, and function, *Chemical Research in Toxicology*, 4 (1991) 4.
- [129] B. Mannervik, Five Decades with Glutathione and the GSTome, *The Journal of Biological Chemistry*, 287 (2012) 3.
- [130] I.C. Crocker, C.Y. Zhou, A.K. Bewtra, W. Kreutner and R.G. Townley, Glucocorticosteroids inhibit leukotriene production, *Annual Allergy Asthma Immunology*, 78 (1997) 5.
- [131] P. Labbé, H. Alout, L., Djogbéno, N. Pasteur and M. Weill, Evolution of Resistance to Insecticide in Disease Vectors. M. Tibayrenc (Eds), in *Genetics and Evolution of Infectious Disease*, Elsevier, London, 2011.
- [132] M.R. Franklin, in *Phase II Biotransformation Reactions-Glutathione-S-Transferase*. S.J Enna and D.B. Bylund (Eds), *The Comprehensive Pharmacology Reference*, Elsevier, New York, 2007.
- [133] M.A. and R.F. Vargo Colman, Heterodimers of wild-type and subunit interface mutant enzymes of glutathione S-transferase A1-1: Interactive or independent active sites, *Protein Science: A Publication of the Protein Society*, 13 (2004) 3.
- [134] S. Zubkov, W.J. Lennarz and S. Mohanty, Structural basis for the function of a minimembrane protein subunit of yeast oligosaccharyltransferase, *Proceedings of the National Academy of Sciences of the United States of America*, 101 (2004) 6.
- [135] D. Sheehan, G. Meade, V.M. Foley and C.A. Dowd, Structure, function and evolution of glutathione transferases: implications for classification of non-mammalian members of an ancient enzyme superfamily, *Biochemical Journal*, 360 (2001) 3.
- [136] H.J. Atkinson and P.C. Babbitt, Glutathione Transferases Are Structural and Functional Outliers in the Thioredoxin Fold, *Biochemistry*, 48 (2009) 6.
- [137] L. Prade, R. Huber, T.H. Manoharan and W.E. Fahl, Structures of class pi glutathione S-transferase from human placenta in complex with substrate, transition-state analogue and inhibitor, *Structure*, 5 (1997) 4.
- [138] D.P. Dixon, A. Laphorn and R. Edwards, Plant glutathione transferases, *Genome Biology*, 3 (2002) 3.
- [139] J.W. Gronwald and K.L. Plaisance, Isolation and Characterization of Glutathione S-Transferase Isozymes from Sorghum, *Plant Physiology*, 117 (1998) 2.
- [140] N.E. Labrou, G.A. Kotzia and Y.D. Clonis, Engineering the xenobiotic substrate specificity of maize glutathione S-transferase I, *Protein Engineering, Design and Selection*, 17 (2004) 2.

- [141] A.B. Juarez-Martinez, R.R. Sotelo-Mundo and E. Rudino-Pinera, Crystal structure of a class-mu glutathione S-transferase from whiteleg shrimp *Litopenaeus vannamei*: structural changes in the xenobiotic binding H-site may alter the spectra of molecules bound, *Journal of Biochemistry Molecular Toxicology*, 31 (2017) 1.
- [142] M.J. Morris, D. Liu, L.M. Weaver, P.G. Board and M.G. Casarotto, A Structural Basis for Cellular Uptake of GST-Fold Proteins, *PLOS ONE*, 13 (2011) 3.
- [143] D. Bartling, R. Radzio, U. Steiner and E.W. Weiler, A glutathione S-transferase with glutathione-peroxidase activity from *Arabidopsis thaliana*, *European J of Biochemistry*, 216 (1993) 2.
- [144] F. Deng and K.K. Hatzios, Characterization and Safener Induction of Multiple Glutathione S-Transferases in Three Genetic Lines of Rice, *Pesticide Biochemistry and Physiology*, 72 (2002) 2.
- [145] Y. Kanaoka, H. Ago, E. Inagaki, T., Nanayama, M., Miyano and R. Kikuno Cloning and crystal structure of hematopoietic prostaglandin D synthase, *Cell*, 90 (1997) 1.
- [146] H. Sies and L. Packer, *Glutathione Transferases and Gamma-Glutamyl Transpeptidases*, Vol. 3, Elsevier, Amsterdam, 2005.
- [147] K.D. Tew, Y. Manevich, C. Grek, Y. Xiong, J. Uys and D.M. Townsend, The Role of Glutathione S-transferase P in signaling pathways and S-glutathionylation in Cancer, *Free Radical Biology and Medicine*, 51 (2011) 2.
- [148] M. Afrand, N. Bashardoost, M.H. Sheikhha and M. Afkhami-Ardekani, Association between Glutathione S-Transferase GSTM1-T1 and P1 Polymorphisms with Metabolic Syndrome in Zoroastrians in Yazd, Iran *Iranian Journal of Public Health*, 44 (2015) 1.
- [149] G. Ginsberg, S. Smolenski, D. Hattis, K.Z. Guyton and D.O. Johns, Genetic Polymorphism in Glutathione Transferases (GST): Population distribution of GSTM1, T1, and P1 conjugating activity, *Journal of Toxicology and Environmental Health Part B*, 12 (2009) 9.
- [150] D. Sheehan, G. Meade, V.M. Foley and C.A. Dowd, Structure, function and evolution of glutathione transferases: implications for classification of non-mammalian members of an ancient enzyme superfamily, *Biochemical Journal*, 360 (2001) 3.
- [151] N. Allocati, M. Masulli, C. Di Ilio and L. Federic, Glutathione transferases: substrates, inhibitors and pro-drugs in cancer and neurodegenerative diseases, *Oncogenesis*, 7 (2018) 8.
- [152] T. Pandey, G. Chhetri, R. Chinta, B. Kumar, D.B. Singh and T. Tripathi, Functional classification and biochemical characterization of a novel rho

- class glutathione S-transferase in *Synechocystis* PCC 6803, *FEBS Open Biology*, 5 (2015) 1.
- [153] A.W. Hayes and C.L. Kruger, *Hayes' Principles and Methods of Toxicology*, Sixth Edition, Taylor & Francis, 2014.
- [154] L.G. Higgins and J.D. Hayes, Mechanisms of induction of cytosolic and microsomal glutathione transferase (GST) genes by xenobiotics and pro-inflammatory agents, *Drug Metabolism Reviews*, 43 (2011) 1.
- [155] P.J. Jakobsson, R. Morgenstern, J. Mancini, A. Ford-Hutchinson and B. Persson, Membrane-associated proteins in eicosanoid and glutathione metabolism (MAPEG). A widespread protein superfamily, *American Journal of Respiratory and Critical Care Medicine*, 161 (2000) 2.
- [156] K. Sato, S. Tsuchida and K. Tamai, Anti-cancer drug resistance and glutathione S-transferases, *Gan To Kagaku Ryoho*, 16 (1989) 1.
- [157] T. Bernig, S. Ritz, G. Brodt, I. Volkmer and M.S. Staeger, Glutathione-S-Transferases and Chemotherapy Resistance of Hodgkin's Lymphoma Cell Lines, *Anticancer Research*, 36 (2016) 5.
- [158] V.J. Findlay, D.M. Townsend and K.D. Tew, in *Glutathione and Glutathione S-Transferases in Drug Resistance*, B. Teicher (Eds), Humana Press, New Jersey, 2006.
- [159] D.M. Townsend and K.D. Tew, The role of glutathione-S-transferase in anti-cancer drug resistance, *Oncogene*, 22 (2003) 2.
- [160] I. Mármol, C. Sánchez-de-Diego, A. Pradilla Dieste, E. Cerrada and M.J. Rodríguez Yoldi, Colorectal Carcinoma: A General Overview and Future Perspectives in Colorectal Cancer, *International Journal of Molecular Sciences*, 18 (2017) 197.
- [161] K. Simon Colorectal cancer development and advances in screening, *Clinical Interventions in Aging*, 11 (2016) 1.
- [162] B.E. Ansa Coughlin, S.S. Alema-Mensah, S.A. Smith, Evaluation of Colorectal Cancer Incidence Trends in the United States (2000–2014), *Journal of Clinical Medicine*, 7 (2018) 22.
- [163] J.S.G. Pestana, S.F.F. Martins, Colorectal cancer: comparative analysis of clinical and pathological characteristics in patients aged above and below 45 years of age and impact on prognosis, *Journal of Coloproctology*, 36 (2016) 2.
- [164] H. Jahangirian, E.G. Lemraski, T.J. Webster, R. Rafiee-Moghaddam and Y.A. Abdollahi, A review of drug delivery systems based on nanotechnology and green chemistry: green nanomedicine, *International Journal of Nanomedicine*, 12 (2017) 8.

- [165] P. Satalkar, B.S. Elger and D.M. Shaw, Defining Nano, Nanotechnology and Nanomedicine: Why Should It Matter?, *Science and Engineering Ethics* 22 (2016) 1.
- [166] B. Walker and C.P. Mouton, Nanotechnology and nanomedicine: a primer, *Journal of the National Medical Association*, 98 (2006) 2.
- [167] J.K. Patra Das, L.F. Fraceto, E.V.R. Campos, M.D.P Rodriguez-Torres and L.S. Acosta-Torres, Nano based drug delivery systems: recent developments and future prospects, *Journal of Nanobiotechnology*, 16 (2018) 1.
- [168] B.V. Bonifácio, P.B. da Silva, M.A.D.S. Ramos, K.M.S. Negri, T.M. Bauab and M. Chorilli Nanotechnology-based drug delivery systems and herbal medicines: a review, *International Journal of Nanomedicine*, 9 (2014) 1.
- [169] B. Fonseca-Santos, M.P.D. Gremião and M. Chorilli, Nanotechnology-based drug delivery systems for the treatment of Alzheimer's disease, *International Journal of Nanomedicine*, 10 (2015) 10.
- [170] R. Bazak, M. Hourri, S.E. Achy, W. Hussein and T. Refaat Passive targeting of nanoparticles to cancer: A comprehensive review of the literature, *Molecular and Clinical Oncology*, 2 (2014) 2.
- [171] V. Sanna, N. Pala and M. Sechi, Targeted therapy using nanotechnology: focus on cancer, *International Journal of Nanomedicine*, 9 (2014) 2.
- [172] E.A. Azzopardi, E.L. Ferguson and D.W. Thomas, The enhanced permeability retention effect: a new paradigm for drug targeting in infection, *Journal of Antimicrobial Chemotherapy*, 68 (2013) 4.
- [173] Y. Nakamura, A. Mochida, P.L. Choyke and H. Kobayash, Nanodrug Delivery: Is the Enhanced Permeability and Retention Effect Sufficient for Curing Cancer, *Bioconjugate Chemistry*, 27 (2016) 2.
- [174] N. Singh, A. Joshi, A.P. Toor and G. Verma, in *Drug delivery: advancements and challenges*, E. Andronescu and A.M. Grumezescu (Eds), Chapter 27, Elsevier, Amsterdam, 2017.
- [175] K. Krishnaswamy and V. Orsat, in *Sustainable Delivery Systems Through Green Nanotechnology*. A.M. Grumezescu (Eds), Chapter 2, Elsevier, Amsterdam, 2017.
- [176] S. Pund and A. Joshi, in *Nanoarchitectures for Neglected Tropical Protozoal Diseases: Challenges and State of the Art*, A.M. Grumezescu (Eds) Chapter 23, Elsevier, Amsterdam, 2017.
- [177] S.P. Egusquiaguirre, J.L. Pedraz, R.M. Hernández and M. Igartua M. in *Nanotherapeutic Platforms for Cancer Treatment: From Preclinical Development to Clinical Application*, A.M. Holban and A.M., Grumezescu (Eds), William Andrew Publishing, England, 2016.



- [178] K.K. Chereddy, G. Vandermeulen and V. Pr eat PLGA based drug delivery systems: Promising carriers for wound healing activity, *Wound Repair and Regeneration*, 24 (2016) 2.
- [179] L. Naves, C. Dhand, L. Almeida, L. Rajamani, S. Ramakrishna and G. Soares, Poly(lactic-co-glycolic) acid drug delivery systems through transdermal pathway: an overview, *Progress in Biomaterials*, 6 (2017) 1.
- [180] D. Kloose, F. Siepmann, K. Elkharraz and J. Siepmann, PLGA-based drug delivery systems: Importance of the type of drug and device geometry, *International Journal of Pharmaceutics*, 354 (2008) 3.
- [181] D.N. Kapoor, A. Bhatia, R. Kaur, R. Sharma, G. Kaur and S. Dhawan, PLGA: a unique polymer for drug delivery, *Therapeutic delivery*, 6 (2015) 1.
- [182] S. Fredenberg, M. Wahlgren, M. Reslow and A. Axelsson The mechanisms of drug release in poly(lactic-co-glycolic acid)-based drug delivery systems- A review, *International Journal of Pharmaceutics*, 415 (2011) 3.
- [183] A. Bolhassani, S. Javanzad, T. Saleh, M. Hashemi, M.R. Aghasadeghi and S.M. Sadat, Polymeric nanoparticles: Potent vectors for vaccine delivery targeting cancer and infectious diseases, *Human Vaccines and Immunotherapeutics*, 10 (2014) 1.
- [184] R. Singh and J.W. Lillard, Nanoparticle-based targeted drug delivery, *Experimental and Molecular Pathology*, 86 (2009) 1.
- [185] N. Horiuchi, K. Nakagawa, Y. Sasaki, K. Minato, Y. Fujiwara and K. Nezu, *In vitro* antitumor activity of mitomycin C derivative (RM-49) and new anticancer antibiotics (FK973) against lung cancer cell lines determined by tetrazolium dye (MTT) assay, *Cancer Chemotherapy Pharmacology*, 22 (1988) 2.
- [186] C.W. Lin, P. Gonzalez and F. Yuan, Cellular pharmacokinetic and pharmacodynamic analyses of ethacrynic acid: Implications in topical drug delivery in the eye, *Molecular Vision*, 17 (2011) 2.
- [187] R. Devulapally, K. Foygel, T.V. Sekar, J.K Willmann. and R. Paulmurugan Gemcitabine and Antisense-microRNA Co-encapsulated PLGA-PEG Polymer Nanoparticles for Hepatocellular Carcinoma Therapy, *ACS Applied Materials and Interfaces*, 8 (2016) 2.
- [188] E. Locatelli and M. Comes Franchini, Biodegradable PLGA-*b*-PEG polymeric nanoparticles: synthesis, properties, and nanomedical applications as drug delivery system, *Journal of Nanoparticle Research*, 14 (2012) 1.
- [189] B. Han, Y. Wang, L. Wang, Z. Shang, S. Wang and J. Pei Preparation of GST Inhibitor Nanoparticle Drug Delivery System and Its Reversal Effect on the Multidrug Resistance in Oral Carcinoma, 5 (2015) 2.

- [190] B. Han, Y. Wang, L. Wang, Z. Shang, S. Wang and J. Pei Preparation of GST Inhibitor Nanoparticle Drug Delivery System and Its Reversal Effect on the Multidrug Resistance in Oral Carcinoma, 5 (2015) 2.
- [191] H. Fessi, F. Puisieux, J.P. Devissaguet, N. Ammoury and S. Benita, Nanocapsule formation by interfacial polymer deposition following solvent displacement, International Journal of Pharmaceutics, 55 (1989) 1.
- [192] Y. Wang, P. Li, T. Truong-Dinh Tran, J. Zhang and L. Kong, Manufacturing Techniques and Surface Engineering of Polymer Based Nanoparticles for Targeted Drug Delivery to Cancer, Nanomaterials, 6 (2016) 26.
- [193] M. Arruebo, M. Valladares and Á. González-Fernández, Antibody-Conjugated Nanoparticles for Biomedical Applications, Journal of Nanomaterials, 24 (2009) 2.
- [194] B. Galateanu, A. Hudita, C. Negrei, R.M. Ion, M. Costache and M. Stan, Impact of multicellular tumor spheroids as an *in vivo*-like tumor model on anticancer drug response, International Journal of Oncology, 48 (2016) 2.
- [195] J. Akhter, P. Yao, L.A. Johnson, S.M. Riordan and D.L. Morris, A new peritoneal carcinomatosis model in cyclosporine immunosuppressed rats, Anticancer Research, 28 (2008) 1.
- [196] S.M. Robinson, J. Mann, A. Vasilaki, J. Mathers, A.D. Burt and F. Oakley Pathogenesis of FOLFOX induced sinusoidal obstruction syndrome in a murine chemotherapy model, Journal of Hepatology, 59 (2013) 2.
- [197] D. Keizman, N. Maimon, M. Ish-Shalom, D. Buchbut, M. Inbar and B. Klein, An animal model for chemotherapy-associated steatohepatitis and its prevention by the oral administration of fatty acid bile acid conjugate, Cancer, 116 (2010) 2.
- [198] M. Tian, and W.P. Schiemann, TGF-beta Stimulation of EMT Programs Elicits Non-genomic ER-alpha Activity and Anti-estrogen Resistance in Breast Cancer Cells, Journal of Cancer Metastasis Treatment, 3 (2017) 1.
- [199] W.C. Lim, H. Kim, Y.J. Kim, K.C. Choi, I.H. Lee and K.H. Lee, Dioscin suppresses TGF-beta1-induced epithelial-mesenchymal transition and suppresses A549 lung cancer migration and invasion, Bioorganic & Medicinal Chemistry Letters, 27 (2017) 2.
- [200] B. Du and J. Shim, Targeting Epithelial–Mesenchymal Transition (EMT) to Overcome Drug Resistance in Cancer, Molecules, 21 (2016) 7.
- [201] M.S. Pino, H. Kikuchi, M. Zeng, M.T. Herraiz, I. Sperduti and D. Berger, The epithelial to mesenchymal transition is impaired in colon cancer cells with microsatellite instability, Gastroenterology, 138 (2010) 7.
- [202] D. D’Eliseo, G. Di Rocco, R. Loria, S. Soddu, A. Santoni and F.J.J. Velotti, Epithelial-to-mesenchymal transition and invasion are upmodulated by tumor-

- expressed granzyme B and inhibited by docosahexaenoic acid in human colorectal cancer cells, *Molecules*, 35 (2016) 24.
- [203] P.V. Angadi, P.V. Patil, V. Angadi, D. Mane, S. Shekar and S. Hallikerimath, Immunoexpression of Epithelial Mesenchymal Transition Proteins E-Cadherin,  $\beta$ -Catenin, and N-Cadherin in Oral Squamous Cell Carcinoma, *International Journal of Surgical Pathology*, 24 (2016) 3.
- [204] H.N. Chen, K. Yuan, N. Xie, K. Wang, Z. Huang and Y. Chen, PDLIM1 Stabilizes the E-Cadherin/ $\beta$ -Catenin Complex to Prevent Epithelial–Mesenchymal Transition and Metastatic Potential of Colorectal Cancer Cells, 76 (2016) 4.
- [205] L. Li, L. Qi, Z. Liang, W. Song, Y. Liu and Y. Wang, Transforming growth factor- $\beta$ 1 induces EMT by the transactivation of epidermal growth factor signaling through HA/CD44 in lung and breast cancer cells, *International Journal of Molecular Medicine*, 36 (2015) 2.
- [206] H. Kasai, J.T. Allen, R.M. Mason, T. Kamimura and Z. Zhang, TGF- $\beta$ 1 induces human alveolar epithelial to mesenchymal cell transition (EMT), *Respiratory Research*, 6 (2005) 3.
- [207] D. Schneider, M. Tarantola and A. Janshoff, Dynamics of TGF- $\beta$  induced epithelial-to-mesenchymal transition monitored by Electric Cell-Substrate Impedance Sensing, *Biochimica et Biophysica Acta (BBA) Molecular Cell Research*, 1813 (2011) 7.
- [208] Z. Chen, D. Zhang, F. Yue, M. Zheng, Z. Kovacevic and D.R. Richardson, The iron chelators Dp44mT and DFO inhibit TGF-beta-induced epithelial-mesenchymal transition via up-regulation of N-Myc downstream-regulated gene 1 (NDRG1), *The Journal of Biological Chemistry*, 287 (2012) 42.
- [209] Z. Yang, S. Liu, M. Zhu, H. Zhang, J. Wang, and Q. Xu, PS341 inhibits hepatocellular and colorectal cancer cells through the FOXO3/CTNNB1 signaling pathway, *Scientific Reports*, 6 (2016) 12.
- [210] S. Lindsey and S.A. Langhans, Crosstalk of Oncogenic Signaling Pathways during Epithelial–Mesenchymal Transition, *Frontiers in Oncology*, 4 (2014) 8.
- [211] B.D. White A.J. Chien and D.W. Dawson Dysregulation of Wnt/ $\beta$ -catenin Signaling in Gastrointestinal Cancers, *Gastroenterology*, 142 (2012) 2.
- [212] S. Yang, Y. Liu, M.Y. Li, S.I. Yang and S. Wang, FOXP3 promotes tumor growth and metastasis by activating Wnt/ $\beta$ -catenin signaling pathway and EMT in non-small cell lung cancer, *Molecular Cancer*, 16 (2017) 124.
- [213] B. Zhou, Y. Liu, M. Kahn, D.K. Ann, A. Han and H. Wang, Interactions Between  $\beta$ -Catenin and Transforming Growth Factor- $\beta$  Signaling Pathways Mediate Epithelial-Mesenchymal Transition and Are Dependent on the Transcriptional Co-activator cAMP-response Element-binding Protein

- (CREB)-binding Protein (CBP), *The Journal of Biological Chemistry*, 287 (2012) 8.
- [214] J. Zhang, X.J. Tian and J. Xing, Signal Transduction Pathways of EMT Induced by TGF- $\beta$ , SHH, and WNT and Their Crosstalks, *Journal of Clinical Medicine*, 5 (2016) 41.
- [215] T. Ipekci, F. Ozden, B. Unal, C. Saygin, D. Uzunaslana and E.J.P. Ates, Epithelial-Mesenchymal Transition Markers  $\beta$ -catenin, Snail, and E-Cadherin do not Predict Disease Free Survival in Prostate Adenocarcinoma: a Prospective Study, *Pathology Oncology Research* 21 (2015) 4.
- [216] L. Sheng, S. Zhang and H. Xu, Effect of Slug-Mediated Down-Regulation of E-Cadherin on Invasiveness and Metastasis of Anaplastic Thyroid Cancer Cells, *Medical Science Monitor, International Medical Journal of Experimental and Clinical Research*, 23 (2017) 138.
- [217] V. Bolos, H. Peinado, M.A. Perez-Moreno, M.F. Fraga, M. Esteller and A. Cano, The transcription factor Slug represses E-cadherin expression and induces epithelial to mesenchymal transitions: a comparison with Snail and E47 repressors, *Journal of Cell Science*, 116 (2003) 8.
- [218] J.C. Cheng, H.M. Chang and P.C. Leung, Transforming growth factor-beta1 inhibits trophoblast cell invasion by inducing Snail-mediated down-regulation of vascular endothelial-cadherin protein, *Journal of Biological Chemistry*, 288 (2013) 2.
- [219] J. Feng, Z. Fu, J. Guo, W. Lu, K. Wen and W. Chen, Overexpression of peroxiredoxin 2 inhibits TGF-beta1-induced epithelial-mesenchymal transition and cell migration in colorectal cancer, *Molecular Medicine Reports*, 10 (2014) 3.
- [220] H. Li, H. Wang, F. Wang, Q. Gu and X. Xu, Snail involves in the transforming growth factor beta1-mediated epithelial-mesenchymal transition of retinal pigment epithelial cells, *PLoS One*, 6 (2011) 2.
- [221] S. Otsuki, M. Inokuchi, M. Enjoji, T. Ishikawa, Y. Takagi and K. Kato, Vimentin expression is associated with decreased survival in gastric cancer, *Oncology Reports*, 25 (2011) 2.
- [222] A. Satelli and S. Li, Vimentin as a potential molecular target in cancer therapy or Vimentin, an overview and its potential as a molecular target for cancer therapy, *Cellular and molecular life sciences*, 68 (2011) 6.
- [223] M.E. Kidd, D.K. Shumaker and K.M. Ridge, The Role of Vimentin Intermediate Filaments in the Progression of Lung Cancer, *American Journal of Respiratory Cell and Molecular Biology*, 50 (2014) 6.

- [224] M. Maeda, K.R. Johnson and M.J. Wheelock, Cadherin switching: essential for behavioral but not morphological changes during an epithelium-to-mesenchyme transition, *Journal of Cell Science*, 118 (2005) 5.
- [225] Y.W. Cao, G.X. Wan, J.P. Sun, X.B. Cui, J.M. Hu and W.H. Liang, Implications of the Notch1-Snail/Slug-epithelial to mesenchymal transition axis for lymph node metastasis in infiltrating ductal carcinoma, *The Kaohsiung Journal of Medical Sciences*, 31 (2015) 6.
- [226] D. Anastassiou, V. Rumjantseva, W. Cheng, J. Huang, P.D. Canoll and D.J. Yamashiro, Human cancer cells express Slug-based epithelial-mesenchymal transition gene expression signature obtained *in vivo*, *BioMed Cancer*, 11 (2011) 529.
- [227] C.S. Scanlon, E.A. Van Tubergen, R.C. Inglehart and N.J. D'Silva, Biomarkers of Epithelial-Mesenchymal Transition in Squamous Cell Carcinoma, *Journal of Dental Research*, 92 (2013) 121.
- [228] A.Y. Kim, J.H. Kwak, N.K. Je, Y. Lee and Y.S. Jung, Epithelial-Mesenchymal Transition is Associated with Acquired Resistance to 5-Fluorouracil in HT-29 Colon Cancer Cells, *Toxicological Research*, 31 (2015) 156.
- [229] D.S. Yu, D.S. Hsieh and S.Y. Chang, Increasing expression of GST-pi MIF, and ID1 genes in chemoresistant prostate cancer cells, *Archives of Andrology*, 52 (2006) 81.
- [230] C.C. Chao, Y.T. Huang, C.M. Ma, W.Y. Chou and S. Lin-Chao, Overexpression of glutathione S-transferase and elevation of thiol pools in a multidrug-resistant human colon cancer cell line, *Molecular Pharmacology*, 41 (1992) 75.
- [231] L. Jankova, G. Robertson, C. Chan, K.L. Tan, M. Kohonen-Corish and C.L.S. Fung, Glutathione S-transferase Pi expression predicts response to adjuvant chemotherapy for stage C colon cancer: a matched historical control study, *BioMed Cancer*, 12 (2012) 196.
- [232] J. Stoehlmacher, D.J. Park, W. Zhang, S. Groshen, D.D. Tsao-Wei and M.C. Yu, Association Between Glutathione S-Transferase P1, T1, and M1 Genetic Polymorphism and Survival of Patients With Metastatic Colorectal Cancer, *Journal of the National Cancer Institute*, 94 (2002) 2.
- [233] A. Singh and J. Settleman, EMT, cancer stem cells and drug resistance: an emerging axis of evil in the war on cancer, *Oncogene*, 29 (2010) 1.
- [234] T. Arumugam, V. Ramachandran, K.F. Fournier, H. Wang, L. Marquis and J.L. Abbruzzese, Epithelial to Mesenchymal Transition Contributes to Drug Resistance in Pancreatic Cancer, *Cancer Research*, 69 (2009) 8.

- [235] Y. Chen, Z. Zhao, Y. Chen, Z. Lv, X. Ding and R. Wang, An epithelial-to-mesenchymal transition-inducing potential of granulocyte macrophage colony-stimulating factor in colon cancer, *Scientific Reports*, 7 (2017) 5.
- [236] M.N. Ebert, A. Klinder, W.H.M. Peters, A. Schäferhenrich, W. Sendt and J. Scheele, Expression of glutathione S-transferases (GSTs) in human colon cells and inducibility of GSTM2 by butyrate, *Carcinogenesis*, 24 (2003) 1.
- [237] P.O. Beaumont, M.J. Moore, K.Ahmad, M.M. Payne, C. Lee and D.S. Riddick, Role of glutathione S-transferases in the resistance of human colon cancer cell lines to doxorubicin, *Cancer Research*, 58 (1998) 2.
- [238] L. Xie, B.K. Law, A.M. Chytil, K.A. Brown, M.E. Aakre and H.L. Moses Activation of the Erk Pathway Is Required for TGF- $\beta$ 1-Induced EMT *In Vitro*, *Neoplasia*, 6 (2004) 1.
- [239] Y. Yang, F. Yin, Q. Hang, X. Dong, J. Chen and L. Li, Regulation of Endothelial Permeability by Glutathione S-Transferase Pi Against Actin Polymerization, *Cellular Physiology and Biochemistry*, 45 (2018) 1.
- [240] D.W. Choi, M.S. Lim, J.W. Lee, W. Chun, S.H. Lee and Y.H. Nam The Cytotoxicity of Kahweol in HT-29 Human Colorectal Cancer Cells Is Mediated by Apoptosis and Suppression of Heat Shock Protein 70 Expression, *Biomolecules & Therapeutics*, 23 (2015) 3.
- [241] R. Koren, S. Wacksberg, G.E. Weitsman and A. Ravid, Calcitriol sensitizes colon cancer cells to H<sub>2</sub>O<sub>2</sub>-induced cytotoxicity while inhibiting caspase activation, *The Journal of Steroid Biochemistry and Molecular Biology*, 101 (2006) 2.
- [242] M.M. Gaschler and B.R. Stockwell, Lipid peroxidation in cell death, *Biochemical and Biophysical Research Communications*, 482 (2017) 5.
- [243] D. Grotto, L.S. Maria, J. Valentini, C. Paniz, G. Schmitt and Garcia S.C. Importance of the lipid peroxidation biomarkers and methodological aspects for malondialdehyde quantification, *Artigos Química Nova*, 32 (2009) 1.
- [244] A. Ayala, M.F. Muñoz and S. Argüelles, Lipid Peroxidation: Production, Metabolism, and Signaling Mechanisms of Malondialdehyde and 4-Hydroxy-2-Nonenal, *Oxidative Medicine and Cellular Longevity*, 3 (2014) 1.
- [245] Y.H. Siddique, G. Ara and M. Afzal, Estimation of Lipid Peroxidation Induced by Hydrogen Peroxide in Cultured Human Lymphocytes, *Dose-Response*, 10 (2012) 10.
- [246] T.C. Carraro, N.M. Khalil and R.M. Mainardes, Amphotericin B-loaded polymeric nanoparticles: formulation optimization by factorial design, *Pharmaceutical Development and Technology*, 21 (2016) 6.
- [247] F. Danhier, E. Ansorena, J.M. Silva, R. Coco, A. Le Breton and V. Preat, PLGA-based nanoparticles: an overview of biomedical applications, *Journal of Control Release*, 161 (2012) 522.

- [248] J.S. Petschauer, A.J. Madden, W.P. Kirschbrown, G. Song and W.C. Zamboni, The effects of nanoparticle drug loading on the pharmacokinetics of anticancer agents, *Nanomedicine*, 10 (2015) 3.
- [249] N. Hoshyar, S. Gray, H. Han and G. Bao, The effect of nanoparticle size on *in vivo* pharmacokinetics and cellular interaction, *Nanomedicine*, 11 (2016) 6.
- [250] F. Lu, S.H. Wu, Y. Hung, C.Y. Mou, Size Effect on Cell Uptake in Well-Suspended, Uniform Mesoporous Silica Nanoparticles, 5 (2009) 13.
- [251] W. Kaiyaly and M. Al Shafiee, Recent advances in the engineering of nanosized active pharmaceutical ingredients: Promises and challenges, *Advances in Colloid and Interface Science*, 228 (2016) 1.
- [252] R.N. Saha, S. Vasanthakumar, G. Bende, and Snehalatha M. Nanoparticulate drug delivery systems for cancer chemotherapy, *Molecular Membrane Biology*, 27 (2010) 1.
- [253] A. Lamprecht, U. Schafer and C.M. Lehr, Size-dependent bioadhesion of micro- and nanoparticulate carriers to the inflamed colonic mucosa, *Pharmacological Research*, 18 (2001) 3.
- [254] A. Shabir, F. Alhusban, Y. Perrie and A.R. Mohammed, Effects of ball-milling on PLGA polymer and its implication on lansoprazole-loaded nanoparticles, *Journal of Basic and Clinical Pharmacy*, 2 (2011) 2.
- [255] L.R. Tefas, I. Tomuta, M. Achim and L. Vlase, Development and optimization of quercetin-loaded PLGA nanoparticles by experimental design, *Clujul Medical*, 88 (2015) 3.
- [256] W. Huang and C. Zhang, Tuning the Size of Poly(lactic-co-glycolic Acid) (PLGA) Nanoparticles Fabricated by Nanoprecipitation, *Biotechnology Journal*, 13 (2018) 1.
- [257] N. Sharma, P. Madan and S. Lin, Effect of process and formulation variables on the preparation of parenteral paclitaxel-loaded biodegradable polymeric nanoparticles: A co-surfactant study, *Asian Journal of Pharmaceutical Sciences*, 11 (2016) 2.
- [258] Fanun M. *Colloids in Biotechnology*, 1<sup>st</sup> edition, CRC Press, Florida, 2010.
- [259] M. Morales-Cruz, G.M. Flores-Fernández, M. Morales-Cruz, E.A. Orellano, J.A. Rodriguez-Martinez and M. Ruiz, Two-step nanoprecipitation for the production of protein-loaded PLGA nanospheres, *Results in Pharma Sciences*, 2 (2012) 5.
- [260] J. Cheng, B.A. Teply, I. Sherifi, J. Sung, G. Luther and F.X. Gu, Formulation of Functionalized PLGA-PEG Nanoparticles for *in vivo* Targeted Drug Delivery, *Biomaterials*, 28 (2007) 6.

- [261] Halayqa M., Domanska U. PLGA biodegradable nanoparticles containing perphenazine or chlorpromazine hydrochloride: effect of formulation and release, *Int J Mol Sci* 2014: 15: 23909-23923.
- [262] Sharma D., Maheshwari D., Philip G., Rana R., Bhatia S., Singh M. et al. Formulation and Optimization of Polymeric Nanoparticles for Intranasal Delivery of Lorazepam Using Box-Behnken Design: *in vitro* and *in vivo* Evaluation, *Journal of BioMed Research International*, 2014: 2014: 14.
- [263] Tekko I., Maaz A., Abdelwahed W., Trefi S. Influence of nanoprecipitation method parameters on nanoparticles loaded with gatifloxacin for ocular drug delivery, *International Journal of Academic and Scientific Research* 2015: 3: 1-12.
- [264] Dalpiaz A., Contado C., Mari L., Perrone D., Pavan B., Paganetto G. et al. Development and characterization of PLGA nanoparticles as delivery systems of a prodrug of zidovudine obtained by its conjugation with ursodeoxycholic acid, *Drug Delivery* 2014: 21: 221-232.
- [265] Fonseca C., Simoes S., Gaspar R. Paclitaxel-loaded PLGA nanoparticles: preparation, physicochemical characterization and *in vitro* anti-tumoral activity, *J Control Release* 2002: 83: 273-286.
- [266] Lancheros R., Guerrero C. A., Godoy-Silva R., #xe9, D. n. Improvement of N-Acetylcysteine Loaded in PLGA Nanoparticles by Nanoprecipitation Method %J *Journal of Nanotechnology*, 2018: 2018: 11.
- [267] Peltonen L., Aitta J., Hyvönen S., Karjalainen M., Hirvonen J. Improved entrapment efficiency of hydrophilic drug substance during nanoprecipitation of poly(l)lactide nanoparticles, *AAPS PharmSciTech* 2009: 5: 115.
- [268] Higuchi T. Mechanism of sustained-action medication. Theoretical analysis of rate of release of solid drugs dispersed in solid matrices, 1963: 52: 1145-1149.
- [269] Yang Q., Xiao H., Cai J., Xie Z., Wang Z., Jing X. Nanoparticle mediated delivery of a GST inhibitor ethacrynic acid for sensitizing platinum based chemotherapy, *RSC Advances* 2014: 4: 61124-61132.
- [270] Branco M. C., Schneider J. P. Self-assembling materials for therapeutic delivery, *Acta biomaterialia* 2009: 5: 817-831.
- [271] Shen S., Wu Y., Liu Y., Wu D. High drug-loading nanomedicines: progress, current status, and prospects, *International Journal of Nanomedicine* 2017: 12: 4085-4109.
- [272] Shen Y. Jin E. Zhang B. Murphy C.J. Sui M. and Zhao J. Prodrugs forming high drug loading multifunctional nanocapsules for intracellular cancer drug delivery, *Journal of the American Chemical Society*, 132 (2010) 12.



- [273] P. Gou, W. Liu, W. Mao, J. Tang, Y. Shen and M. Sui Self-assembling doxorubicin prodrug forming nanoparticles for cancer chemotherapy: synthesis and anticancer study *in vitro* and *in vivo*, Journal of Materials Chemistry B, 1 (2013) 1.
- [274] H. Zhang, J. Wang, W. Mao, J. Huang, X. Wu and Y. Shen, Novel SN38 conjugate-forming nanoparticles as anticancer prodrug: *in vitro* and *in vivo* studies, Journal of Control Release, 166 (2013) 2.
- [275] Z. Zhou, O. Munyaradzi, X. Xia, D.S. Green and D. Bong, High-Capacity Drug Carriers from Common Polymer Amphiphiles, Biomacromolecules, 17 (2016) 1.
- [276] S.J. Wallace, J. Li, R.L. Nation and B.J. Boyd, Drug release from nanomedicines: Selection of appropriate encapsulation and release methodology, Drug Delivery and Translational Research, 2 (2012) 2.
- [277] M. Sethi, R. Sukumar, S. Karve, M.E. Werner, E.C. Wang and D.T. Moore, Effect of Drug Release Kinetics on Nanoparticle Therapeutic Efficacy and Toxicity, Nanoscale, 6 (2014) 1.
- [278] S.A. Abouelmagd, B. Sun, A.C. Chang, Y.J. Ku and Y. Yeo, Release Kinetics Study of Poorly Water-Soluble Drugs from Nanoparticles: Are We Doing It Right?, Molecular Pharmaceutics, 12 (2015) 1.
- [279] S. Souza, A Review of *In Vitro* Drug Release Test Methods for Nano-Sized Dosage Forms, Journal of Advances in Pharmaceutics, 12 (2014) 3.
- [280] A.L. Ortega, S. Mena and J.M. Estrela, Glutathione in Cancer Cell Death, Cancers, 3 (2011) 12.
- [281] N. Traverso, R. Ricciarelli, M. Nitti, B. Marengo, A.L. Furfaro and M.A. Pronzato, Role of Glutathione in Cancer Progression and Chemoresistance, Journal of Oxidative Medicine and Cellular Longevity, 10 (2013) 1.
- [282] G. Ma, and Z.G. Su, Microspheres and Microcapsules in Biotechnology: Design, Preparation and Applications: Pan Stanford, 2013.
- [283] S.B. Sun, P. Liu, F.M. Shao and Q.L. Miao, Formulation and evaluation of PLGA nanoparticles loaded capecitabine for prostate cancer, International Journal of Clinical and Experimental Medicine, 8 (2015) 1.
- [284] B. Mukherjee, K. Santra, G. Pattnaik and S. Ghosh, Preparation, characterization and *in-vitro* evaluation of sustained release protein-loaded nanoparticles based on biodegradable polymers, International Journal of Nanomedicine, 3 (2008) 6.
- [285] S. Davaran, M.R. Rashidi, B. Pourabbas, M. Dadashzadeh and N.M. Haghshenas, Adriamycin release from poly(lactide-co-glycolide)-polyethylene glycol nanoparticles: synthesis, and *in vitro* characterization, International Journal of Nanomedicine, 1 (2006) 9.

- [286] D.J. Hines and D.L. Kaplan Poly (lactic-co-glycolic acid) controlled release systems: experimental and modeling insights, *Critical Reviews In Therapeutic Drug Carrier Systems*, 30 (2013) 6.
- [287] F.U. Amin, S.A. Shah, H. Badshah, M. Khan and M. Kim, Anthocyanins encapsulated by PLGA-PEG nanoparticles potentially improved its free radical scavenging capabilities via p38/JNK pathway against A $\beta$ 1–42-induced oxidative stress, *Journal of Nanobiotechnology*, 15 (2017) 12.
- [288] M. Omid, A. Fatehinya, M. Farahani, Z. Akbari, S. Shahmoradi and F. Yazdian, Characterization of biomaterials. In: L. Tayebi and K. Moharamzadeh (Eds). *Biomaterials for Oral and Dental Tissue Engineering*: Woodhead Publishing, Cambridge, 2017.
- [289] E. Koliniotou-Koubia, P. Dionysopoulos, E.A. Koulaouzidou, A.H. Kortsaris and Y. Papadogiannis, *In vitro* cytotoxicity of six dentin bonding agents, *Journal of Oral Rehabilitation*, 28 (2001) 5.
- [290] G. Ciapetti, S. Stea, E. Cenni, A. Sudanese, D. Marraro and A. Toni, Cytotoxicity testing of cyanoacrylates using direct contact assay on cell cultures, *Biomaterials*, 15 (1994) 67.
- [291] X. Liu, M. Tang, T. Zhang, Y. Hu, S. Zhang and L. Kong, Determination of a threshold dose to reduce or eliminate CdTe-induced toxicity in L929 cells by controlling the exposure dose, *PLoS One*, 8 (2013) 1.
- [292] J.D. Coyne, Necrobiotic palisading granulomas associated with breast carcinoma, *Journal of Clinical Pathology*, 58 (2005) 12.
- [293] Z. Zhao, X. Zhu, K. Cui, J. Mancuso, R. Federley and K. Fischer, *In vivo* visualization and characterization of epithelial-mesenchymal transition in breast tumors, *Cancer Research*, 76 (2016) 3.

# CURRICULUM VITAE

## Credentials

Name, Surname :Burçin Özçelik  
Place of Birth :İstanbul  
Marital Status Single  
e-mail :burcinozclk@gmail.com  
Adress :Ulukavak Mah. No:289/13 Çorum

## Education

High School : Zonguldak Fen Lisesi  
Bsc. : Biology Education  
PhD. : Division of Nanotechnology and Nanomedicine

## Foreign Languages

English : Advanced (Score: 78.75, ÜDS)

## Work Experience

Research asistant : Department of Biology, Hitit University, Çorum

## **Areas of Experiences**

Nanotechnology, Nanomedicine, Novel Drug Delivery Systems, Drug Resistance Mechanisms in Cancer Therapy, Polymeric Nanoparticles, Polymer-Drug Conjugation

## **Projects and Budgets**

- 1- The Role of Glutathione S-Transferase (GST) in Epithelial Mesenchymal Transition (EMT) Model of Colorectal Cancer and the Enhancement of Adjuvant Therapy Efficiency by Targeting GST Inhibitor, The Scientific and Technological Research Council of Turkey, Project Number:116S347, Project Budget: 400.208 TL.
- 2- The Role of Glutathione S-Transferase (GST) in Epithelial Mesenchymal Transition (EMT) Model of Colorectal Cancer and the Enhancement of Adjuvant Therapy Efficiency by Targeting GST Inhibitor, Scientific Research Fund of Hacettepe University, Project Number: TSA-2017-15520, Project Budget: 103.453,24 TL.

## **Publications**

-

## **Oral and Poster Presentations**

- 1- The 7<sup>th</sup> EMBO Meeting, September 2016, Mannheim, Germany (Poster presentation).
- 2- 18<sup>th</sup> International Pharmaceutical Technology Symposium: IPTS 2016, September 2016, Antalya, Turkey (Poster presentation).
- 3- International Multidisciplinary Symposium on Drug Research and Development (DRD 2017): October, 2017, Erzurum, Turkey (Poster presentation).
- 4- 19<sup>th</sup> International Pharmaceutical Technology Symposium: IPTS 2016, September 2018, Antalya, Turkey (Poster presentation).



## DENEY HAYVANLARI KULLANIM SERTİFİKASI

**BURÇİN ÖZÇELİK**

Ankara Üniversitesi Sürekli Eğitim Merkezi (ANKÜSEM) ve Hayvan Deneyleri Yerel Etik Kurulu İşbirliği çerçevesinde 04 Mayıs - 13 Mayıs 2015 tarihleri arasında düzenlenen "Deney Hayvanları Kullanım Sertifikası" eğitimini başarı ile tamamlayarak sertifika almaya hak kazanmıştır.



Prof. Dr. Ögüz SARIMENEMETOĞLU

Hayvan Deneyleri Yerel Etik Kurulu Başkanı

Eğitim Programını Kategorisi ve Süresi : 8 Kategorisi - 81 Saat



Prof. Dr. Erkan İBİŞ  
Rektör



Prof. Dr. Mualla SİLTÜRK  
ANKÜSEM Müdürü

Belge No: 6298



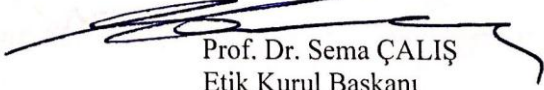
T.C.  
**HACETTEPE ÜNİVERSİTESİ**  
Hayvan Deneyleri Yerel Etik Kurulu

Sayı : 52338575 - 48

**HAYVAN DENEYLERİ YEREL ETİK KURUL KARARI**

<b>TOPLANTI TARİHİ</b>	: 28.03.2017 (SALI)
<b>TOPLANTI SAYISI</b>	: 2017/03
<b>DOSYA KAYIT NUMARASI</b>	: 2017/26
<b>KARAR NUMARASI</b>	: 2017/26 -10
<b>ARAŞTIRMA YÜRÜTÜCÜSÜ</b>	: Prof. Dr. Alper B. İSKİT
<b>HAYVAN DENEYLERİNDEN SORUMLU ARAŞTIRMACI</b>	: Prof. Dr. Alper B. İSKİT, Arş. Gör. Burçin ÖZÇELİK, Arş. Gör. Dr. Açelya ERİKÇİ
<b>YARDIMCI ARAŞTIRMACILAR</b>	: Prof. Dr. Gülberk UÇAR, Doç. Dr. İpek EROĞLU, Yrd. Doç. Dr. Kemal KÖSEMEHMETOĞLU, Arş. Gör. Dr. Açelya ERİKÇİ, Arş. Gör. Burçin ÖZÇELİK
<b>ONAYLANAN HAYVAN TÜRÜ ve SAYISI</b>	: 78 Adet Wistar Sıçan (6-8 Hafta)

Üniversitemiz Tıp Fakültesi Tıbbi Farmakoloji Anabilim Dalı öğretim üyelerinden Prof. Dr. Alper B. İSKİT' in araştırma yürütücüsü olduğu 2017/26 kayıt numaralı "*Kolorektal Kanserde Epitelyalmezankimal Geçiş (EMT) Modellemesinde Glutasyon-S-Transferaz'ın Rolü Ve Glutasyon-S-Transferaz İnhibitörü Hedeflenerek Adjuvan Terapi Etkinliğinin İn Vivo Şartlarda Arttırılması*" isimli çalışma Hayvan Deneyleri Yerel Etik Kurulu Yönergesi'ne göre uygun bulunarak oy birliği ile onaylanmasına karar verilmiştir.

  
Prof. Dr. Sema ÇALIŞ  
Etik Kurul Başkanı





HACETTEPE UNIVERSITY  
GRADUATE SCHOOL OF SCIENCE AND ENGINEERING  
DISSERTATION ORIGINALITY REPORT

HACETTEPE UNIVERSITY  
GRADUATE SCHOOL OF SCIENCE AND ENGINEERING  
TO THE DEPARTMENT OF NANOTECHNOLOGY and NANOMEDICINE

Date: 10/01/2019

Thesis Title / Topic: The Role of Glutathione-S-Transferase in Epithelial Mesenchymal Transition (EMT) Model in Colorectal Cancer And the Enhancement of Adjuvant Therapy by Targeting Glutathione-S-Transferase Inhibitor

According to the originality report obtained by my thesis advisor by using the *Turnitin* plagiarism detection software and by applying the filtering options stated below on 10/01/2019 for the total of 120. pages including the a) Title Page, b) Introduction, c) Main Chapters, d) Conclusion sections of my thesis entitled as above, the similarity index of my thesis is 11 %.

Filtering options applied:

1. Bibliography/Works Cited excluded
2. Quotes excluded
3. Match size up to 5 words excluded

I declare that I have carefully read Hacettepe University Graduate School of Science and Engineering Guidelines for Obtaining and Using Thesis Originality Reports; that according to the maximum similarity index values specified in the Guidelines, my thesis does not include any form of plagiarism; that in any future detection of possible infringement of the regulations I accept all legal responsibility; and that all the information I have provided is correct to the best of my knowledge.

I respectfully submit this for approval.

  
10.01.2019

Name Surname: BURÇİN ÖZÇELİK

Student No: N12141038

Department: NANOTECHNOLOGY and NANOMEDICINE

Program: NANOTECHNOLOGY and NANOMEDICINE

Status:  Masters  Ph.D.  Integrated Ph.D.

**ADVISOR APPROVAL**

APPROVED

  
Prof. Dr. Alper B. İSKİT

Prof. Dr. Alper B. İSKİT

(Title, Name Surname, Signature)